5-1-1985

Pseudo-Random Codes for Single-Mode and Simultaneous Multi-Mode Operation in Ultrasonic Imaging Systems

B. B. Lee
Purdue University

E. S. Furgason
Purdue University

Pseudo-Random Codes for Single-Mode and Simultaneous Multi-Mode Operation in Ultrasonic Imaging Systems

B. B. Lee
E. S. Furgason

TR-EE 85-10
May 1985

School of Electrical Engineering
Purdue University
West Lafayette, Indiana 47907

PSEUDO-RANDOM CODES FOR SINGLE-MODE AND SIMULTANEOUS MULTI-MODE OPERATION IN ULTRASONIC IMAGING SYSTEMS

by

B. B. Lee

E. S. Furgason

School of Electrical Engineering

Purdue University

West Lafayette, Indiana 47907

TR-EE 85-10

May 1985

TABLE OF CONTENTS

ABSTRACT

Conventional pulse-echo imaging systems used in ultrasonics can become limited in average transmit power by transmitter, transducer, and medium peak-power limitations. In addition, imaging systems which use multi-element arrays are limited in speed by the necessity to transmit sequentially when scanning in more than one direction in order to avoid interfering echoes. A new system is studied which can overcome both the speed and power limitations by using correlation receivers and pseudo-random transmit codes. First, the performance of several single-mode correlation systems are compared to conventional pulse-echo systems in the presence of clutter and moving targets. The system which uses special pseudo-random codes called Golay codes is shown to provide the best overall performance. A multi-mode correlation system is then studied which images in many different modes (e.g. scan directions) simultaneously. This multi-mode system is studied under the effects of moving targets, clutter and background receiver noise. A comparison with the operation of conventional sequentially-scanned phased array systems is made under a variety of signal-to-noise ratio (SNR) conditions and operating speeds to determine the optimal type of imaging system. Results indicate that under many conditions, a simultaneous multi-mode system can provide improved SNR and/or speed over conventional sequential multi-mode systems. The multi-mode system which uses Golay codes is shown to provide the best overall performance.

CHAPTER I - INTRODUCTION

Conventional ultrasonic systems are fundamentally limited in both range and scan speed due, respectively, to average power limitations and an inability to transmit in more than one scan direction at a time. In the following paper a new ultrasonic system is presented and analyzed which overcomes both these limitations.

Conventional Pulse-Echo Imaging

Ultrasound provides a convenient method for nondestructively probing deep within any medium which is conducive to ultrasonic propagation, such as metal structures or the human body. Any discontinuity in acoustic impedance within the medium disrupts and scatters the propagating ultrasonic wave. Encoded in the scattered ultrasound is a wealth of information about the material characteristics along the ultrasonic travel path including, density, velocity and attenuation. From this information the relative locations and size of cracks, flaws, voids and the location or motion of interfaces can be readily deduced. In ultrasonics there are, thus, two basic tasks. The first is to obtain the ultrasonic information in an optimal manner, typically with high resolution, high signal-to-noise ratio and the highest possible speed. The second is to process the data to best utilize the available information, e.g., for an optimal flaw location decision.

Obviously, from an overall system point of view, these two tasks are not independent. Good data presupposes more information for better processing and good processing techniques can handle poor data. However, it is also obvious that good processing techniques will always be better if the quality of the input-data is improved.

Unfortunately, the most widely utilized ultrasonic transmitter/receiver design has remained nearly unchanged since ultrasonic pulse-echo techniques were first used to provide one-dimensional A-scan images [1]. The conventional pulse-echo technique involves exciting a wideband piezoelectric transducer with

a narrow, high-amplitude pulse to transmit a short burst of ultrasound into the medium under inspection. Discontinuities in acoustic impedance produce reflections which are received by the same transducer as used for transmission. (The use of a single transducer for both transmission and reception has a number of advantages, including simplified usage and reduced cost.) The received echoes are then processed to provide some form of visual display for human inspection.

Unfortunately, average transmit power is constrained in conventional pulse-echo systems because the peak transmit power is limited by transmitter design and transducer breakdown. The system must transmit narrow pulses so that the resolution of the system will only be limited by the impulse response of the transducer. Bilgutay et al. [2] described this power limitation on a pulse-echo system as

$$\frac{\textit{maximum range}}{\textit{maximum resolution}} \leq \frac{\textit{burst interval}}{\textit{burst width}} = \frac{\textit{peak power}}{\textit{average power}} . \qquad (1.1)$$

This relationship indicates that when conventional pulse-echo systems are peak-power limited, their average transmit power cannot be increased without sacrificing either range or resolution. If some method could be applied in which the average transmit power could be increased without degrading the resolution, an increase in the output signal-to-noise ratio would result. As will be shown, the use of correlation processing with large time-bandwidth signals can overcome these limitations.

Improved Single-Mode Imaging

In order to overcome the average transmit power limitation Furgason et al. [3] proposed a flaw detection system similar to a radar system developed by Cooper et al. [4] which transmits large time-bandwidth random signals and then uses a correlation receiver to compress the long transmit signals into short, high-resolution bursts. A basic diagram of this system is shown in Figure 1-1. The system uses a water delay line to store a copy of the transmit signal. The output of the delay line is multiplied by the return echo signals and then integrated by a lowpass filter. This operation produces an approximation to the correlation function of the transmit signal which results in an output signal which is compressed compared to the transmit signal. A

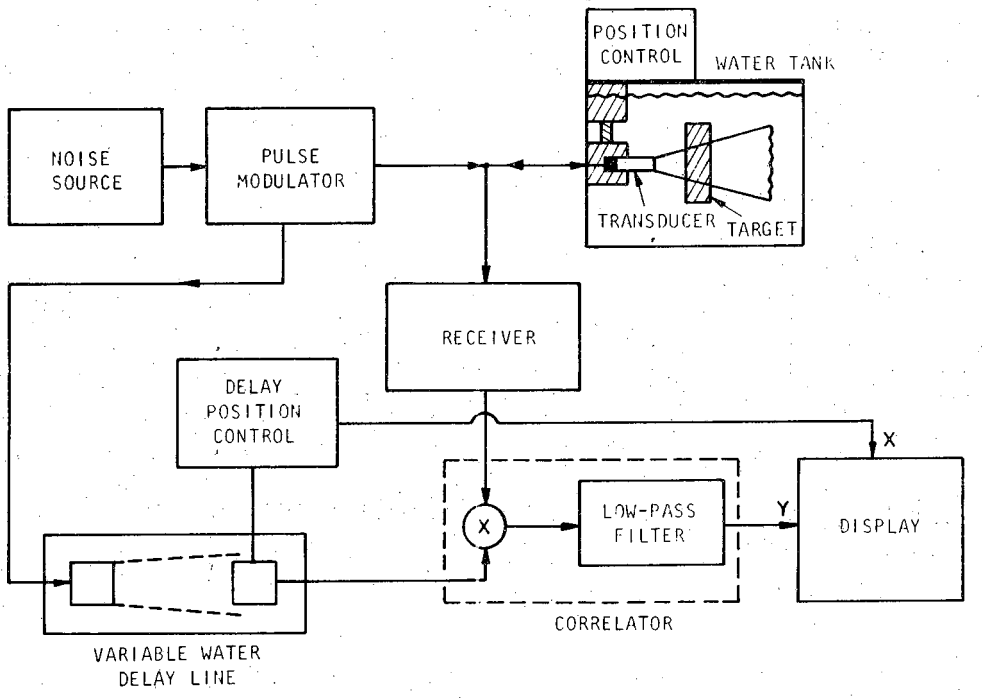

Figure 1–1 Original random signal analog correlation system.

more thorough description of this correlation process will be provided later in this paper. This original analog correlation system was shown to provide improved signal-to-noise ratio enhancement *SNRE*, on the order of 10,000 [2]. This enhancement ability allows the random signal flaw detection system to retrieve signals which are buried in receiver noise. Thus the system can probe much deeper into highly attenuative materials, such as ceramics and porous metals, than conventional pulse-echo systems.

As an example of the improved performance provided by correlation systems, consider the plexiglas target of Figure 1-2. Four concentric flat-bottom holes have been drilled in one end. Because of the high attenuation of plexiglas, it was not possible to discriminate the return echoes of the concentric holes from background receiver noise using a conventional pulse-echo system. However, the random signal system was easily able to detect the echoes, as shown in Figure 1-3.

Several other types of transmit signals besides random signals have been used in more recently developed ultrasonic correlation systems. These include clipped sampled random noise [5], m-sequences [6,7], and m-sequence modulated r.f. signals [8-11]. Since these signals are all binary in nature they are able to utilize digital delays to overcome some disadvantages of the analog delay line used in the original random signal flaw detection system. These disadvantages include slow scan time, slow reset time, and limited bandwidth [8].

Although correlation systems offer a significant improvement in *SNR*, all the previous systems, except the correlation flaw detection systems which use continuously transmitted m-sequences [8,9], suffer from an inherent limitation which becomes significant at higher operating speeds. This limitation is called self-noise, and is produced during the correlation process due to finite integration time. An example of self-noise for a short pseudo-random m-sequence of finite length, as shown in Figure 1-4a, can be seen in the correlation function shown in Figure 1-4b, as the hash surrounding the large central peak.

Self-noise causes interference in two important situations, when a large reflector is located close to a desired target, and when a desired target is surrounded by a large number of small reflectors such as grains in NDE [10], or clutter in radar [11] and sonar [12]. In order to reduce self-noise to tolerable levels, previous correlation systems were constrained to long correlation times [15], or separate transmitting and receiving transducers were used for continuous transmission of m-sequences [9,10]. Long correlation times are

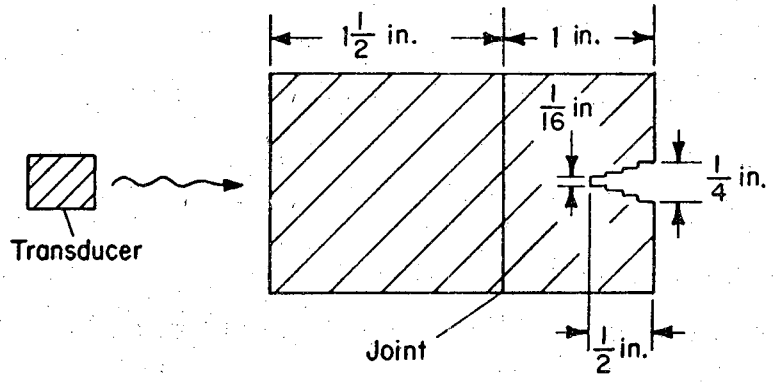

Figure 1–2 Plexiglas target with four concentric flat-bottom holes.

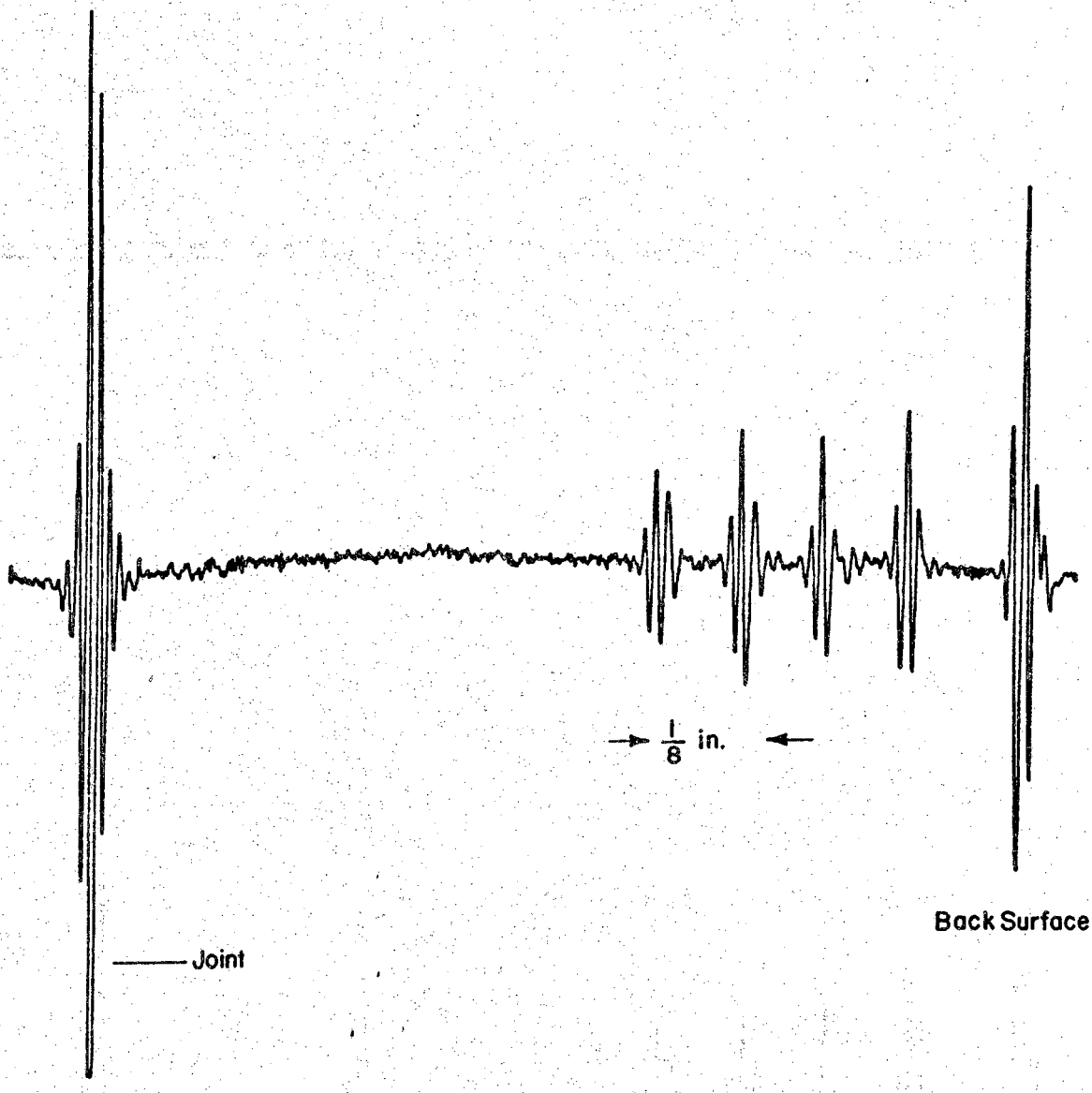

Figure 1–3 Random signal correlation scan of the plexiglas target of Figure 1-2.

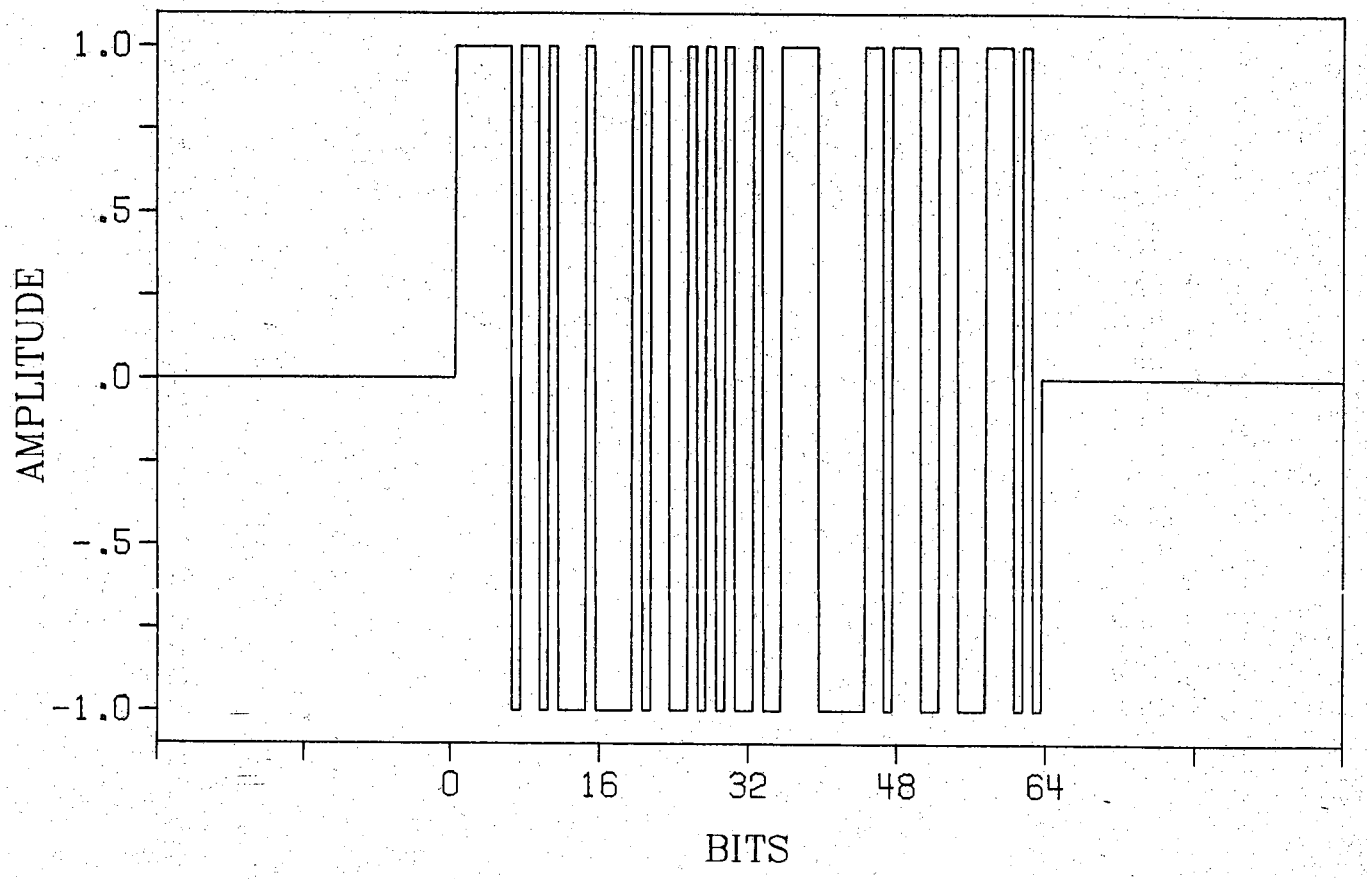

a. M-sequence

Figure 1–4 Autocorrelation function of a 63 bit m-sequence.

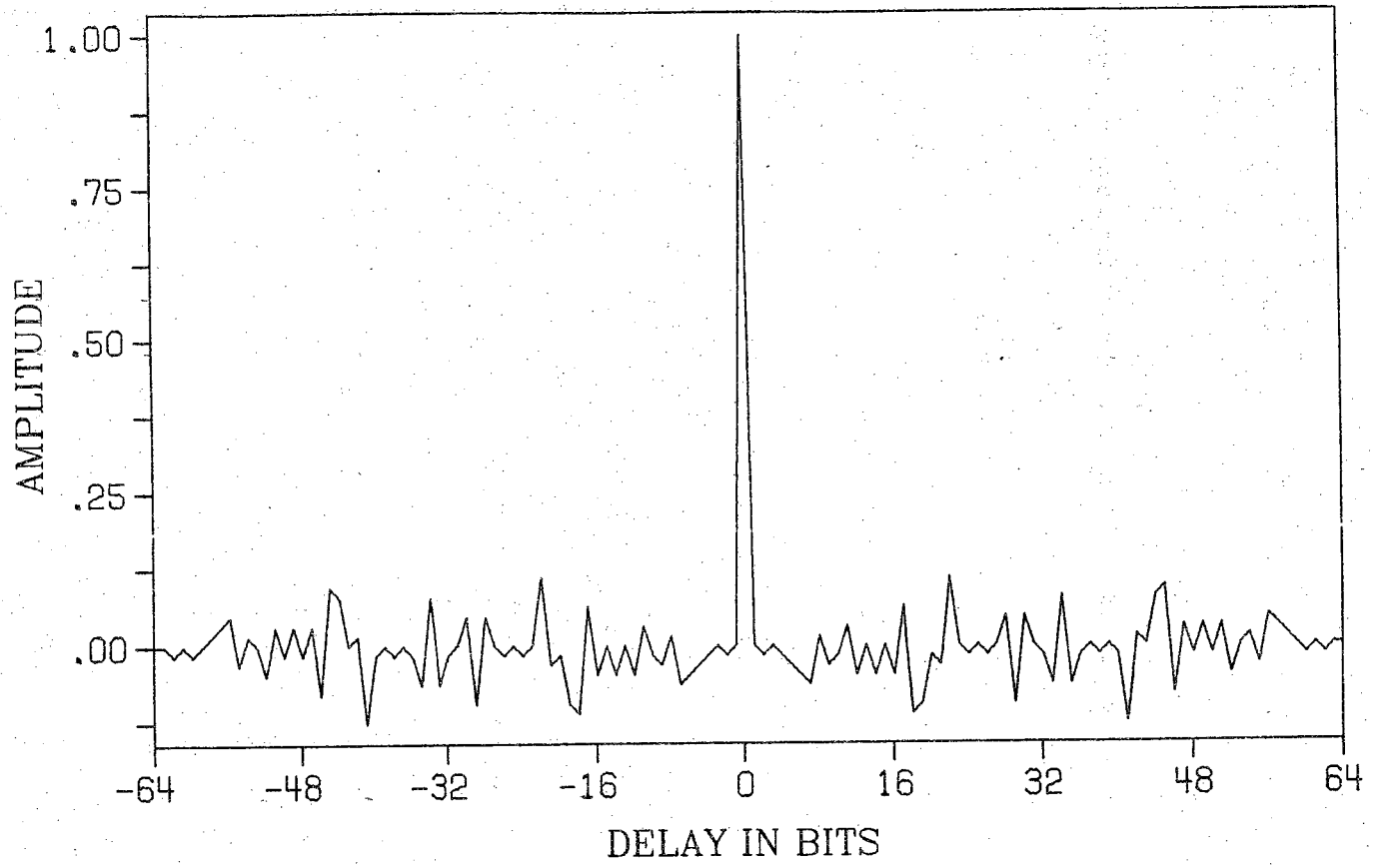

b. Autocorrelation function

Figure 1–4 (continued).

unnecessary in high input signal-to-noise ratio situations, and separate transmitting and receiving transducers impose limitations in many flaw detection situations. For these reasons, and since conventional pulse-echo systems only require one transducer for transmission and reception, we have restricted our studies to developing an ultrasonic correlation system which would overcome the problem of self-noise and still operate in a pulse-echo mode with a single transducer. In this study a special type of pseudo-random codes called Golay codes is used to overcome the problem of self-noise using only two transmit bursts.

Improved Multi-Mode Imaging

Since the introduction of the original pulse-echo method, one of the most important further developments in ultrasonic imaging has been the development of rapid scanning techniques for creating two dimensional images of moving targets. Systems which use rapid scanning have allowed medical specialists to make "real time" B-scan images of fetuses and fast moving organs such as the heart. Such techniques require sequential multiple-mode operation in which the modes correspond to different scan directions. Each directional scan is similar to the same A-scan produced by the basic pulse-echo technique. These different scan directions can correspond to different transducer elements in a linear array, different rotation positions in a mechanical scanner, or different steering angles in an electronically steered phased array. A thorough review of these techniques can be found in a recent article by Ramm and Smith [14]. The basic advantage of a linear or phased array is that no physical movement of the ultrasonic transducer is needed to create an ultrasonic image since all the steering of scan directions is done electronically. Avoiding mechanical movement of the transducer has made it possible to create much higher resolution ultrasonic images [14].

Unfortunately, the scan speed of a conventional pulse-echo multi-mode system is limited because the system control must wait until all the detectable echoes from one mode have been received before it can switch to the next mode. If each sequential mode requires the same amount of time, T, and M modes are required to complete an image, the sequential system requires an amount of time MT to complete an image. If all M modes can be completed simultaneously over a period of time less than MT, an improvement in system speed will be realized.

Ideally, such a system will increase the system operation speed by a factor of M. However, in practice, cross-talk interference between the modes will occur which will require extra time to reduce. From a different standpoint, if an improvement in system speed is not required, an improvement in system signal-to-noise ratio can be realized by transmitting M modes simultaneously, and time averaging over the time MT.

It would be desirable to use a detection method which minimizes interference, or, in other words, maximizes signal-to-noise ratio. Matched filters might seem to be an obvious choice for such a task. One such matched filter technique is a multiple frequency method in which a frequency is assigned to each mode and then narrow band-pass filters (a type of matched filter) are used to detect the signals [15,16]. However the resolution of such a system would be restricted by the narrow bandwidth of these filters and if there was sufficient spread between frequencies to allow wide band signals to be used, the nature of the beam pattern would be different in each of the various modes. Nonetheless, in sonar and radar applications where targets are generally much larger than a wavelength, the resolution requirements are not necessarily as stringent as in ultrasound applications where targets are on the order of a wavelength in size. Consequently, narrowband multiple-frequency techniques may be suitable in sonar and radar but are of little value in ultrasonic imaging and flaw detection.

The ability of correlation systems to retrieve signals buried in noise implies that it would also be possible to use a correlation system to retrieve a desired transmitted signal even in the presence of other transmitted noise signals which occupy the same spectral region. In a previous study [17], we have proposed a system which would transmit a set of broadband random or pseudo-random signals simultaneously, and then isolate the different modes upon reception with correlation receivers matched to the transmit signals. A simplified example of a simple two-direction simultaneous phased array system is shown in Figure 1-5. The number of scan directions can be extended beyond the two shown by adding more signal sources and delay lines. Preliminary studies of similar systems have also been made by Tournois [16], and Miwa et al. [15]. Results have indicated that such a system will provide an increase in speed over sequential systems provided the beams do not completely overlap. The speed improvement is somewhat less than N because extra correlation time is required to reduce the cross-talk interference between the modes.

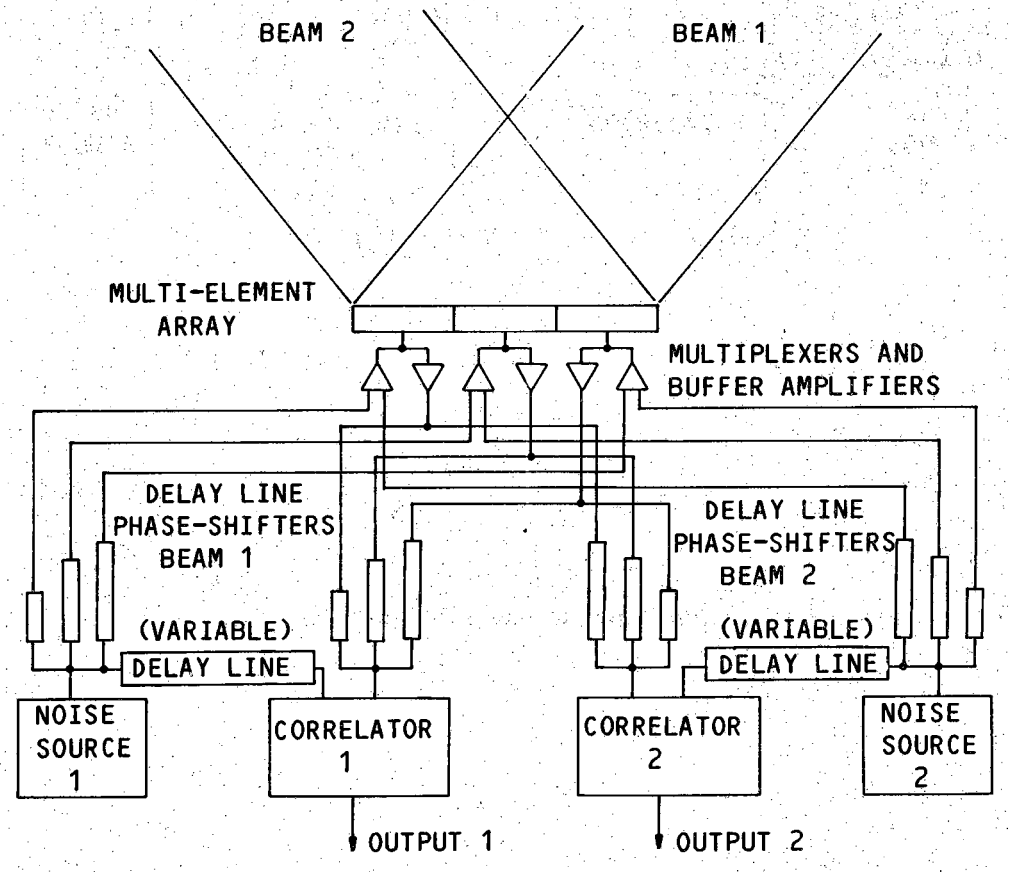

Figure 1–5 A two-mode simultaneous transmission phased array.

Summary

In Chapter II of this study, a background review of the history of single-mode correlation systems is presented, followed by a comparison of their application to ultrasonics, radar, and sonar. The second section of Chapter II then extends the background discussion to multi-mode systems.

The rest of this dissertation is divided into two major parts consisting of two related, yet distinct, topics. The first part is the most extensive and consists of a thorough study of single-mode pulse-echo correlation systems under the presence of clutter, noise, and moving targets. The second part consists of one chapter, Chapter VII. This chapter extends the single-mode results of the first part of the thesis, to include the presence of simultaneously transmitted interfering channels, in a multi-mode correlation system.

In Chapter III the principles of single-mode correlation systems are discussed in terms of their signal-to-noise ratio enhancement, fundamental descriptive formulas and resolution capabilities. The important problem of self-noise due to finite correlation times is introduced, and the effects of this self-noise are discussed under the presence of large interfering targets, clutter, and moving targets.

In Chapter IV the various details of implementing single-mode correlation systems are covered. The different types of correlation system architectures are first discussed, followed by a review and discussion of large time-bandwidth transmit signals, modulation techniques, delay lines, multipliers and integrators. As an addition to the examination of modulation schemes, a brief simulation study of optimal clock rate for direct transmission is presented. Finally, the important effects of time-gain-control receivers on correlation receivers are examined.

In Chapter V a working single-mode digital correlation system is discussed, demonstrated and analyzed under a number of different input signal-to-noise ratio and clutter situations using both m-sequences and clipped sampled random signals.

In Chapter VI, the final chapter on single-mode correlation systems, a modified version of the digital correlation system described in Chapter V is presented which can transmit special paired pseudo-random codes called Golay codes. This system is compared experimentally and theoretically to the system of Chapter V as well as to conventional pulse-echo systems, under a variety of signal-to-noise ratio and clutter conditions. Computer simulations are used to determine the sensitivity of Golay code self-noise cancellation to DC offsets and

dissimilar turn-on and turn-off times of the transmit signal. The motion sensitivity of self-noise cancellation is also determined through the use of the generalized ambiguity function. The results of this moving target analysis are then included in a system signal-to-noise ratio formula.

Under certain simplifying assumptions, this system signal-to-noise ratio formula is then used in a performance evaluation of the Golay code system in which the system is compared to conventional pulse-echo systems to determine the optimal type of system for a given situation.

In Chapter VII a complete comparative analysis is then made of a simultaneous multi-mode correlation system which uses a set of pseudo-random transmit signals. This system is analyzed, for operation with Golay codes, pseudo-random m-sequences, and random signals, through a system signal-to-noise ratio formula which includes the effects of moving clutter, moving targets, and background receiver noise. After making certain simplifying assumptions criterion are developed which can be used to choose the optimum type of transmit signal and imaging system for a given application or situation.

The final chapter of this dissertation summarizes, and discusses the important results of the studies on improved single and multi-mode imaging systems.

CHAPTER II - BACKGROUND

Correlation Systems

The first application of correlation receivers occurred in radar systems in the 1940's [18,19]. Frequency modulated (FM) transmit signals were the first type of transmit signal to be used in radar correlation systems, and in fact, the FM transmit signal is still one of the most widely used radar signals.

Other types of correlation systems which have also been used in radar include systems which transmit pseudo-random m-sequences [20], random signals [4], polyphase pseudo-random codes [21,22], and complementary Golay codes [23-26]. In depth reviews and discussions of radar correlation systems can be found in references [26-29].

Shortly after being introduced into radar, correlation systems were also successfully applied to pulse-echo sonar systems. Sonar pulse-echo systems are analogous to radar pulse-echo systems except for the type of wave propagated, and the range of transmit frequencies. The propagation of waves in sonar is acoustic in nature whereas radar signals are electromagnetic, and the transmit frequencies of sonar systems are much lower than radar transmit frequencies. A good discussion and review of sonar correlation systems can be found in references [30] and [31].

It was not until 1974 that correlation detection was first introduced to ultrasound, by researchers in our lab, through the development of a random signal flaw detection system [2]. This original random signal flaw detection system was shown in Figure 1-1. A detailed description of this system with circuit diagrams can be found in a technical report by Mitchell [32]. This early system relied on a mechanically scanned water delay line which has two transducers facing each other in a long plexiglas water tank. The reference signal travels through the water bath while the transmit signal is interrogating the sample under study. This system was shown to provide very good performance under noise-limited conditions. Unfortunately, a mechanically-scanned delay line is slow, and requires considerable time between scans. The system was also shown to provide slightly lower resolution than m-sequence

correlation systems because of the band-limiting which occurs in the delay line [7].

More recently both Elias [6] and Chapelon et al. [7] have demonstrated similar correlation flaw detection systems which use special binary pseudo-random codes called m-sequences as a replacement for random signals. These systems have the same *SNR* enhancement and pulse compression properties as the original random signal system, but have the advantage of not requiring the bulky water delay line used in the correlation receiver of the random signal system. They replace this water delay line with a short binary shift register set which generates a pseudo-random code identical to that which is transmitted, Figure 2-1. This new development made the pseudo-random system more portable than the original random signal system.

In this thesis a digital flaw detection system is described which replaces the bulky water delay line of the original random signal system with a set of high-speed digital shift registers. This new digital system is not restricted to operation with only pseudo-random m-sequences and can be used to transmit any type of binary code including clipped sampled noise. A demonstration of a modified version of this system which uses Golay codes will be presented in Chapter VI. code system.

The following study is intended to be somewhat general in nature, so that, although the major emphasis is on ultrasonic applications, the results will be applicable, with appropriate modification, to the important fields of sonar and radar. Sonar, radar, and ultrasonic pulse-echo systems each require the same fundamental system design and operate in the same fundamental manner, yet they each have unique design and performance requirements due to the underlying physics of transmission, propagation phenomenon, mission scenario, and specific purpose of the system.

Sonar, radar, and ultrasonic pulse-echo systems can all be represented by the generic system of Figure 2-2. They require a transmit source, a modulator to prepare the transmit signal for transmission (a modulator may not be needed for some transmitters and transmit signals), a power amplifier to maximize the transmit power, and a transmitter which converts a percentage of the electrical signal into a form of energy appropriate for maximum coupling into the propagation medium. They all interrogate some environment which includes targets of interest; as well as interfering targets, both large and small.

The targets produce backscattered propagating waves, and by reciprocity the transmitter then acts as a receiver and converts a percentage of the returning waves to electrical signals which undergo further processing. A

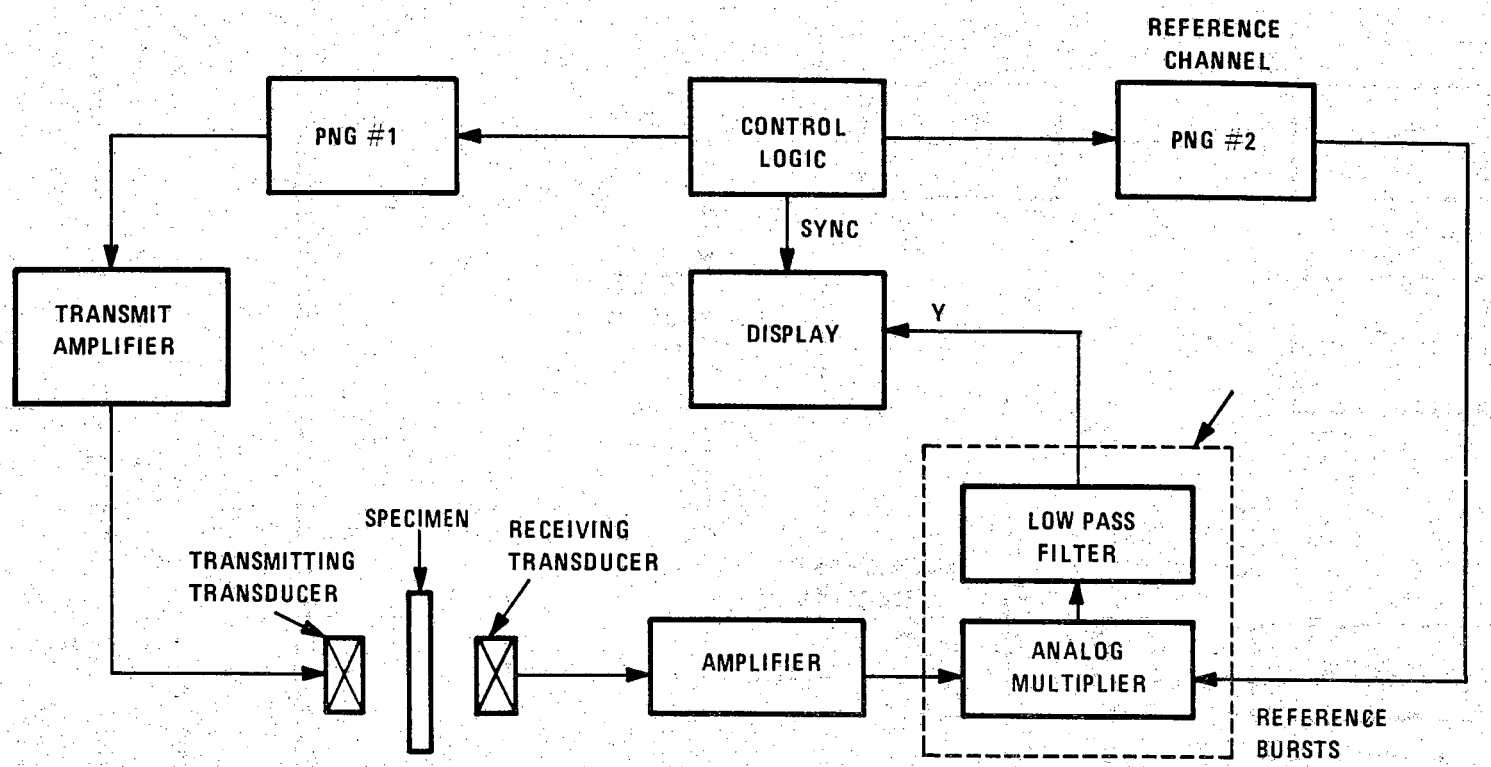

Figure 2–1 M-sequence correlation system.

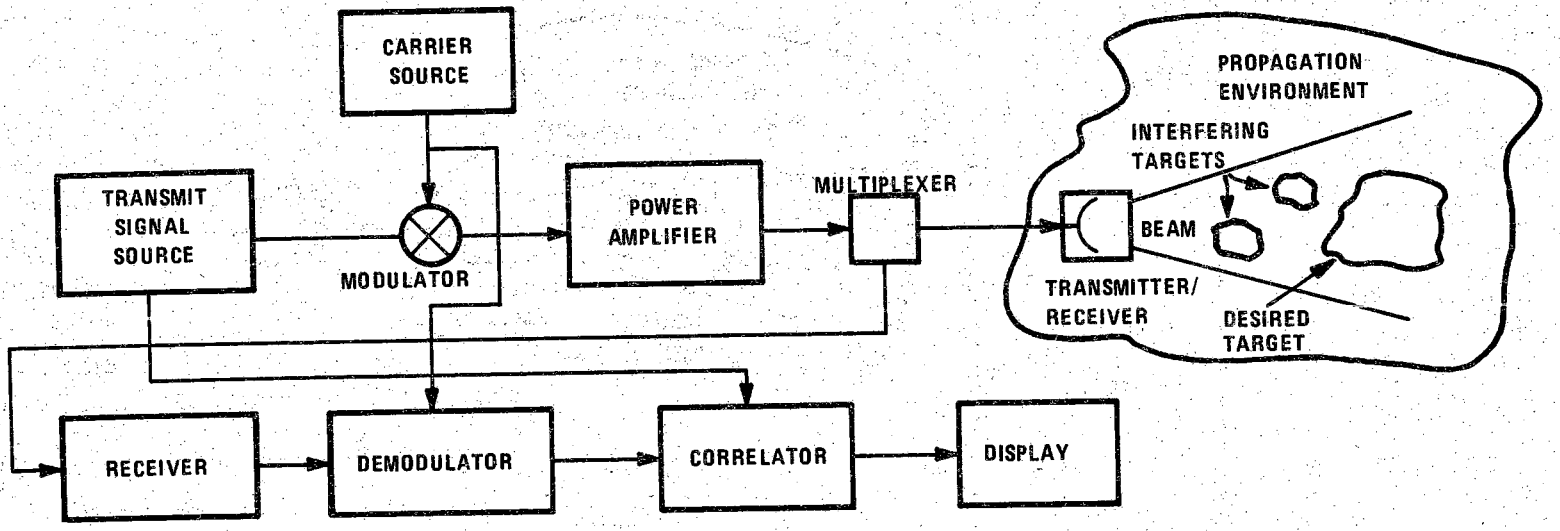

Figure 2–2 Generic pulse-echo correlation system.

receiver filters and/or amplifies the electrical signal to reduce the effects of noise, and the signal is demodulated from the original carrier (once again, the demodulation may not be needed). This signal then undergoes further processing to make it suitable for some visual display device.

As mentioned before, although the systems operate in the same fundamental manner, there are basic differences between the physics and mission scenarios of radar, sonar, and ultrasound, which affect system performance requirements and design. The underlying fundamental differences include velocity of propagation, attenuation, scan range, target sizes, target velocities, clutter levels, and transmitter limitations. These result in a need for different center frequencies, percentage bandwidths, pulse-widths, and repetition rates; which in turn require different types of receivers and demodulators, since no single type of receiver or demodulator can perform optimally for all bandwidths and frequencies.

A summary of some of the important parameters of ultrasonic, sonar, and radar systems is shown in Table 2-1. The velocity of propagation of a radar signal is the speed of light in air, 3×10^8 m/sec, whereas ultrasound and sonar waves travel at the speed of sound, which is approximately 1500 m/sec in water. Depending on the application, radar systems generally transmit at center frequencies between 100 MHz and 100 GHz [33], ultrasonic systems typically transmit at center frequencies between 100 KHz and 30 MHz [34], and sonar systems generally transmit between 100 Hz and 100 KHz [35]. Ultrasound pulse-echo systems are typically much higher in percentage bandwidth than radar or sonar due to several factors: the more stringent resolution requirements of ultrasound applications (resolution is inversely proportional to bandwidth), the difficulty of processing the large bandwidths which would be required for a high percentage bandwidth radar, and the greater difficulty in manufacturing efficient wideband radar and sonar transmitters. (Efficiency is inversely proportional to bandwidth). High efficiency is important because signal-to-noise ratio is nearly always a limitation in pulse-echo systems.

These differences in percentage bandwidth result in several interesting similarities and differences between radar, sonar and ultrasonic systems. Although radar systems transmit at much higher center frequencies than sonar or ultrasound systems, because their percentage bandwidth is low in radar systems the received signal can be demodulated to produce an intermediate center frequency typically in the 1 to 20 MHz range, with a corresponding bandwidth of 1 to 20 MHz. This frequency range is essentially the same as in

Table 2–1 Important parameters of sonar, radar, and ultrasonic pulse-echo systems.

	Pulse-Echo Correlation Systems		
	Sonar	Radar	Ultrasound
Propagation Velocity (v_p)	1.5×10^3 meters/sec	3×10^8 m/sec	1.5×10^3 m/sec
Center Frequency (f_c)	100 Hz to 100 KHz	100 MHz to 100 GHz	.1 to 30 MHz
% 3 dB Bandwidth (BW)	1 to 40%	.01 to 1%	20 to 100%
Scan Range (R)	100 m to 10 Km	1 to 100 Km	1 to 100 cm
Max. Rep Rate $= v_p/(2R) = f_R$	.1 to 10 Hz	2 to 200 KHz	1 to 100 KHz
Max. Burst Length (MBL) $= \frac{1}{2}\frac{1}{f_R}$	50 msec to 5 sec	25 to 250 μsec	5 to 500 μsec
Code Clock Rate $\simeq 2 f_c = CK$	200 Hz to 200 KHz	1 to 20 MHz	.2 to 30 MHz
Code length per burst $= n$ $= (MBL)(CK)$	500 to 50,000 (at CK=10 KHz)	25 to 2500 (at CK=10 MHz)	50 to 3000 (at CK=10 MHz)

ultrasonic systems, and thus, after demodulation, radar and ultrasonic systems can utilize the same type of technology for amplifier design and high-speed A/D conversion. Sonar systems, however, have a much lower center frequency with a corresponding smaller bandwidth of approximately 100 Hz to 100 KHz. Thus, amplifier design, sampling, and signal processing are much less difficult for sonar system designers than either radar or ultrasound systems.

Ultrasound and radar also have very similar maximum repetition frequencies. As is well known, the maximum repetition frequency of a pulse-echo system is the reciprocal of the time-of-flight from the source to the furthest target of interest, and back again. This time-of-flight is related to both the propagation velocity and the target distance. Although the velocity of a radar signal in air is approximately $2x10^5$ times faster than ultrasound in water, the range of a radar is roughly 1 to 100 km, while the range of ultrasound is roughly 1 to 100 cm, which corresponds to a factor of 10^5, therefore implying similar repetition frequencies. This equivalence in maximum repetition frequency also results in nearly the same maximum transmit burst length for both radar and ultrasound. In addition since the bandwidths are also similar the pseudo-random code lengths which are chosen for transmission will also be nearly equivalent. (This correspondence between bandwidth and code length for a fixed transmit time will be shown in Chapter IV.)

Since the maximum range of a sonar system is much greater than the range of ultrasound systems and the propagation velocity of a sonar signal is the same as an ultrasonic signal, the repetition frequency is much lower for sonar, and the transmit burst can be much longer. The transmit frequency and bandwidth are also lower for sonar, resulting in much lower data rates and which allows more time for more sophisticated data processing. The transmit code length can also be much longer in a sonar system because of the low repetition period. This is in spite of lower clock rates which are required because of the lower transducer center frequencies of sonar systems.(This relationship between clock frequency and transducer frequency is shown in the subsection on optimal clock rate in Chapter IV.) This longer transmit code length is an important advantage of sonar correlation systems since the length of the code determines the signal-to-noise ratio and self-noise level which results from pulse-compression.

Multi-Mode Systems

Most ultrasonic imaging applications require that a scan be made of a two-dimensional area or a 3-dimensional volume. In imaging applications where targets of interest are fixed or slow-moving (slow relative to mechanical scanning speed limitations) this scanning can be done by mechanically repositioning a single transducer while using a single transmitter/receiver channel [36]. However, in many applications mechanical scanning is not fast enough to image moving targets, or a decrease in imaging time is desired. For these applications special multi-mode scanning systems have been developed which electronically scan the beam by electronically switching the transmit signal from element-to-element in a large array of small transducer elements.

Consider a conventional pulse-echo imaging system which sequentially performs a series of scanning operations. Such a system must sequentially change one or a combination of the following factors:

1) rotational position of the transmitter/receiver,
2) focal distance of a set of phased elements,
3) translational position of the transmitter/receiver,
4) or the scan direction of a set of phased elements.

For any of the above changes, the scan line position can either be varied by mechanically moving a single transducer element, or by switching from one element to another. This switching can, of course, be done either electronically or mechanically.

Several good examples of the rotational scanning system are the conventional rotating radar [37] and the inter-esophogeal ultrasonic imaging system described in reference [36]. In these scanning systems, the resulting images are best represented as scan lines in a polar coordinate system. The advantage to this kind of rotational scanning is that it can be done using a small number of independent transmitter elements which produce minimal interference since they can direct their beams in widely different directions. Unfortunately, they operate only in applications in which the transmitters can be centrally located.

An example of a system which sequentially changes its focal point has been developed by Burckhardt [38]. His system uses an ultrasonic transducer which is composed of concentric annular rings and is focussed electronically by varying a set of electronic delays, one for each annulus. It can only focus to

one depth on transmission, but can focus on reception at a number of depths. This system is dynamically focussed on reception over a long range to produce a narrow pencil beam. Unfortunately, this focussing system is limited to only focussing along a single given direction, and cannot, therefore, be used for more general imaging applications.

An example of a scanning system which sequentially changes the translational position of the transmitter/receiver is the scanned linear array [37]. This linear array is composed of a line of small transmitter/receiver elements and is used in medical imaging for providing a narrow 2-D scan along the array direction The result is a 2-D pulse-echo image corresponding to a beam-wide "slice" into the medium of interest. This linear scan is limited to applications in which a wide "viewing" area is available to place the transducer. Linear arrays are thus typically most useful in applications such as abdominal scans during pregnancy.

An example of a system which controls the scan direction by adjusting the delays to a set of transducer elements is the celebrated phased array. The phased array has been applied to radar, sonar, and ultrasound. A simple example of a phased array was shown in Figure 1-5. The phased array is the most flexible of the imaging systems since it can scan a relatively large imaging region from a small "window" into the medium. It is thus the most effective heart imaging system since it can peer between the ribs.

Because of their inherent flexibility the most widely used multi-mode systems are the linear and phased arrays. For this reason the multi-mode analysis will focus on these two systems. The analysis will be kept sufficiently general, however, so that it can easily be extended to other other types of multi-mode systems.

The operation of the linear and phased arrays are fundamentally different in a number of important ways which affect multi-mode operation. The phased array transmits from every element, simultaneously. It then sequentially scans the environment by sequentially changing the delays to the phased array elements between scans. However the linear array transmits sequentially from each element along the linear array. Each scan line in the resulting image then corresponds to the "view" from a different linear array element.

Two types of simultaneous transmission phased array systems have been proposed. The first, denoted here as "beam-coded" transmission, is the simultaneous transmission scheme depicted in Figure 1-5 and first described by Newhouse and Furgason [39,40]. In this approach a different signal source and receiver is associated with each chosen beam mode (e.g. beam direction). This

approach requires a set of phased arrays for each transmit beam mode to steer or focus on transmission and each receive beam mode to steer or focus on reception.

The second simultaneous transmission system denoted here as a "coloured" transmission system was proposed by Tournois [16], and is shown in Figure 2-3. This approach assigns a signal source to each element of the array. All beam steering or focusing is done only on reception. In this system the beam steering on transmission is realized after reception by utilizing a second set of delay lines. Each of these delay lines contains a correlation receiver which only correlates (matches) with a signal originating from one of the phased array elements. By summing a set of these matched and delayed signals, each signal originating from a different transmit element, the system effectively recreates what would have occurred with steering on transmission.

Several hardware differences between these two approaches are apparent. The coloured-transmission approach may require significantly more signal sources since there must be a different signal source for each element. The coloured transmission source may also require more correlators, since one correlator is needed for each element in the array. It thus appears that the coloured transmission system would be extremely costly in terms of hardware complexity, without necessarily gaining any advantage over the beam-coded transmission system.

Subsequent to the introduction of the beam-coded transmission system by Furgason, Newhouse and Lee [39,40], a full analysis of a beam-coded simultaneous transmission system which uses random transmit signals was carried out by Lee and Furgason [17]. This study showed the feasibility of simultaneous transmission through a successful experimental demonstration of a simultaneous multi-mode system operating with two modes, the two modes corresponding to two transmitters focussed on one receiver. These two-mode results were then extended in a complete study of an N-mode random signal simultaneous transmission system. A signal-to-noise ratio formula was derived which included the effects of clutter, cross-talk, self-noise, and background receiver noise. This formula was verified by making noise power measurements, in a sponge-clutter medium, with the random signal flaw detection system.

Using the verified signal-to-noise ratio formula, a comparison was made between an N-mode sequential transmission system and an N-mode simultaneous transmission system, each of which were assumed to employ

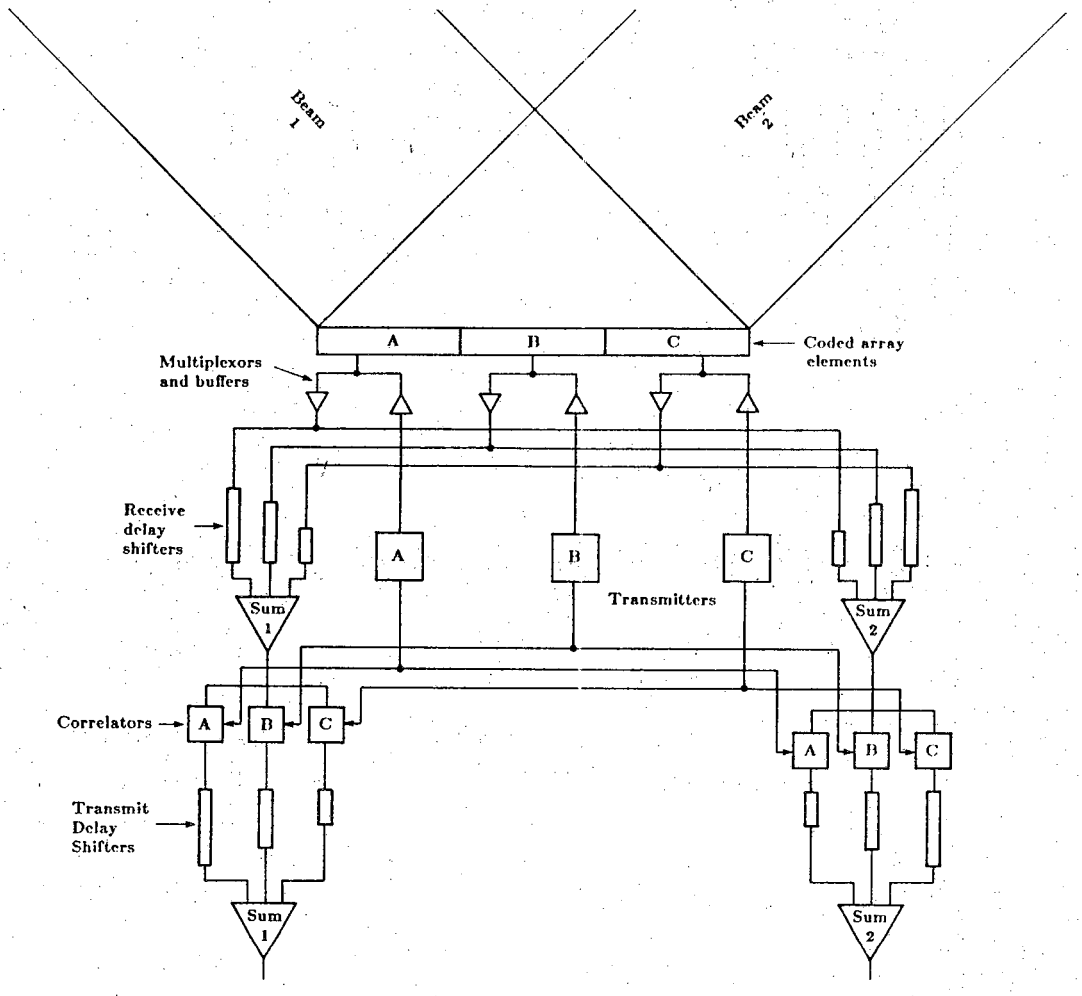

Figure 1–6 A two-mode "coloured" transmission system.

random signal correlation detection schemes. In order to simplify the equations, it was assumed that all N modes were identical, each having the same beam pattern, the same clutter level and the same cross-talk constant. The transmitted pulse-width was assumed to be large in order to make it possible to neglect some of the noise terms, including the background receiver noise and the noise from the interfering signals which are reflected by large desired targets.

Results indicated that even in clutter limited environments, systems which have a small cross-talk coefficient can benefit in speed and/or signal-to-noise ratio from a simultaneous transmission system using a correlation receiver. This is true in particular for phased arrays which would have central beams aimed in N different directions. Even though extra integration time might be required, the simultaneous system can still be faster, since it is possible to have μ quite small in a phased array. Note that a simultaneous system, such as the one depicted in Figure 1-5, would transmit as well as receive in more than one mode at a time. The beam pattern for the array is thus squared, which decreases the spatial sidelobe level and thus decreases the cross-talk coefficient.

In this thesis, the topic of simultaneous transmission systems is revisited in Chapter VII to include the effects of moving targets, and to study and compare the promising pseudo-random Golay codes to other transmit signals in a simultaneous transmission system.

CHAPTER III - PRINCIPLES OF SINGLE-MODE CORRELATION SYSTEMS

Fundamentals

To evaluate the performance of a correlation system it is first necessary to consider the basic operating principles of the correlation system. If $x(t)$ is the broadband noise signal or pseudo-random code applied to the transducer, the echo received from a point target is of the form

$$y(t) = x(t) * h(t) * h(t), \tag{3.1}$$

where $h(t)$ is the impulse response of the transducer and $*$ is the convolution operator. For simplicity, the medium is assumed to be lossless and the time delay due to propagation is also neglected.

Since correlation detectors are equivalent to matched filters, they obtain their enhancement by minimizing, through correlation with a reference signal, the mean-squared error of an estimate of the desired signal.

If $x(t)$ is wide-sense stationary, an ideal correlation receiver produces the output

$$R_{yx}(\tau) = \lim_{T \to \infty} \frac{1}{\alpha T} \int_{t-\alpha T}^{t} y(u)x(u-\tau)\, du, \tag{3.2}$$

where $x(t-\tau)$ is the reference signal and T is the time difference between the received and reference signal. This output can then be represented as

$$R_{yx}(\tau) = y(\tau) * x(-\tau) = h(\tau) * h(\tau) * R_{xx}(\tau). \tag{3.3}$$

If $x(t)$ is assumed to be very broadband so that the autocorrelation function $R_{xx}(\tau) \simeq \delta(t)$, the Dirac delta function, so that the frequency content of $y(t)$ is

determined primarily by $h(t)$ and the output can be rewritten as

$$R_{yx}(\tau) = h(\tau) * h(\tau), \tag{3.4}$$

the same output that would be produced by a pulse-echo system in which the excitation is an ideal impulse. For finite integration times, equation (3.2) becomes

$$\bar{R}_{yx}(t,\tau,\alpha T) = \frac{1}{\alpha T}\int_{t-\alpha T}^{t} y(u)x(u-\tau)\,du, \tag{3.5}$$

where $R_{yx}(t,\tau)$ is now a time-varying random variable with a mean given by equation (3.2) and a variance given by [41]

$$\sigma^2_{yx}(t,\tau,\alpha T) = \frac{1}{\alpha T}\int_{o}^{2\alpha T}(1-\xi/2\alpha T)\left[R_{\phi\phi}(\xi) - R^2_{yx}(\tau)\right]d\xi, \tag{3.6}$$

where $R_{\phi\phi}(\psi)$ is the fourth product moment and has the following form

$$R_{\phi\phi}(\xi) = E\{x(t+\tau+\xi)\,y(t-\xi)\,x(t+\tau)\,y(t)\}, \tag{3.7}$$

where E denotes the expectation operator.

The signal-to-noise ratio enhancement ($SNRE$) of a correlation receiver, is given by the band compression of the receiver so that [2]

$$SNRE = \frac{SNR_{out}}{SNR_{in}} = \frac{\alpha B_{in}}{B_{out}} \simeq \alpha BT, \tag{3.8}$$

where α is the duty cycle of the transmitted signal, T is the system integration time, and $B_{in} = Bout$ and B_{out} are respectively the half-power bandwidths of the received signal and the output low-pass filter. Another way to represent equation (3.8) which is more convenient for digital signals is

$$SNRE = nNB\delta, \tag{3.9}$$

where n is the number of bits in the transmit burst, N is the number of transmit bursts correlated, and δ is the width of one bit. For a given repetition rate, R, and a given number of transmit bursts, the optimum integration time is

$$T = N/R. \tag{3.10}$$

Note that the *SNRE* can theoretically be increased, without limit, merely by increasing the integration time. Therefore, in practice the available *SNRE* is limited only by the stability of the integrator and the rigidity of the measurement system.

Self-Noise

Equation (3.6) describes the power variation of an error term in the finite integration time approximation to the ideal correlator output. This error term has been called self-noise for both random and pseudo-random signals.

The self noise of pseudo-random m-sequences is also referred to as range sidelobes in the literature because of their non-random nature. In the rest of the paper we will use the term "self-noise" as the general term referring to the self-interference noise process for both random and pseudo-random signals and the term "range sidelobes" will be restricted to the measured samples of self-interference noise of a specific pseudo-random code, or sample of random signal.

This self-noise problem can be seen in Figure 3-1, which shows a computer simulation of the autocorrelation function for a short 63 bit, m-sequence. Interfering self-noise can be easily seen in the area around the large desired echo. It can be seen that the self-noise reduces in amplitude as the code strength is increased but the extent of the noise increases.

If an entire m-sequence of length m is continuously repeated or circularly correlated, its autocorrelation has constant range sidelobe levels of height $1/m$ relative to the peak. But if the m-sequence is transmitted in a discontinuous pulsed mode, its autocorrelation function has non-constant range sibelobe levels. Cooper [42] has found that the variance of the self noise of random or

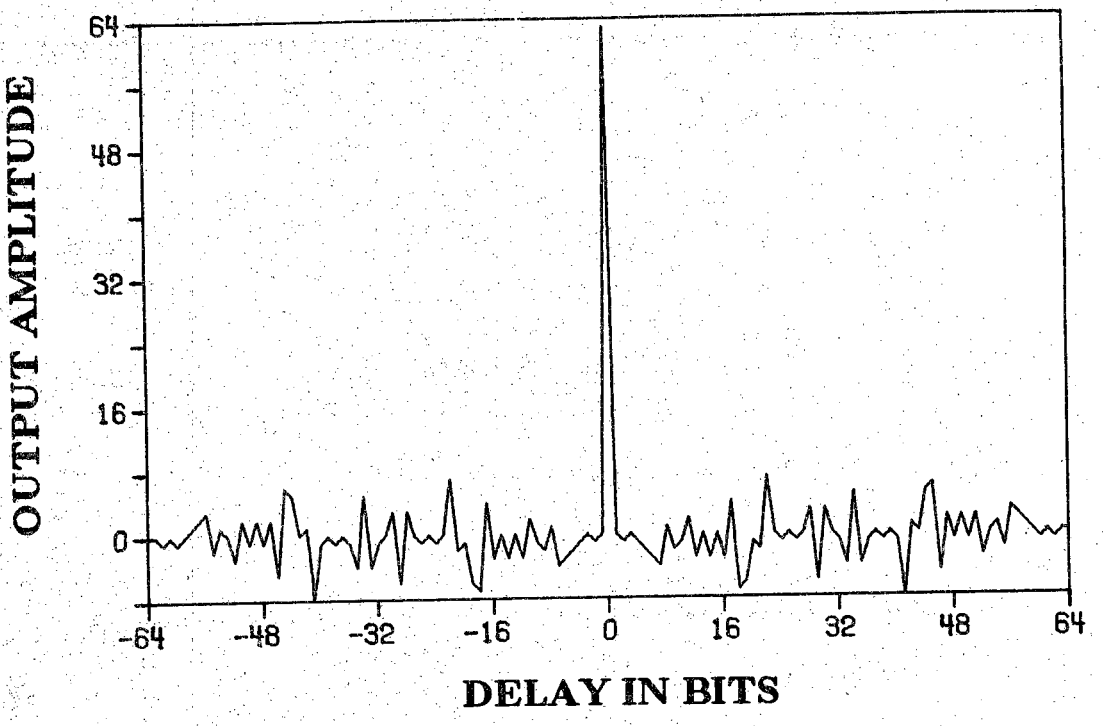

a. Simulated autocorrelation function of a 63 bit m-sequence.

Figure 3–1 Self-noise of an m-sequence.

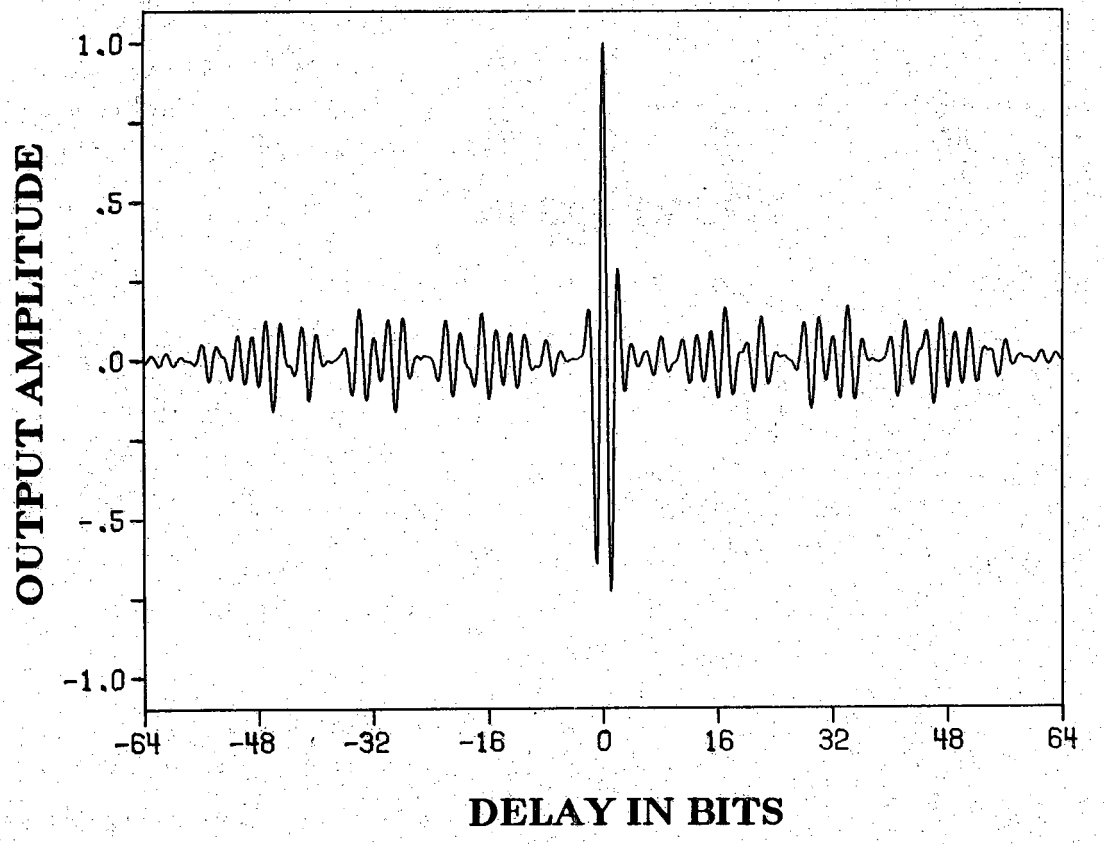

b. Function of a. convolved with typical transducer impulse response.

Figure 3–1 (continued).

pseudo-random codes is bounded such that

$$\sigma_{zz}^2 \leq \frac{\delta}{\alpha T}, \qquad \textit{for all } \tau, \tag{3.11}$$

where δ is again the pulse-width of a single binary bit of code.

Under band limited conditions (e.g., Figure 3-1b), Siebert [43] calculates that the autocorrelation function of any maximal-length sequence which is not continuously repeated will have range sidelobes of maximum height relative to the peak, H_m bounded by

$$H_m \leq \frac{1}{\sqrt{\alpha BT}} = \frac{1}{\sqrt{nLB\delta}}, \tag{3.12}$$

where n must be less than or equal to m.

For the case where the m-sequence is band-limited to approximately its half-power point, $B = 1/(2\delta)$, the bound of the peak sidelobe power computer using equation (3.12) is consistent with the bound for the average sidelobe power presented in equation (3.11).

Equation (3.11) has considerable intuitive appeal and would seem to apply to both m-sequences and random codes. If one considers the correlation of a band-limited random code or m-sequence, for values of τ such that $n\delta/2 >> \tau >> 0$, the correlated signals appear similar to background receiver noise. Equation (3.8) would then predict peak self-noise power levels, relative to the peak power, of $1/\alpha BT$. This indicates that the amplitude levels of the self-noise would be on the order of $1/\sqrt{\alpha BT}$, in agreement with equation (3.12). This result is verified in a later study presented in this thesis which compares range sidelobe levels of typical samples of random signal to the range sidelobe levels of typical m-sequences.

Large Target Effects

The level and range extent of self-noise are particularly important in two frequently encountered situations. One is when a small target of interest is located next to a much larger target, and the other is when a desired target is surrounded by many smaller targets called clutter. The presence of self-noise

causes spatial interference in both cases and thus degrades system performance.

The interference effects of a larger close target are fairly obvious and limit the dynamic range of target sizes which can be discriminated. In a pulse-echo system, the dynamic range is limited by the height of the edges of the system impulse response for the case where a small target is located next to a large target. A correlation system will suffer from this same fundamental dynamic range limitation since it is imposed by the transducer response. A method for overcoming this limitation in either system involves the use of inverse filtering operations like the constrained deconvolution operation described in reference [44]. In addition, for short correlation times the correlation system may be further limited in dynamic range by the presence of the self-noise. This can easily be seen in the computer simulations of Figure 3-2. As can be seen, the dynamic range will then be given by the ratio of the peak signal level to the self-noise level given in equation (3.12). If only a single transmit signal is integrated (to allow high speed operation) a dynamic range of 30 dB, for example, can only be reached for extremely long codes on the order of 500 μsec assuming a bandwidth B of 2 MHz. At the speed of sound in water this requires that the target be located at a distance of 3/8 meters, for use in a pulse-echo mode. This distance is prohibitively long for most practical ultrasonic situations.

Clutter Effects

The interference effects produced by clutter are not so obvious. The size and distribution of clutter targets, as well as the length of the transmit burst, will influence the amount of interference present. The size and distribution of clutter targets are fixed characteristics of the medium and only special non-linear processing such as the split-spectrum processing described in reference [45] has been found to provide an improvement. Although, using a longer transmit burst will reduce the self-noise levels relative to the autocorrelation peak; the time extent of the self-noise is twice the length of a transmit burst (see Figure 3-1) so that the self-noise from adjacent targets will increase their amount of overlap with increasing transmit burst length.

To evaluate the effects of parameter changes, such as pulse-width, we assume a very simple clutter situation. Consider a uniform distribution of randomly distributed clutter targets, each with the same relative orientation and back-scattering cross-section. If ρ is the average spatial density of the

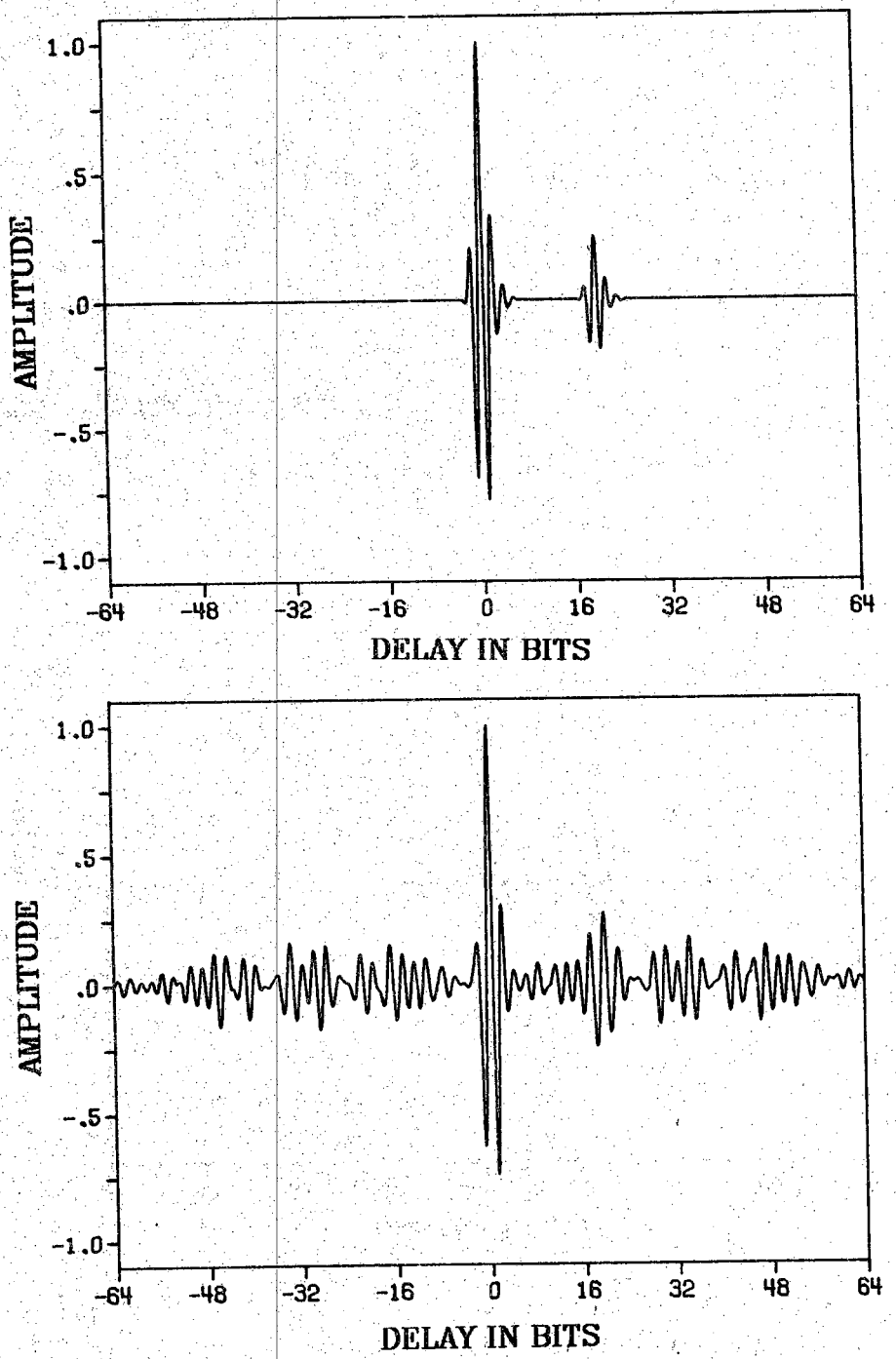

Figure 3–2 Large target effects of self-noise

clutter and the beam of the transducer is assumed to have a nearly constant cross-sectional area, A, then

$$\rho_l = \rho A. \tag{3.13}$$

The average number of clutter targets or grains, γ, contributing interference at any particular delay can be computed by convolving the ultrasonic signal with the clutter target distribution. Since the target distribution was assumed to be uniform, the number of grains contributing to the interference is simply

$$\gamma = \rho_l w. \tag{3.14}$$

where w is the width or effective spatial extent of the ultrasound signal. The actual spatial extent of the ultrasonic signal is determined solely by the transmitting transducer, its excitation, and the sound velocity of the medium. However, in terms of the overall system performance, the effective width of the pulse is also influenced by the bandwidth of the receiving transducer and receiver. In a correlation system, the effective width of the ultrasonic signal is also influenced by the autocorrelation function of the transmit signal (see equation (3-3).

For a given transducer and medium of characteristic velocity, v, the minimum ultrasonic pulse-width is approximately $w=v/B$, the output pulse-width of an ideal pulse-echo system. This return echo pulse is produced by applying a rectangular pulse to the transducer which has a duration less than or equal to one-half of a cycle of the fundamental frequency component (the center frequency, f_c) of the ultrasonic transducer, $1/(2f_c)$. The minimum number of interfering targets contributing interference to the pulse-echo output at any range is then

$$\gamma_o = \rho_l v/B. \tag{3.15}$$

Since in the correlation system output the autocorrelation function of the transmit signal is convolved with the clutter, the autocorrelation function for pseudo-random and random signals can be considered to be composed of two parts; the desired large central triangular pulse of width 2δ, shown in Figure 3-

1 and interfering range sidelobes of extend $2n\delta$ and relative height bounded by H_m of equation (3-12). From equation (3.4) the desired central triangular pulse produces an output signal nearly identical to a pulse-echo system output which is of length $1/B$. Thus, in the ideal case, the correlation system would produce the same minimum number of interfering targets as given by equation (3-15). However the self-noise will add additional interfering targets and the number of additional interfering targets will be approximately

$$\gamma_a = \rho_l v[2n\delta] , \qquad n\delta > 1/(2f_c) . \tag{3.16}$$

Assuming the scattering cross-section of the average clutter target is so small that multiple scattering can be ignored, we can then add the powers of the interference signal from each particle [46]. If we further assume that the peak power returned from an isolated clutter target is C_i, then the minimum clutter interference power, C_o, that would be seen by an ideal pulse-echo system is then given as

$$C_o = \gamma_o C_i . \tag{3.17}$$

In a correlation system the bound on the amplitude of the self-noise given by equation (3.12) indicates that the average power in the self-noise due to a clutter target will be given by

$$C_r = rH_m^2 C_i = rC_i/(nNB\delta) \leq C_i/(nNB\delta), \tag{3.18}$$

where r is some constant and $0 < r \leq 1$. Consequently, when N unique transmit bursts of length $n\delta$ are correlated, the additional clutter power in the correlator output signal due to self-noise is

$$C_a = \gamma_a C_r = [\rho_l v 2r/NB] C_i . \tag{3.19}$$

Special care must be exercised in extending and interpreting the above equations for the case where $n\delta \leq 1/(2f_c)$. Under these circumstances the output bandwidth of the correlator is greater than the input bandwidth and such a system actually degrades the output signal-to-noise ratio compared to

pulse-echo systems. However, in practical correlation systems $n\delta \gg 1/(2f_c)$, thus, this limiting case is of no practical importance.

To complete the discussion of clutter effects, we cast the final equations in terms of a dimensionless parameter. Let the ratio of shift register clock frequency to the bandwidth of the transducer be defined as

$$b = \frac{1}{\delta B}. \tag{3.20}$$

The total signal-to-clutter ratio, SCR, for the correlation system is then just the ratio of the power of the desired signal P to the total output clutter power

$$\begin{aligned} SCR &= P/[C_o + C_a] = P/[C_o(1 + \frac{2r}{N})], \qquad n\delta > \frac{1}{2f_c}, \\ &= P/C_o, \qquad n\delta \leq \frac{1}{2f_c}, \end{aligned} \tag{3.21}$$

where the case $n\delta \leq 1/(2f_c)$ also describes the signal-to-clutter ratio for a conventional pulse-echo system. Including the background receiver noise η, and assuming that the noise sources are all uncorrelated so that their powers add a total signal-to-noise ratio for the correlation system is given by

$$SNR = \frac{P}{C_o(1 + \frac{2r}{N}) + \eta(\frac{b}{nN})}. \tag{3.22}$$

The total signal-to-noise ratio for the conventional pulse-echo system is described by equation (3-23) with $r = 0$ and $b/(nN) = 1$. An alternative definition for the SNR of a correlation system, which is particularly useful in nondestructive evaluation, measures the ability to identify the location of a particular signal in the presence of background noise which surrounds the desired target. In this case, the range-sidelobes of the target must also be taken into account since they contribute to the noise level in the vicinity of the target. Thus comparing the peak signal power to the total power level of all the noise surrounding the target yields

$$SNR = \frac{P}{C_o(1 + \frac{2r}{N}) + \eta(\frac{b}{nN}) + P(\frac{b}{nN})} . \tag{3.23}$$

Moving Target Effects

Since the self-noise cancellation requires the summation of two autocorrelation functions, which correspond to transmit bursts separated by the transmit repetition period, movement of the target between transmit bursts will produce correlation functions which will not align as required for peak superposition and self-noise cancellation. Takeuchi studied a phase-modulated system using Golay codes and estimated that Doppler shifts would cause self-noise which follows a curve similar to $\cos 1/\theta$), where θ is the phase difference between received complementary codes due to Doppler shift.

It is well known that moving targets add a Doppler shift onto a single frequency transmit signal in direct proportion to the velocity of the target and the frequency of transmission [48]. In the case of a broad-band, (multi-frequency waveform) the effect of the moving target can best be described as a compression or stretching of the time-domain waveform in proportion to the target velocity [49]. In a conventional pulse-echo system the result is a longer or shorter burst. In a correlation system the returning waveform from a moving target no longer matches the reference signal. In order to determine the effects of this mismatch on wideband signals, Kelly and Wishner [49] have developed a generalized form of the original well-known narrow-band ambiguity function developed by Woodward [48].

Kelly and Wishner's generalized ambiguity function can be represented in a number of equivalent integral forms. Assuming, for simplicity, that the source/receiver is stationary and that the target has zero acceleration, one convenient form of the generalized ambiguity function is

$$G(\tau,\nu) = \int_{-\infty}^{\infty} A(\omega)\, A^*(\omega\nu)\, e^{-j2\pi\omega\nu\tau} d\omega, \tag{3.24}$$

where τ is the time delay difference between the received signal and the reference signal, $A(\omega)$ is the complex frequency spectrum of the transmit signal, and $\nu \simeq (1-2v/c)$; where v is the target velocity, and c is the velocity of sound. Note that for a given ν, $G(\tau,\nu)$ represents the output of a correlation system

for a moving target. A simple substitution of τ/ν for τ shows that for a fixed ν, the integral can be viewed as the inverse Fourier transform of $A(\omega)A^*(\omega\nu)$, which maps into the τ domain scaled by the factor ν. The variable ν is normally very close to unity since c is very large compared to v for practical imaging situations. Thus $G(\tau/\nu,\nu)\simeq G(\tau,\nu)$ and the scale factor on τ can be ignored in the inverse Fourier Transform calculation for simulations.

Using this formula it is possible to simulate the generalized function for a given transmit signal, merely by performing an inverse Fourier transform on the multiplied spectra $A(\omega)$ and $A^*(\omega\nu)$. This simulation is carried out later in Chapter VI using FFT processing.

CHAPTER IV- IMPLEMENTATION OF SINGLE-MODE CORRELATION SYSTEMS

Correlation Architectures

The correlation process described by equation (3.5) can be implemented in hardware or software via a number of different architectures. The three basic correlation system structures are, the transversal filter which produces a high speed serial output [50], the time-integrating correlator which produces a parallel set of outputs one for each delay [51], and the FFT convolution processor [52] which can be implemented in array processors or software. In these systems the delay between the received signal $y(t)$, and the reference signal $x(t)$, can be synthesized by adding delays to one or both signals. This delay has been implemented in hardware by a number of different analog and digital methods, including digital shift registers, charge coupled delay lines (CCD)[50], surface acoustic wave (SAW) delay lines [53], liquid delay lines [2], and digital delay lines. The multiplication and integration processes of equation (3.5) can also be implemented in hardware by a number of different analog and digital methods. As should be obvious, the best type of delay line, multiplier, and integrator will partly depend upon the form of signal to be correlated. Accordingly, an appropriate delay line for a binary signal, for example, is obviously a set of digital shift registers. In the following section a discussion and comparison is made between the basic types of correlation architectures and between the system components which are presently available.

The transversal implementation of a correlator is shown in Figure 4-1. The received echo signals are sent through a multi-tap delay line in which the taps are separated by a delay increment equal to the clock period of the pseudo-random transmit signal. If the transmit signal is random, the delay increment is chosen to fulfill the Nyquist sampling rate for the signal bandwidth. The correlation reference signal is stored in digital memory or hardware and is used to weight the outputs of the tapped delay line. These weighted signals are then summed to produce the correlation output in serial form.

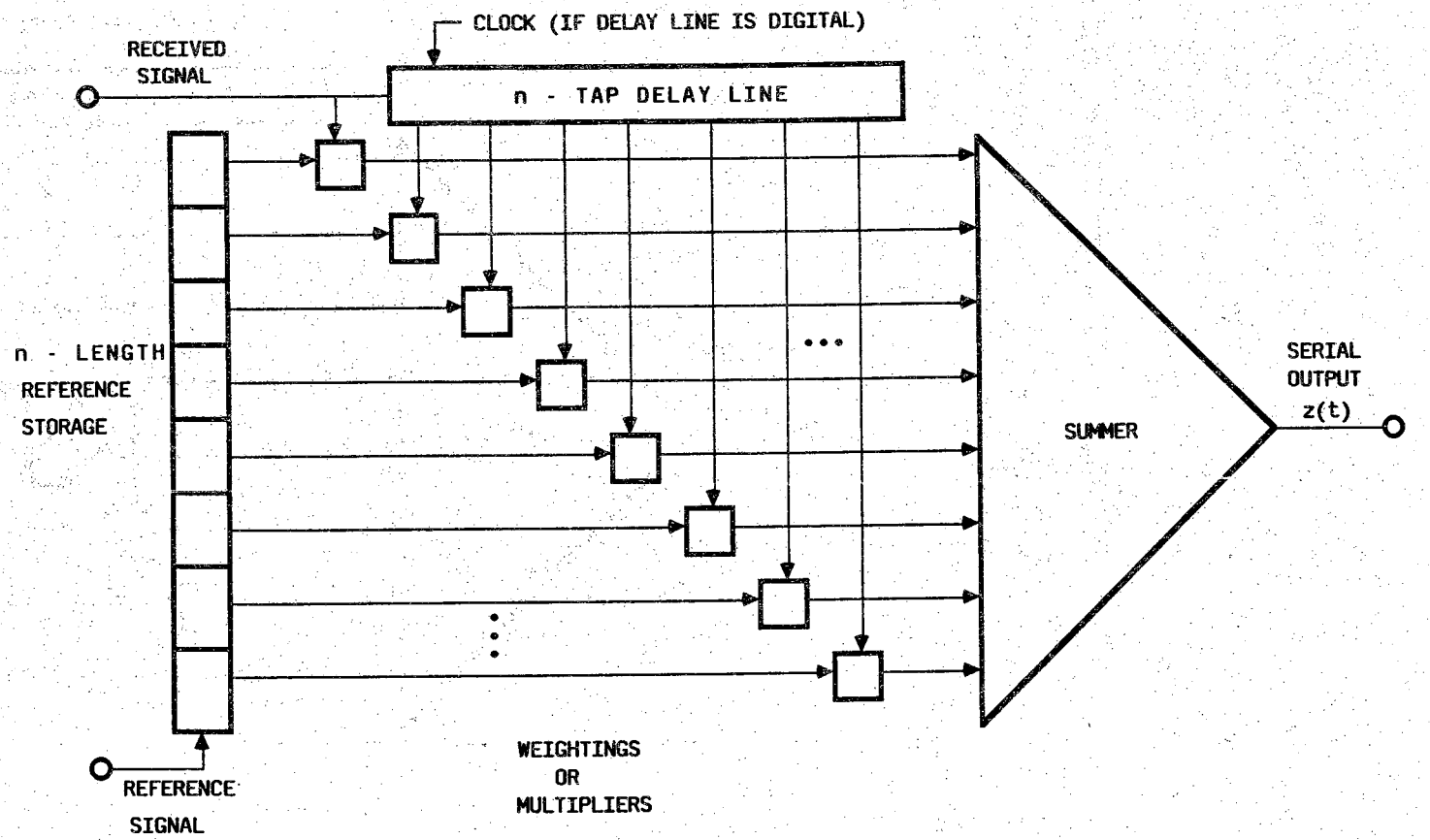

Figure 4–1 Transversal filter correlator.

The transversal filter of Figure 4-1 can be easily shown to produce the desired correlation process. If $y(t-\tau_o)$ is the received echo signal from a single point reflector at distance $v\tau_o/2$ and $x(t)$ is the reference signal, the output of the summer of Figure 4-1 is

$$z(t) = \sum_{j=1}^{n} x(j)\, y(t + j\Delta\tau - n\Delta\tau - \tau_0) \tag{4.1}$$

where j is an integer representing the jth tap from the right, $\Delta\tau$ is the time delay between taps of the delay line, and n is the code length.

This equation represents a sampled version of the autocorrelation function. It can be transformed into the familiar correlation integral formula by using the sifting property of the Dirac delta function [54]. The integral form of equation 4-1 is then

$$z(t) = \int_0^{n\Delta\tau} x(\frac{u}{\Delta\tau}) \left[\sum_{j=1}^{n} \delta(u - j\Delta\tau)\, y(t + u - T - \tau_0) \right] du, \tag{4.2}$$

where $T = n\Delta\tau$ and $\delta(t)$ is the Dirac delta function. Let $\tau = t-T-\tau_o$, so that τ is a function of time, and $s(u) = \sum_{j=0}^{n} \delta(u-j\Delta\tau)x(\frac{u}{\Delta\tau})$, then

$$R(\tau\,;\, t) = z(\tau+T+\tau_0) = \int_0^{n\Delta\tau} s(u)\, y(u+\tau)du, \tag{4.3}$$

which is the familiar integral form of the correlation function, where $s(u)$ is a sampled version of the reference signal, $x(u)$.

A time-integrating version of the correlator is shown in Figure 4-2. Instead of delaying the received signal, the reference signal is delayed with a multi-tap delay line. The received signal is then correlated separately with each delayed version of the reference signal using m multipliers and integrators, where m is the number of ranges of interest. As in the transversal filter, the delay increment between range samples is chosen to satisfy the Nyquist sampling rate for the pulse-echo waveform. The m correlation ranges are thus produced in parallel, and the output for each range can be described by a slightly modified version of equation (3.5). A practical integrator does not

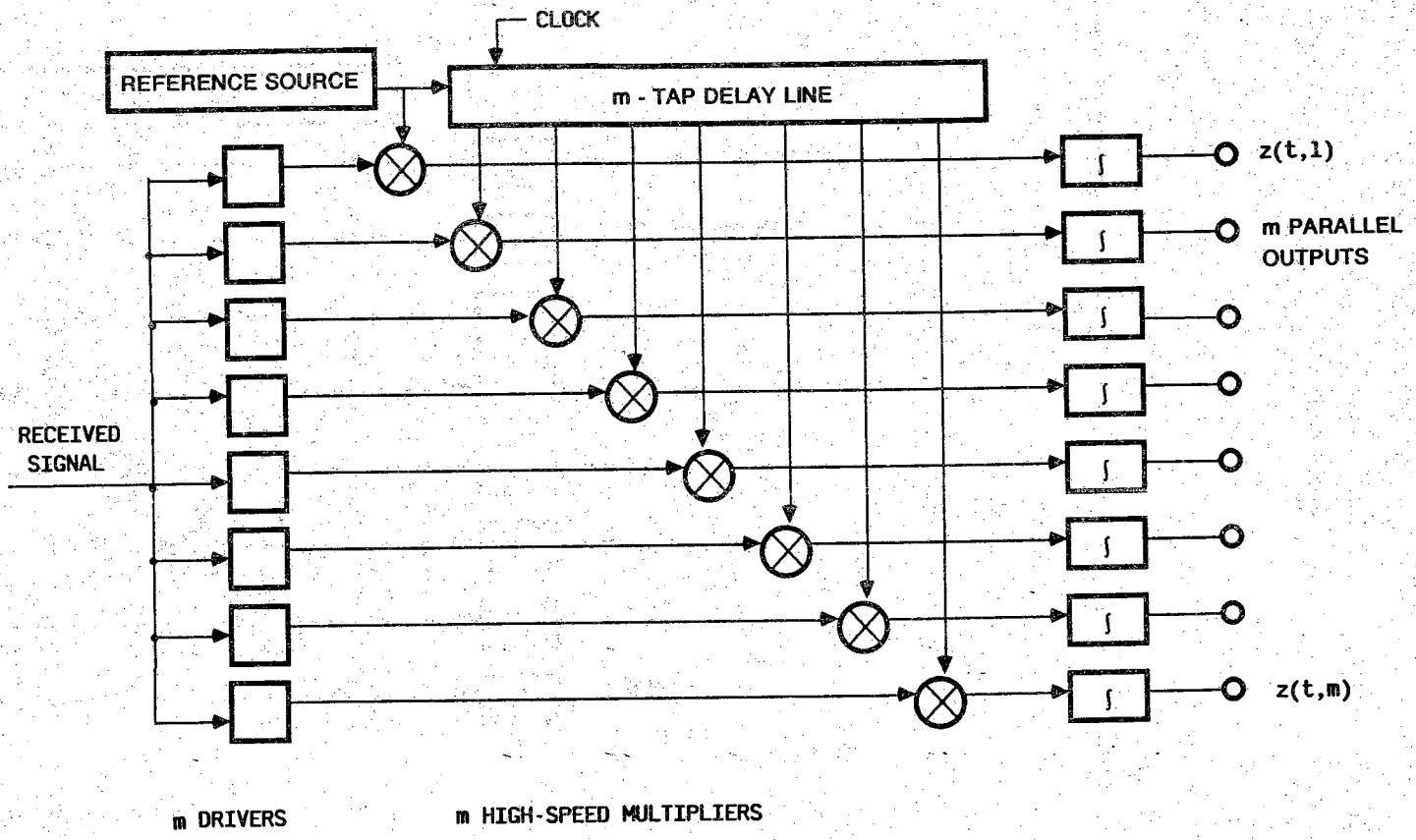

Figure 4–2 Time-integrating correlator.

normalize by the factor αT , and the delay τ will be an initial delay, τ_o, plus $m\delta$, where δ is the delay increment, so that

$$z(t,m) = \int_{t-nN\Delta\tau}^{t} y(u)x[u-(\tau_0+m\delta)]\,du. \tag{4.4}$$

Note that the lower integral limit includes a factor N which allows for an integration of more than one transmit burst. Integrating more then one transmit burst is equivalent to time averaging, a process which produces additional signal-to-noise ratio improvement, as described by equation 4-9. This inherent time averaging ability is the prime advantage of the time integrating correlator over the transversal filter correlator.

After some thought, one may realize that since the basic requirement of the correlation hardware is to produce a delay difference between the received signal and the reference signal, it should be possible to exchange the input signals, $y(t-\tau)$ and $x(t)$, to both the transversal filter and the time integrating correlator. However, some slight modifications are required in the hardware for the interchanged version of the transversal filter, Figure 4-3, due to the inherent range uncertainty in the time of reception of the received pulse-echo signal.

If $y(t)$ is the transmit signal, the received pulse-echo signal is $y(t-\tau_o)$ where $\tau_o = 2x/v$; where x is the distance to the reflector and v is the average propagation velocity along the flight path. Since τ_o is the variable to be estimated, the best that can usually be known apriori is that τ_o is within some range $\tau_i =< \tau_o =< \tau_i + m\Delta t$. (Ordinarily, in practice, the only targets one is really interested in are located in this chosen range of delays.)

In this transversal filter implementation, the received signal $y(t-\tau_o)$ is sampled at a rate greater than the Nyquist rate such that

$$s(i) = \sum_{i=1}^{m+n\frac{\Delta\tau}{\Delta t}} y(t-\tau_0)\delta(t-\tau_i+i\Delta t-(m+n\frac{\Delta\tau}{\Delta t})\Delta t \tag{4.5}$$

$$= \sum_{i=1}^{m+n\frac{\Delta\tau}{\Delta t}} y(t-\tau_0+\tau_i)\delta(t-i\Delta t+m\Delta t+n\Delta\tau),$$

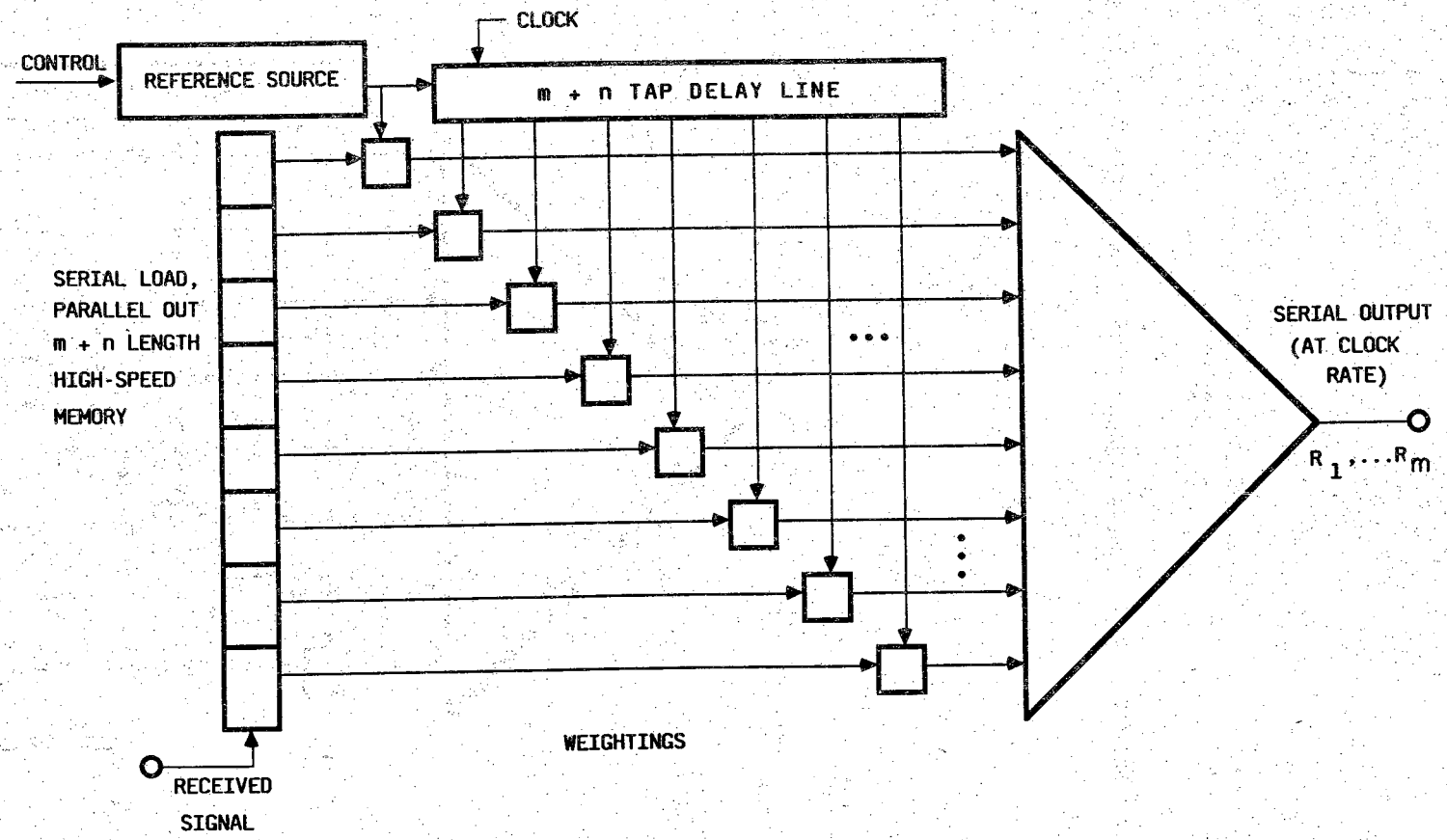

Figure 4–3 Input-exchanged transversal filter correlator.

where: $s(i)$ is the sampled, stored sequence,

i is an integer such that $1 \leq i \leq (m + n\frac{\Delta\tau}{\Delta t})$

n is the burst length,

m is the number of ranges being correlated,

$\Delta\tau$ is the code bit width, and

Δt is the sampling period.

The sampled version of $y(t-\tau_o)$ thus begins in the memory location at the nearest i greater than $[m\Delta t + n\Delta\tau + \tau_i + \tau_o]\frac{1}{\Delta t}$.

Once the echo signal has been stored in the parallel-out memory, the reference signal can be generated at any delay, τ_r, and clock rate, CK, such that $\tau_r > \tau_i$. This can be a major benefit of this approach, if there are hardware speed constraints in the transversal filter implementation.

The output of the input-exchanged transversal filter is then

$$z(t) = \sum_{j=1}^{[m+n\frac{\Delta\tau}{\Delta t}]} s(j)x(t-j\Delta t+m\Delta t-n\Delta\tau-\tau_r), \tag{4.6}$$

In integral form this becomes

$$z(t) = \int_0^{\substack{m\Delta t \\ +n\Delta\tau}} \sum_{j=1}^{m+n\frac{\Delta\tau}{\Delta t}} \delta(u-j\delta)y(-u+\tau_o-\tau_i+m\Delta t+n\Delta t) \times x(t-u+m\Delta t-n\Delta t-\tau_r)du \tag{4.7}$$

substituting $v = -u+m\Delta t+n\Delta\tau-\tau_o+\tau_i$, and letting $t=m\Delta t+n\Delta t$ and $tau=t-\tau_o-\tau$, then:

$$R(\tau) = \int_{t_o}^{t_o+T} q(v)x(v+\tau)dv, \tag{4.8}$$

where $q(v) = \sum_{j=1}^{m+\frac{N\Delta\tau}{\Delta t}} \delta(u-j\delta)y(v)$.

Although the system design of the input-exchanged version of the time-integrating correlator shown in Figure 4-4 is identical to the time-integrating correlator design, the actual hardware of the input-exchanged version is always limited to using a delay line which can store a dynamic range of signals as required in the final output. However, when the reference signal is delayed, Figure 4-4, if the reference signal is binary the delay line can also be in binary form. This can be a considerable advantage in hardware requirements.

Another type of correlation architecture, the FFT convolution correlator, takes advantage of the fact that convolution in the time domain can be represented as a multiplication in the frequency domain. Since correlation and convolution are very similar, it is possible to transform to the frequency domain and perform a correlation by multiplication.

The convolution operation $*$ is described by

$$y(t) * x^*(t) = \int_{-\infty}^{\infty} y(u)x^*(t-u)du, \tag{4.9}$$

where $x^*(t)$ is the complex conjugate of $x(t)$. This can easily be seen to be a correlation operation on $y(t)$ and $x(t)$, if $x^*(t)$ is replaced by $x^*(-t)$, so that

$$R_{yx}(t) = y(t) * x^*(-t) = \int_{-\infty}^{\infty} y(u)x(u-\tau)du, \tag{4.10}$$

which is identical to equation (3.5), except for the finite limits of integration required in equation (3.5) for a practical implementation.

Now, as is well known, convolution in the time domain is equivalent to multiplication in the frequency domain. Therefore,

$$R_{yx}(t) = F^{-1}\Big\{F[y(t)]\ F[x^*(-t)]\Big\}, \tag{4.11}$$

where $F[\,]$ and $F^{-1}[\,]$ are the Fourier and inverse Fourier transforms respectively.

This convolution correlator can readily be implemented through pipeline FFT processors [55] in schemes similar to that shown in Figure 4-5. The advantage to this type of processor is that the correlation values for all delays

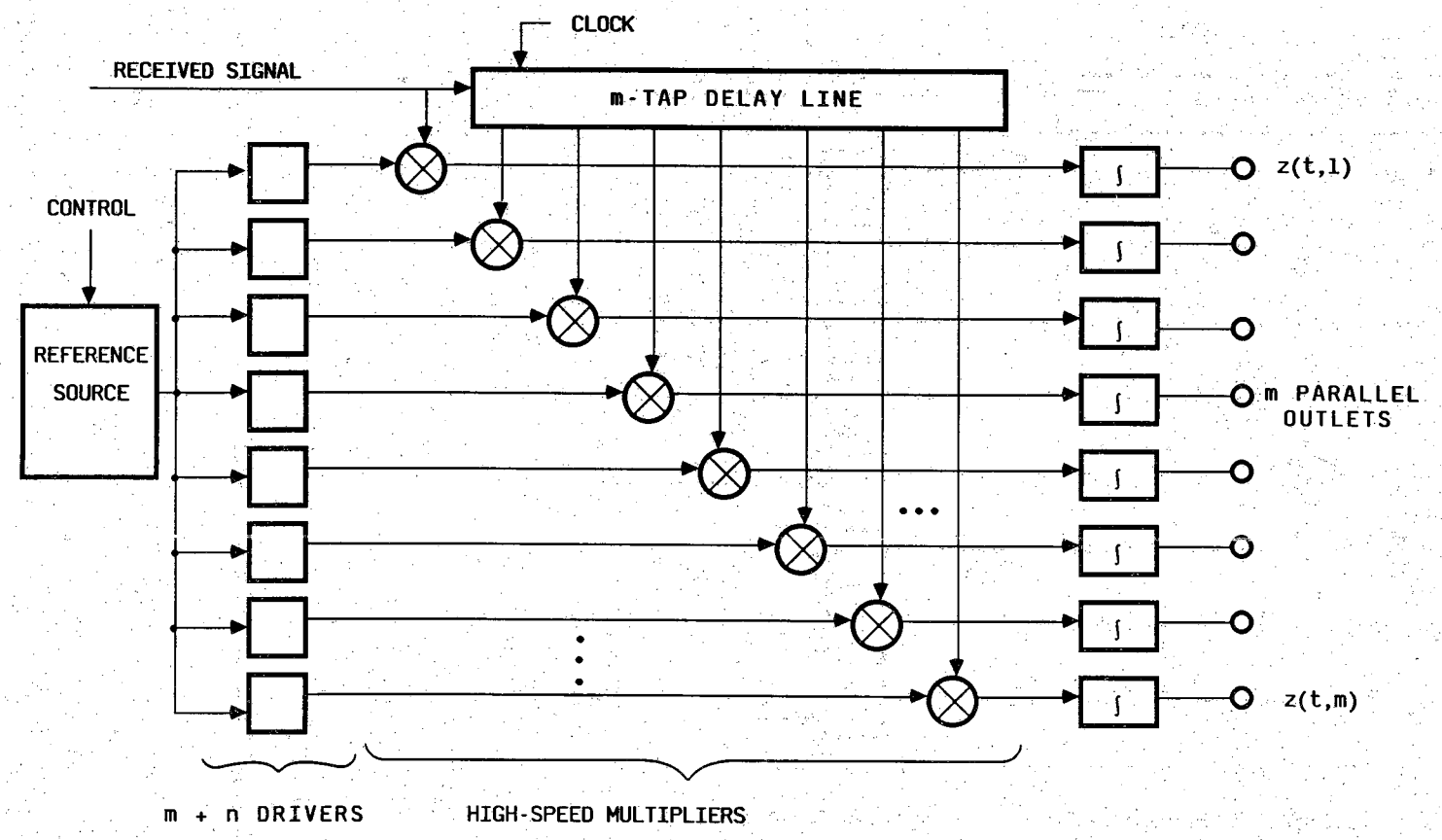

Figure 4–4 Input-exchanged time-integrating correlator.

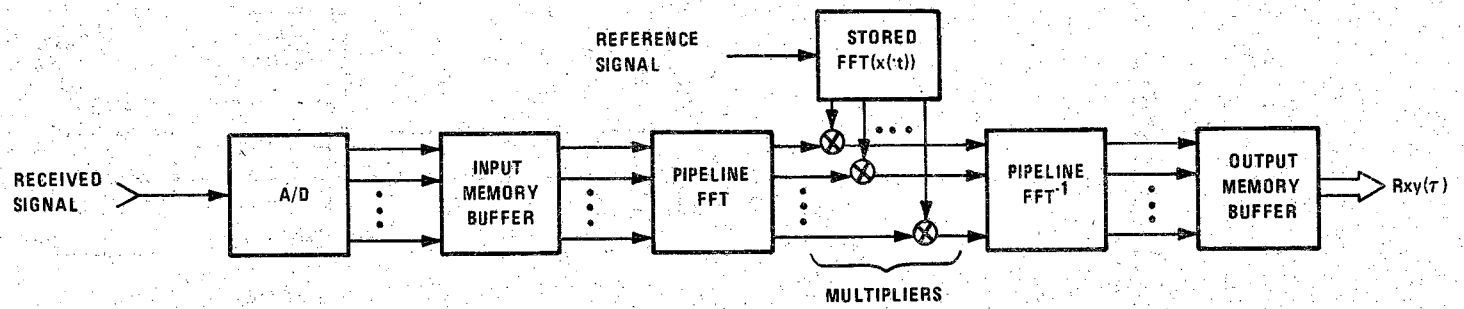

Figure 4–5 Pipeline FFT convolution correlator.

are calculated simultaneously during the frequency domain multiplication. In addition, efficient high-speed FFT processors are becoming a standard function within LSI technology, especially in radar [55]. These pipeline FFT processors are modular in form and increased data lengths from increased scan range can be handled merely by augmenting the processor with additional modules.

All of the preceding architectures have their own merits and disadvantages. The hardware components required are different for each, as will be discussed next. The transversal filter lends itself well to high-speed one-burst correlation because hardware requirements are minimal. The delay line must only be long enough to store the burst length; whereas the other processing methods must incorporate enough delays to handle the scan length, which may be much longer than the burst length. However, as mentioned before, the time-integrating correlator has the advantage of providing improved signal-to-noise ratio which is obtained merely by increasing the integration time.

The correlation architecture, used for demonstrations in the following study, is a simplified version of the time-integrating correlator. This system is called a box-car correlator because of the serial box-car way in which the ranges are processed, Figure 4-6. It trades processing speed for simplicity by utilizing only one of the parallel output range channels of Figure 4-2. The entire range is scanned serially by incrementally changing the initial delay time of the reference signal, after N transmit bursts have been integrated. If the scan covers r range bins and the time between transmit bursts is P then it takes rPN amount of time to finish a range scan. This method is not effective for tracking fast moving targets, but it has the advantages of reduced hardware and a reduced sampling rate for data storage, which allows for a more accurate, and cheaper A/D converters. Conventional inexpensive low-speed microprocessors can then be used to control the data acquisition, even though the processed bandwidths are very high.

Hardware Components

There are three or four components required for the correlation architectures discussed in the previous sections: delay lines, multipliers and integrators; and digital memory for some implementations. Each of these components can be implemented by a number of different methods.

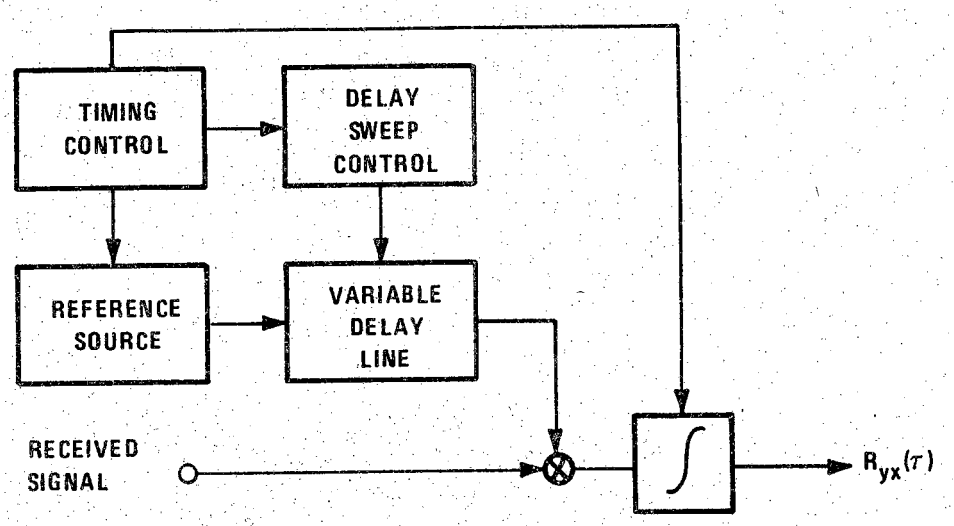

Figure 4–6 Box-car correlator.

Delay Lines

Delay lines fall into two major categories – acoustic and electronic. Acoustic delay lines are analog in nature and fall into several sub-categories – liquid, solid bulk-mode, and solid surface-mode. Electronic delay lines fall into a number of sub-categories including digital high speed memories, charge-coupled delay lines and digital shift registers.

Acoustic delay lines are analog in nature and require some type of acoustic medium in which an acoustic wave is transmitted and received using electro-acoustic transducers.

A liquid delay line was used in the original random signal flaw detection system. This liquid delay line, Figure 4-7, consisted of two piezo-electric transducers, identical to the transducer used for the transmitter/receiver, placed in a water bath and scanned mechanically. This method has the advantages of extreme simplicity, can be operated bi-directionally for producing identically matched delay [7], and produces a continuous range of delays. It has the disadvantages of being large and unwieldy in size, it degrades the resolution by limiting the bandwidth of the reference signal due to the transducers [7], and it produces slow scans and slow resets due to mechanical limitations. It also does not easily allow for multiple taps, since the receive transducers are large and interfere with the continuity of the propagating signal. Other types of liquids could also be used instead of water, and reductions in size and increased efficiency may be possible by using liquids with lower propagation velocity and higher density, respectively. Water, however, is cheap and readily available.

Solid versions of the liquid delay line have been created using materials such as quartz. Quartz delay lines can be made compact by using reflections to increase the path length. Unfortunately, these delay lines are only suitable for fixed delays and although it would be possible to produce parallel outputs by using more than one delay line, cost and size can become prohibitive.

Surface wave devices are another commonly used method for producing delays [53]. A typical SAW delay line is shown in Figure 4-8. The fingerlike structures are the transmit and receive electrodes. Surface waves are produced which travel between the electrodes when an appropriate signal is applied to the transmit electrodes. The surface waves are generally slower than the bulk-mode waves so that the devices are somewhat smaller than the previously described delay line devices. It is also possible to use a number of receive electrodes, to produce a multi-tap delay line. Unfortunately, these SAW delay

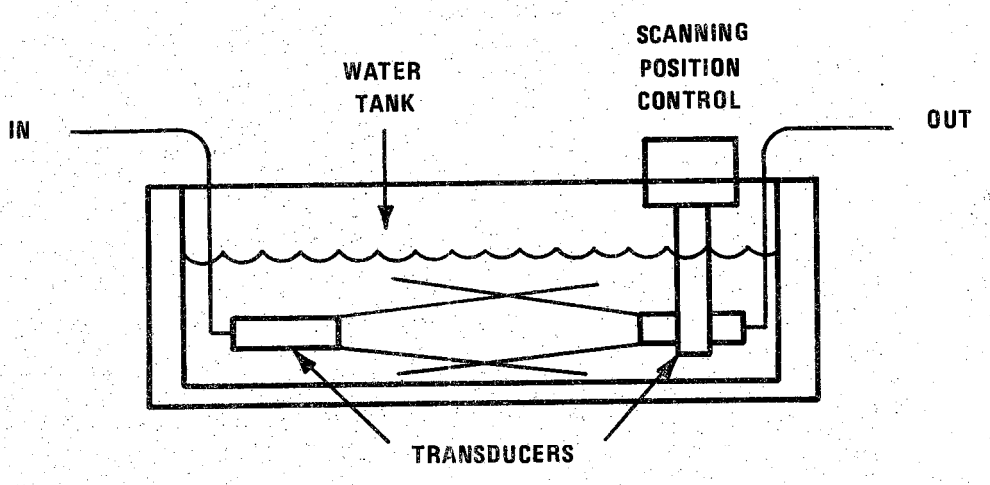

Figure 4–7 Water delay line.

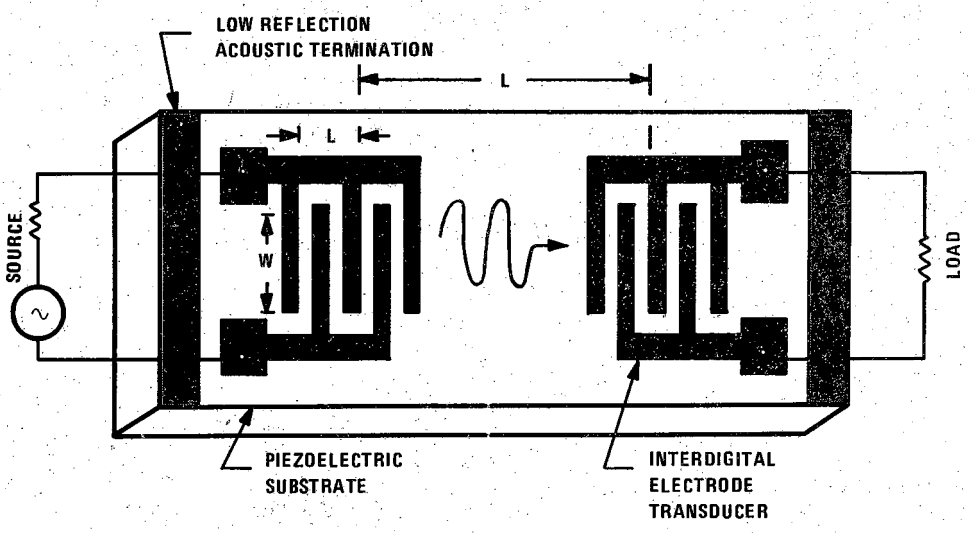

Figure 4–8 SAW delay line

lines can suffer from several limitations, some of which are identical to the previous delay lines. They are rather large for long delay times, can limit the bandwidth of the reference signal, and good SAW delay line devices bandwidths have only been constructed at frequencies above about 50 MHz. Of course it is possible to use modulation to use high frequency devices to delay low frequency signals, but complexity becomes a problem and size is also a problem, because long delay lines on the order of 50 μsec are required. However, these devices have the advantage of providing additional signal processing on the device itself. Filters, convolvers, etc. have all been built on SAW devices.

The most promising delay lines are electronic in nature. Electronic delay lines interface more efficiently with standard digital components and filters, retain wider bandwidth, provide easy multi-tap access, and with improvements in technology are becoming smaller faster, and lower in power consumption.

The most promising electronic delay line is the CCD, or charge-coupled delay line shown in Figure 4-9. These devices retain the best properties of both analog and digital delay lines. Although the amplitude information is analog in nature, the delays are incremental, and thus digital in nature. CCD delay lines allow for small size, (silicon LSI technology) easy multi-tap access, and wide bandwidth, while retaining large dynamic range without the requirement for multi-bit hardware. These devices consist of a series of charge storage areas which are separated by one way charge transfer paths. The exchange of charges are controlled by electronic gates. Charges proportional in amplitude to the input signal, at the sampling times, are stored and transferred through the length of the delay line during the presence of a synchronized clock signals. Unfortunately, CCD delay lines at frequencies above 5 MHz are only in the development stage.

The last type of delay line to be discussed here, multi-bit digital delay lines, can be created by using a set of binary digital delay lines in parallel, as shown in Figure 4-10. This delay line has A/D and D/A converters at the input and output, respectively, to emulate an analog delay line. The dynamic range of signals which such a delay line can store, DR, is the same as that of an A/D converter, so that

$$DR = 2^n \tag{4.12}$$

where n is the number of bits stored at each delay.

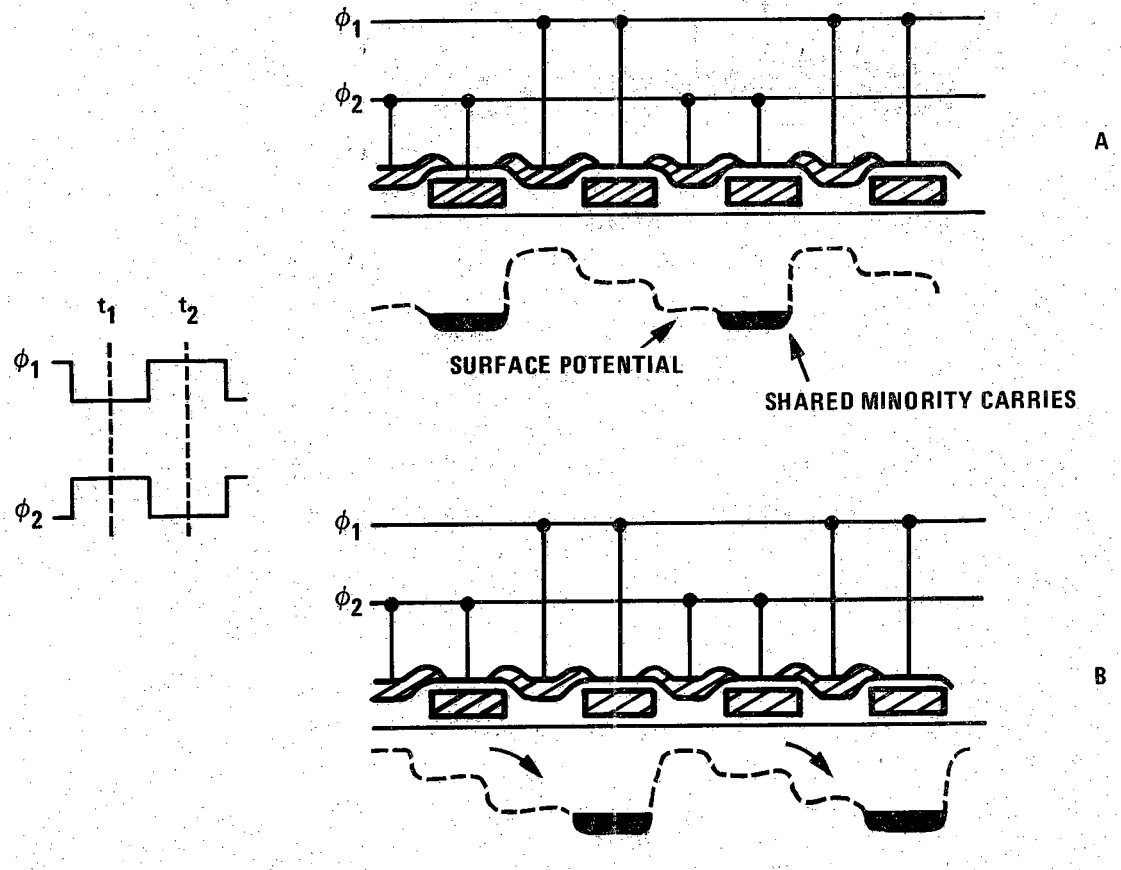

Figure 4–9 Electronic CCD delay line.

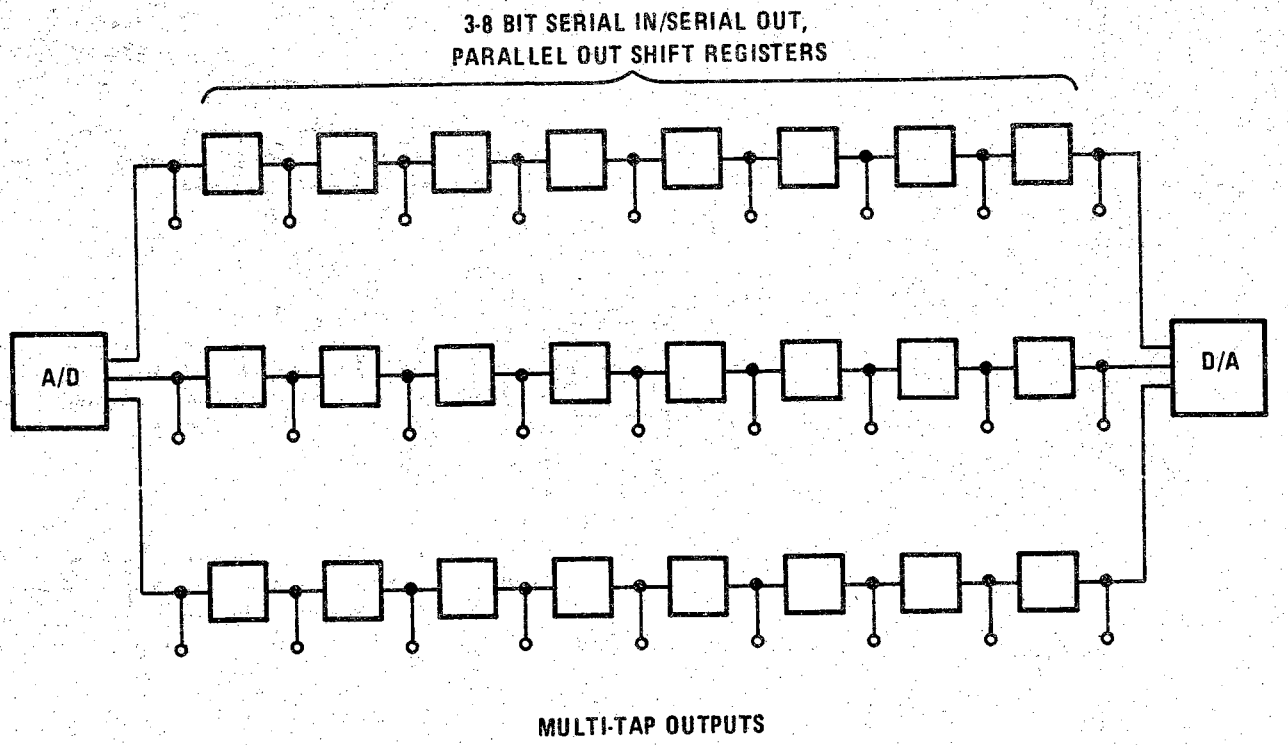

Figure 4–10 Multi-bit digital delay line.

Digital shift registers are readily available in M.O.S. to 20 MHz clock rates, TTL. to 100 MHz clock rates and ECL. to 200 MHz clock rates. As the frequency goes up, there is a corresponding increase in chip power requirements and an increase in the number of chips required. Multi-bit digital delay lines have the advantage of operating at high clock speeds and thus can handle high bandwidth signals, are easily amenable to LSI technology, are readily available, and can be used in multi-tap format. They have the disadvantages of requiring many parallel registers if a large dynamic range is required, and can require a considerable amount of space and power. They also have the disadvantage of requiring an A/D convertor at the front end. Currently integrated A/D convertors can only sample at approximately 20 MHz. However, as technology is advanced into faster, cheaper and lower powered devices these disadvantages will continue to be reduced.

In this study, the correlator architecture shown in Figure 4-6 was used. Because of this approach it was not necessary to store the received signal $y(t - \tau)$ in a multi-bit delay line. Only a one-bit wide (binary) digital delay line was required to delay the binary reference signal. In spite of the relative simplicity of this approach, multiplication by a binary reference signal retains all of the desired amplitude information present in the received signal. The dynamic range of the system is still very high because the return signal $y(t - \tau)$ contains the dynamic range information.

Multipliers

Multipliers fall into three general types – analog, digital and hybrid multipliers. The most common analog multipliers are traditionally called mixers and are typically constructed using diodes as shown in Figure 4-11.

This device can be shown to provide the product if the inputs are constrained to be less than a certain maximum voltage, above which their response becomes nonlinear. They have the advantage of being very wide in bandwidth. These devices have the disadvantage of requiring the use of discrete inductors and diodes. They are also somewhat limited in dynamic range, require matching impedance networks, and produce a slight loss in signal strength. Newer models however, are becoming smaller, wider in dynamic range and less lossy.

If the correlator input signals are digital streams of data, a high speed digital multiplier can be used. Digital multiplication can also be easily

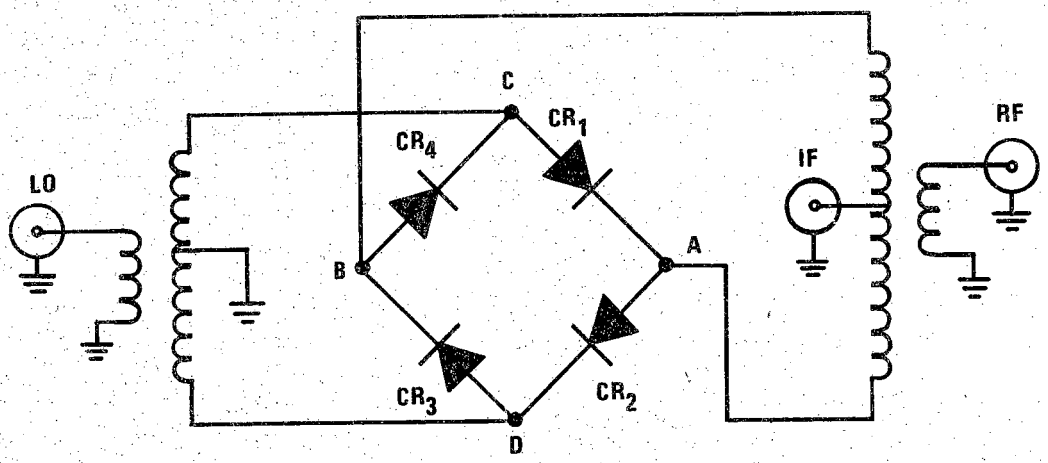

Figure 4–11 Analog mixer multiplier.

implemented by multiplies in software if the signals have been stored. An example of a high-speed multiplier scheme is drawn in Figure 4-12.

Integrators

Several analog methods can be used to perform integration in practical applications. Operational amplifiers with a capacitor in the feedback loop can perform near-ideal integration especially for short integration times. For long integration times. DC offsets at the amplifier inputs can cause severe drift problems. If a long integration time is required, passive lowpass filters can be used to approximate an ideal integrator and will not suffer the same stability problems as an operational amplifier integrator. The integration time of a low-pass filter can be determined by equating the energies present in the impulse responses of the low-pass filter and an ideal finite-time integrator. Using this method it can be shown that the integration time of a single-pole low-pass filter is

$$T = \frac{1}{\pi f_l}, \tag{4.13}$$

where f_l is the half-power cutoff frequency of the filter. For higher order filters of order σ, using a similar impulse response comparison and Parseval's theorem, it can be shown that

$$T \simeq \left(\frac{2\sigma - 1}{4\sigma}\right)\left(\frac{1}{f_l}\right). \tag{4.14}$$

This approximation increases in accuracy with increasing σ and is most accurate for maximally flat (Butterworth) filters.

Optimum Transmit Codes

Two types of large time-bandwidth signals have previously been studied for use in ultrasonic flaw detection systems, random signals [2, 3, 6] and pseudo-random m-sequences [6-11]. These signals were chosen because they are

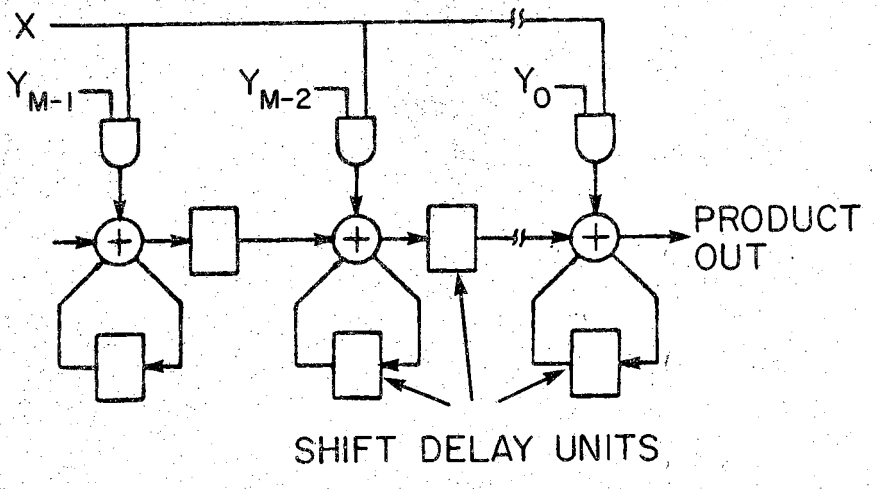

Figure 4–12 High-speed digital multiplier.

easily generated and have bandwidths which are essentially independent of the transmitted signal duration.

Random signals can be produced very easily by amplifying the thermal noise present in any number of sources including resistors [56], vacuum tubes [56], and diodes [56]. This noise can be transmitted in analog fashion as in the original analog random signal system [3], or after clipping and sampling as in the high speed digital correlation system to be described.

M-sequences are special pseudo-random codes described by Golomb [57] which are, by definition, the maximal-length sequences which can be produced by any finite-length shift register. The length of the m-sequence produced by a shift register of length k is

$$m = 2^k - 1 \tag{4.15}$$

A number of different m-sequences can be produced for any given shift register length, by using modulo-2 addition and special feedback configurations [57]. In this study, the m-sequences which are normally in binary form, were changed to a bipolar form, where +1 and -1 were substituted for the binary values 1 and 0, to remove the DC offset and make the transmit signal compatible with the bandpass characteristics of the ultrasonic transducer.

If m-sequences are transmitted continuously they produce constant sidelobes of height $-1/m$, where m is the code length given by equation (4.15). If AC coupled transducers are used, this constant DC offset will not effect the output, and thus, the range sidelobes will be zero.

Several continuous transmission correlation systems using m-sequences have recently been developed, including a Doppler flow measurement system described by Cathignol [58] and flaw detection systems described by Lam and Hui [8] and Pederson [9]. However, as mentioned before, these systems require the use of separate transmitting and receiving transducers, which can impose limitations on their use in many flaw detection situations.

If m-sequences are transmitted in discontinuous bursts, as in the NDE ultrasonic correlation systems described by Elias [6] and Chapelon et al. [7], their autocorrelation functions have finite range sidelobes of approximate height $m^{-1/2}$[43]. The longest known binary code which can be transmitted discontinuously and which has the minimum possible range sidelobes of height $1/m$, is the Barker code of length 13 [59]. This longest Barker code is obviously too short to produce sufficient *SNRE* for most practical NDE applications.

If it is possible to sum the correlation outputs of two sequential transmit bursts, two types of pseudo-random codes can theoretically be used to produce zero self-noise levels in a non-continuous transmit/receive mode using a single transducer. They are the binary pseudo-random codes called Golay codes [60] and the quaternary pseudo-random codes called E-codes [61].

Golay codes are pairs of complementary binary codes which have been thoroughly characterized by Golay [60]. They have the special property that the autocorrelation functions from each code in a pair have a large central peak and have range sidelobes of identical shape but of opposite sign as shown in Figures 4-13a and 4-13b. The addition of the autocorrelation functions from a pair of complementary codes produces a large central peak with no range sidelobes as shown in Figure 4-13c.

Golay codes cannot be as easily generated as m-sequences, but Golay [60] describes a set of algorithms for determining long codes from shorter codes. For a given short complementary Golay code, pair another complementary Golay code pair can be generated from the shorter pair which is twice as long, and which retains the range sidelobe cancellation. This generation can easily be done by either appending or interleaving using the original code pair. In the appending method, given a short complementary code pair A and D, the new longer code pair will be AD and $A\overline{D}$, where the overbar indicates that the code bits are complemented. In the interleaving method, the bits of A and D are interleaved for one code and those of A and $\overline{D}$ for the complementary code. Other similar methods can also be used to generate new codes from two pairs of unrelated complementary codes.

Many codes exist for any given code length, and the length of Golay code usable by a correlation system is limited only by the generation capabilities of the system.

These codes were originally used to determine the slit patterns for optical multislit spectrometry [60]. More recently, Golay codes have been used with good success at very low frequencies, approximately 2 to 100 Hz, in a seismic prospecting system [62]. They have not, to our knowledge, been studied for application in ultrasonics, except theoretically by Takeuchi in a proposed medical imaging system [63, 64].

Quaternary E-codes have also been shown to have this zero range sidelobe property [61]. Quaternary E-codes are four symbol codes which have been described by Welti [61]. These codes are restricted to lengths which are powers of two and can be generated from basis binary codes called D-codes. Turyn [65] has shown the equivalence of Golay codes and certain E-codes with respect

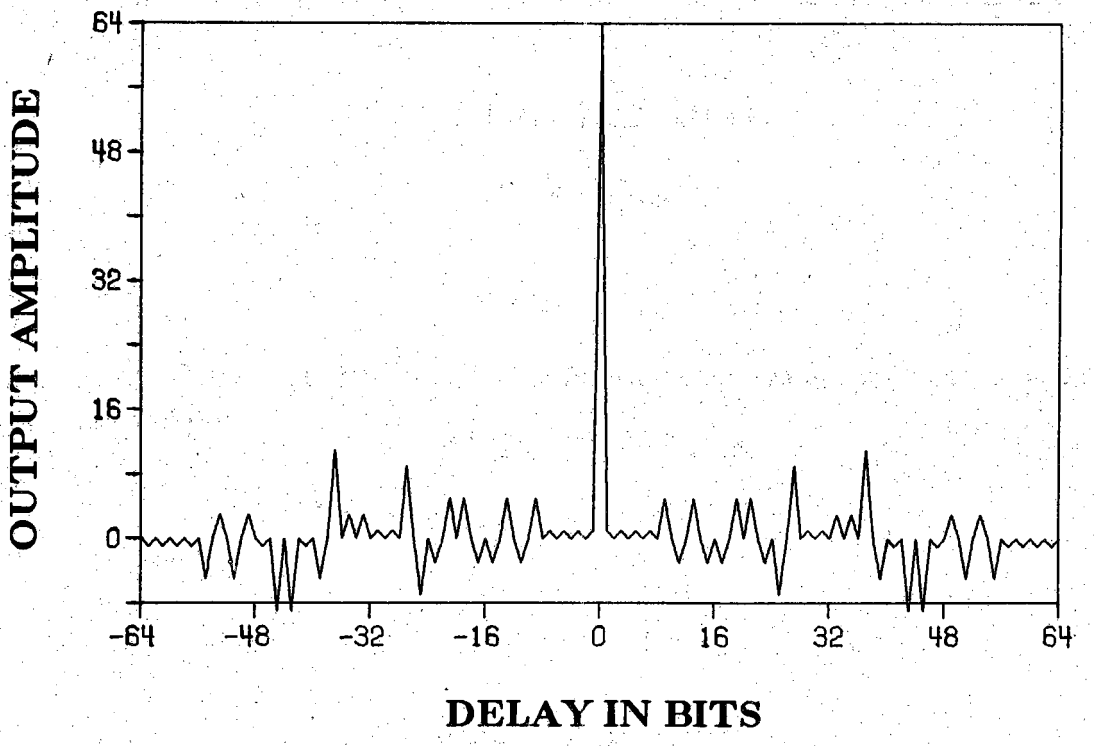

a. Golay Code A

Figure 4–13 Golay code autocorrelation functions and range sidelobe cancellation.

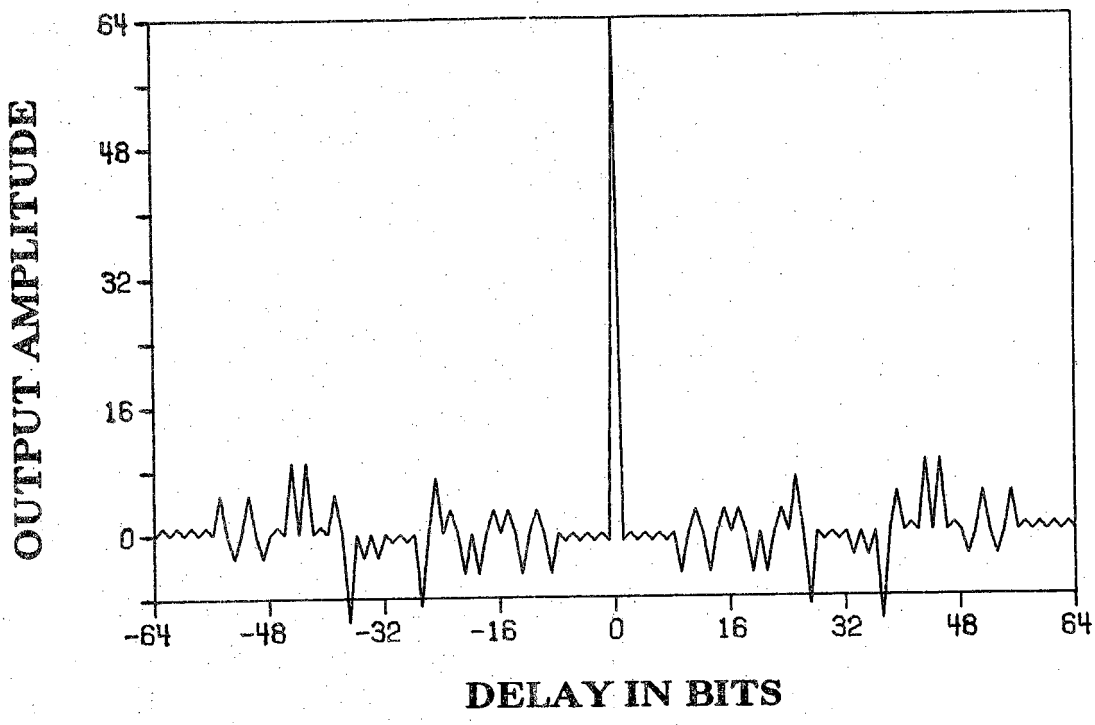

b. Golay Code B

Figure 4-13 (continued).

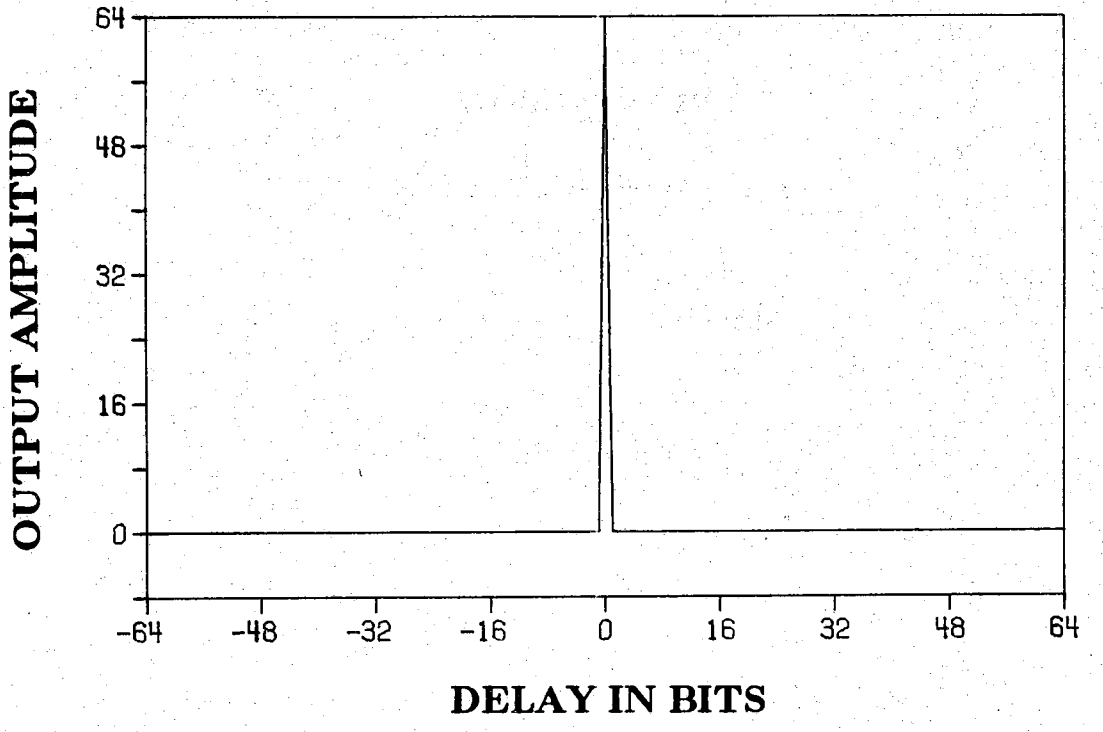

c. Normalized sum of a. and b.

Figure 4–13 (continued).

to side-lobe cancellation. Because of this equivalence and because the binary form of Golay codes makes Golay codes much easier to implement, the E-codes were not investigated further for this study.

Modulation Methods

In the random signal correlation system the random thermal noise was amplified, bandpass filtered and then directly transmitted. However, two types of modulation schemes have been proposed for systems which use pseudo-random m-sequences – direct transmission and phase modulation. In direct transmission, Figures 4-14a and 4-14b, the code is clocked at a rate which is greater than the upper cutoff frequency of the transducer so that the resolution of the system will be determined only by the transducer, as previously mentioned. In phase modulation, Figures 4-14c and 4-14d, the code is clocked at approximately half the rate required for the direct transmission method and used to phase modulate a carrier at the center frequency of the transducer. A simple comparison of these two techniques shows that phase modulation is a more efficient means of transmission [66], simply because much less of the signal spectrum falls outside the transducer pass-band and therefore is not wasted as in the directly sequenced system. This can easily be seen in the spectrums shown in Figure 4-14. However, Chapelon et al. [7] have shown that by filtering the directly sequenced code before transmission, the efficiency of both systems is essentially the same. This filtering then protects the ultrasonic transducer from the low frequency energy produced in direct sequencing transmission. Both Nahamoo and Kak [66] and Chapelon et al. [7] agree that phase modulation is more complicated to implement than direct sequencing. In this study we use direct sequencing transmission in a digital version of the original random signal system, because of its relative simplicity of implementation and its utilization of maximum transducer bandwidth.

Optimum Clock Rate

Equation (3.3) indicates that, assuming the autocorrelation function of a large time-bandwidth signal is a delta function, the correlation output is the impulse response of the system. In practice, however, the code bit-width (transmit clock rate) is chosen in order to maximize the output signal-to-noise ratio. When this is true, the ideal triangular autocorrelation function of the

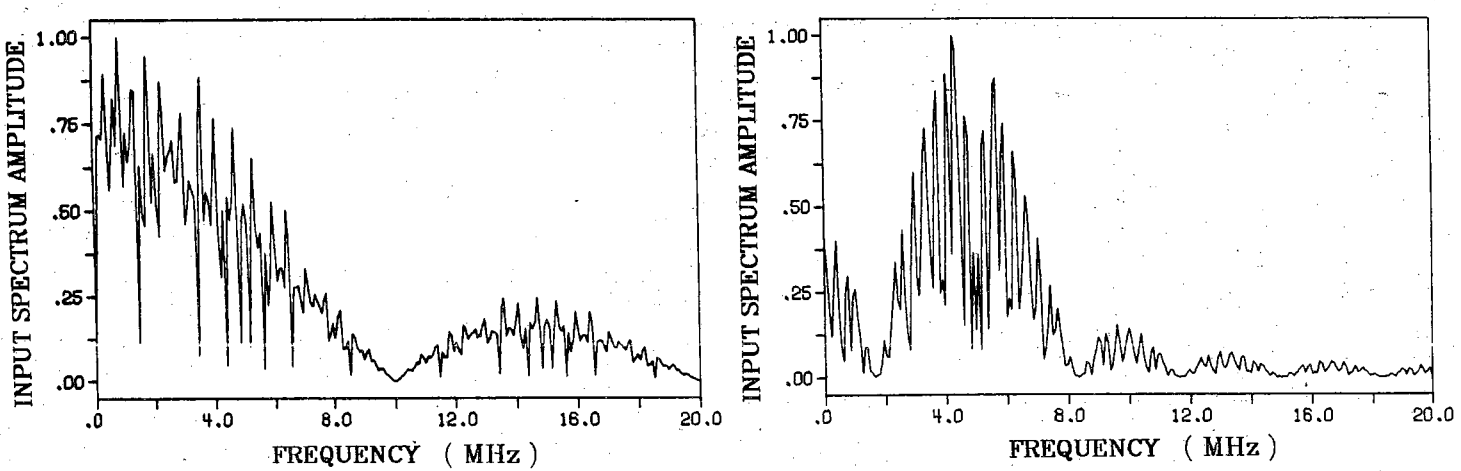

a. Direct transmission

b. Signal spectrum of a.

Figure 4–14 Transmit signals and associated spectrums.

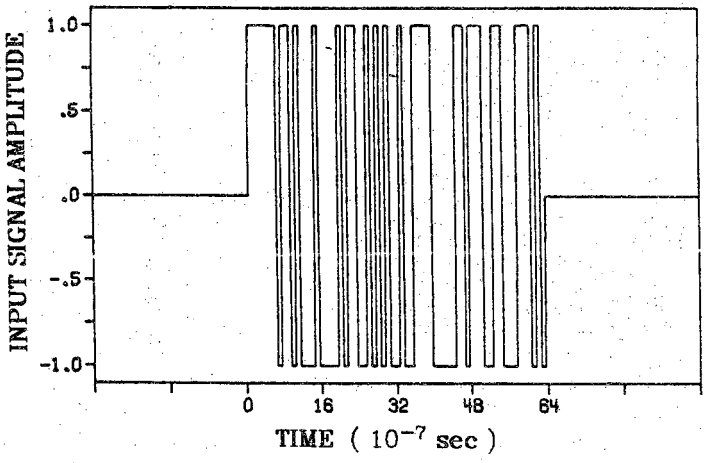

c. Phase modulated signal.

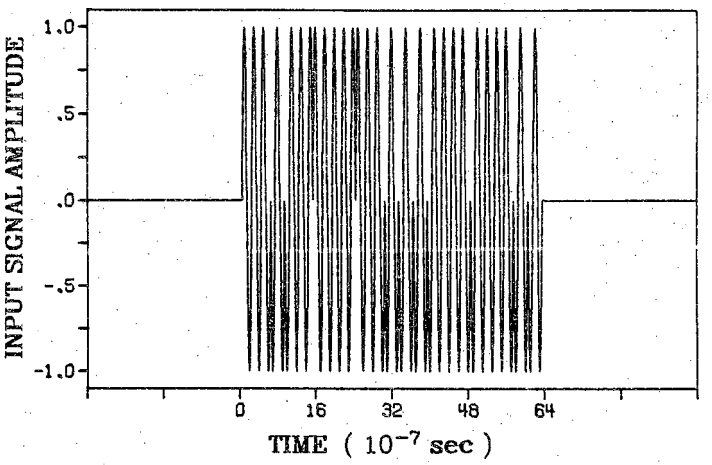

d. Spectrum of c.

Figure 4–14 (continued).

large time-bandwidth signal has a basewidth of 2δ and therefore is not necessarily a good approximation to a delta function. In a pulse-echo system the stimulating waveform is not triangular, but is a smoothed rectangular pulse with unequal rise and fall times. If this pulse is approximated by an ideal rectangular pulse the optimal pulse-width for a pulse-echo system is $1/2f_c$.

In order to determine an optimum transmit clock rate for the correlation system, the operation of the correlation system, as described by equation (3.3), was simulated with a computer program. The impulse response, $h(\tau)*h(\tau)$, of a 40% bandwidth transducer was first measured experimentally in a pulse-echo mode. A functional fit was then made to simulate the measured impulse response on the computer. The ideal triangular autocorrelation function, $R_{xx}(\tau)$, was generated by convolving two identical rectangular pulses which where a single bit-width, δ, in length. This triangular pulse was then convolved with the simulated impulse response to produce the output, as described by equation (3.3). The power of the simulated output was measured by summing the squares of the digital samples of output, and the output noise power was assumed to be linearly related to δ since the length of a transmit burst varies in a linear manner with δ, assuming a constant number of bits in each transmit burst. The ratio of these two powers then produced an output signal-to-noise ratio for the correlation system.

The plot in Figure 4-15 shows the analytically determined output signal-to-noise ratio versus the shift register clock rate, $f_s = 1/\delta$. As can be seen for $1.4f_c < f_s < 3.4f_c$ the signal-to-noise ratio reaches a maximum at approximately $f_m = 2f_c$, and varies less than 2 dB within this range. When operating at the optimal clock rate, f_m, the simulated output waveform appears as shown with the solid line of Figure 4-16. This output is nearly identical to the impulse response of the transducer represented by the dashed line of Figure 4-16. The simulated output for a pulse-echo system operating at the optimum pulse-width is not shown, but is located between the solid and dashed lines of Figure 4-16. Thus, even for the fairly wide triangular autocorrelation function resulting from operation at the optimum signal-to-noise ratio, the simulations predict that the correlation system resolution is essentially the same as the resolution of an ideal pulse-echo system.

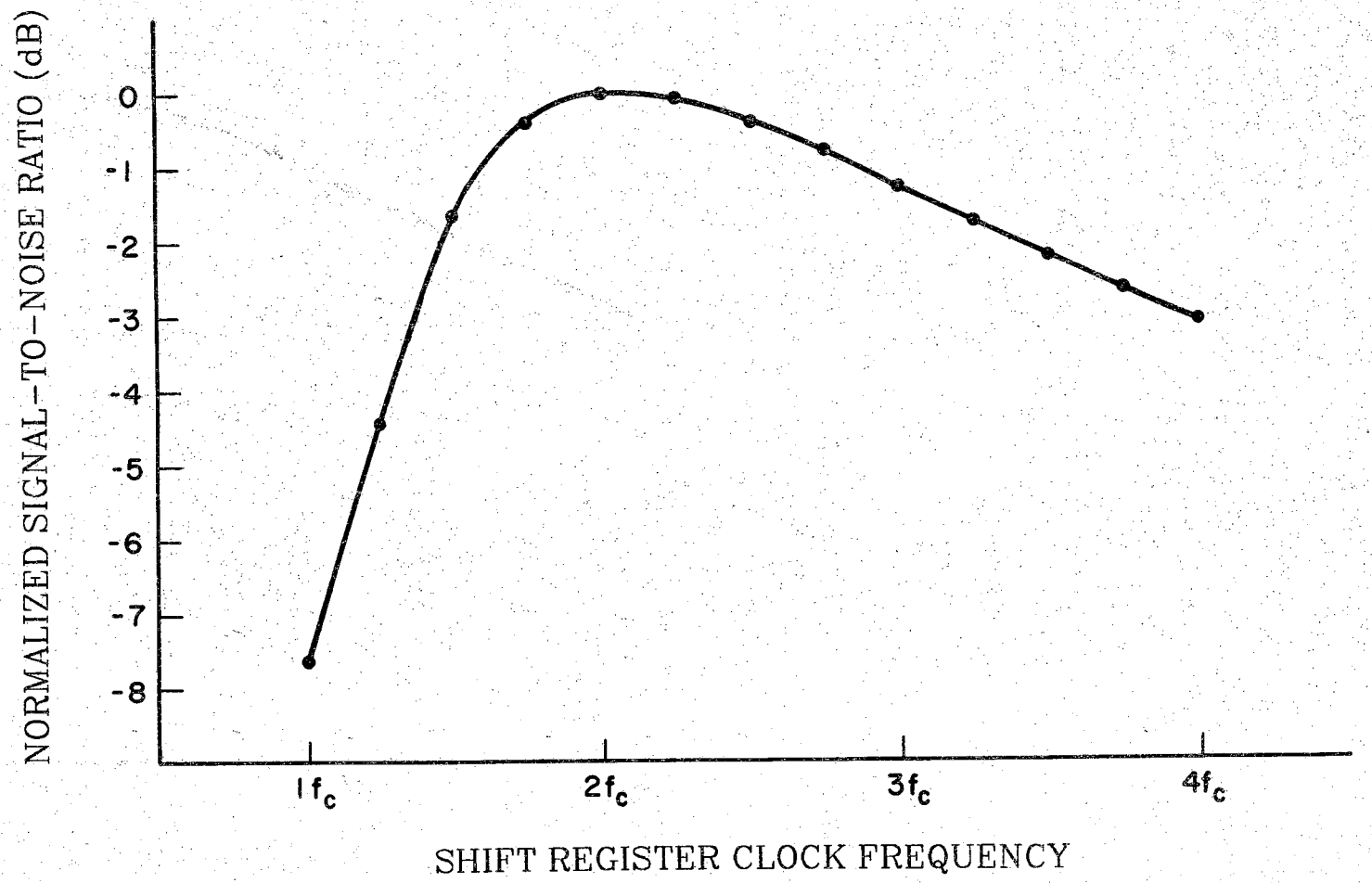

Figure 4–15 Correlation system output signal-to-noise ratio versus shift register clock frequency.

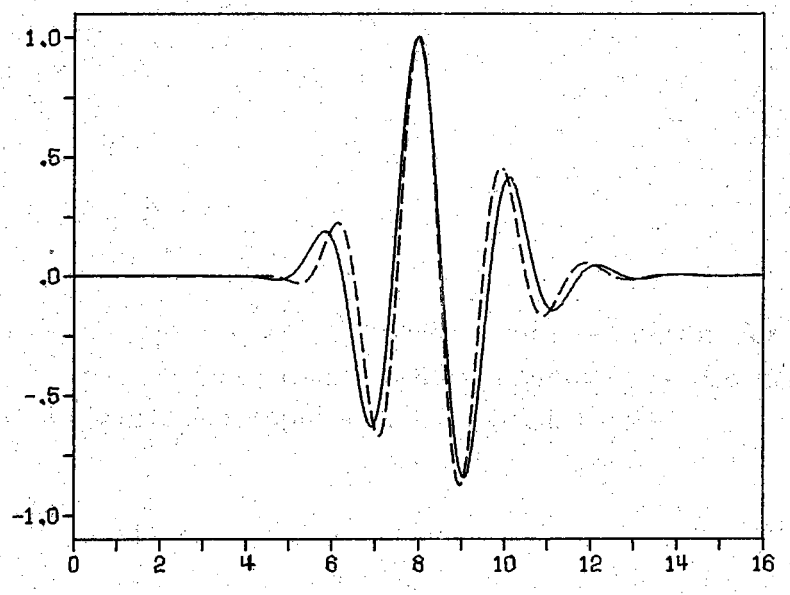

Figure 4–16 Comparison of a computer simulated output for a correlation system operating at the optimum clock frequency and the transducer impulse response (dashed line).

Time-Gain-Control Effects

A practical ultrasonic imaging system for medical applications typically uses a method called time-gain-control (TGC) to compensate for the exponential decrease in signal strength which occurs in tissue, Figure 4-17. Unfortunately, TGC can produce adverse effects if improperly used in a correlation system. A TGC amplifier varies its gain with time according to a curve like the dashed line. Ideally, the net return signal strength for a target will then be independent of its depth, as shown by the straight line of Figure 4-17. The desired result is a decrease in the dynamic range requirements of all the subsequent electronic stages, including the final display device. In conventional pulse-echo systems, TGC is implemented in the front-end receiver in order to optimize the signal-to-noise ratio and reduce the dynamic range requirements of the subsequent stages.

Unfortunately, if implemented in the conventional manner, the TGC receiver can adversely effect the operation of a correlation system which uses long transmit signals.

The TGC receiver will exponentially modulate the long received signal as shown in Figure 4-18. If the correlator then blindly attempts to correlate with a copy of the transmit signal, the signals are no longer optimally matched, and the resulting signal is distorted. Takeuchi proposed to compensate for this TGC term [63,64] by either transmitting the long transmit signals with an inverse exponential weighting, or by inverse exponential weighting, on reception, in the correlator. Both of these methods are somewhat complicated since they require a careful match between the signal weighting and the TGC amplifier. They also reduce the output signal-to-noise ratio of the system since the optimum signal or code amplitude would not be used at all times.

An alternate method not discussed by Takeuchi, is to apply the TGC after the detection system. Since the detection process compresses the long transmit signals, there will be no need for complicated inverse weighting. For systems which operate in real time, as is the case in medical imaging systems that image moving objects, a simple synchronized TGC amplifier could be used at the output of the detection process. Such a system would have a constant gain receiver with a gain equal to the minimum gain of the TGC receiver.

Based on the system design parameters presented in the second part of Takeuchi's paper [64], it is possible to estimate the amount of additional noise resulting from the use of a constant gain receiver. Using typical noise figures for a multi-stage receiver, this additional noise is very small, resulting in about

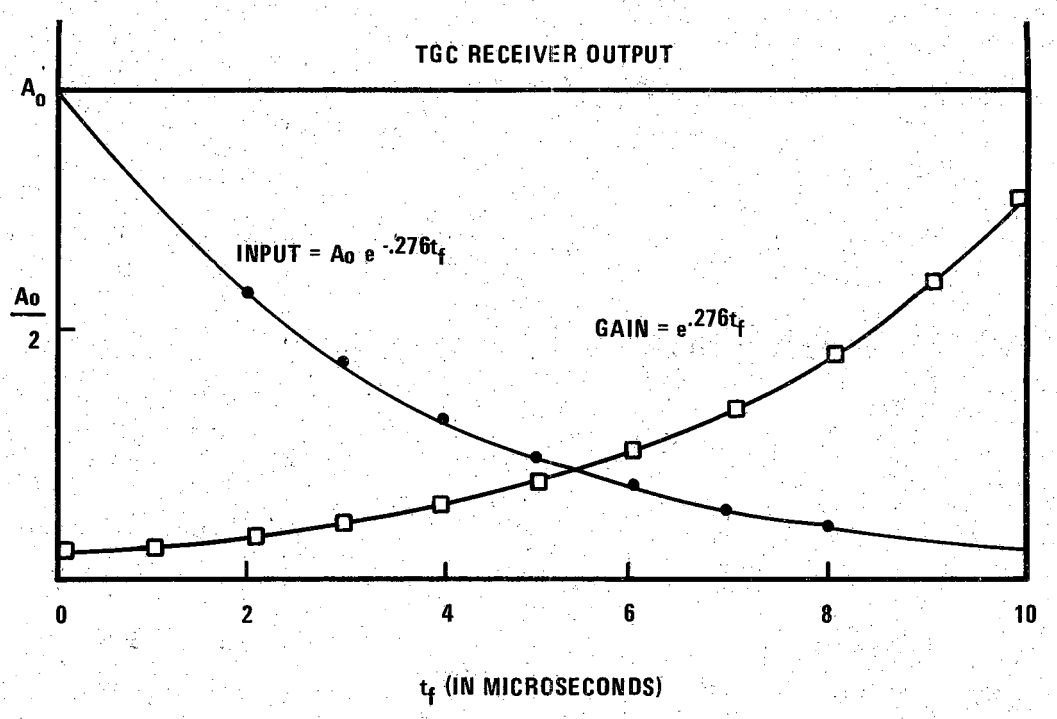

Figure 4–17 TGC amplifier effects.

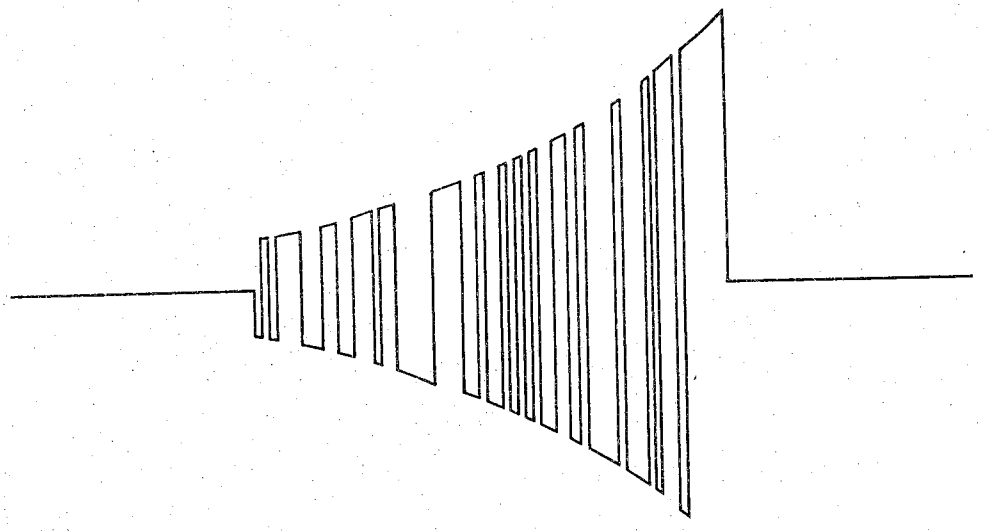

Figure 4–18 TGC effects on an m-sequence burst.

1 to 2 dB of output signal-to-noise ratio degradation.

This signal-to-noise ratio degradation can easily be overcome by the use of a constant signal strength throughout the pulse-length of the transmitted signal. Following Takeuchi's example of a 12 bit code, a 20% signal bandwidth and a 6 dB change in amplitude, between the beginning and end of an exponential pulse, there is approximately 3 dB less average power in an exponential pulse compared to the average power present in a constant maximum signal strength pulse. This 3 dB difference easily compensates for the degradation estimated above. Further signal-to-noise ratio improvement can also be obtained by lengthening the pulse-width of the transmitted signal. The pulse-length is no longer restricted as it is in the proposed Golay code system, where only 6 dB or slightly more gain change could occur over one pulse sequence.

In systems that image stationary objects, as is the case in flaw detection systems, it would be possible to use a different kind of gain compensation. Since the targets are not moving, a real-time scan is not required and it is possible to integrate or average more than one pulse at each range [2]. It would be possible to vary the net integration time, $nN\delta$, with depth, to compensate for attenuation effects so that

$$nN\delta = K^{2a(x_2-x_1)} \tag{4.16}$$

where a is the attenuation constant of the medium, x_1 is some reference depth of penetration, x_2 is the depth for which compensation is desired, and K is some constant. If the integration time, is increased exponentially with depth, the scan time will thus also increase exponentially with scan depth.

This method of gain compensation, using varying integration time, has several benefits over conventional TGC. The output noise level of a variable integration time system will stay constant throughout a scan, whereas conventional TGC produces an exponentially increasing noise level. The depth of penetration of a variable integration time system is not limited by the transmitted signal strength and attenuation, as it is in real-time systems. The only limitations on the depth of penetration are the stability of the integrator and the rigidity of the scan device and the medium. Because of the available *SNRE* the center frequency of operation and the bandwidth of the transmitted signal can easily be increased, causing a corresponding increase in the lateral and axial resolutions, respectively. Of course an increase in integration time

means that the system will not operate in real time, but in flaw detection where high resolution and maximum penetration are more important than scan speed a spread energy system with variable integration time gain compensation, using a system similar to Takeuchi's [63,64], is feasible.

CHAPTER V - A DIGITAL CORRELATION SYSTEM FOR BINARY TRANSMIT SIGNALS

Following the development of the original random signal correlation flaw detection system [2], a new flaw detection system was developed which replaced the analog water delay line of the original system with a set of high-speed digital shift registers. Initially this system was used to transmit random signals, with a sampled version of the random transmit signal stored in the delay line. This method was found to be an inefficient use of the transmit power and for the work in this paper the initial system was modified to transmit the binary sampled version of the random signal, or any type of binary transmit signal, such as m-sequences.

In the following chapter this new digital flaw detection system is described, tested, compared to simulations, and evaluated in a number of critical situations.

System Description

The new digital flaw detection system is shown in Figure 5-1. This system can store a pair of reference signals each containing up to 256 bits, which corresponds to a 12.8 μs reference signals at a 20 MHz clock frequency. Clock frequencies of up to 30 MHz can be used in the present system. Using a clock of frequency f_c, the digital delay line produces random signals and m-sequences of half-power bandwidth $.45f_c$. the digital delay line will thus produce reference signals of much wider bandwidth than the water delay line, provided the transducer upper half-power frequency is below $.45f_c$. The scan rate, initial delay time, and scan range of the digital flaw detection system are all controlled by digital signals, allowing the system to be interfaced with a microprocessor.

The operation of the system is as follows: first a digital controller loads and unloads the shift registers according to three settings: initial delay,

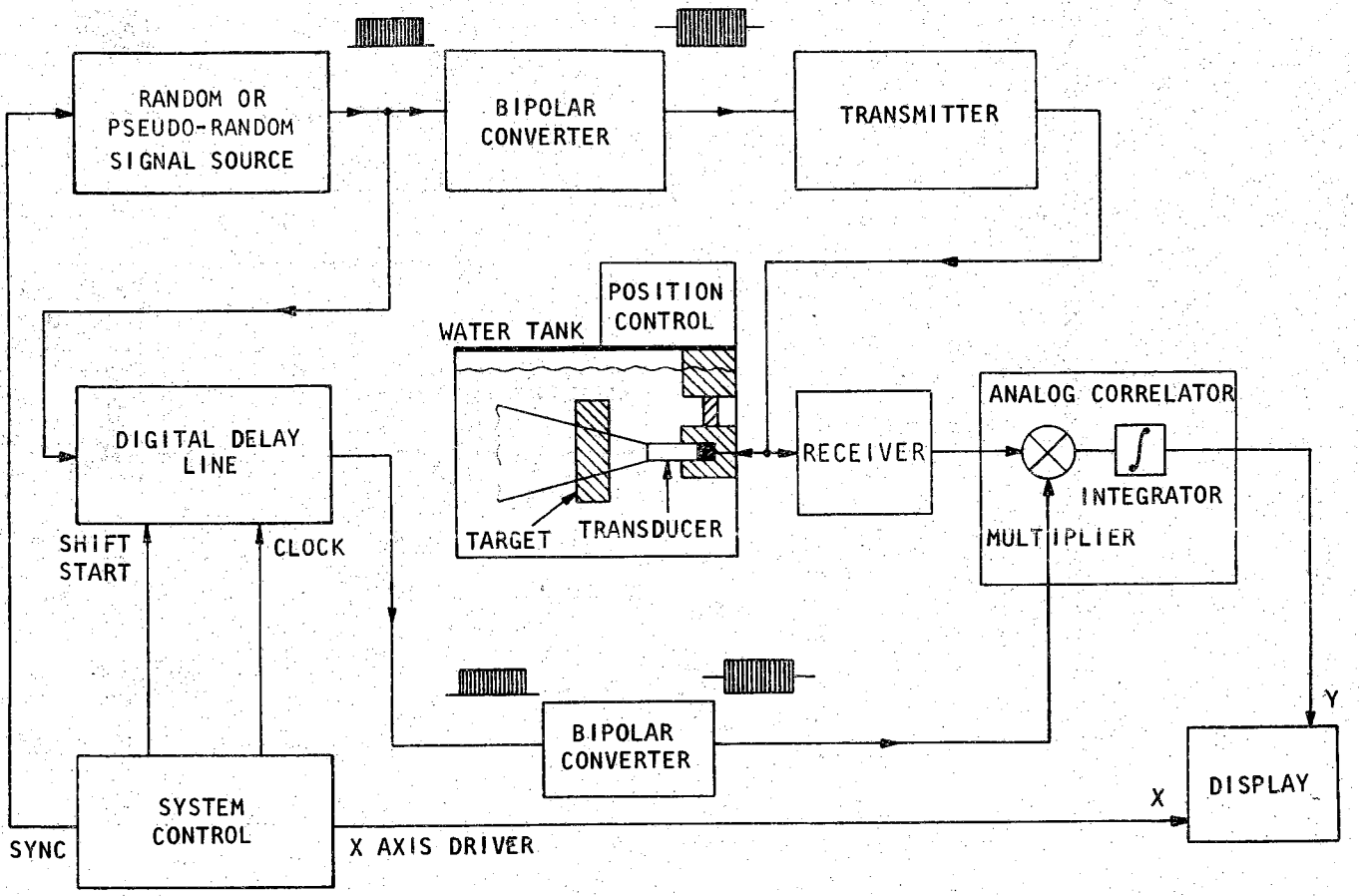

Figure 5–1 Digital correlation system.

samples per cell, and number of cells. (A cell is a delay increment and is equal to $1/f_c$ in this system.) On the transmit cycle, the controller signals the source to transmit, and loads the transmit signal, into the shift register set (Figure 5-1). After transmission, the controller counts clock pulses until the interval delay count is reached. In the correlation cycle the controller subsequently dumps the contents of the shift register for correlation with any returning echo signals. It then waits for the next transmit cycle command, the timing of which is determined by an external repetition rate setting, and again reloads the shift registers. The delay count is subsequently either incremented by one for a new range cell, or zero for the same range cell, depending on the external samples per cell setting. This transmit/correlate cycle continues until the entire scan, as controlled by the external number of cells setting, has been completed. The system then resets itself and starts a new scan with the delay count reset to the initial delay setting.

In an actual practical operating system, the position of the transducer would be varied between scans, to interrogate the entire sample under study. A D/A converter transforms the digital scan position into a continuous smooth ramp which drives the x-input of an x-y recorder or oscilloscope (Figure 5-1). The output of the correlator indicates location of targets and is displayed on the y axis. For optimum system operation, the integration time of the correlator is set at approximately the number of samples per cell multiplied by the repetition period. Since the output of the correlator is at a frequency approximately equal to the scan rate, which is always much lower than the transmitted frequency, an A/D conversion of the system output can easily be accomplished under microprocessor control, eliminating the need for a high-speed transient recorder. Thus the system is ideally suited to provide high *SNR* output signals for use in conjunction with additional signal processing.

Experiments were performed to verify proper system operation and to compare m-sequences with clipped sampled random signals for both short and long code lengths. In order to test short codes, simulating high-speed operation, the digital flaw detection system was modified to recirculate the contents of the digital shift register and thus transmit the same code in every transmit burst.

For long code operation, the codes were produced from external signal sources and loaded in 192 bit sections. A 8,388,607 bit m-sequence was generated using a 23 bit shift register set and was loaded synchronously into the digital delay line. Clipped sampled random signals were generated using a Model 1380 20 Hz-20 MHz General Radio random noise generator. The analog random signal produced by the noise generator was clipped symmetrically using

a Schmitt trigger and then sampled and loaded into the digital delay line at the system clock frequency.

Simulation

Computer simulations were made for comparison and were implemented in the following manner. The impulse response of an approximately 5 MHz center frequency, 2 MHz bandwidth, transducer was measured, as in the previous section, by operating the system in a pulse-echo mode, using the same transmitter as used in the correlation system measurements. The Fourier transform of the impulse response yielded the frequency response of the transducer, which was used to weight the spectrum of the transmitted code. The inverse Fourier transform of the weighted spectrum produced the computer simulated output.

Single-Target Measurements

Low *SNR* Results

The advantages of the signal-to-noise ratio enhancement offered by the correlation system can be clearly seen in a direct comparison of the two systems operating under high noise conditions. Figure 5-2a shows the received echo signal produced by a conventional pulse-echo system from a flat stainless steel target placed in a water bath and oriented parallel to the transducer face. The signal-to-noise ratio was adjusted to approximately unity and many scans were recorded to help identify the target location.

The correlation system output produced by using a single 256 bit m-sequence transmit signal ($n = 256$ and $N=1$), and having the same input signal-to-noise ratio and target/transducer configuration as the pulse-echo system, is shown in Figure 5-2b.

The expected reduction in background receiver noise, given by the *SNRE* formula of equation (3.9), is 23 dB for the 10 MHz bandwidth receiver and 12.5 MHz clock frequency used in this measurement. However, in addition to the original thermal noise of the receiver, the figure shows a deterministic (non-random) term due to self-noise. The level of the self-noise in the vicinity of the

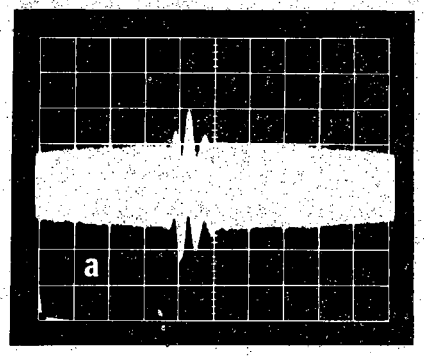

a. Multiple pulse-echo scans

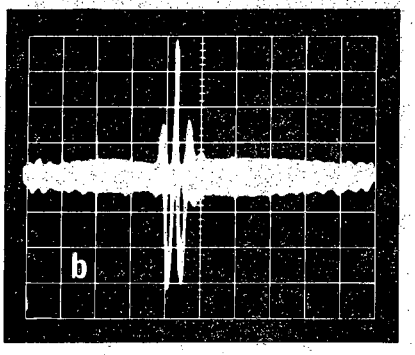

b. Multiple correlator scans (n=256,N=1)

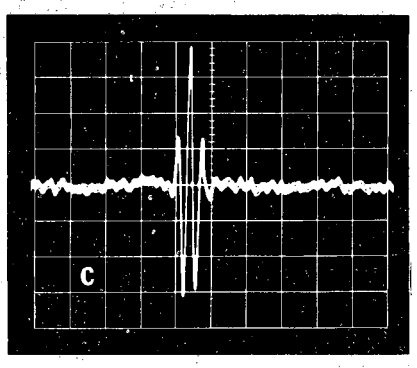

c. Single correlator scan (n=1,N=256)

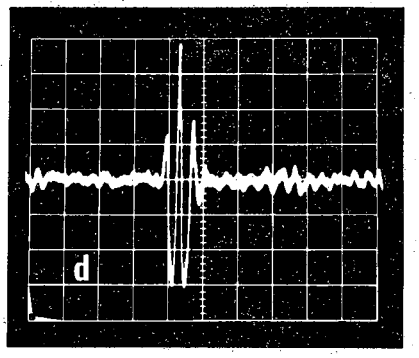

d. Single correlator scan (n=256,N=1)

Figure 5–2 Comparison of pulse-echo and correlator outputs for unity input signal-to-noise ratio.

desired target is given by equation (3.12). For this particular measurement, the range sidelobes should be 16 dB below the peak signal. When these two independent noise sources are added, the peak signal power to background noise ratio is about 15 dB. Figure 5-2 clearly shows the expected factor of six improvement in signal-to-noise amplitude ratio. As a comparison, setting $n = 1$ and $N = 256$ produced the single scan correlation system output displayed in Figure 5-2c. Setting $n = 1$ and $N = 256$ is equivalent to time averaging in a pulse-echo system, where the averaging is done point-by-point throughout the scan range, thus the system is 256 times slower than when operating with $n = 256$. Although the scan is much slower, Figure 5-2c does represent an output with better signal-to-noise ratio due to the absence of range sidelobes. In this case, the *SNRE* is close to the expected level of 23 dB. A single trace of the high speed correlation scan (Figure 5-2d) is reproduced in Figure 5-2d to permit a more convenient comparison of the two operating modes.

High *SNR* Results

The experimental and computer simulated correlation outputs for both a 64 bit clipped sampled random signal and a slightly modified 63 bit m-sequence clocked at 20 MHz are shown in Figures 5-3 and 5-4 (The 63 bit m-sequence was modified by adding an extra bit, equal to the bit at the beginning of the m-sequence, to simplify implementation). As can be seen, the measured outputs match well with the computer simulations. All of the short code outputs show significant range sidelobes present around the desired echo. Other 64 bit samples of random signal and 63 bit m-sequences were also tested and were found to have different range sidelobe patterns, however the sidelobe levels remained within 3 dB of the sidelobes of the signals shown in Figure 5-3 and 5-4.

Equation (3.12) predicts the upper bound of range sidelobes for the short 64 bit codes to be at least 8.2 dB lower than the peak amplitude compared to measured values of 12 dB for the short random code and 14 dB for the short m-sequence. The slightly lower range sidelobes of the m-sequence have the special property that when continuously repeated they produce a constant range sidelobe level [8].

The measured correlation outputs for 1024 consecutive 192 bit sections of a 8,388,607 bit m-sequence, and a clipped sampled random signal are shown in

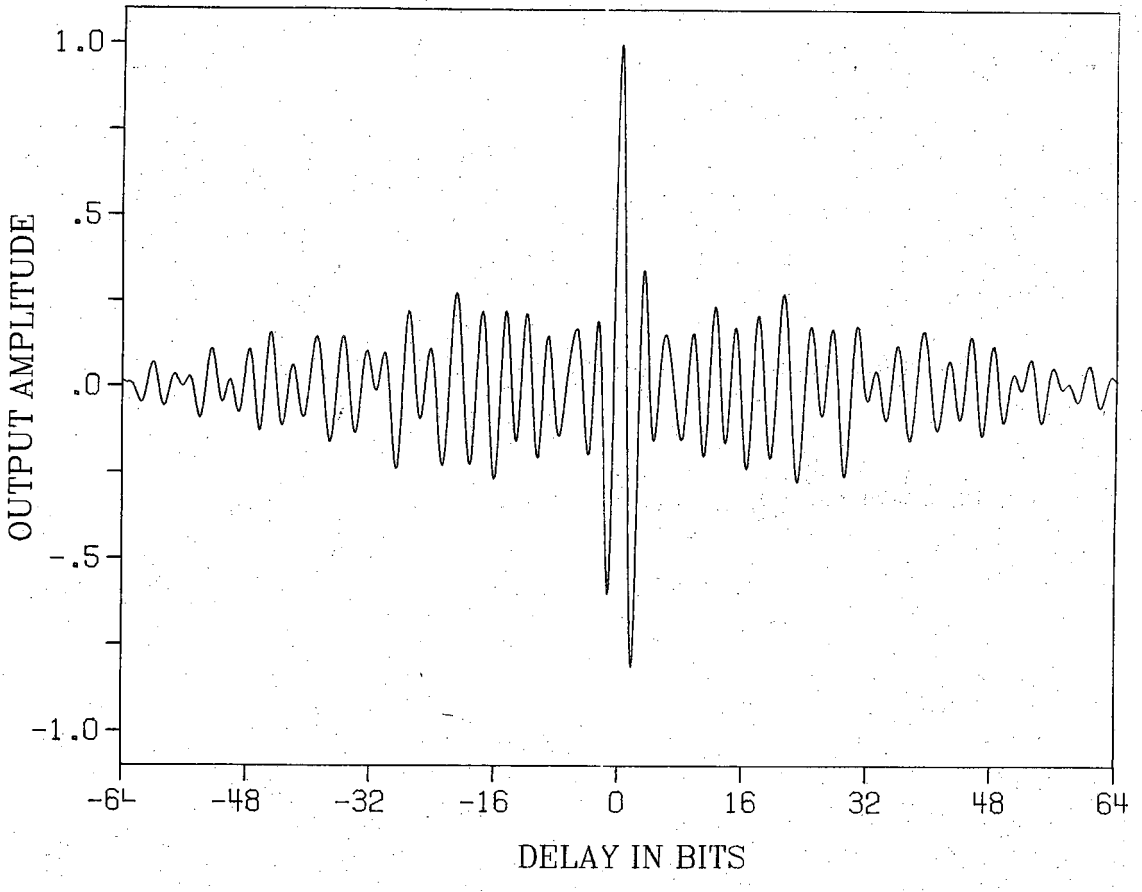

a. Self-correlation function of a random sequence.

Figure 5–3 Self-correlation function of a random sequence.

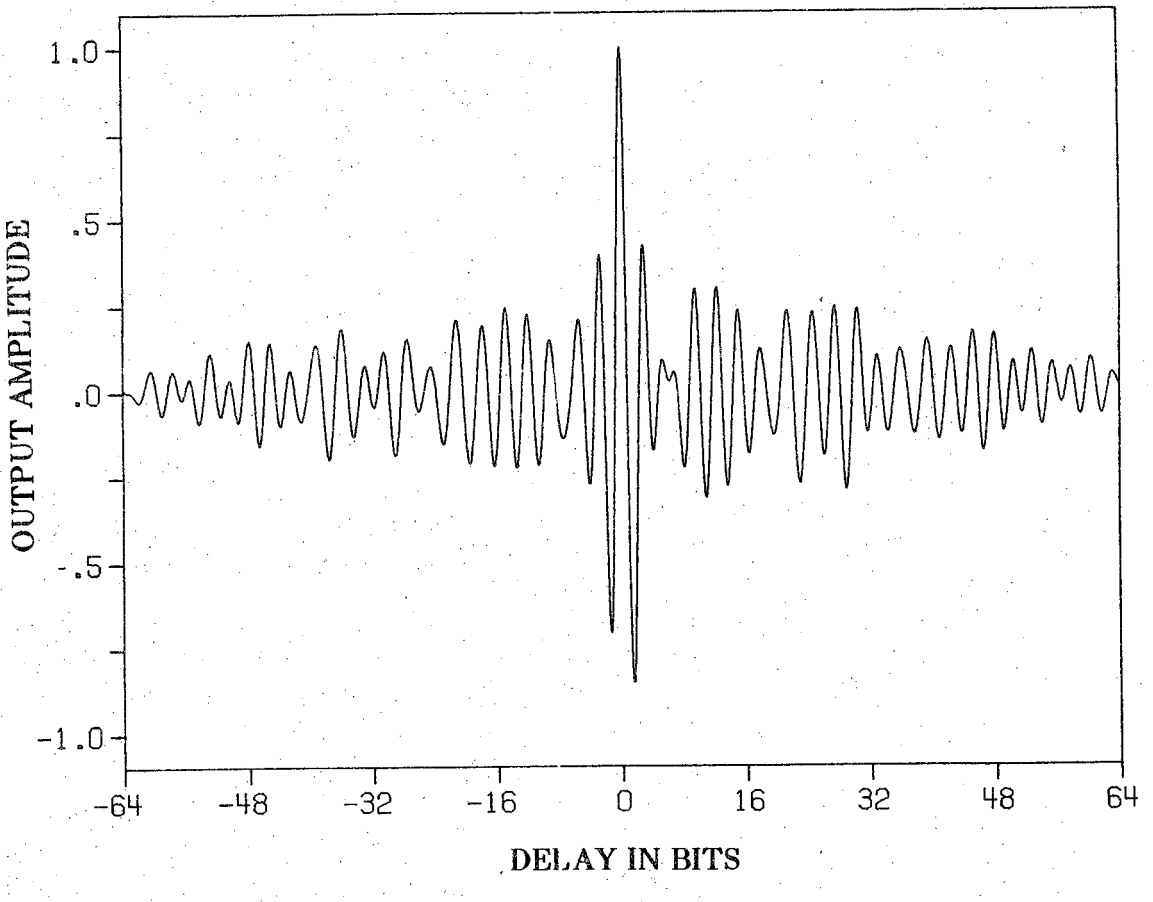

b. computer simulation of a.

Figure 5--3 (continued).

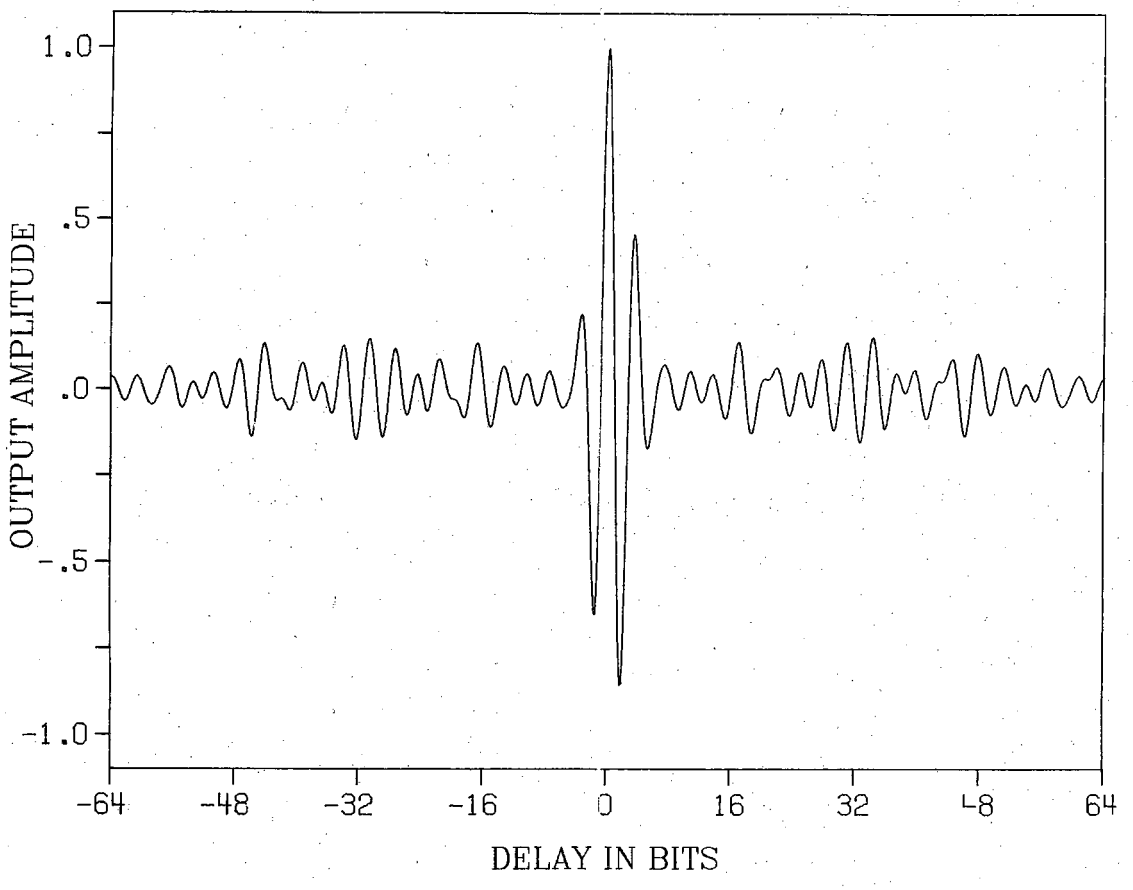

a. Self-correlation function of an m-sequence.

Figure 5–4 Self-correlation function of an m-sequence.

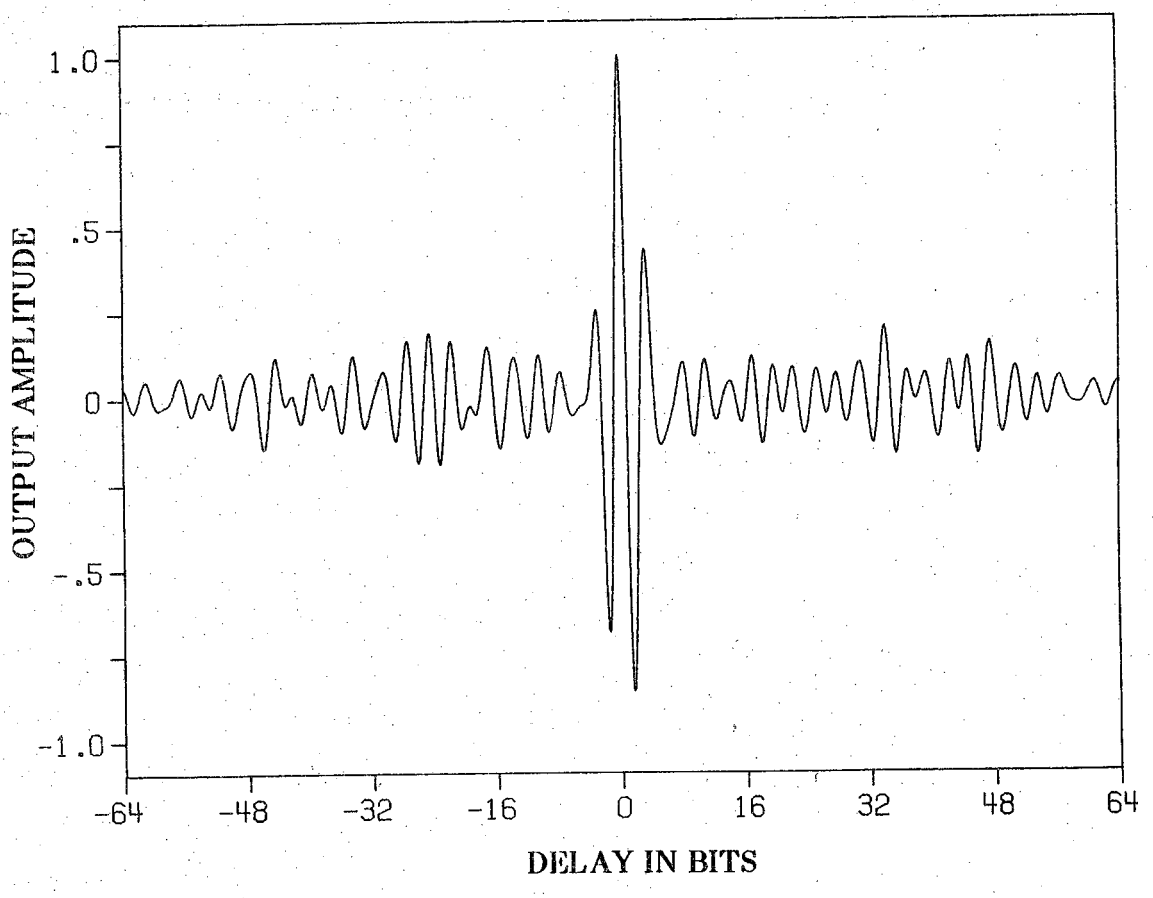

b. Computer simulation of a.

Figure 5–4 (continued).

Figure 5-5. Notice that the range sidelobe level of the m-sequence is about the same as that of the clipped sampled random signal at approximately 42 dB below the peak amplitude. This agrees with the value of 43 dB predicted from equation (3.12). As can be seen, the output signal of the correlation system is nearly identical to the simulations of Figure 4-16. Thus as expected, the correlation system has the same resolution as an ordinary pulse-echo system. However, equation (3.9) shows that the correlation system has a signal-to-noise ratio enhancement of 20,644 which is not available in a conventional pulse-echo system.

Clutter Measurements

Measurements were made to verify the formula for signal-to-noise ratio in clutter, equation (3.21) by using the grain boundaries in a cylindrical block of 303 austenitic stainless steel to simulate a practical clutter situation, Figure 5-6. The grain size was enhanced by heat treatment for one hour at $1387^{o}\,C$, which yielded a measured grain size of 160 μm [45]. The target thus simulated the clutter-limited situation typically encountered in the heat-affected-zone (HAZ) of a weld. The transducer used is one inch in diameter and has a center frequency of 5 MHz and a half-power bandwidth of approximately 2 MHz. The end of the target opposite the transducer was coupled to a second large metal block to help reduce back surface reflections and thus multiple reverberations. Shear wave couplant was used for all surface contacts.

The number of transmit bits, n, and the number of transmit bursts, N, were varied to investigate their influence on the output clutter power seen by a random signal correlation receiver. The average minimum clutter power from a region of the sample, C_o, was determined from both direct pulse-echo measurements and correlation system measurements in which many unique m-sequence bursts of long duration were integrated. A typical correlation output for this sample taken under conditions of long integration of long codes is presented in Figure 5-7a.

The total clutter power was also measured for short code operation using 63 bit m-sequences and varying the number of unique transmit signals integrated in each range cell. A typical plot of the clutter present with short code operation is shown in Figure 5-7b. Subtracting the previously measured value of C_o from the total clutter power measurements isolated the additional clutter power C_a contributed by the self-noise, Figure 5-8 displays the

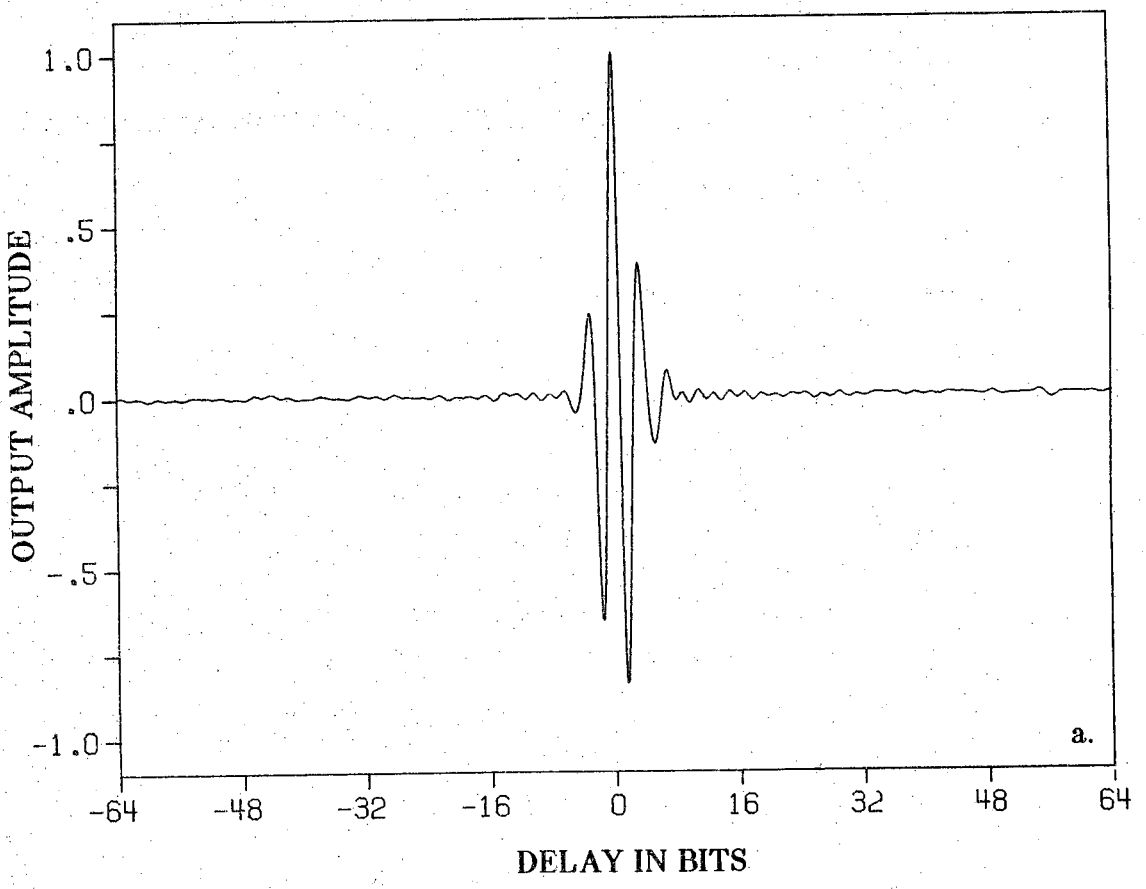

a. 8,388,607 bit m-sequence.

Figure 5–5 Measured correlation outputs for approximately 196,608 bits of code.

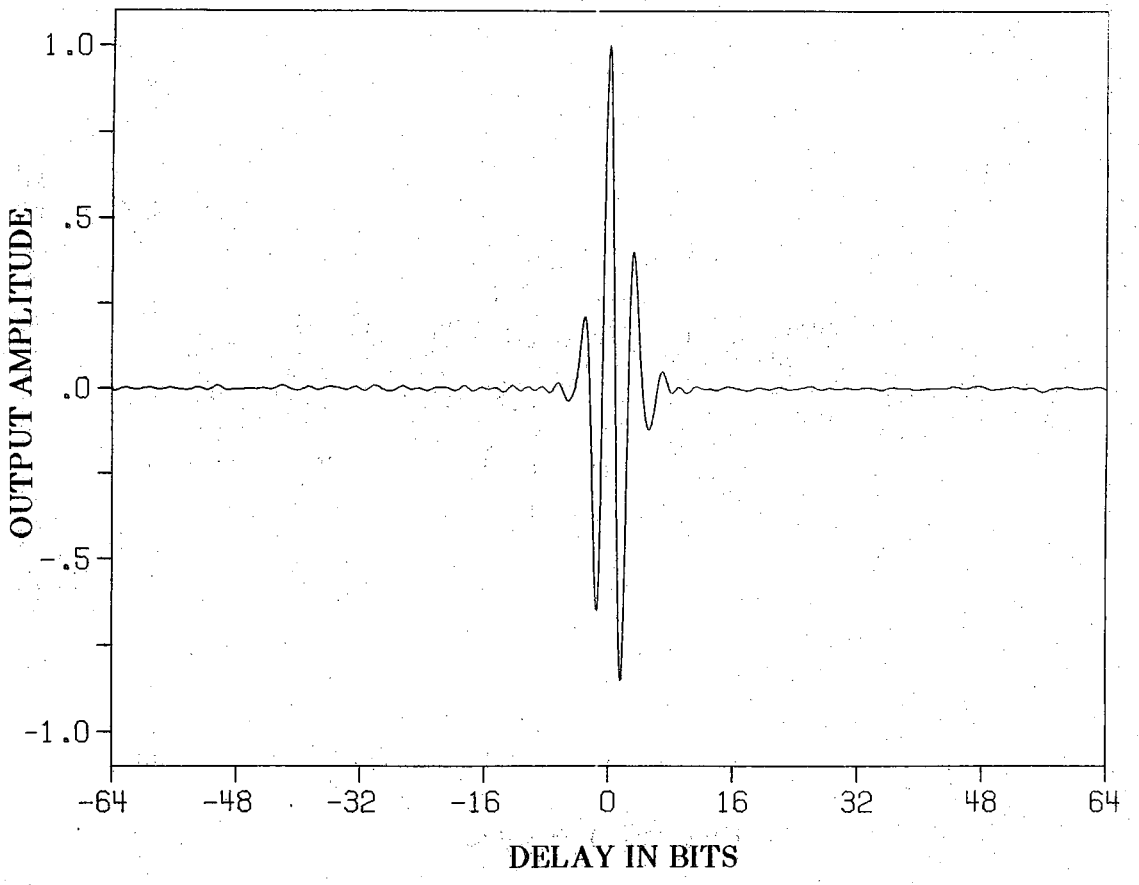

b. Clipped sampled random signal.

Figure 5–5 (continued).

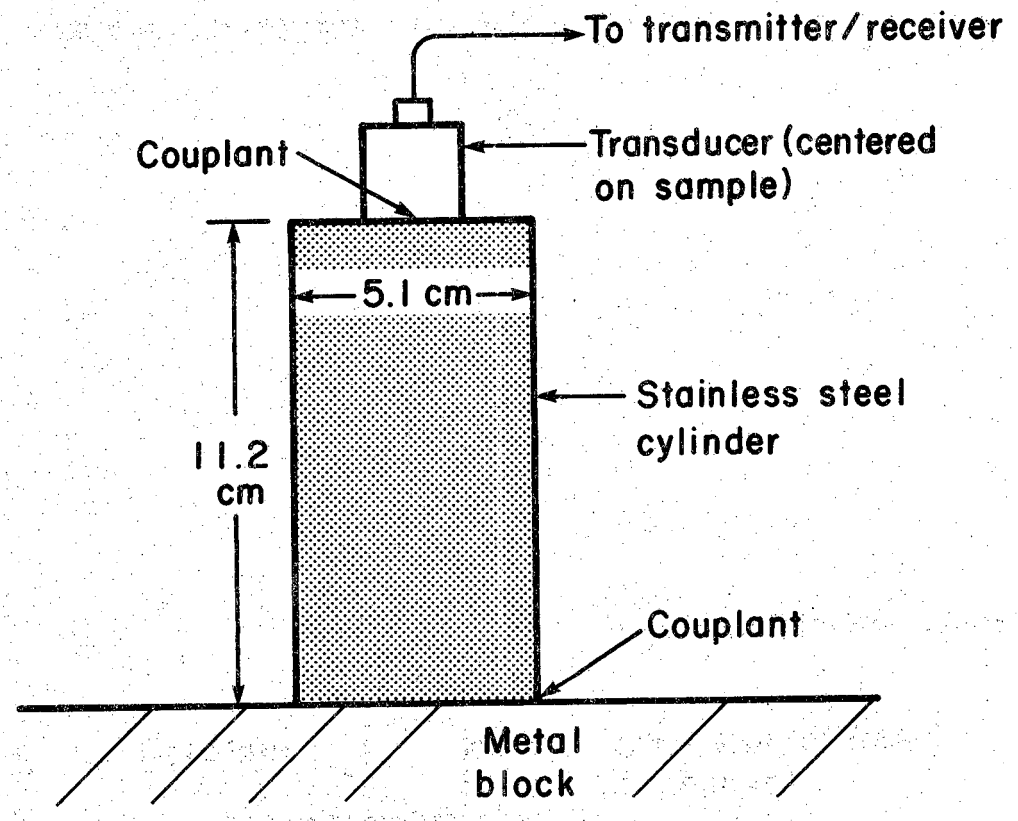

Figure 5–6 Experimental setup for clutter (grain) measurements.

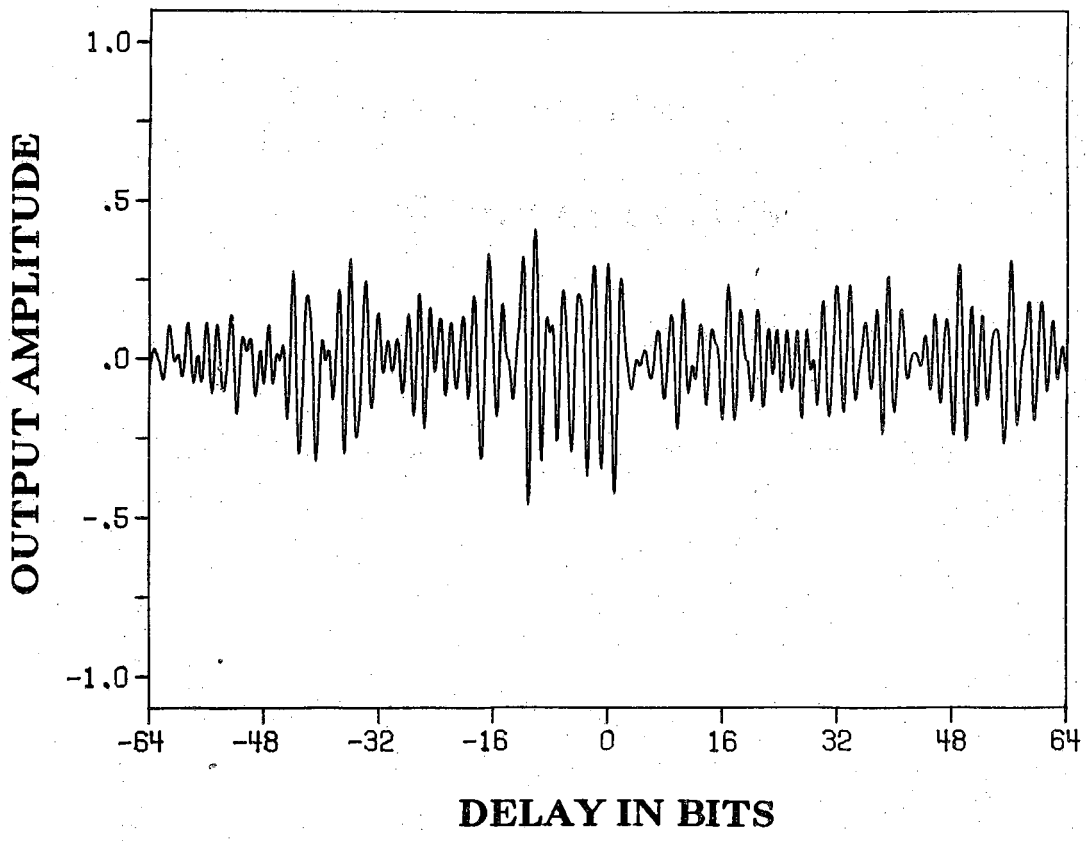

a. 512, 64 bit sections of a 8,388,607 bit m-sequence.

Figure 5–7 Typical correlator scans of a large grain stainless steel target.

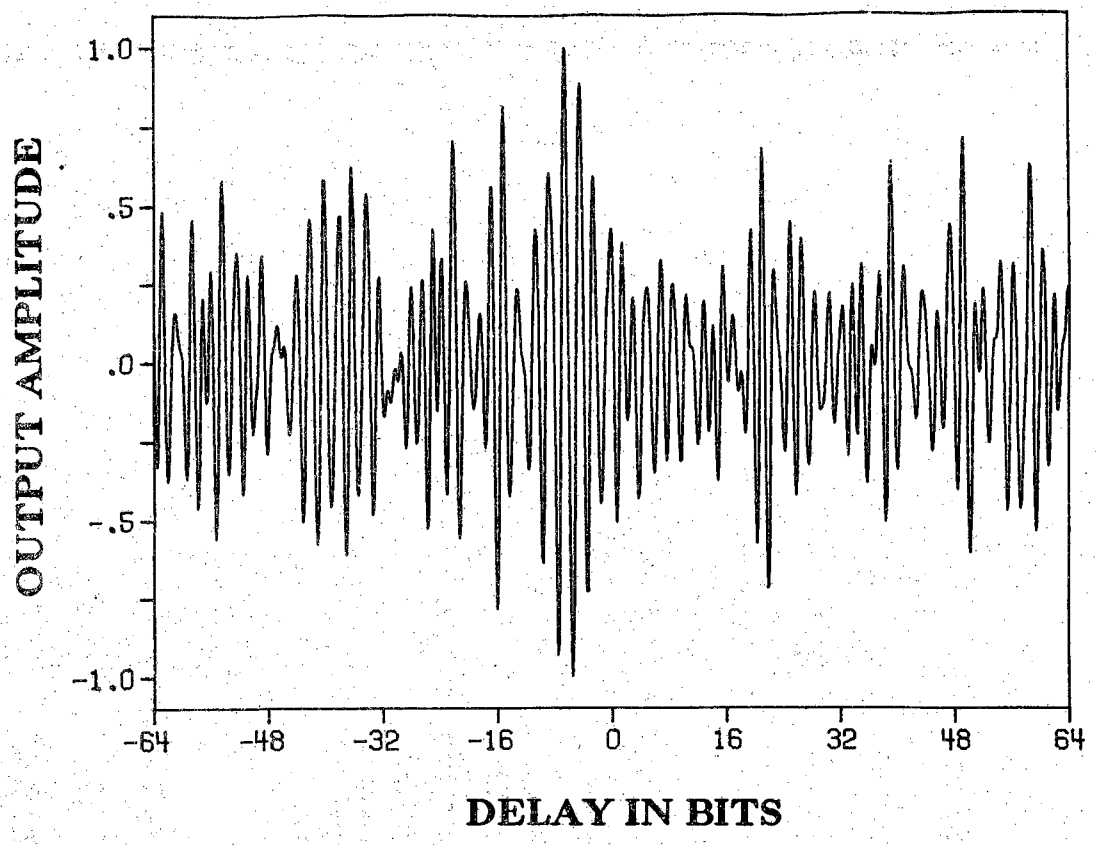

b. 63 bit m-sequence (same scale as a.).

Figure 5–7 (continued).

calculated upper bound for the added clutter noise together with the experimental measurements. The dispersion in the measurements at each value of N can be accounted for by variations in the power present in the range sidelobes of the different codes tested. These measurements verify the predicted $1/N$ variation of the added clutter noise and indicate that the practical value of r is approximately 1/2.

An additional set of clutter measurements was made by varying the length of the transmitted m-sequence, n, while integrating over a single transmitted burst. Since the integration time and repetition rate were held constant as the transmit burst length increased, the duty cycle increased in direct proportion to the burst length. In the lowpass filter approximation to equation (3.5) the normalizing factor, αT, is missing, so that the correlation output increases in direct proportion to the duty cycle and the output power thus increases as the square of the duty cycle. Figure 5-9 shows the calculated upper bound of the added clutter noise and the experimental values for C_o determined by subtracting C_o from the total measured clutter power. Three codes were tested at each value of n and, as can be seen, the experimental values are again slightly dependent on the particular transmit code. The results of a linear regression fit to the data indicated a slope of approximately two as predicted by a square law dependence on α. Since the output power from a target imbedded in the clutter would also increase with the square of the duty cycle, Figure 5-9 demonstrates the independence of SCR in terms of the number of bits per transmitted burst as predicted by equation (3.19). Having verified the results of the clutter analysis given in equation (3.21), we can now proceed with an overall system performance analysis.

System Performance Analysis

Examination of equation (3.23) reveals that there exist three distinct sources of noise which degrade the performance of a random or pseudo-random signal correlation receiver. To compare the operating characteristics of the correlation system with conventional flaw detection systems, the effect of each of the noise sources will be examined. The response of the correlation system to the various noise sources will dictate the circumstances under which a correlation system can be used effectively to replace conventional pulse-echo systems.

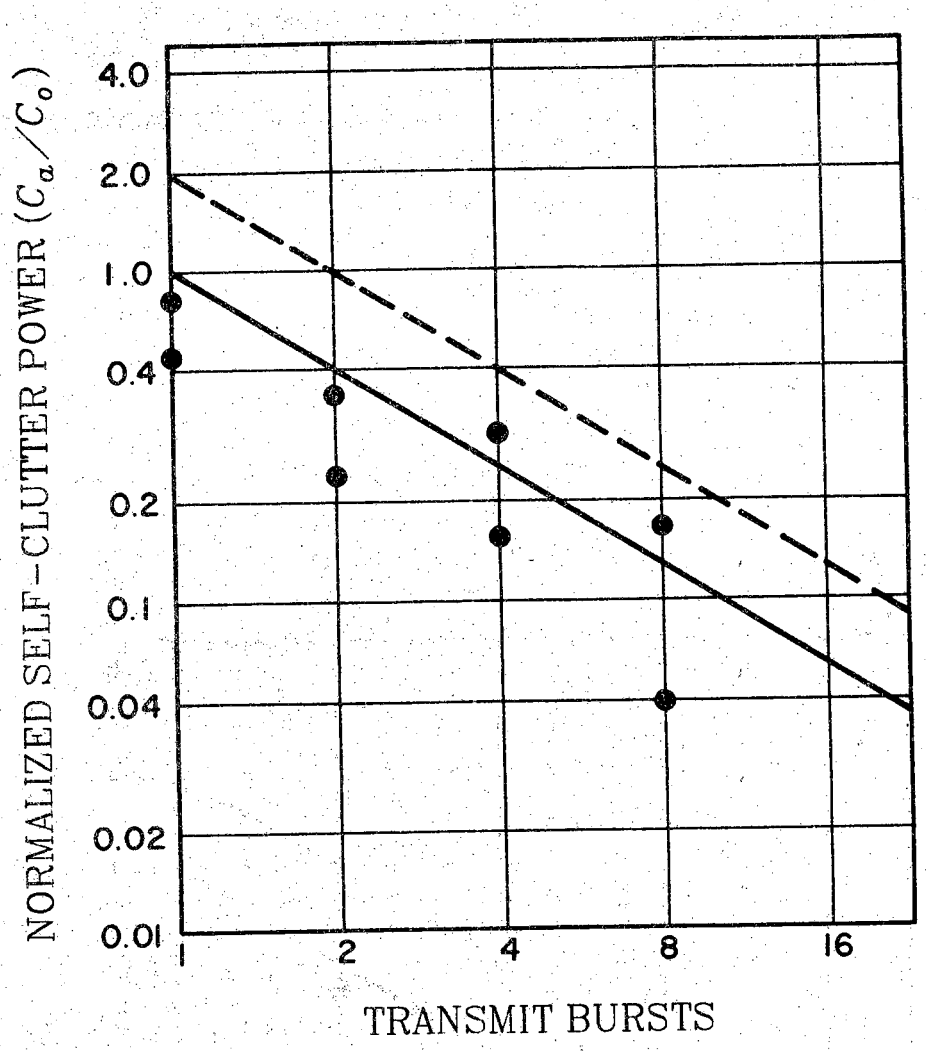

Figure 5–8 Experimental measurements of added clutter power as a function of the number of transmit bursts.

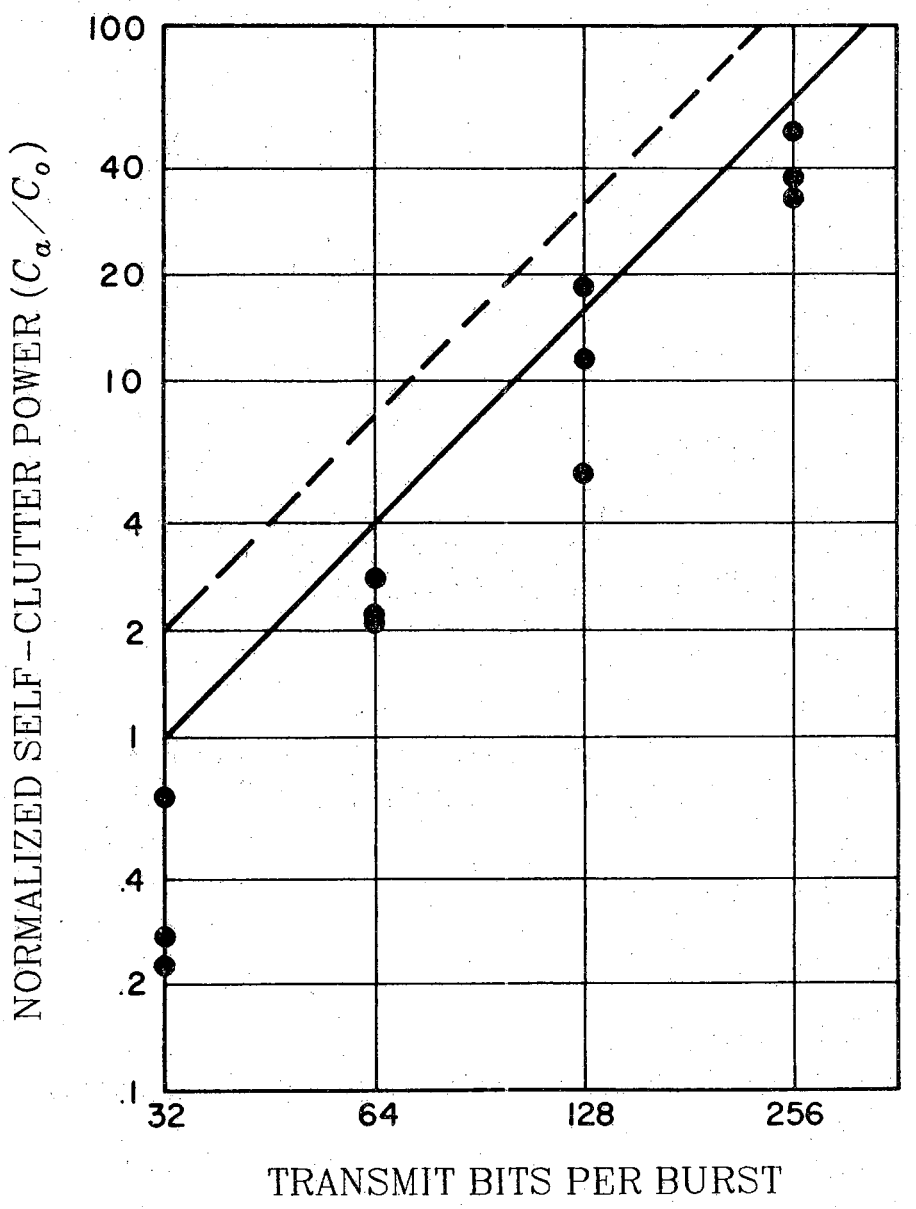

Figure 5–9 Experimental measurements of added clutter power as a function of the number of transmit bits.

High Input *SNR* Operation

The first source of noise to be considered, self-noise, is an unfortunate consequence of incomplete pulse compression. In those circumstances where the echo signal is much larger than the thermal receiver noise, so that $P \gg \eta$, the self-noise of the correlation function imposes a fundamental limitation on system performance. This limitation is of particular importance when high speed or real time imaging is required for targets which provide strong ultrasonic echoes.

The requirement of high speed operation usually translates to a severe restriction on the number of transmit pulses, so that $N \simeq 1$. An additional limitation will be imposed by the minimum target range. Consequently, the maximum width of the transmitted burst will also be restricted. Assuming temporarily that clutter is not important in such imaging, equation (3.23) reduces to

$$SNR \simeq \frac{P}{P(b/nN)} = \frac{nN}{b} = nN\delta B. \tag{5.1}$$

This is the reciprocal of the upper bound on the relative sidelobe power level predicted by equation (3.12).

For a transducer of 5 MHz center frequency and 2 MHz bandwidth with a 10 μs limit on pulse duration, the *SNR* will be only 13 dB. This is a signal-to-noise ratio similar to the *SNR* of the signals presented in Figures 5-3 and 5-4. Equation (5.1) shows that the output signal-to-noise ratio for this self-limiting case is independent of the transmit power, P, so long as the returned echoes are larger than the noise introduced by the receiving system. Clearly this is not a situation in which a correlation system would be of much benefit. Fortunately, this situation is of little practical importance since by assumption conventional pulse-echo systems can be used to produce high quality images.

Clutter Limited Operation

A more interesting situation arises when the receiving system is clutter limited. To define this situation, we first assume that the clutter signals are larger than the noise introduced by the receiving system. Since the comparison is being made with a conventional pulse-echo system, we require that

$C_o >> \eta$. However, in order to detect a target with any linear detection system we must also have $P > C_o$, otherwise the target will be lost in the clutter noise. In the clutter limited case, equation (3.23) reduces to

$$SNR \simeq \frac{P}{C_o(1 + \frac{2r}{N}) + P(\frac{b}{nN})}. \tag{5.2}$$

This suggests that the performance of the random signal or m-sequence correlation system may again be limited by the range sidelobes of the correlation function associated with the desired target. To ensure that this is not the case, we assume that $C_o(1 + 2r/N) > P/n\delta BN$ and apply the above inequalities to yield the weak condition $(N+2r)(n\delta B) > (P/C_o) > 1$. This condition is easily satisfied by utilizing a transmit burst which is slightly longer than that used in a pulse-echo system. Thus, for almost any correlation system, the *SNR* presented in equation (5.2) reduces to the *SCR* formula given previously as equation (3.21). Therefore, in the case of real time imaging with only one transmit burst, $N = 1$, equation (3.21) predicts that in the worst case, $r = 1$, the correlation system will provide a signal-to-noise ratio within 4.8 dB of pulse-echo systems. However, the grain measurements of Figure 5-5 indicate that the value of r is approximately 1/2 and that in an actual clutter situation the signal-to-noise ratio of the random signal or m-sequence correlation system is within 3 dB of a pulse-echo system.

Although the performance of the random signal or m-sequence correlation system is slightly inferior to that of a pulse-echo system, as the number of unique transmit bursts which are correlated is increased, the performance of random signal or m-sequence correlation system rapidly approaches that of an ideal pulse-echo system. It is important to note that the additional clutter noise present in the correlation system output can appear in two distinct forms depending on the type of transmitted signal. In the case of the random signal system, the small additional noise term will appear as random noise in the output. For an m-sequence system which interrogates each range cell with the same code or set of codes, the additional noise will appear as a deterministic signal which can be exactly reproduced on successive scans of the clutter.

Practical Clutter Situations

The clutter limited case, as presented above, is somewhat artificial since the assumption of strong clutter signals implies that considerable energy is scattered out of the ultrasound beam. Thus with increasing depth, the scattering losses will rapidly reduce the backscattered energy level to values comparable to the receiver noise. A more realistic description of the case where strongly reflecting clutter targets are present is $C_o \simeq N$ or $C_o < N$. To detect a target, we must still require that $P > C_o$. Thus as discussed above, self-noise produced by the range sidelobes of the target will not play an important role.

In the practical case of clutter dominated performance, equation (5.24) becomes

$$SNR = \frac{P}{C_o(1 + \frac{2r}{N}) + \eta(\frac{b}{nN})} . \tag{5.3}$$

Even for relatively high speed operation, $N \simeq 4$, with $r = 1/2$ the clutter noise level will be nearly the theoretical minimum, C_o, thus

$$SNR \simeq \frac{P}{C_o + \eta(\frac{b}{nN})} \tag{5.4}$$

As the inspection depth within the clutter region increases, both the target signal power, P, and the clutter noise power, C_o, will decrease relative to the receiver noise due to scattering losses and absorption. Equation (5.44) clearly demonstrates, however, that by appropriate selection of the code length and the number of transmit bursts, the random or pseudo-random signal correlation system can maintain ideal clutter limited performance throughout the scan range. To obtain similar performance using a pulse-echo system, coherent averaging of the received echoes could be utilized. In this frequently encountered situation, the correlation system offers a significant advantage in operating speed. The random signal correlation system will be faster by a factor of n/b since it effectively combines pulse compression with coherent time averaging.

Receiver Noise Limited Operation

The final case to be considered is noise limited performance. An extreme example of this situation can be found in the inspection of plastics and composites for which $C_o \simeq 0$. More frequently encountered situations are the inspection of ceramics or thick metal sections where absorption and scattering from small grains severely reduce the echo intensities, although grain echoes as such are not the limiting factor.

In the receiver noise limited case, the signal-to-noise ratio for the random signal or m-sequence correlation system takes the simple form

$$SNR \simeq \frac{nN}{b}\left(\frac{P}{\eta}\right), \tag{5.5}$$

which is the product of the *SNRE* given in equation (5.9) and the *SNR* for a conventional pulse-echo system.

Optimum System Threshold Criterion

In order to determine the optimum imaging system for a given application it is helpful to have a threshold level dictating which system, conventional pulse-echo or random signal/m-sequence correlation, will produce a higher output signal-to-noise ratio. Assuming that the signal-to-noise ratio for a conventional pulse-echo system is given by equation (3.22) with $r = 0$ and $b/(nN) = 1$, the ratio of equation (3.23) to the special case of equation (3.22) can be considered to be an extension of the signal-to-noise ratio enhancement formula of equation (3.9) to include the effects of clutter and self-noise, and is given by

$$SNRE = \frac{C_o + \eta}{C_o\left(1 + \frac{2r}{N}\right) + P\left(\frac{b}{nN}\right) + \eta\left(\frac{b}{nN}\right)} \tag{5.6}$$

Rearranging equation (5.6), by applying the condition that the *SNRE* be greater than unity, results in the threshold condition

$$\eta > \frac{Pb + C_o 2rn}{nN - b}. \tag{5.7}$$

which indicates the level of receiver noise for which a random signal or m-sequence correlation system will provide a better output signal-to-noise ratio than a conventional pulse-echo system. If $n \gg Pb/(C_o 2r)$ and $nN \gg b$ then equation (5.7) can be simplified to the form

$$\frac{C_o}{\eta} < N \tag{5.8}$$

and the correlation system will produce a higher signal-to-noise ratio than a conventional pulse-echo system if the clutter-to-noise ratio is less than N. In applications where the clutter-to-noise ratio is greater than N it will be necessary to use the special codes described in the following chapter.

CHAPTER VI - A HIGH-SPEED DIGITAL GOLAY CODE CORRELATION SYSTEM

In order to use a correlation system under high input signal-to-noise ratio situations and high-speed operation, it would be advantageous to use pseudo-random codes which produce correlation outputs with zero range sidelobes. The output *SNR* would then be given by

$$SNR = \frac{P}{C + \frac{\eta}{nNB\delta}}. \tag{6.1}$$

The output signal-to-noise ratio of a conventional pulse-echo system is

$$SNR = \frac{P}{C + \eta}. \tag{6.2}$$

These equations indicates that if $nNb\delta$ is chosen to be greater than unity, a zero self-noise correlation system will always produce a better output signal-to-noise ratio than a conventional pulse-echo system, shown in equation (6.2), or previous correlation systems, shown in equation (3.23). However, under many conditions the difference in *SNR* of a zero self-noise correlation system compared to previous correlation systems may only be significant for low values of N, i.e., high operation speed. As mentioned in Chapter IV, two types of pseudo-random codes have been discovered which can be used to produce zero range sidelobes – continuously transmitted m-sequences and Golay codes. Since m-sequences cannot be used in a pulse-echo mode using a single transducer, this study concentrates on developing and analyzing an improved system which uses Golay codes.

In an actual correlation system employing Golay codes, the sidelobes will not cancel completely, resulting in vestigial sidelobes. The *SNR* of such a system can then be represented as a modified version of equation (3.23) such that

$$SNR = \frac{P}{C_o(1 + rq) + \eta(b/nN) + P(b/(2n))q}, \tag{6.3}$$

where $N = 2j$, such that j is a positive integer, and the ratio q is defined as

$$q = \frac{2(\textit{average vestigial power})}{\textit{average power in the sidelobes for one burst}}. \tag{6.4}$$

The factor 2 is included since in correlation systems which do not use Golay codes, two-burst correlation reduces the power in the sidelobes by the factor 2.

However, if a different set of Golay code pairs is transmitted every second burst, the vestigial sidelobes will be reduced relative to the peak power. If the vestigial sidelobe signal for different Golay code pairs are considered to be uncorrelated noise signals, the power in the sum of these vestigial sidelobe signals will reduce as $2/N$ relative to the peak signal power. The SNR for such a system is then

$$SNR = \frac{P}{C_o(1 + 2rq/N) + \eta(b/nN) + P(b/nN)q} \tag{6.5}$$

where $N = 2j$; such that j is a positive integer.

For very low input noise and clutter situations,

$$SNR \simeq q(nN/b) \tag{6.6}$$

Thus the available signal-to-noise is only dependent upon the self-noise cancellation produced in the system implementation.

System Description

The new Golay code correlation system shown in Figure 6-1 is a modification of the digital correlation system described in the previous chapter. The signal source generates the Golay codes according to the algorithms developed by Golay and loads them into the digital delay line. After waiting a predetermined delay period, the system control signals the digital delay line to

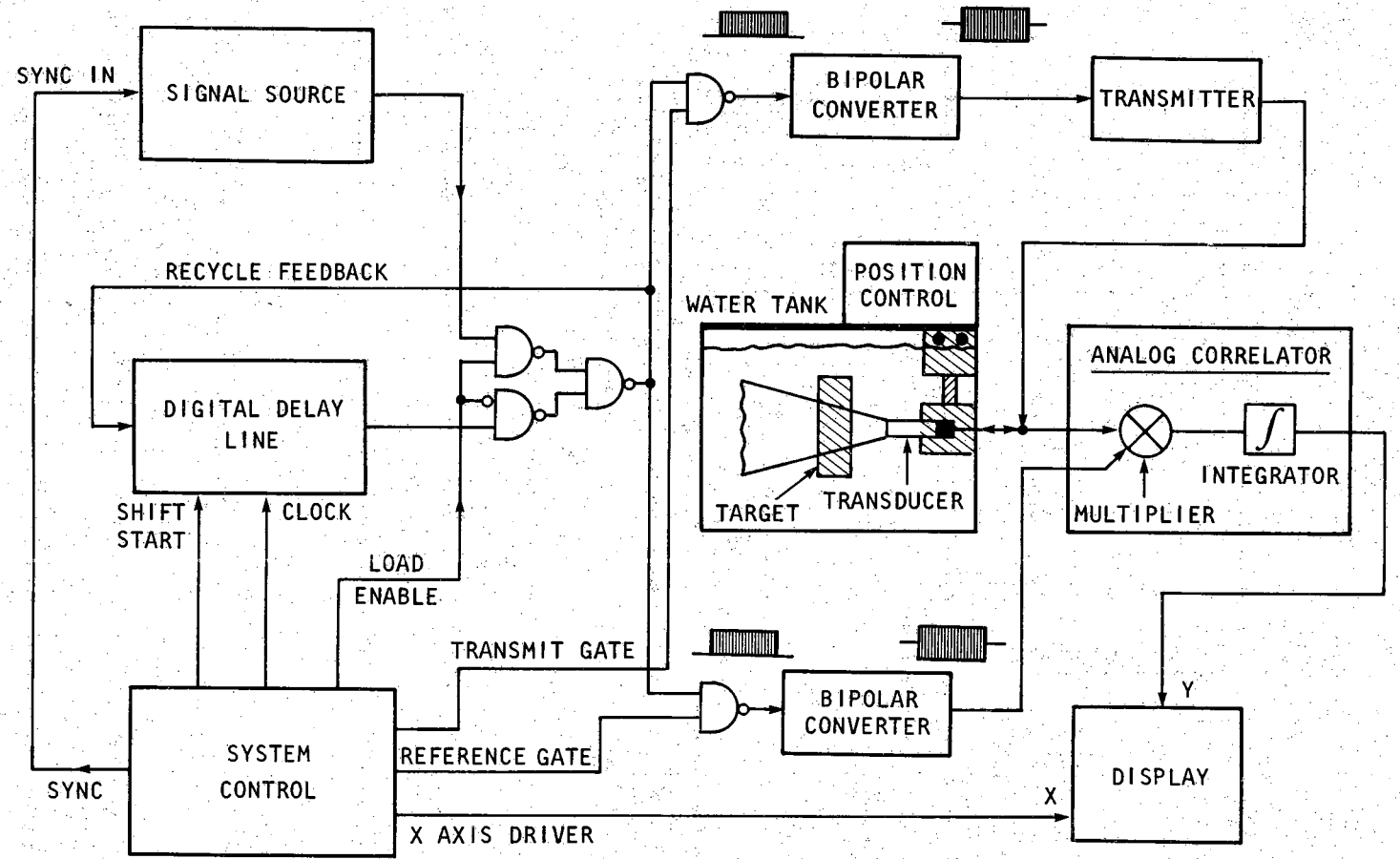

Figure 6–1 Single-mode digital Golay code correlation system.

unload the shift registers for correlation with the return echo signals. In this high-speed Golay code system, the contents of the delay line are recycled on every unload command, except during the initial load from the signal source. In practice, the source could either be a hard-wired generator or a microprocessor, since all control parameters in the new system are digital.

In order to sum the self-correlation functions (not autocorrelation functions since the transmitted signal is filtered by the transducer) from the two complementary codes, the codes were transmitted and correlated in a sequential mode. Two copies each of a 64 bit Golay code and its complement were stored sequentially in a 256 bit shift register. The contents of this shift register were circulated by 64 bits on each transmit or correlate cycle. When the integration time of the correlator is any multiple of the time required to transmit two bursts, the correlation functions of the two complementary Golay codes are effectively summed.

For the high-speed system the integrator was constructed using an operational amplifier. The integrator was reset to zero at the end of each integration interval by shorting a feedback capacitor with an FET. The integration value at the end of an integration interval was retained by a sample-and-hold until the end of the next integration interval. This output was either A/D sampled for computer processing or low-pass filtered for direct display. In previous correlation systems low-pass filters were used to approximate integrators [2, 3, 6]. However, unlike the integrator, the low-pass filter does not control the start and end of an integration interval as required to cancel self-noise in two transmit bursts. If a situation requires the correlation of many transmit bursts, as when a large signal-to-noise ratio enhancement is required, it will be shown that it is also possible to use a low-pass integrator to effectively sum the outputs from the complementary codes.

Computer Simulations of Single-Target Measurements

Computer simulations, generated for comparison, were implemented in the a manner slightly different than the computer simulations of the previous chapter in order to make the simulations match the actual measurements more accurately. The impulse response of a transducer, having approximately a 5 MHz center frequency and a 2 MHz bandwidth, was first measured experimentally and then approximated analytically using a cosine damped by two fourth-order exponential terms, corresponding to positive and negative

time. The Fourier transform of this simulated impulse response function yielded a simulated frequency response for the transducer, which was used to weight the spectrum of the autocorrelation function for the transmitted code. The inverse Fourier transform of this weighted spectrum then produced a simulated output for the correlation system, since it can be shown that the output of the correlation system is the convolution of the autocorrelation function with the impulse response of the system.

Single-Target Measurements

Measurements were made with the new Golay code system using a 5 MHz center frequency, 2 MHz bandwidth transducer, and using a shift register clock frequency of 10 MHz. This particular shift register clock frequency was chosen since it was shown in the optimum clock rate study of Chapter IV to be near optimal for a 5 MHz transducer. All measurements were made in a water tank using the flat end of a large cylindrical Plexiglas target to produce a single return echo.

Measured results using the new Golay code system, with the high-speed integrator and two transmit burst correlation, are shown in Figure 6-2. The outputs in Figure 6-2, parts a and b, are each for transmission of a single 64 bit member of a complementary Golay code pair and the output shown in Figure 6-2c is for the transmission of the two complementary Golay codes in sequential transmit bursts. For comparison, computer simulated results are shown in Figure 6-3. As can be seen, considerable cancellation of the range-sidelobes has occurred in the measured Golay code output of Figure 6-2c, and the measured Golay code results are essentially the same as the computer simulations and the ideal pulse-echo system output. However, residual range sidelobes are still noticeable in the Golay code output of Figure 6-2c, and are approximately 35 dB lower than the central peak. These residual range sidelobes are probably due to errors in pulse shape and pulse-width introduce during the bipolar conversion of the binary codes, therefore further improvement seems possible.

Nevertheless, the residual range sidelobes of the Golay code output are considerably lower than those of the output produced by sequential transmission of two different 63 bit m-sequences, as shown in Figure 6-4 (An additional bit was added to the end of each m-sequence, equal to the beginning bit of each code to make implementation easier). Furthermore, it would

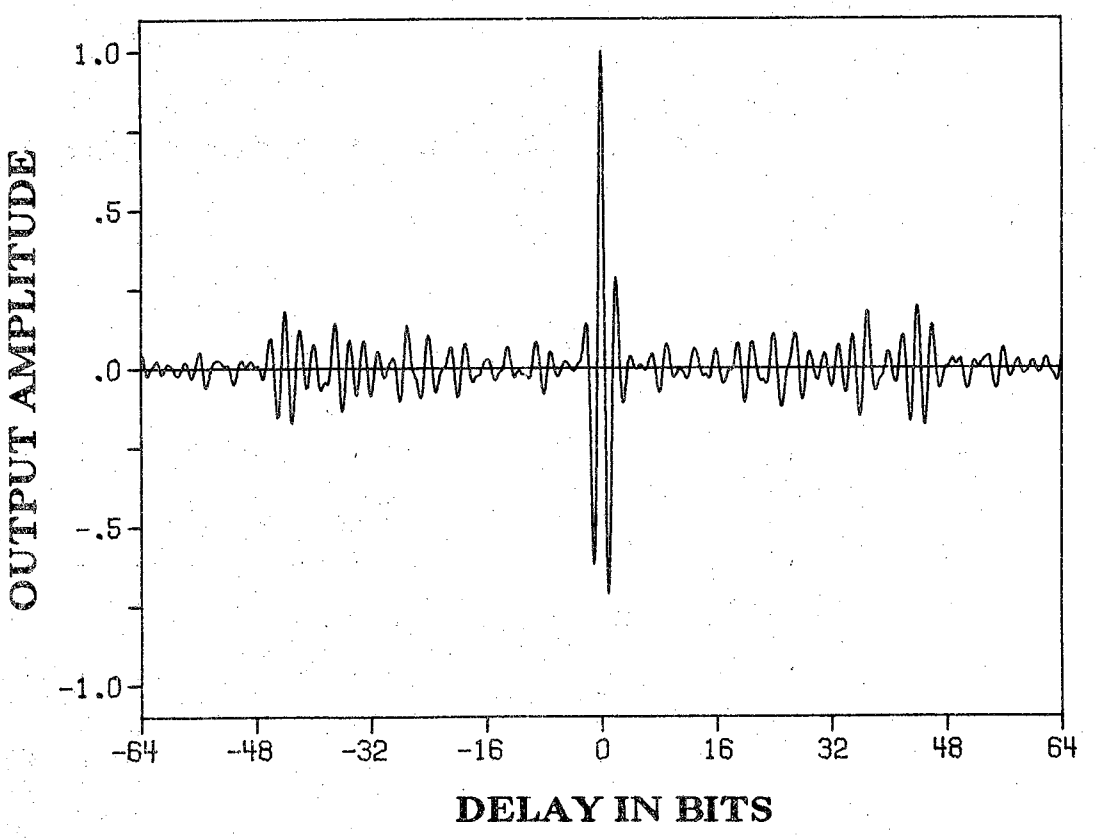

a. Measured self-correlation function of Golay code A.

Figure 6–2 Measured Golay code self-correlation functions.

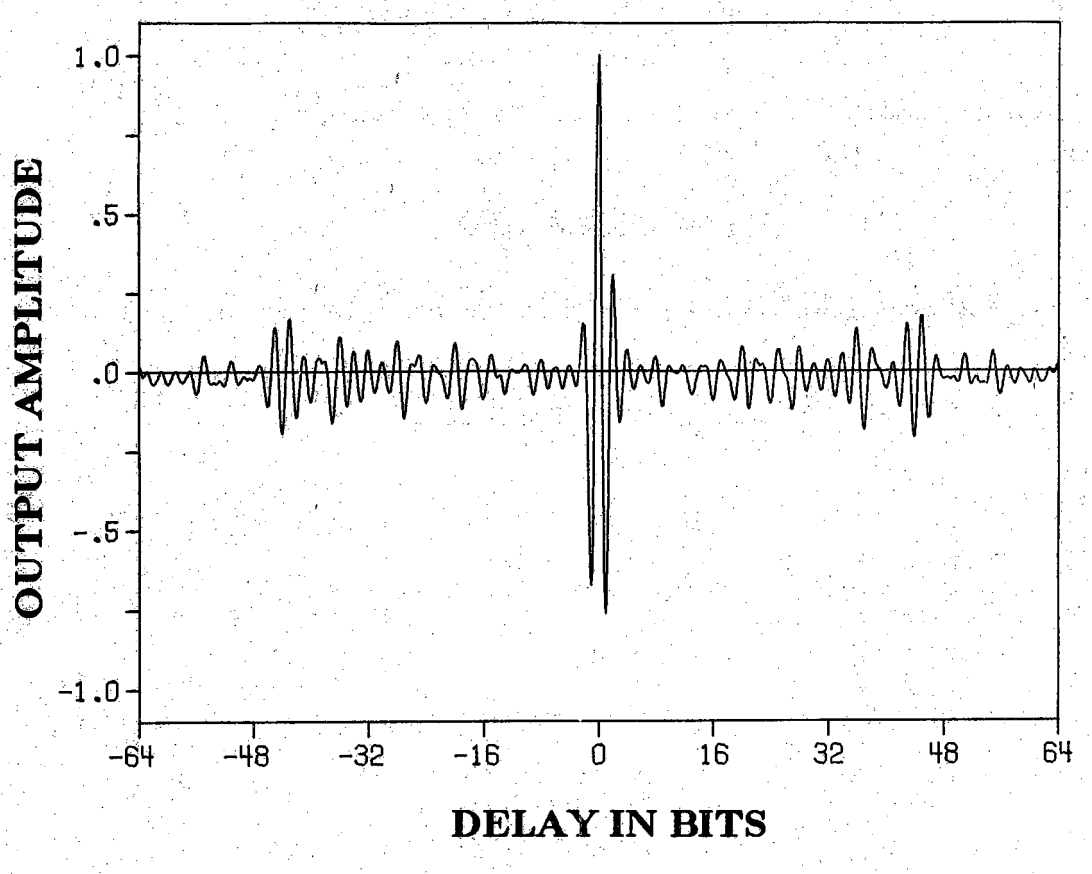

b. Measured self-correlation function of Golay code B.

Figure 6–2 (continued).

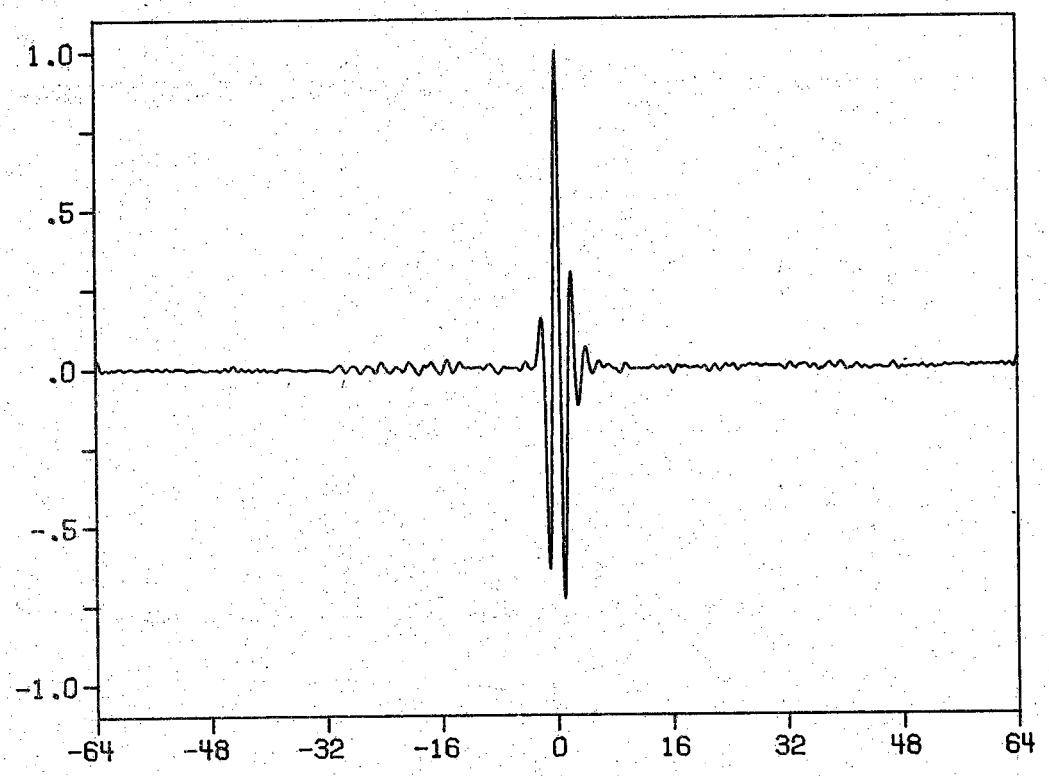

c. Measured self-correlation function when Golay codes A and B are transmitted alternately.

Figure 6–2 (continued).

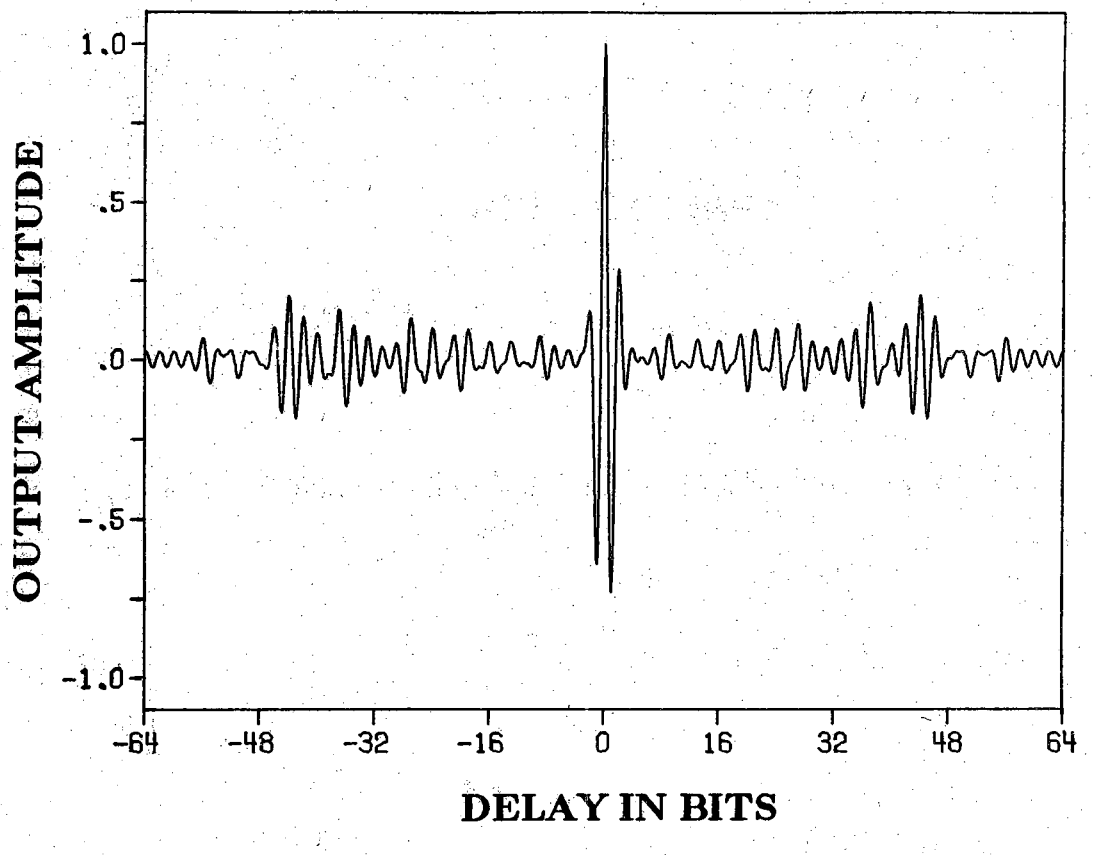

a. Computer simulation of self-correlation function of Golay code A.

Figure 6–3 Computer simulated Golay code self-correlation functions.

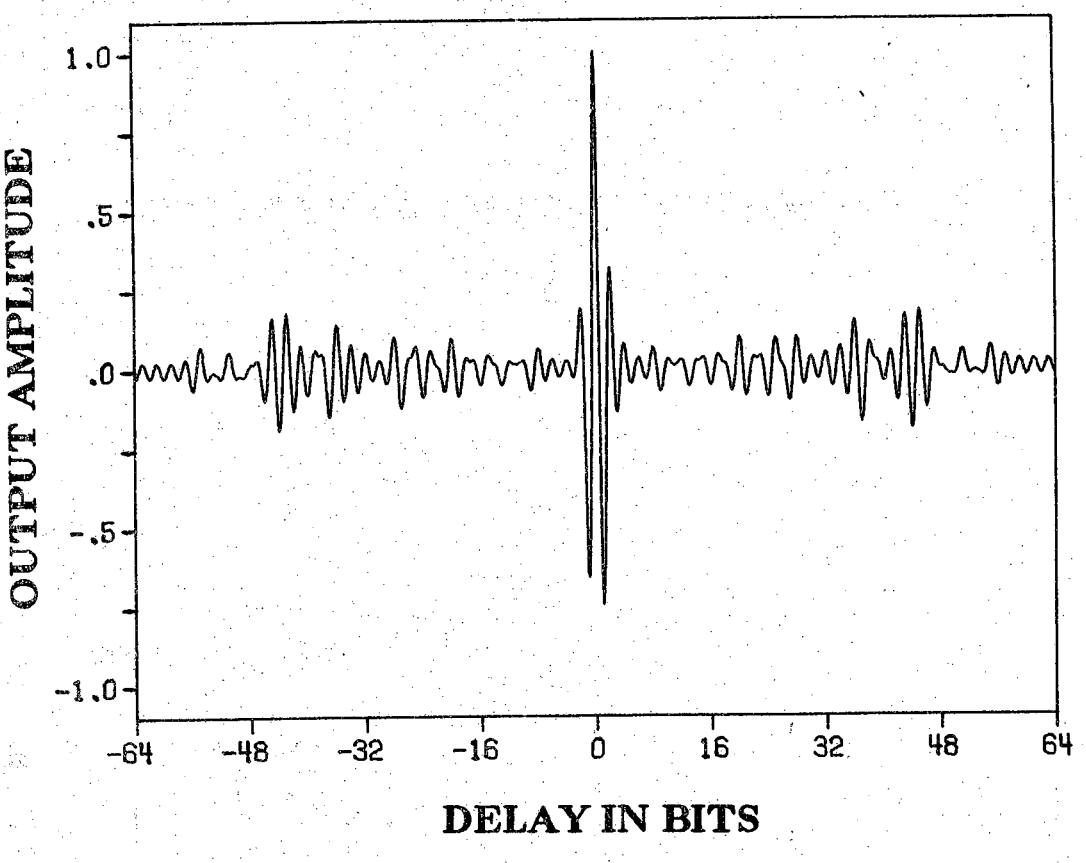

b. Computer simulation of self-correlation function of Golay code B.

Figure 6–3 (continued).

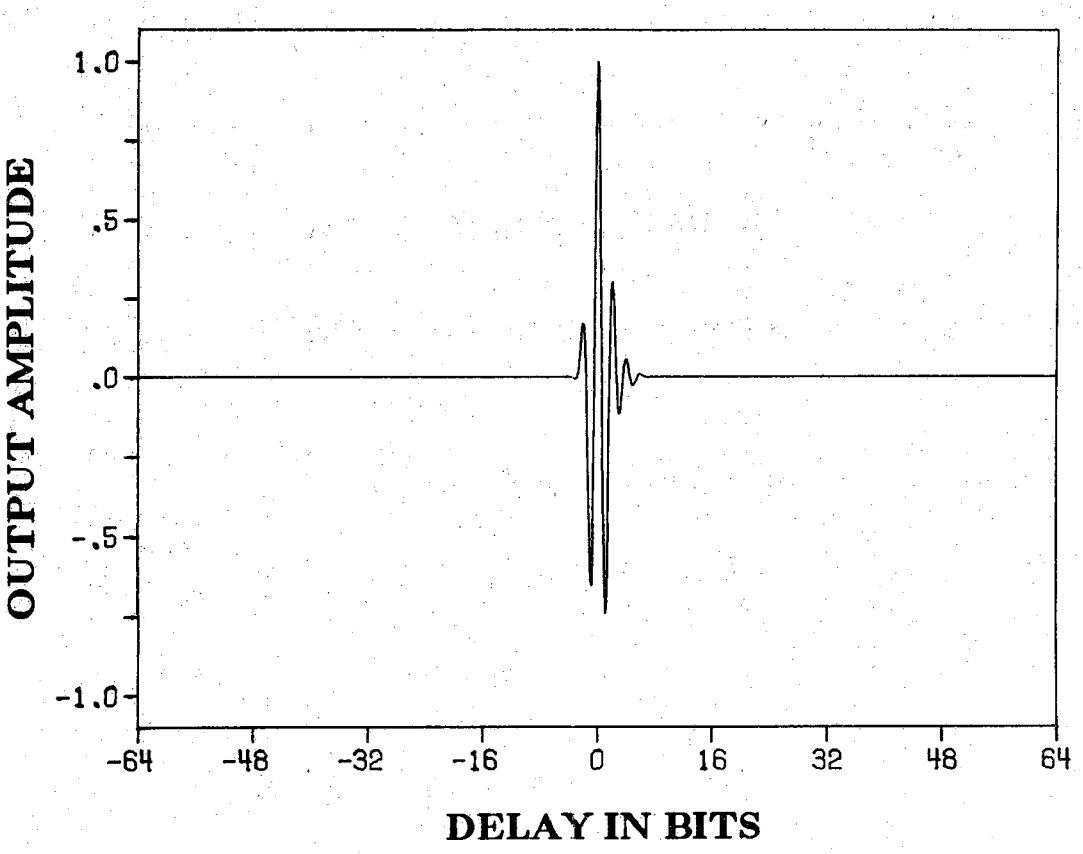

c. One-half the sum of computer simulations a. and b.

Figure 6–3 (continued).

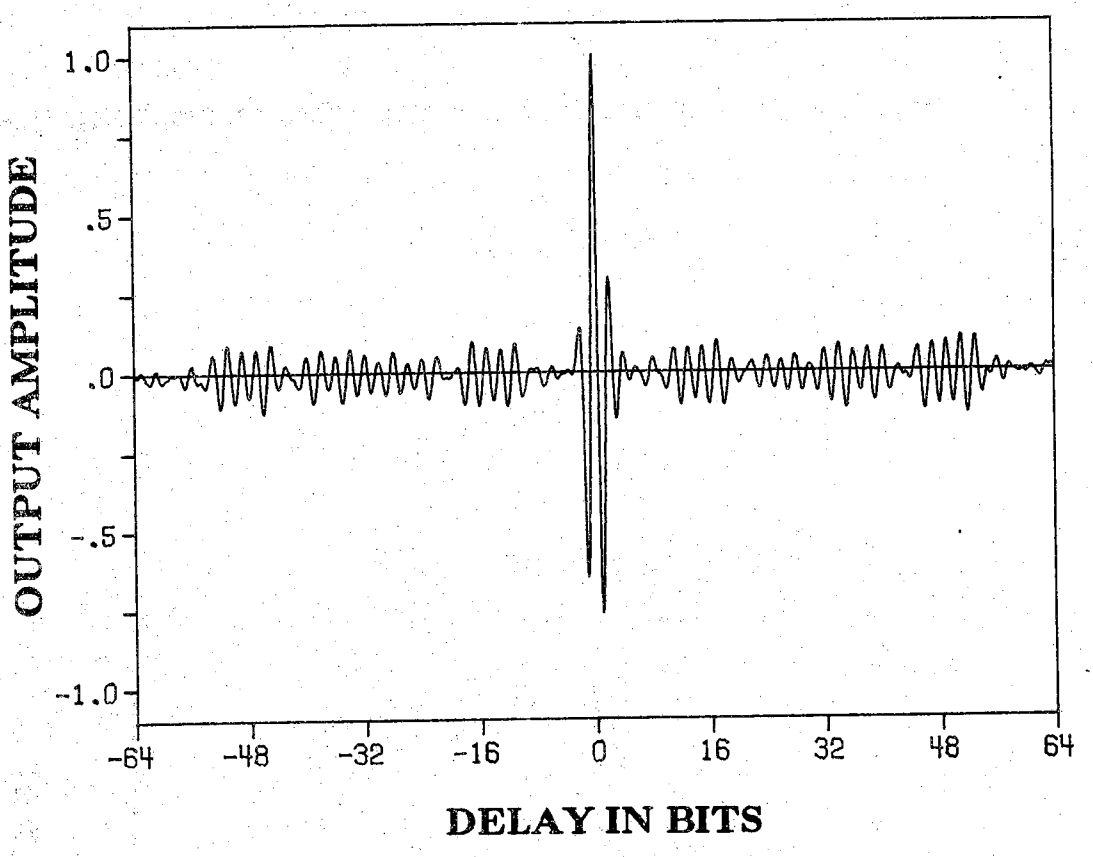

Figure 6–4 Output of a correlation system using a high speed integrator for sequential transmission of two different 63 bit m-sequences

require correlation of approximately 258, 64 bit sections of a long m-sequence, as shown in Figure 6-5, to produce range sidelobe levels equivalent to the Golay code output which was achieved in only two transmit bursts.

Several additional measurements were made to determine whether a low-pass filter, used to approximate an integrator in previous correlation systems, could also be used to cancel the self-noise. To determine this, the high-speed integrator was replaced by a four-pole Butterworth low-pass filter with a 3 dB cutoff frequency chosen to correspond to an integration time of two transmit periods. High-speed operation, using sequential transmission of the same Golay code pair as before and two burst correlation with the low-pass filter produced the output shown in Figure 6-6. As can be seen, the self-noise cancellation is poor and the shape of the impulse response is distorted. The distortion results from spreading of energy between range cells since the low-pass integrator is not cleared between range cells. The poor self-noise cancellation occurs in part for the same reason as the distortion and also because the correlation level for a burst of code decays between transmit bursts. However, if the system is adjusted to correlate more bursts per cell with a corresponding change in the low-pass filter bandwidth to integrate over the required number of transmit periods, the cancellation improves, and even if as few as 18 bursts are correlated per range cell, low-pass integration produces essentially the same output as the high-speed integrator, as shown in Figure 6-7.

Grain Measurements

Further measurements were also made to test the Golay code system operation in the presence of grains. For sequential transmission of two 64 bit complementary Golay codes, an A-scan of the grain sample appeared as in Figure 6-8a. The power of this signal is about 2/3 as large as the power of the grain scan produced by the 63 bit m-sequence, Figure 5-7b. This result is as expected since there is a large reduction in sidelobe level when using Golay codes. As a more fair comparison, a grain scan was made using sequential transmission of two 63 bit m-sequences, Figure 6-8b. The power of this signal is slightly lower than the power in the signal of Figure 5-7b and is still larger by a factor of about 1.2 than the power in the Golay code output.

From these results in the presence of single-targets and grainy materials, it is apparent that the Golay code system is optimal for all conditions involving stationary targets. Thus it the Golay code correlation system is ideal for

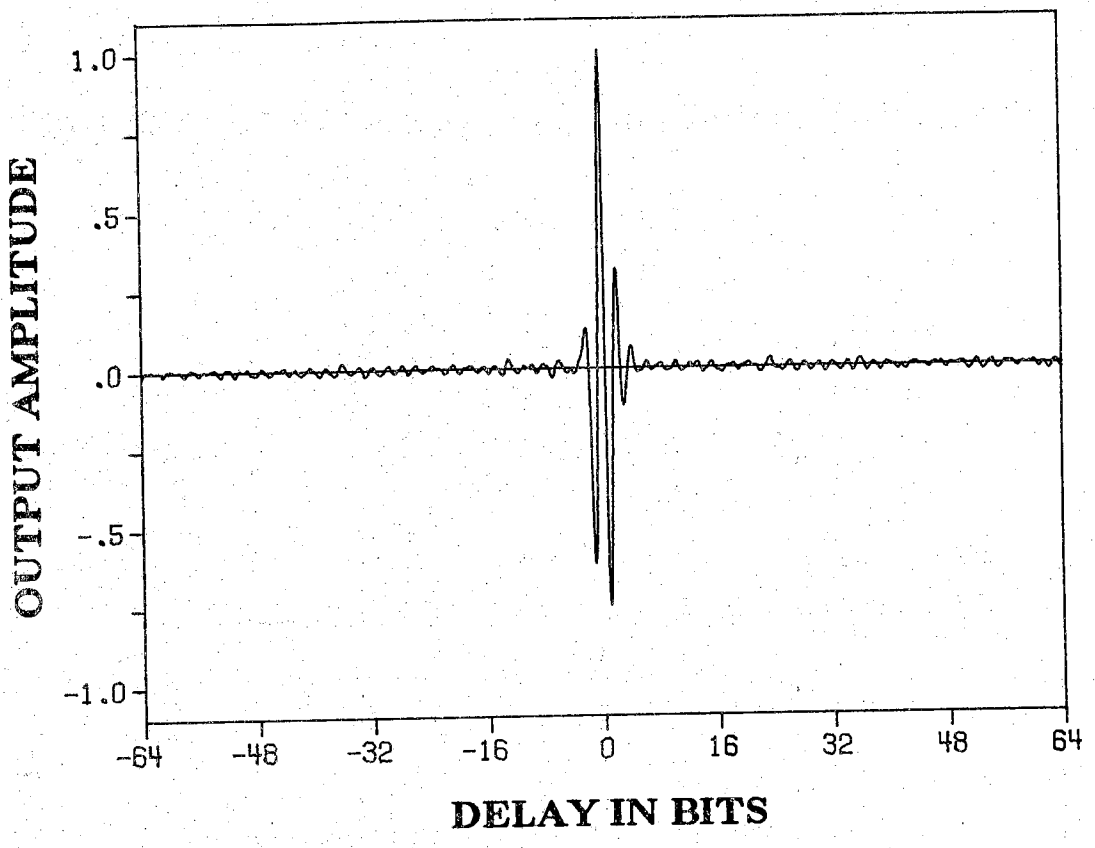

Figure 6–5 Output of a correlation system using a low-pass integrator for correlation of 258, 64 bit sections of an 8,388,607 bit m-sequence.

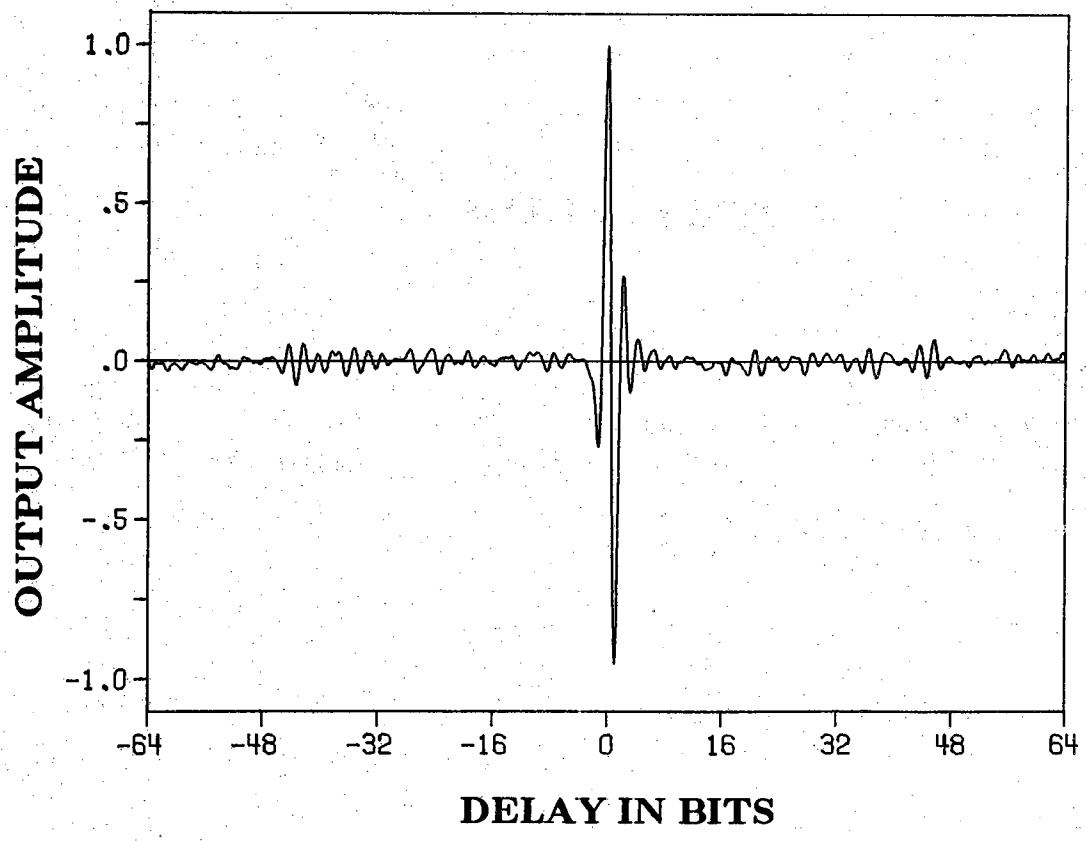

Figure 6–6 Golay code system output using a low-pass integrator with a two transmit period integration time.

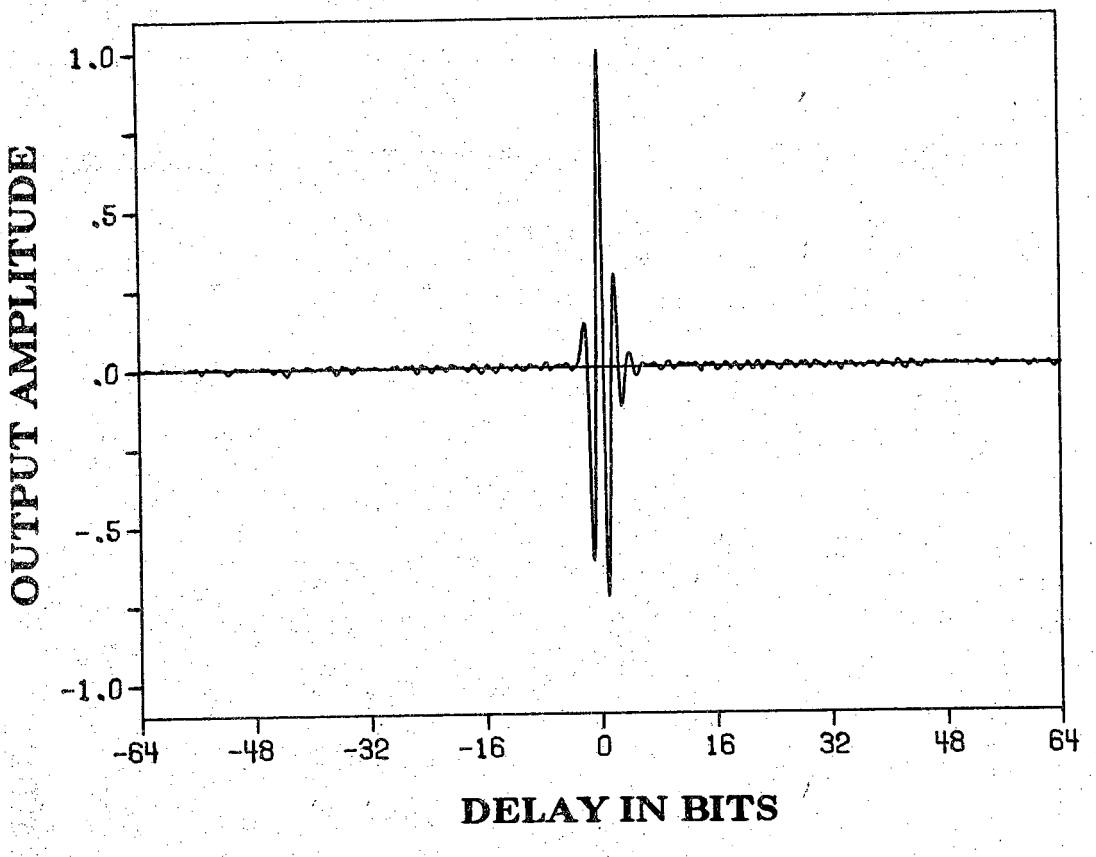

Figure 6–7 Golay code system output obtained using a low-pass integrator with an 18 transmit period integration time.

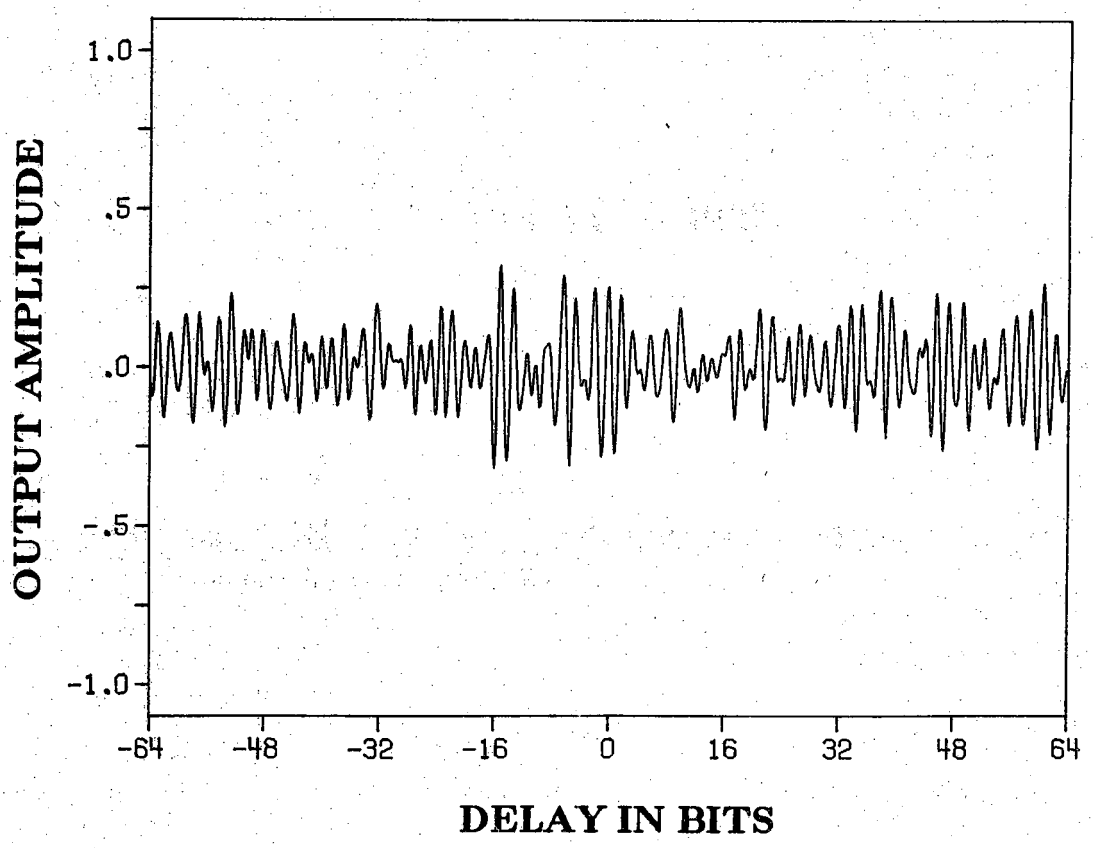

a. two 64 bit complementary Golay codes.

Figure 6–8 Correlation A-scan of a sample of large grain stainless steel using sequential transmission of

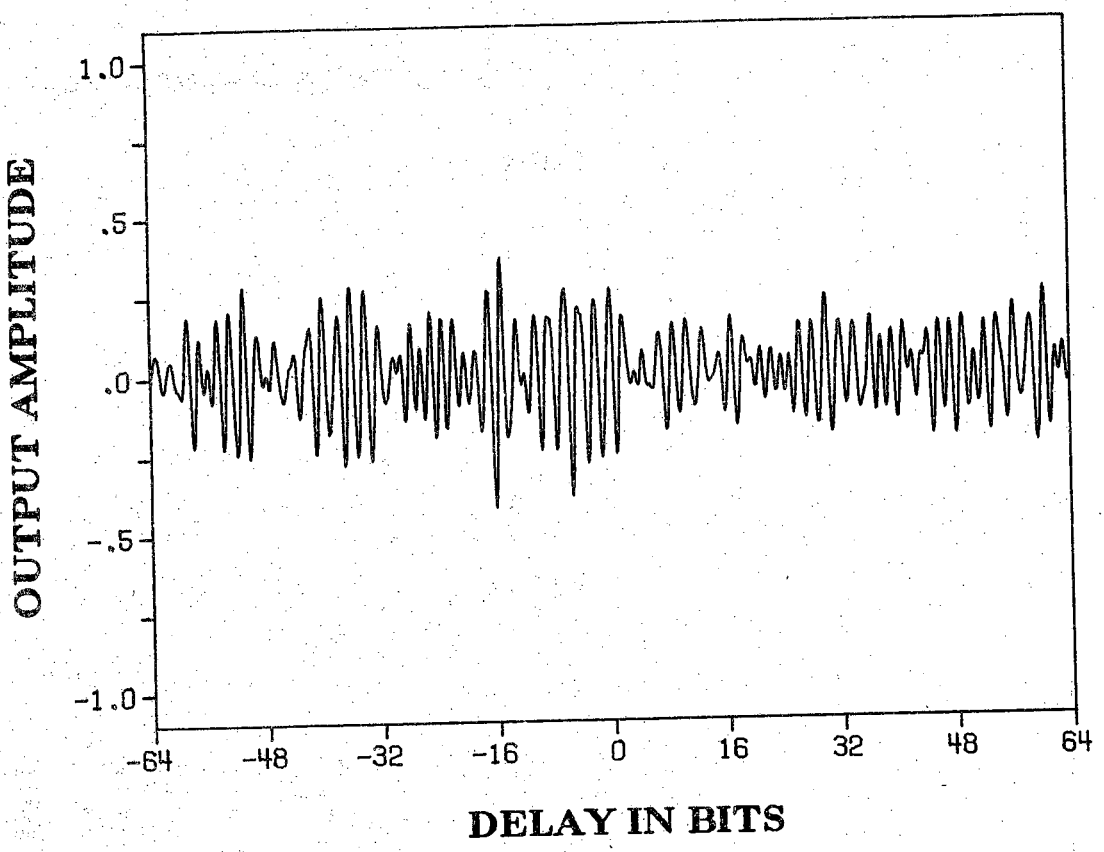

b. two 63 bit m-sequences.

Figure 6–8 (continued).

nondestructive testing applications. However, in more dynamic applications where the targets move, such as in medical applications, or radar and sonar applications with noncooperative targets, the targets will move between transmit bursts. As a result the correlation outputs may not properly align for the proper cancellation of the range sidelobes. To what extent the range sidelobes will cancel under the presence of a moving target is the topic of the next section.

Moving Target Simulation

The effects of moving targets on self-noise cancellation can be simulated by using the ambiguity function defined in equation (3.24). This ambiguity function simulation is straightforward and was carried out in the following manner:

The transmit waveform was first band limited in the frequency domain by truncating the spectrum at the first null, which corresponds to the code clock rate. This spectrum was then weighted using a Hamming window to reduce truncation sidelobes. An inverse digital Fourier transform was then calculated in which each discrete frequency component was shifted an amount in frequency corresponding to the velocity of the target. This produced a compressed time waveform corresponding to the received Doppler shifted waveform. The Fourier transform of the Doppler shifted wave form produces $A[\omega\nu]$. The generalized ambiguity function over τ, for a constant Doppler frequency shift ν, is then the inverse Fourier transform of the product of $A[\omega]$ and $A*[\omega\nu]$.

By varying the value of ν and calculating the inverse Fourier transform to produce a correlation function at each value of ν it is then possible to generate the generalized ambiguity function over all τ and ν of interest.

Since the Doppler shift, ν, is related to the target velocity by the relationship

$$\nu = \left[\frac{v}{v_p}\right] f_u, \tag{6.7}$$

where v is the target velocity, v_p is the velocity of propagation in the medium of interest, and f_u is the upper frequency response of the imaging system, it is

also possible to plot the ambiguity function in terms of target velocity.

However, if the ambiguity function were plotted in terms of absolute target velocity, the resulting ambiguity function would vary with the selected transmit repetition rate of the imaging system. In order to plot an ambiguity function which is independent of the repetition rate it is necessary to plot it in terms of a normalized velocity related to the repetition rate of the system, f_r. It is well known that in order that the Nyquist sampling criterion is not exceeded, we must have $\nu < \frac{1}{2} f_r$ so that the constraint on the velocity, v, is

$$v < \frac{1}{2} \left[\frac{f_r}{f_u} \right] v_p \tag{6.8}$$

The maximum unambiguous velocitys, v_a, which can be tracked is then

$$v_a = \frac{1}{2} \left[\frac{f_r}{f_u} \right] v_p . \tag{6.9}$$

We will thus define the simulated ambiguity functions in terms of the target velocity, v, normalized to this maximum unambiguous velocity, v_a.

Using this simulation approach the ambiguity functions were then simulated for sequential transmission of two complementary Golay codes, a single burst of an m-sequence, and for an ideal single transmit pulse for comparison. The simulated ideal ambiguity function for a ideal target locating system appears as shown in Figure 6-9. The "picket fence" indicates that the resolution in the range axis is determined by a triangular spike and that there is no resolution on the Doppler axis. Thus the motion of the transmitter or a target has no effect on the range resolution of the ideal correlation system.

The generalized ambiguity functions for a 31 bit m-sequence and for two 32 bit complementary Golay codes are shown in Figure 6-10. In the m-sequence ambiguity function the self-noise changes in form but remains essentially constant in power for different velocities. The Golay code ambiguity function, however, has zero self-noise for zero velocity but the self-noise increases with increasing velocity to approximately the same amplitude as the m-sequence self-noise. In order to get a more precise indication of the amount of self-noise cancellation which occurs a measurement of the ratio of peak power to the average self-noise power was made versus velocity as shown in

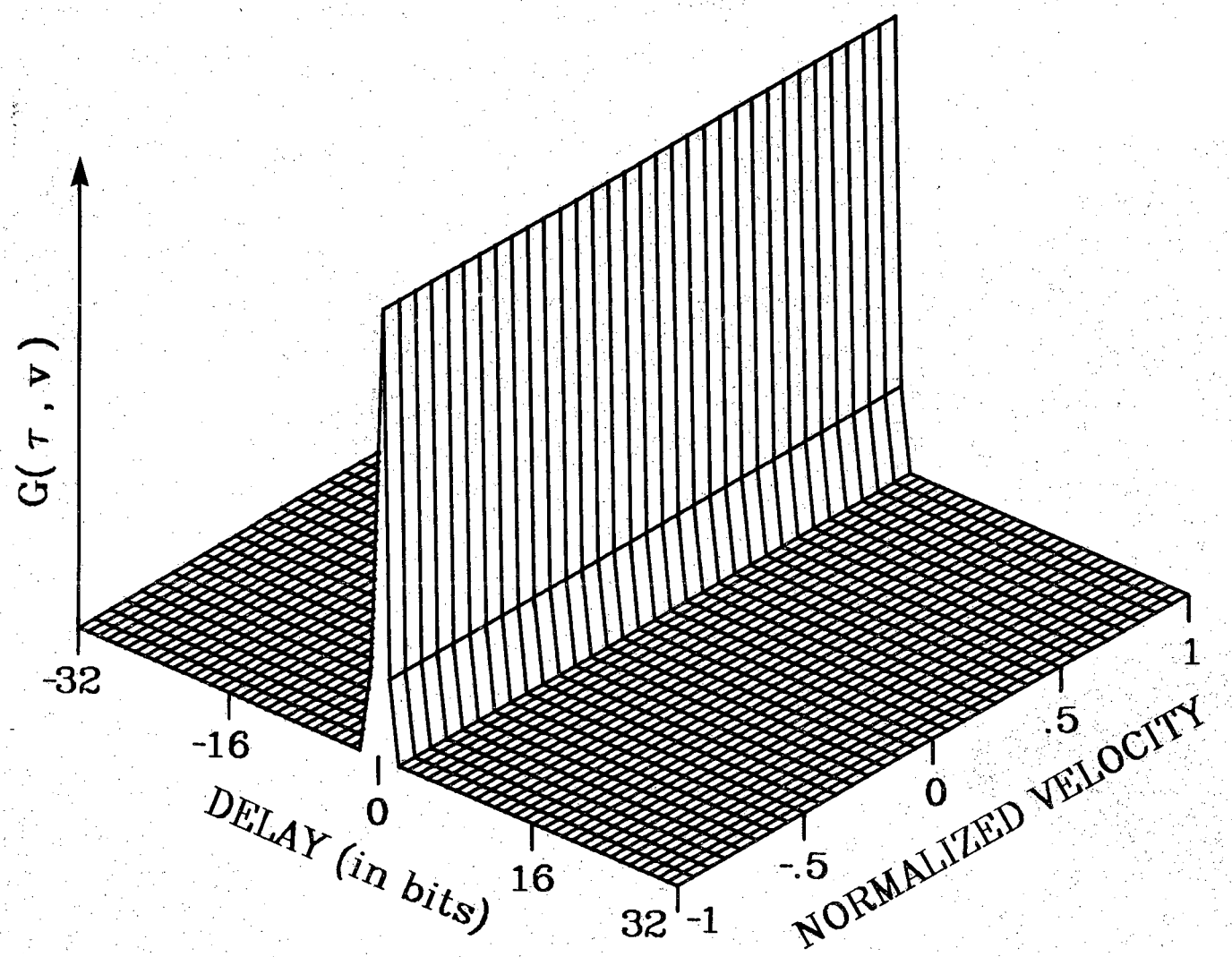

Figure 6–9 Generalized ambiguity function for a single pulse of width δ.

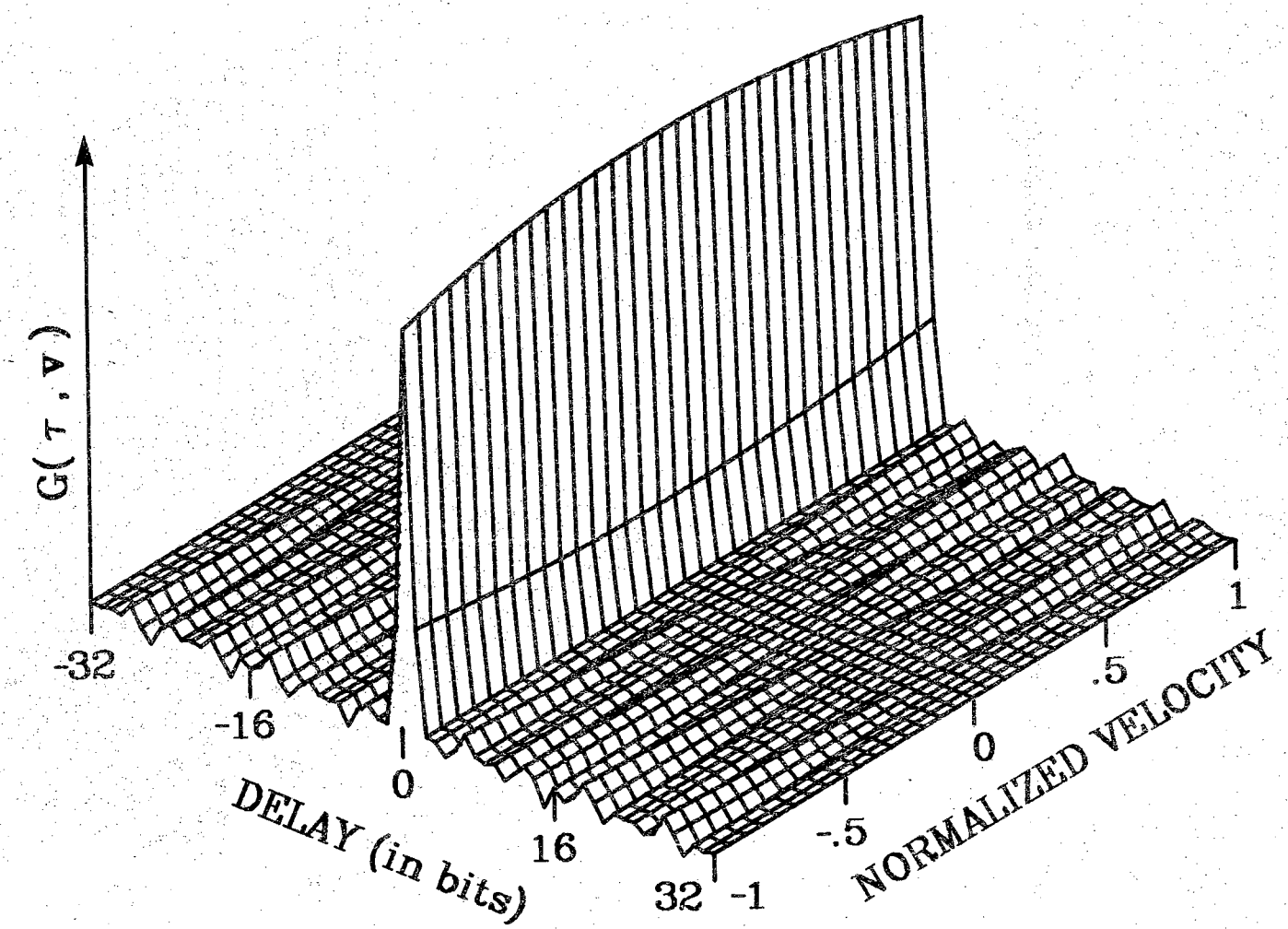

a. two 32 bit Golay code pairs.

Figure 6–10 Computer simulated generalized ambiguity functions.

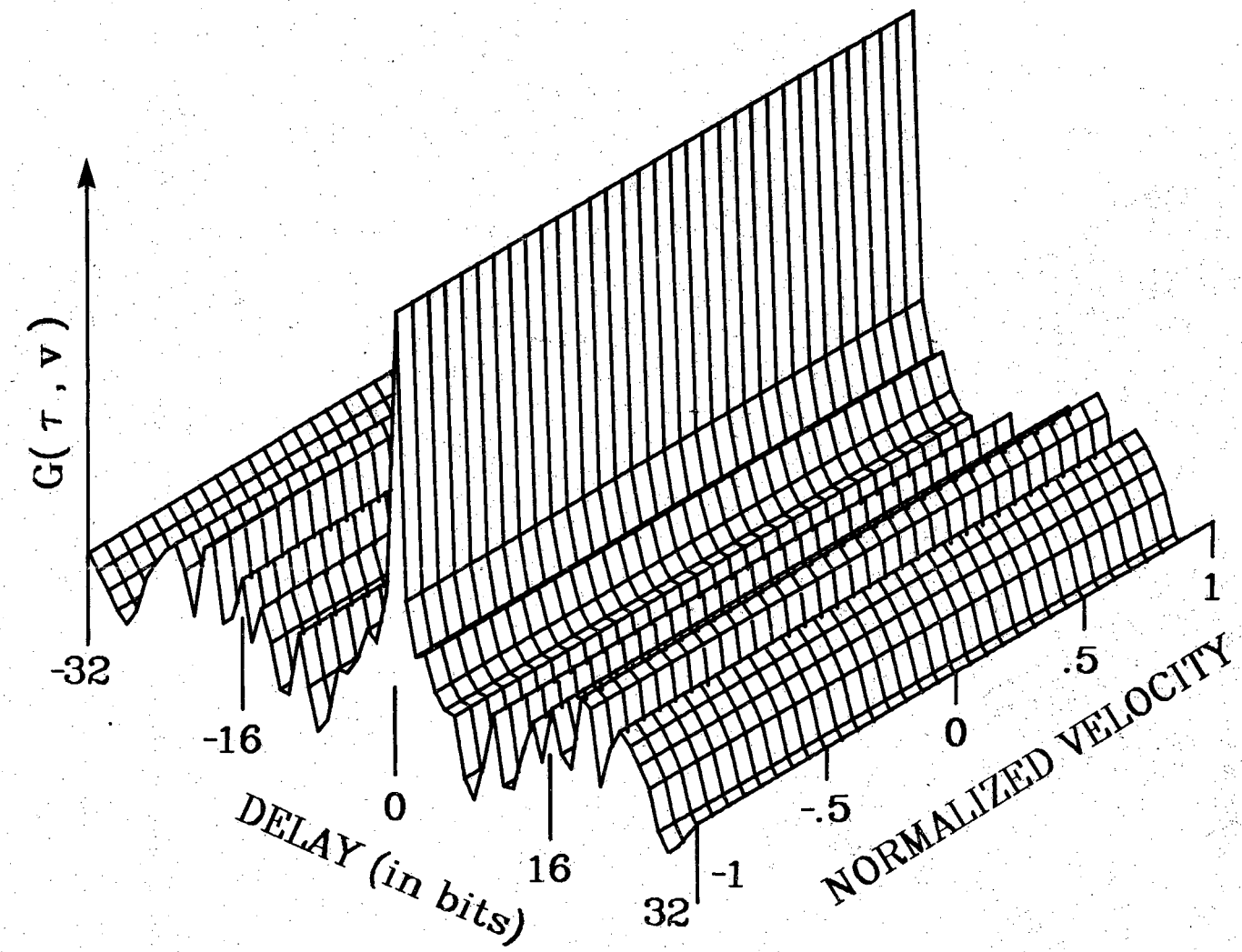

b. one 31 bit m-sequence.

Figure 6–10 (continued).

Figure 6-11. As can be seen this ratio falls below 60 dB for Doppler shifts greater than 0.1% of the repetition rate of the system. Significant self-noise cancellation of greater than 20 dB occurs for values up to 30% of the maximum unambiguous velocity.

If two pulse time averaging is employed by correlating two single pulses in consecutive transmit cycles, the ambiguity function changes to the sum of two slanted ridges, as shown in Figure 6-12. This two pulse averaging is equivalent to the Golay code addition without the presence of self-noise. The triangular correlation function can be seen to decrease in amplitude and widen with increasing velocity. Thus the benefits of time averaging are also degraded when applied to moving targets.

Improving Self-Noise Cancellation

A study was made to determine the system and application limitations on Golay code self-noise cancellation, in order to identify methods for improving the cancellation below the level of 35 dB. In order to identify methods for improving the cancellation of self-noise it is necessary to determine the sensitivity of the self-noise cancellation to the various parameters of the transmit signal which would cause it to deviate from an ideal waveform. In the transmitter designed used in the previous measurements two variables are subject to error -- the shape of the pulses, and the DC offset of these pulses. In order to investigate the effects of DC offsets and misshaped pulses it would be possible to actually "tweak" these parameters in the laboratory. However, in actual high-frequency circuits it is difficult to control all other variables while varying only one. It is thus more straightforward to simulate the errors through computer simulations of the correlation functions.

The misshaped pulses were simulated by increasing the length of code bits which occurred before every one/zero transition to roughly simulate the difference in turn on and turn off times which occurs in TTL circuitry. A plot of the peak power to average self-noise power versus the percentage increase in the code bit width before a one/zero transition is shown in Figure 6-13a. As can be seen, the system is very sensitive to this parameter, and a maximum percentage increase of 1.6% must be maintained to keep average self-noise power 60 dB lower than the power in the correlation peak.

The effects of DC offset were also simulated and the self-noise cancellation was found to be much less sensitive to the addition of DC offset to the Golay

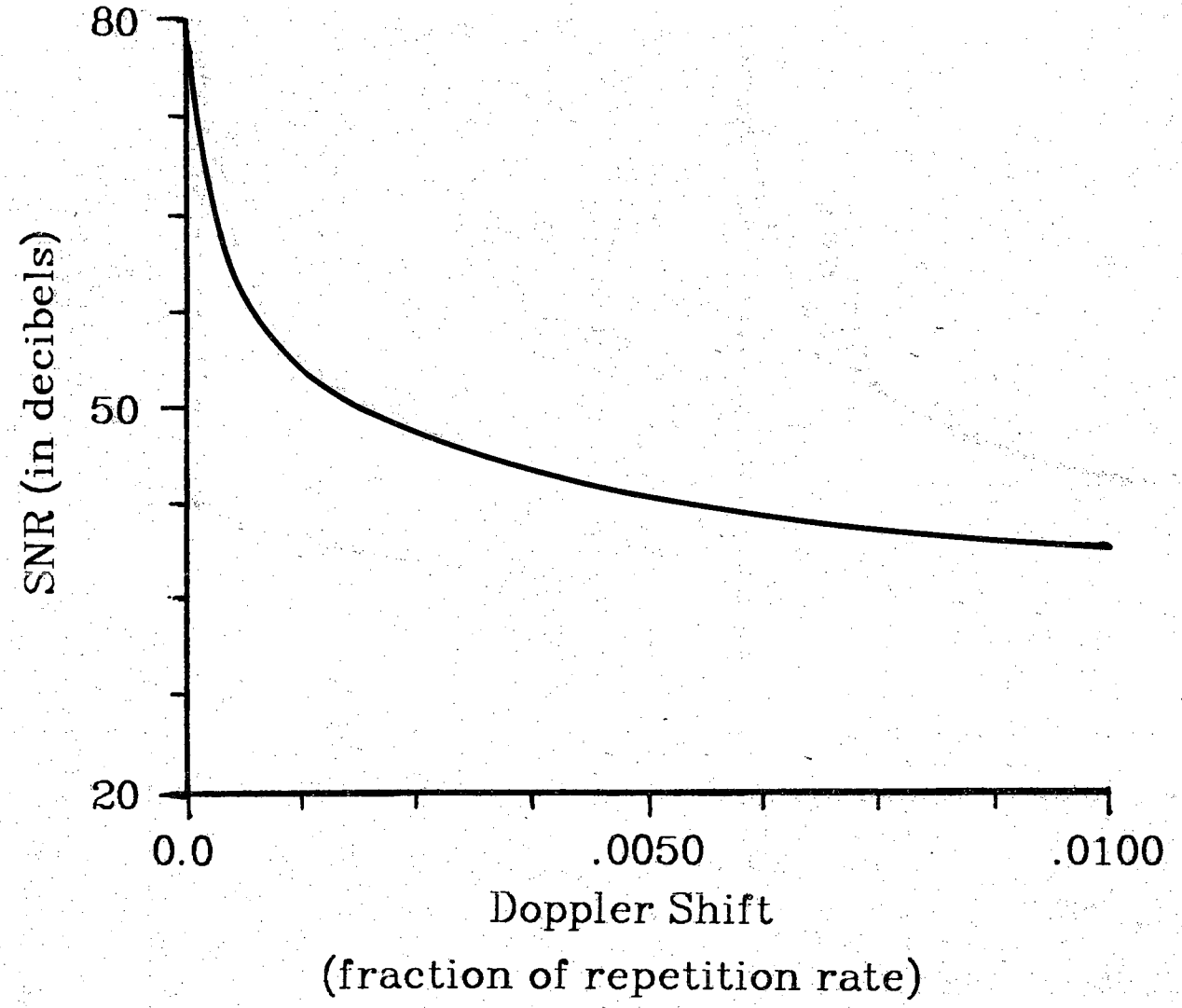

Figure 6–11 Peak-to-average self-noise power versus velocity.

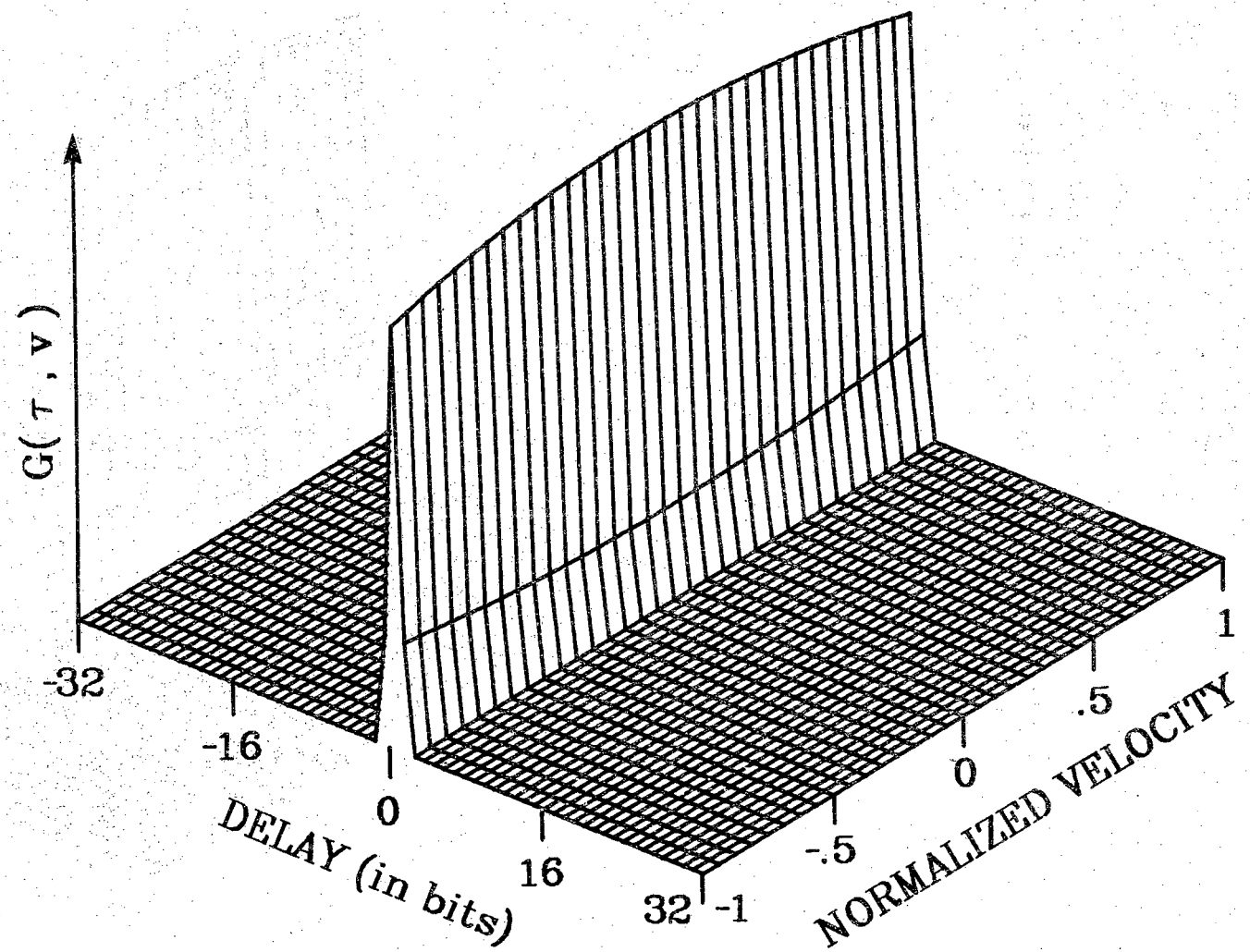

Figure 6–12 Generalized ambiguity function for two single pulses of width δ separated by one repetition period.

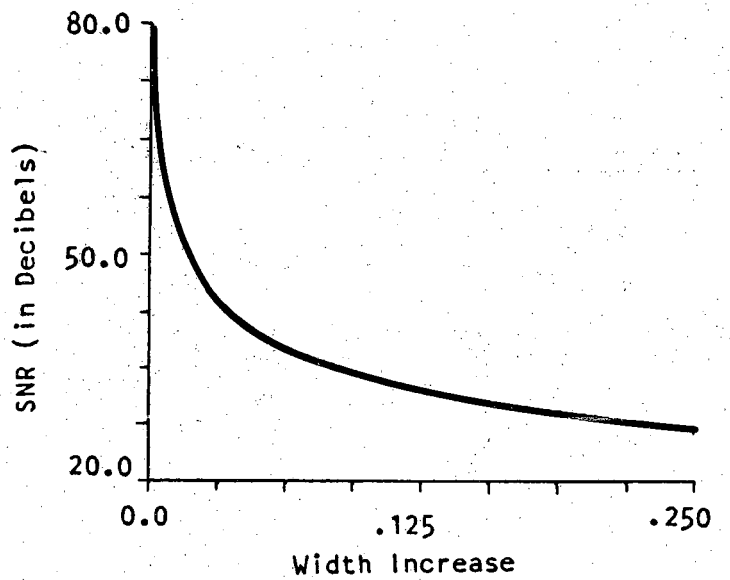

a. Versus percentage increase in the code bit-width.

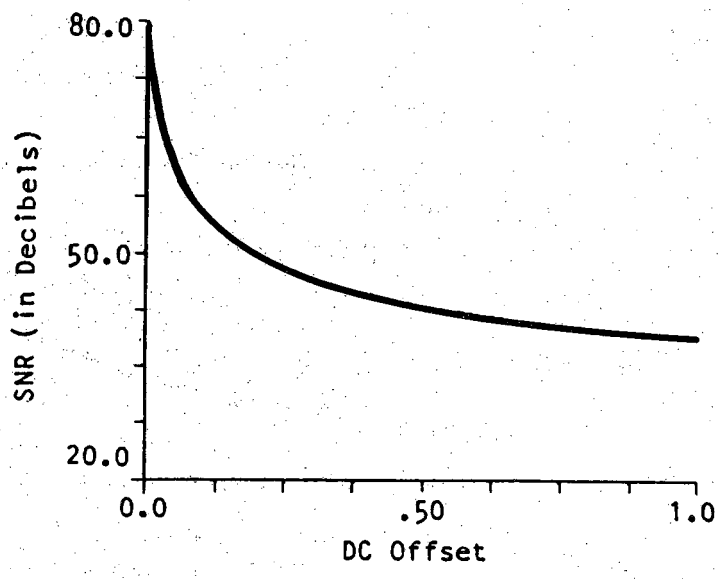

b. Versus DC offset.

Figure 6–13 Peak-to-average self-noise power variation with transmit code parameters.

code bursts as shown in Figure 6-13b. Even with a percentage offset of 7.9% of the peak, the average self-noise power is still 60 dB lower than the peak power of the correlation function.

In conclusion, results indicate that care should be taken to scan the transducer at a rate much less than the repetition rate, that the turn on and turn off times are matched so that the increase in the length of code bits before a one/zero transition is less than 1.6% of the code bit width, and that the DC offset is less than 7.9% of the desired burst height. Under these conditions Golay code sidelobe cancellation to between 50 and 60 dB will be maintained.

SNR Effects of Moving Targets

In Chapter III a signal-to-noise ratio formula (3.23) was presented which included the effects of self-noise, clutter, and background receiver noise. This signal-to-noise ratio formula is exact for flaw detection applications since it was assumed that the desired target and the clutter targets were all stationary with respect to the transducer. However, if the effects of movement are included, the signal-to-noise ratio must be modified so that

$$SNR = \frac{P\ S(v_t)}{C[Q(v_c) + (\frac{2r}{N})R(v_c)] + \eta(\frac{b}{nN}) + P(\frac{b}{nN})R(v_t)}, \qquad (6.10)$$

where $S(v_t)$ is the peak power variation of the desired signal with target velocity, $Q(v_c)$ is the variation in the average power of the desired signal with clutter velocity, and $R(v_t)$ is the variation of the average self-noise power with target velocity.

The velocity dependent terms, $S(v)$, $Q(v)$ and $R(v)$ can be determined using the previously described generalized ambiguity function. The peak and average power of the correlation function of the desired signal vary with velocity if two transmit burst averaging is used, regardless of the form of the transmit burst. The generalized ambiguity function for two transmit burst averaging using a single pulse in each transmit burst, Figure 6-12, describes the effects of velocity variations on the ideal peak without any effects of self-noise present. The peak and average power variations with velocity, $S(v)$ and $Q(v)$ are shown in Figure 6-14.

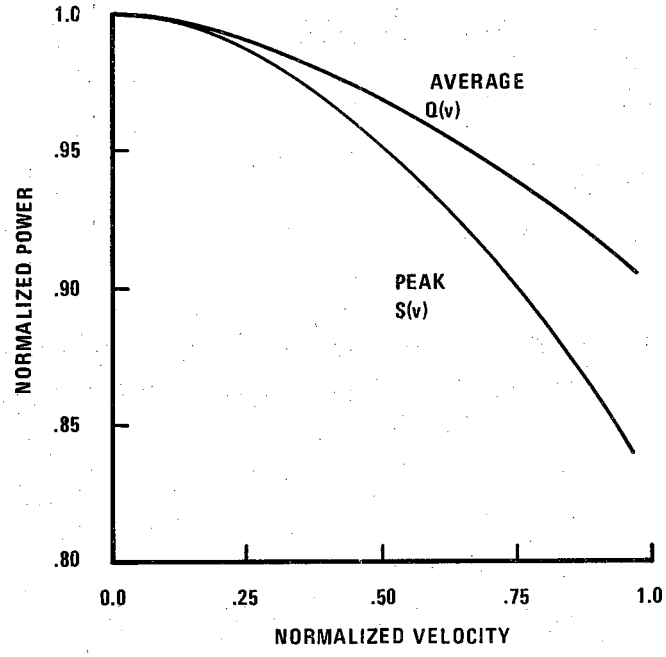

Figure 6–14 Normalized peak power variation with velocity, S(v), and normalized average power variation with velocity, Q(v), for two transmit burst averaging.

The variable $R(v)$ is code dependent and can be determined by subtracting the generalized ambiguity function of Figure 6-12 from the generalized ambiguity function of the given code. This isolates the self-noise variation with velocity. The variable $R(v)$ can then be calculated by determining the average self-noise power variation with velocity and dividing this by the average self-noise power in the correlation function for a single burst of code. Using this process on the Golay code ambiguity function results in an average self-noise power variation with velocity as shown in Figure 6-15. Without averaging the self-noise power of a pseudo-random code does not vary with velocity as can easily be seen in Figure 6-10b.

The signal-to-noise ratio formula can now be used to determine the optimum type of system to use for given clutter level and target velocity, whether Golay code correlation or conventional pulse-echo. Similar assumptions and comparisons to those made in Chapter V can be made for different target and clutter velocities and clutter and noise levels.

System Performance Analysis

The system performance analysis for the random and pseudo-random flaw detection system did not include the effects of moving targets on the system signal-to-noise ratio. As pointed out in the first part of Chapter VI, the major advantage to using Golay codes over other transmit signals is that much shorter code lengths and integration times are required to produce low sidelobe levels. Accordingly, it becomes possible to apply a Golay code correlation system to faster scanning and faster moving-target situations to which the previously described flaw detection systems were not well suited. In the following analysis, the performance of the high-speed Golay code flaw detection system is analyzed under the same conditions as the analysis of the m-sequence and random signal system, except that the effects of moving targets are also studied.

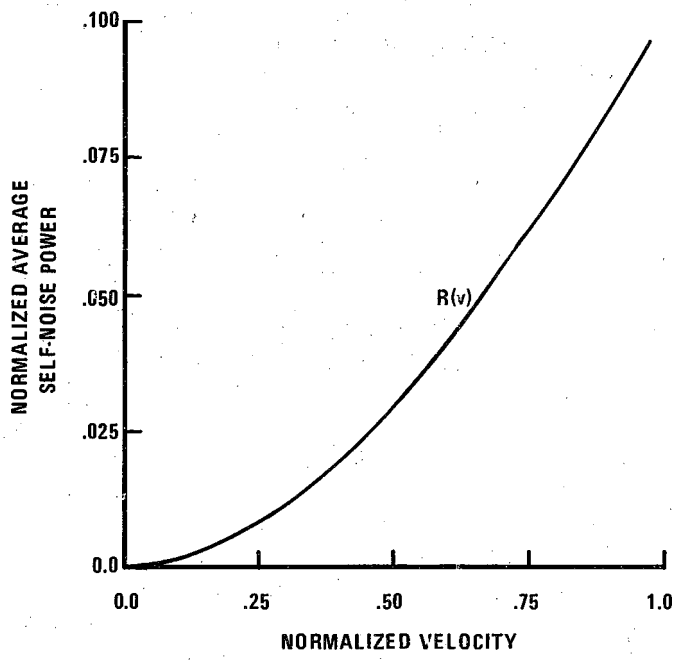

Figure 6–15 Normalized average self-noise power variation with velocity, R(v), of two complementary 32 bit Golay codes.

Non-Moving Targets

As determined in the introduction to Chapter VI, in the case of stationary targets, the Golay code system *SNR* is given by equation (6.1). Since this equation consists of a number of variables it is difficult to consider all the possible combinations. We thus choose to take a practical approach to the problem and consider a practical scanning situation.

For practical ultrasonic applications, P/η can be approximated by an exponential function of the time-of-flight, t_f [46], so that $P/\eta = A_o e^{-\alpha t_f}$. Now since the time-of-flight limits the maximum number of code bits which can be transmitted, n, it is possible to define n in terms of t_f and then make a comparative evaluation of the different types of correlation systems through substitution of P/η and t_f in the *SNR* formulas (3.22), (6.1), and (6.2). With the addition of different levels of clutter to these equations it is then possible to produce *SNR* plots versus time-of-flight for various levels of clutter, as well.

Assuming as an example that $P/\eta = 10^6 e^{-.276\alpha t_f}$, where t_f is the time-of-flight in seconds, and $n = t_f/\delta$, and selecting $b = 2$, $\delta = .1\mu$sec, and $r = 1/2$ as typical values for ultrasonic applications then equations (3.22), (6.1), and (6.2) become:

m−sequence or random signal

$$SNR = \frac{5t_f}{[10t_f \frac{C_o}{P} + 10^{-6}e^{.276t_f} + 1]} \tag{6.11}$$

Golay Code

$$SNR = \frac{5t_f}{[5t_f \frac{C_o}{P} + 10^{-6}e^{.276t_f}]} \tag{6.12}$$

Conventional

$$SNR = \frac{1}{[\frac{C_o}{P} + 10^{-6}e^{.276t_f}]} \tag{6.13}$$

Plotting these *SNR* equations, produces the sets of curves shown in Figure 6-16. For approximately $t_f < .8t_c$, where $t_c = -[ln(P/A_o C_o)]$, the signal-to-noise ratios for the Golay code system are essentially the same as a conventional pulse-echo system. This corresponds to the region where clutter

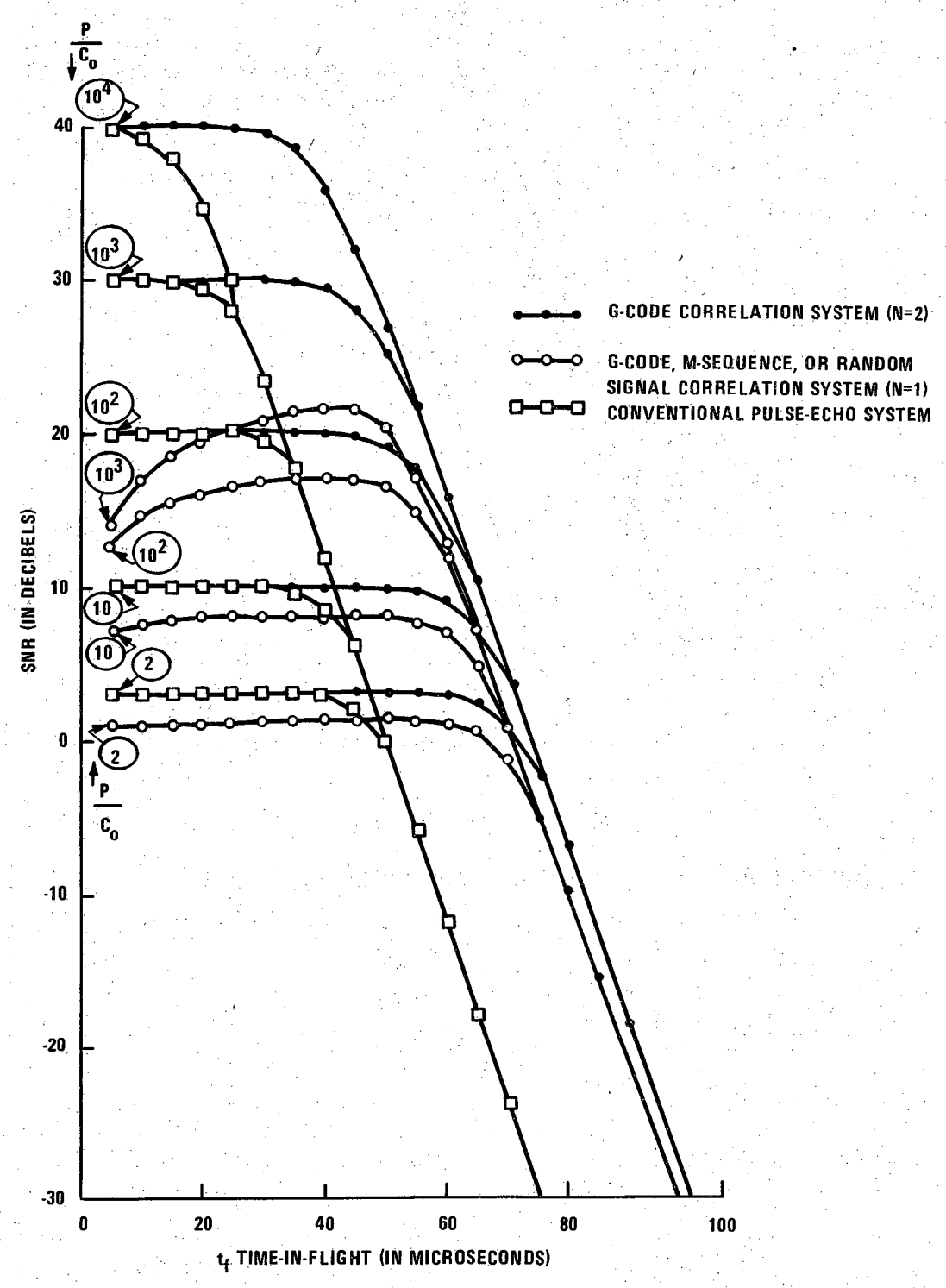

Figure 6–16 SNR versus time-of-flight and clutter level for high-speed operation.

dominates. For values of $t_f > .8t_c$, the Golay code system provides better signal-to-noise ratio than a conventional pulse-echo system. When the noise power becomes approximately 25 dB greater than the clutter power the correlation systems produce approximately the same *SNR* as they do in the clutter-free plots, Figure 6-16.

As mentioned in the system performance analysis of Chapter V if the number of integrated transmit bursts, N, is increased, the *SNR* of the m-sequence and random signal systems in clutter approaches the *SNR* of a Golay code system for the same value of N, as shown in the example curves of Figure 6-17.

For very low clutter situations, $C_o << \eta(b/(nN))$, the *SNR* formulas of equations (6.11) through (6.13) can be simplified by removing the clutter term and the *SNR* formulas can again be plotted as a function for t_f as shown in Figure 6-18. Once again, the Golay code system produces the best signal-to-noise ratio of the three systems.

Thus in the simplified case of stationary targets, it is clear that the ideal Golay code system is optimal for even N, under all conditions. However, in a realistic Golay code system, there are vestigial sidelobes due to mis-cancellation, as described in the *SNR* equation (6.4). Since this *SNR* equation is nearly the same in form as equation (3.23), an analysis equivalent to that in the system performance analysis section of Chapter V can be made. As a result, it is easily shown that the threshold receiver noise level for which a Golay code correlation system produces improved signal-to-noise compared to conventional pulse-echo systems is reduced from the value given in equation (5.7) by the sidelobe cancellation factor, q, of equation (6.3). The *SNR* will also follow curves similar to those shown in Figure 6-17, with N replaced by N/q.

Moving Targets

In order for any imaging system to adequately represent the position of a moving target, the position of the target must be sampled at greater than the Nyquist rate. If the target velocity is high enough, this can restrict the maximum number of integrated bursts to one, $N = 1$. Under the condition $N = 1$, the Golay code system and the m-sequence and random signal systems produce essentially the same sidelobe level and thus the same output *SNR*. The *SNR* formula for a Golay code system with $N = 1$ is then given by equation (3.23) since the velocity effects described by equation (6.10) are

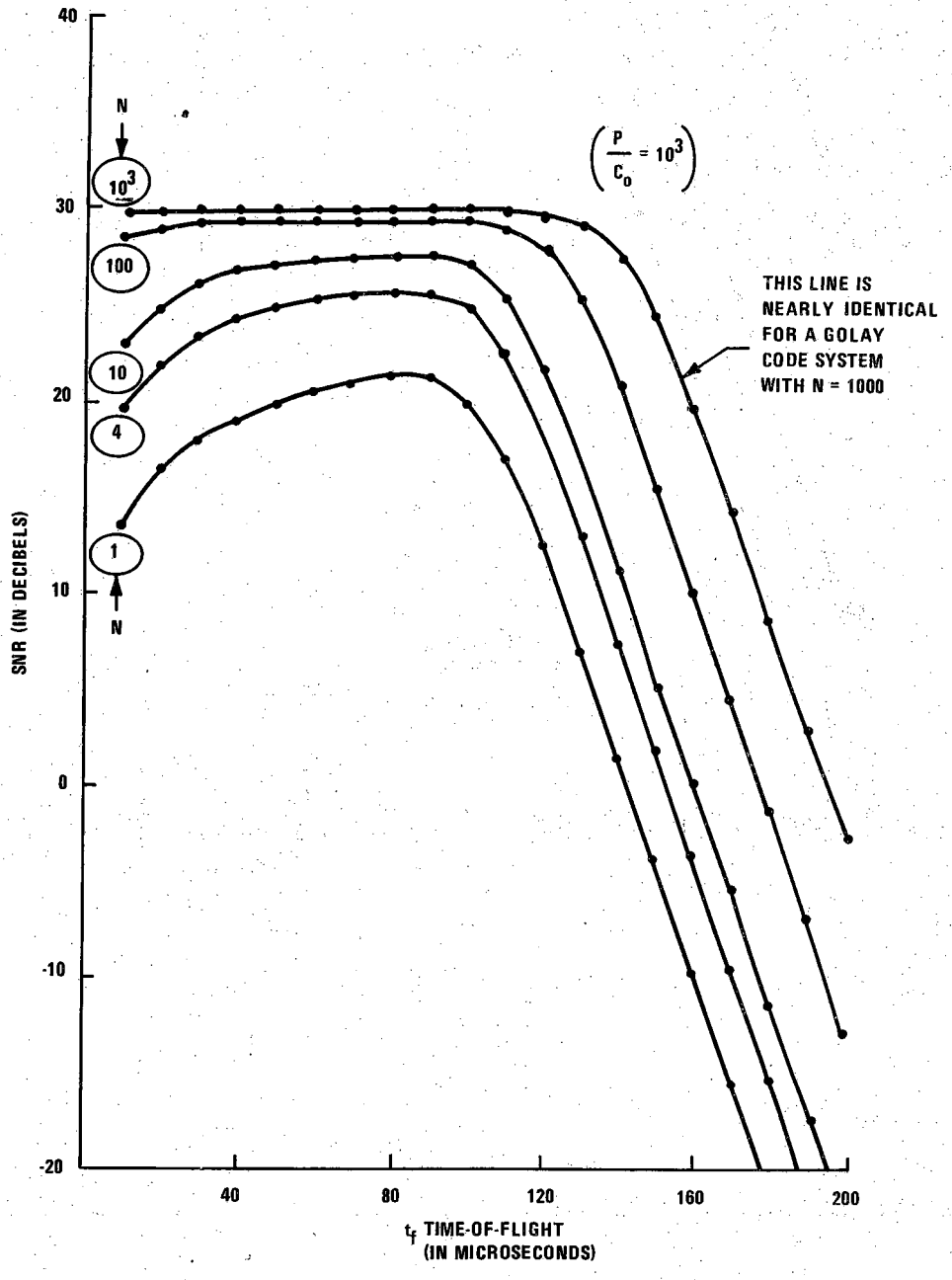

Figure 6–17 M-sequence/random signal correlation system SNR versus time-of-flight and N.

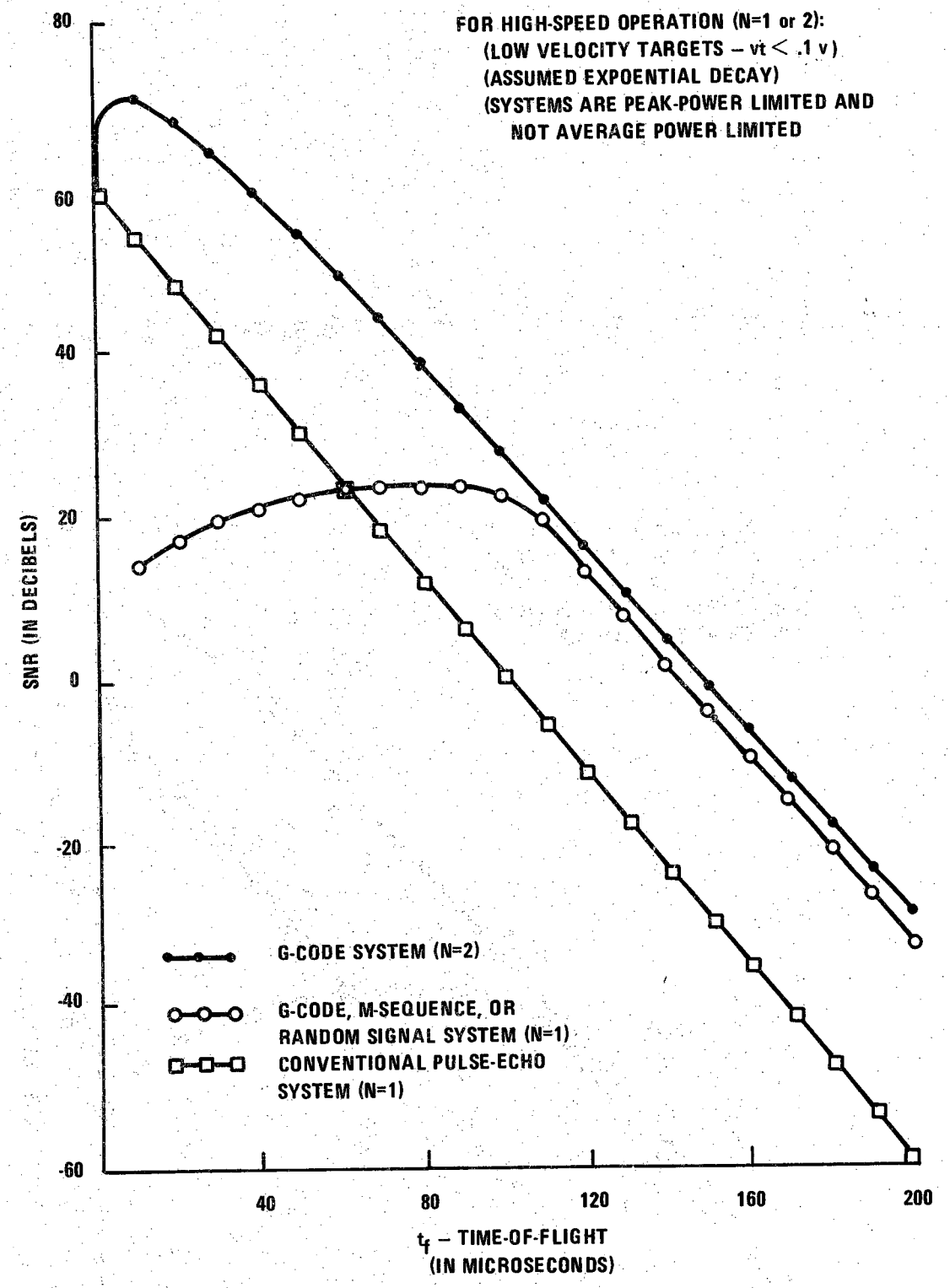

Figure 6–18 Zero clutter SNR versus time-of-flight for high-speed operation.

negligible for $N = 1$. This signal-to-noise ratio formula was examined before in much detail and it was found that the condition on η described by equation (5.7) was necessary in order for a correlation system to provide an improvement over a conventional pulse-echo system. Using equation (5.7) in the case $N = 1$, with $n >> b$, and no clutter, $C_o = 0$, leads to a constraint on n such that

$$n > Pb/\eta. \tag{6.14}$$

Since n is proportional to the transmit burst length $n\delta$, and the maximum transmit burst length is limited to the time of flight to the target and back, t_f, the correlation system will provide improved *SNR* for

$$\frac{P}{\eta} < \frac{t_f}{\delta b}. \tag{6.15}$$

Thus, as the distance to the target of interest is increased, the correlation system provides improved performance for a greater range of input single-to-noise ratios. Now, since the returning power P decreases with increasing t_f (exponentially in many practical cases) the ranges over which performance can be improved can easily be found by determining the intersection of the P/η versus t_f curve and the $P/\eta = t_f/(\delta b)$ line, Figure 6-19. For clutter limited situations, if $n >> Pb/C_o$, and $n >> b$, the correlation system will provide improved signal-to-noise ratio provided $C_o/\eta < 1$.

For moving targets which have a velocity which is less than half the maximum unambiguous velocity for one-burst integration, it becomes possible to use two-burst integration. In this case the Golay code system performance is as good as, or better than, the random signal or m-sequence systems, since the Golay code sidelobe level is less than or equal to the sidelobe levels of either of the other systems.

In order to analyze the performance of the system for $N = 2$ it becomes necessary to use equation (6.10). As determined in the moving target simulation results of Chapter VI, the velocity dependent terms are close to their zero-velocity values for velocities less than 30% of the ambiguous velocity, v_a. Under this situation the analysis and results are the same as the analysis and results for stationary targets.

For situations where $v_t > .3v_a$ and $v_c > .3v_a$, the *SNR* of equation (6.10) compared must be compared directly with pulse-echo system signal-to-noise

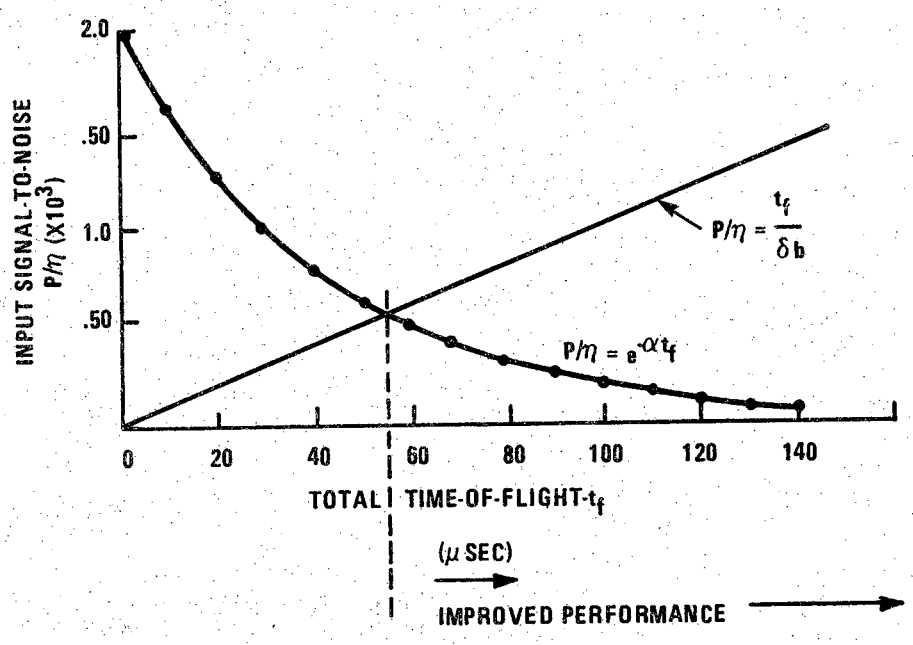

Figure 6–19 The SNR crossover point indicates the required minimum time-of-flight for improved SNR.

ratio to determine when a Golay code system will provide improvement over conventional pulse-echo systems. The signal-to-noise ratio of a Golay code system will be better than a conventional system when

$$\frac{1}{S(v_t) - \frac{b}{nN}}\left[[Q(v_c) - S(v_t) + \frac{2r}{N}R(v_c)] + \frac{P}{C_o}[\frac{b}{nN}R(v_t)]\right] < \frac{\eta}{C_o} \quad (6.16)$$

Choosing $r = 1/2$, $b = 2$, $N = 2$ and $v_t = v_c = v$, as typical values; and assuming n is large enough so that $S(v) >> 1/n$, then the constraint formula becomes

$$\frac{1}{S(v)}[Q(v) - S(v) + \frac{R(v)}{2} + \frac{P}{C_o n}R(v)] < \frac{\eta}{C_o}. \quad (6.17)$$

A graph of the left-hand side as $T(v)$, a function of v for different values of $P/(C_o n)$, can be determined by using the measured values of $R(v)$, $S(v)$, and $Q(v)$ from the moving target simulation. The result is shown in Figure 6-20 as sets of $T(v)$ versus v/v_a curves. This set of curves can be used to determine the best system for a given application. For a given value of $P/(C_o n)$ the plotted curve describes the ranges of velocities and associated minimum η/C_o values, for which a Golay code system will provide improved performance. If, for example, $P/C_o = 128$ and $n = 64$, then the associated curve indicates that improved performance will occur for $v/v_a < 1$ as long as $\eta/C_o < -4dB$.

No Clutter

For the particular case of no clutter, $C_o = 0$ and assuming $S(v) >> b/(nN)$ the *SNR* improvement, *SNRI*, available from a Golay code system is

$$SNRI = (\frac{nN}{b})\frac{S(v)}{1 + \frac{P}{\eta}R(v)}. \quad (6.18)$$

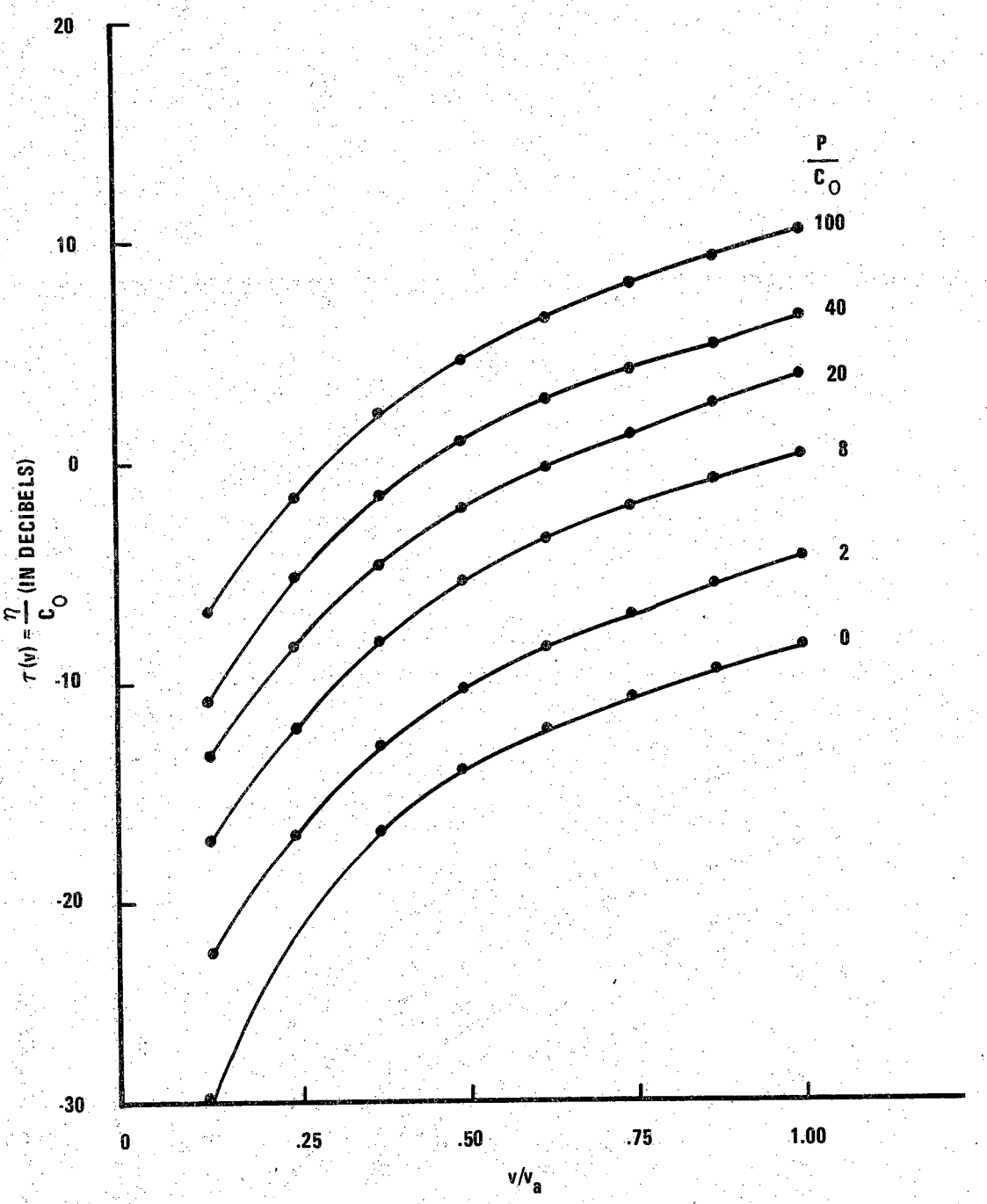

Figure 6–20 T(v) Threshold curves, for improved Golay code system SNR compared to conventional systems, versus target velocity and clutter level.

The quantity nN/b is the *SNRE* available from a Golay code system. The second multiplicative term reduces the signal-to-noise as shown in Figure 6-21. The maximum input signal-to-noise ratio below which improvement occurs is

$$\frac{P}{\eta} < \frac{S(v)}{R(v)} \left(\frac{nN}{b}\right). \tag{6.19}$$

This threshold constraint is plotted as a function of v in Figure 6-22.

Thus, in this example only when the input signal-to-noise ratio is less than $[9.24 + 10log(n/b)]$ dB, will a Golay code system provide improved signal-to-noise ratio over conventional pulse-echo systems.

It is thus obvious that the performance of the Golay code system will be reduced for moving targets, and suffers even more under the presence of moving clutter. However, it is clear that for many medium velocity conditions the Golay code system will provide better performance than conventional pulse-echo systems and will always provide as good as, or better performance than an m-sequence or random signal system.

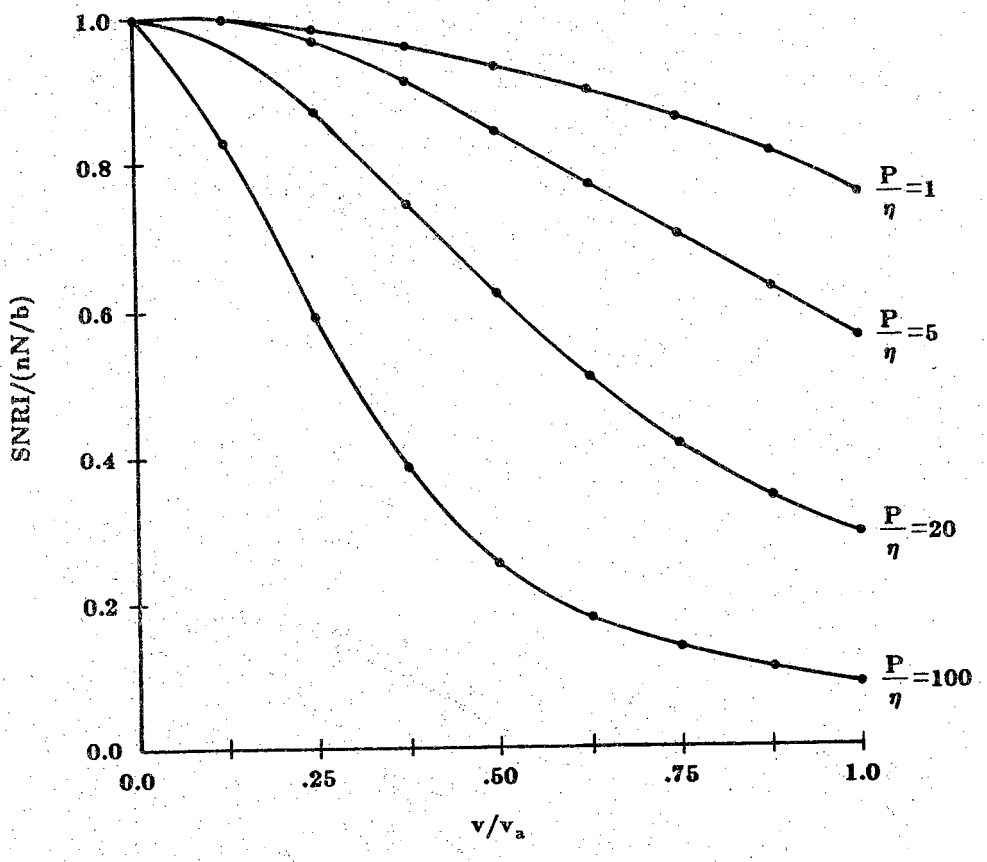

Figure 6–21 Effects of velocity with zero clutter on the Golay code system SNR improvement.

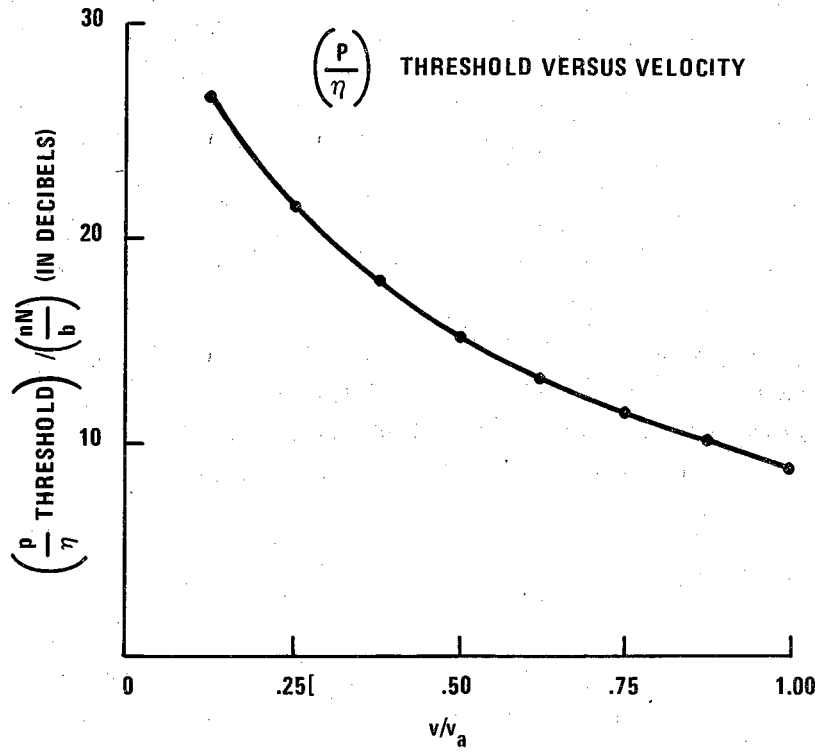

Figure 6–22 Zero clutter input SNR threshold versus target velocity, for which a Golay code system provides improved SNR over conventional systems.

CHAPTER VII - MULTI-MODE SIMULTANEOUS TRANSMISSION

In this chapter the results of the single-mode study are extended to evaluate a system which uses a number of optimal single-mode correlation systems, operating simultaneously in parallel. Subsequent to the derivation of a general system signal-to-noise ratio, a comparison is made between a simultaneous transmission system which uses Golay codes and a simultaneous transmission system which uses pseudo-random m-sequences. The criterion for comparison is based on the improvement these systems provide over conventional sequential multi-mode systems.

As in parallel computer architectures, the primary potential benefit of a simultaneous multi-mode pulse-echo system is an increase in processing speed. Unfortunately, unlike parallel computer architectures, the presence of parallel channels in a pulse-echo system degrades the signal-to-noise of each individual channel.

With this specific noise interference problem in mind, a signal-to-noise ratio formula is used as the primary gauge to analyze and evaluate the performance of the proposed multi-mode system. At this point, the reader familiar with parallel computer architectures may recognize that the simultaneous multi-mode system will suffer from one of the major drawbacks of parallel computer architectures – the increased hardware (and associated power) that such a system requires. Although, this problem is of prime importance to the engineer developing such a system, it is not the purpose of this thesis to deal with the many technological problems of implementation. Any such technology-based study would soon be outdated due to the technological improvements which continually occur in electronic integrated circuits. The purpose of this study is thus to analyze the benefits and limitations of using a simultaneous multi-mode system based on the primary gauges of signal-to-noise ratio and operating speed.

Fundamentals

In order to evaluate the performance of an ultrasonic simultaneous transmission system it is first necessary to formulate and analyze the basic operating principles of the system.

A simultaneous transmission system will have M transmit signals corresponding to the M different operating modes. In an ultrasonic imaging system which operates in a pulse-echo mode, the modes can correspond to one of a number of beam characteristics including beam direction, focal point, beam width, etc., as well as combinations of these characteristics.

These beam characteristics are incorporated in the correlation system impulse response function, $h(t)$, of equation (3.1). If this single-mode equation is expanded to include the $M-1$ interfering signals that are present in an M-mode simultaneous transmission system, a system analysis made using the expanded equation will apply in general to any multi-mode system and its corresponding multi-mode beam characteristics.

The received signal, $y_i(t)$, from a single ideal point reflector in the i-th mode of a multi-mode system is

$$y_i(t) = x_i(t) * h_i(t) * h_i(t) + \sum_{\substack{j=1 \\ j \neq i}}^{M} x_j(t) * h_{j(t)} * h_i(t) \qquad (7.1)$$

where $x_k(t)$ are the M transmit signals, and $h_k(t)$ are the impulse responses of the M operating modes. Note that no attempt has been made here to account for the variation of $h_i(t)$ with the position of the target. This variation is implicit in $h_i(t)$.

If $y_i(t)$ is processed by a correlation receiver which uses a reference signal, $x_i(t)$, the output will be represented by equation (3.2) with $y(u)$ replaced by $y_i(u)$ and $x(u-\tau)$ replaced by $x_i(u-\tau)$ such that

$$R_{y_i x_i}(\tau) = y_i(\tau) * x_i(-\tau)$$

$$= h_i(\tau) * h_i(\tau) * R_{x_i x_i}(\tau) + \sum_{\substack{j=1 \\ j \neq i}}^{M} h_j(\tau) * h_i(\tau) * R_{x_i x_j}(\tau). \qquad (7.2)$$

The output of the i-th mode is the same as the output of the single-mode correlation system, equation (3.3), with the addition of $M-1$ interfering signals.

In order to minimize the interference from these signals it is necessary to reduce the coupling between modes, through control of $h_i(\tau)$ and $h_j(\tau)$ and/or by utilizing $x_i(t)$ which produce low cross-correlation values, $R_{x_i x_j}(\tau)$.

Cross-Correlation Noise

If $x_i(t)$ and $x_j(t)$ are uncorrelated signals such that $R_{x_i x_j}(\tau) = 0$ for all τ, the multi-mode signal-to-noise ratio will be identical to that of an ideal single-mode system. However, for a practical finite correlation time, signals x_i and x_j have not been found which are uncorrelated for all τ.

In studies using bandlimited random signals, the cross-correlation of random signals produced from different noise sources were shown to decrease in power in direct proportion to the integration time [17]. This corresponds with the decrease in the power of the self-noise for single-mode systems as given by equation (3.11). This correspondence is not surprising since self-noise and cross-correlation noise both arise due to the finite integration time correlation of two different pseudo-random signals. Self-noise is produced from correlating signals which correspond to the front and back ends of the same code.

In the finite-time correlation of a desired signal with a reference copy of the transmit signal, the result is a signal whose mean is the ideal correlation function, and whose variance describes the amount of self-noise present, as given by equation (3.6). For a finite-time cross-correlation of two different pseudo-random or random signals, the result is a signal whose mean is zero and whose variance describes the amount of cross-correlation noise which is present, as also given by equation (3.6).

The cross-correlation of any two codes is not easily predetermined. In general, finding a set of codes with low cross-correlation requires much searching and testing.

Beam Overlap

In addition to choosing low cross-correlation codes, the interference between simultaneous modes can also be controlled through the beam patterns of each mode. If the overlap of the beam patterns is zero, as when the transducers are facing in opposite directions, the cross-correlation level between codes is irrelevant and the same codes can be transmitted in each mode. However, this is not the generally the case in phased or linear arrays.

In order to determine the amount of beam overlap which occurs it is necessary describe the beam patterns of each mode using directivity functions. If the directivity function of the i-th mode is defined in spherical coordinates, as $D_i(r,\theta,\phi)$ then the impulse response of the i-th mode can be defined as $h_i(t) = D_i(r,\theta,\phi)\, p_i(t)$, where $p_i(t)$ is the impulse response of the i-th set of array elements and their associated electronics. As a result the impulse response between channels from a point reflector in the far field can be approximated by two multiplicative terms such that

$$h_i(t) * h_j(t) = [p_i(t) * p_j(t)]D_i(r,\theta,\phi)D_j(r,\theta,\phi). \tag{7.3}$$

If the electronics and array elements in each mode are identical, i.e. $p_i(t) = p_j(t)$ for all t, then minimizing the coupling between modes requires minimizing the overlap of D_i and D_j.

A normalized figure of merit, u_j^i, can then be defined which indicates the beam coupling between modes:

$$\mu_j^i = \frac{\int_v D_i(r,\theta,\phi)\, D_j(r,\theta,\phi)\, dv}{\int_v D_i^2\,(r,\theta,\phi)\, dv}. \tag{7.4}$$

This equation describes the average percentage of the i-th beam which overlaps the j-th beam. This average definition of overlap is useful when the effects of distributed clutter are considered.

Minimizing u_j^i requires careful control of the directivity functions and the minimization of the directivity sidelobes by methods such as random arrays [67]. In phased array scanning systems, the directivity function $D_i(r,\theta,\phi)$ may also be a function of time and a minimization of u_j^i for all t may also be necessary.

Large Target Effects

As in the single-mode self-noise discussed in Chapter III, the cross-correlation noise due to a large target can bury the desired return from a small target. The dynamic range (DR) of targets which can be distinguished can be approximately described by the ratio of the amplitude of the large target return, A, to the root-mean-squared (RMS) sum of the power from the undesired cross-correlation signals from the large target, (assuming that the interfering signals are uncorrelated) such that

$$DR \simeq \frac{A}{\left[\frac{A^2}{nNB\delta} + \sum_{\substack{j=j \\ j\neq i}}^{M}(D_i D_j R_{x_i x_j})^2\right]^{1/2}}, \tag{7.5}$$

where $R_{x_i x_j}$ is the cross-correlation between the ith received signal and the jth reference signal. The dynamic range of closely spaced targets which can be distinguished in a simultaneous multi-mode system is thus dependent on both the self-noise and the cross-correlation noise from each additional mode. In the worst case where $D_i = D_j = 1$ for all j, and assuming for simplicity that the power in each of the cross-correlation terms is $P/nNB\delta$, the dynamic range will be

$$DR \simeq \left[\frac{nNB\delta}{M}\right]^{1/2}. \tag{7.6}$$

Thus the available dynamic range of target return amplitudes which can be distinguished will increase in proportion to the square root of the signal-to-noise ratio enhancement, but will decrease in proportion to square root of the number of modes, M.

Clutter Effects

As shown in the single-mode clutter analysis, the increase in overlap of undesired self-noise signals with increased code length can degrade the signal-to-noise ratio. Since cross-correlation noise is similar in nature to self-noise, one would expect cross-correlation noise to produce similar effects in clutter. This was verified in cross-correlation measurements using band-limited random noise signals [17].

In a simultaneous multi-mode transmission system there will be $M-1$ cross-correlation signals from clutter present. (From here on the cross-correlation from clutter will be loosely referred to as cross-clutter.) The received signal under such a situation is the same as equation (7.1) but with additional cross-clutter terms such that

$$s_i(t) = \underbrace{x_i(t) * h_i(t) * h_i(t)}_{target\ echo} + \underbrace{x_i(t) * h_i(t) * b_i(t) * h_i(t)}_{self-clutter} + \sum_{\substack{j=1 \\ j\neq i}}^{M} (\mu_j^i)^2\, x_j(t) * p_j(t) \Big[\underbrace{1}_{\substack{target \\ cross-talk}} + \underbrace{b_j(t)}_{cross-clutter} \Big] * p_i(t) \tag{7.7}$$

where:

$x_k(t)$ is the transmitted signal from the k-th source.

$h_k(t)$ is the reflectivity function of the desired target illuminated by the k-th source.

$b_k(t)$ is the reflectivity function of the clutter targets illuminated by the k-th source.

Since the cross-clutter signals for each interfering mode behave the same as the self-clutter, the same clutter power analysis as in the Clutter Effects section of Chapter III can be used, and the additional interference power due to cross-clutter is then

$$C_i = \sum_{\substack{j=1 \\ i\neq i}}^{M} (\mu_j^i)^2 C_j\left(\frac{2r}{N}\right), \tag{7.8}$$

where C_j is equivalent to C_o of equation (3.17) and is the cross-clutter power

in the kth mode that would be seen by an ideal pulse-echo system.

The total output clutter power is a sum of the single-mode terms, C_o and C_a, with the additional simultaneous multi-mode clutter power, C_i, so that the output signal-to-clutter ratio is

$$SCR = \frac{P}{C_o + C_a + C_i} = \frac{P}{C_o(1 + \frac{2r}{N}) + \sum_{\substack{j=1 \\ j \neq i}}^{M} (\mu_j^i)^2 C_j(\frac{2r}{N})}. \quad (7.9)$$

Moving Target Effects

As in the single-mode study, in applications where the targets are moving, the received signals become stretched or compressed in time. In order to determine the exact effects of moving targets on the operation of a simultaneous multi-mode system it is necessary to extend the single-mode moving target analysis discussed previously in Chapter III. The single-mode analysis required the use of a generalized ambiguity function which describes the variation of the single-mode correlation output with velocity. In a simultaneous multi-mode system it is also necessary to define a generalized cross-ambiguity function to describe the effects of moving targets on the cross-correlation between channels. A generalized cross-ambiguity function can be defined as

$$C(\tau,\nu) = \int_{-\infty}^{\infty} B(\omega)A^*(\omega\nu)e^{-j2\pi\omega\nu\tau}\, d\omega \quad (7.10)$$

where $A(\omega\nu)$ and $B(\omega)$ are the Fourier transforms of $a(t)$ and $b(t)$, respectively; where $a(t)$ is the received signal from one of the simultaneous transmit sources and $b(t)$ is the correlation reference signal.

This formula can be used to simulate the effects of moving targets on the cross-correlation output, just as in the single-mode study of Chapter VI.

Zero Cross-Correlation Golay Codes

Certain special pairs of complementary Golay code pairs have been shown to have the unique property of zero cross-correlation, in two transmit bursts [68], for relative delays less than one repetition period. The zero cross-correlation property remains invariant when synthesis techniques are applied to generate long Golay codes from shorter Golay codes with the zero cross-correlation property.

As an example consider the shortest pair of complementary Golay codes which consist of two bit codes. It can easily be seen that all two bit Golay code pairs can be easily generated from any single two bit pair using the six operations of interchange and alteration described by Golay [60]. Now consider the pair of binary Golay codes represented as -1, +1 and +1, +1. A simple interchange of these two complementary codes produces a new pair, +1, +1 and -1, +1. The cross-correlation between the first two codes in each pair is shown in Figure 7-1a, and the cross-correlation between the second two codes in each pair is shown in Figure 7-1b. The sum of the two cross-correlation functions is identically zero, as shown in Figure 7-1c.

This cross-correlation cancellation is indeed nice, but this is only a trivial set of codes, since very little signal-to-noise ratio enhancement occurs for such short codes. However, if these short codes are appended in the manner described by Golay [60] the zero cross-correlation properties are retained. In Figure 7-2, two 64 bit Golay code pairs, which were generated from the previous two bit codes, are cross-correlated and then summed and the resultant is identically zero. The cancellation of the cross-correlation functions for the longer codes is due to the inherent symmetries of the paired Golay codes and the synthesis algorithms.

As discussed in Chapter VI several methods of synthesizing long codes from short codes have been described by Golay [60]. Briefly summarized, they include the appending of two codes, the interleaving of two codes, and two methods which use two pairs of codes and parity changes. The zero cross-correlation property is invariant under synthesis using either appending or interleaving, but the synthesis methods which involves two pairs of codes does not realize zero cross-correlation codes.

In addition, even non-zero cross-correlation functions remained invariant under synthesis into longer codes using either appending or interleaving. In other words, it is possible to "freeze" the cross-correlation function at some length and form and then recreate the same cross-correlation function for any

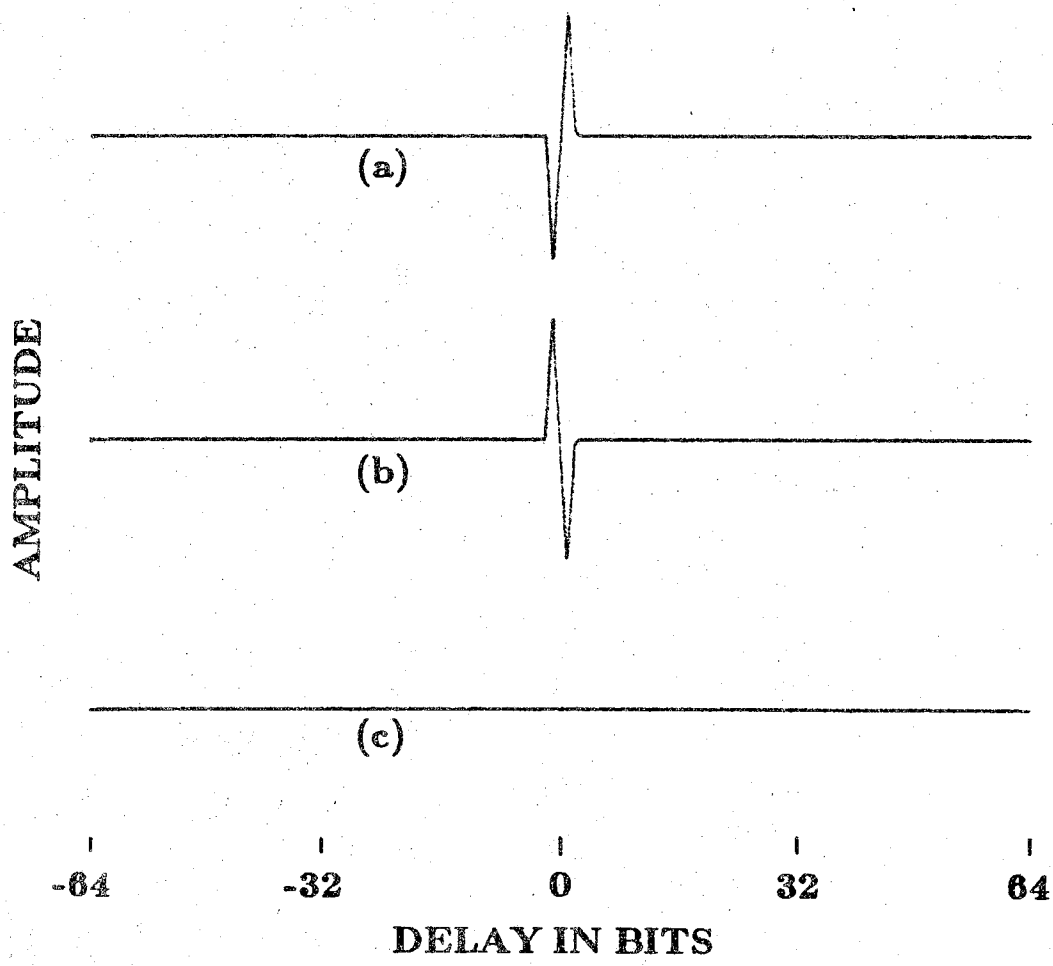

Figure 7–1 Demonstration of zero cross-correlation for 2-bit Golay code pairs.

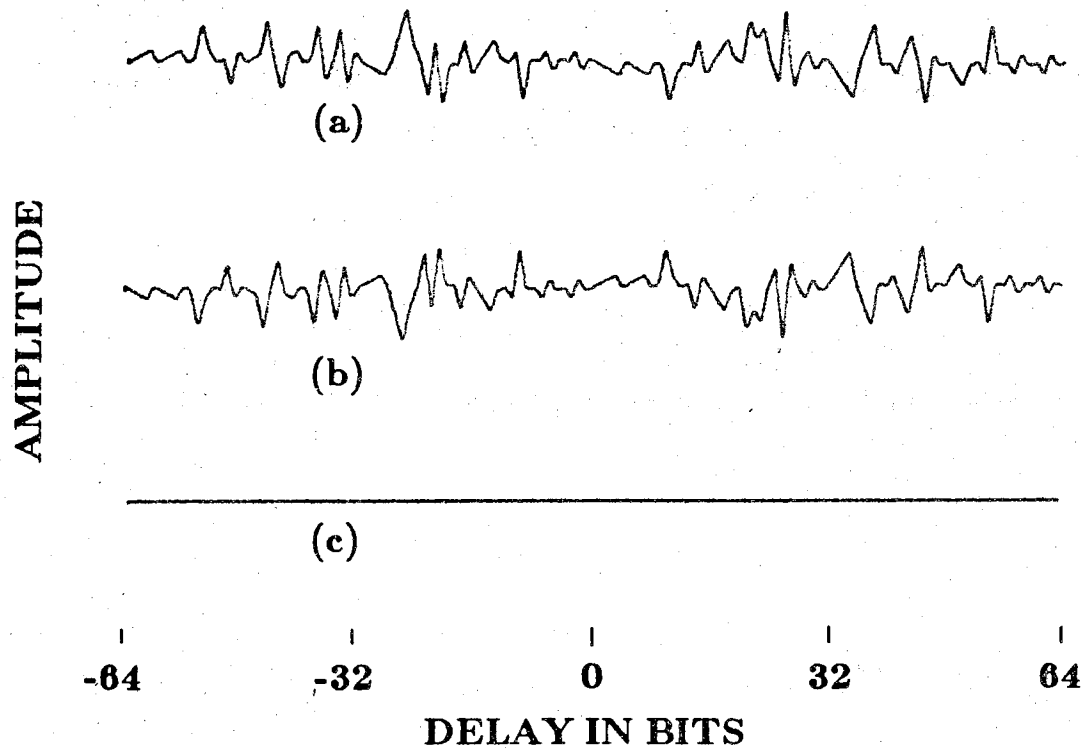

Figure 7–2 Demonstration of zero cross-correlation for 64-bit Golay code pairs.

length Golay code, merely by using the same appending or interleaving synthesis method on both Golay codes.

A larger set of eight Golay codes can be generated which retain the pairwise zero cross-correlation property. Consider the four short complementary pairs:

$$\begin{aligned} A &= +1, +1 \mid +1, -1 \\ B &= +1, -1 \mid +1, +1 \\ C &= -1, -1 \mid +1, -1 \\ D &= +1, -1 \mid -1, -1 \end{aligned}$$

The dividing line, $\mid$, delineates the two complementary codes required to produce the zero range sidelobes.

When the synthesis method involving appending is used on all four code pairs the zero cross-correlation is retained between the codes derived from C and D, however, when the codes synthesized from A and B are cross-correlated with the codes synthesized from C and D, the cross-correlations are identical in form to the cross-correlation functions of the original short codes. This is because of the recreation property just mentioned. But if the second method of synthesis – interleaving, is used on codes C and D, the cross-correlation between the codes derived by appending using A and D and the codes derived from interleaving codes C and D appear as shown in Figure 7-3a. The amplitude of this representative Golay code cross-correlation function compare favorably with the amplitude of the cross-correlation function between the two halves of two 127 bit m-sequences, Figure 7-3b. The particular m-sequences were chosen because they were preferred pairs as described in reference [57]. Preferred pairs have been noted for their low periodic cross-correlation properties [57].

The size of this four pair set can be doubled to eight merely by reversing all the codes. To verify that we have a good set of Golay codes, all the possible cross-correlations between all eight Golay code pairs were generated by computer simulation and the maximum cross-correlation amplitude remained less than 25% of the peak of the correlation function. To get these simulated results the autocorrelation functions of the Golay codes were convolved with a typical transducer impulse response.

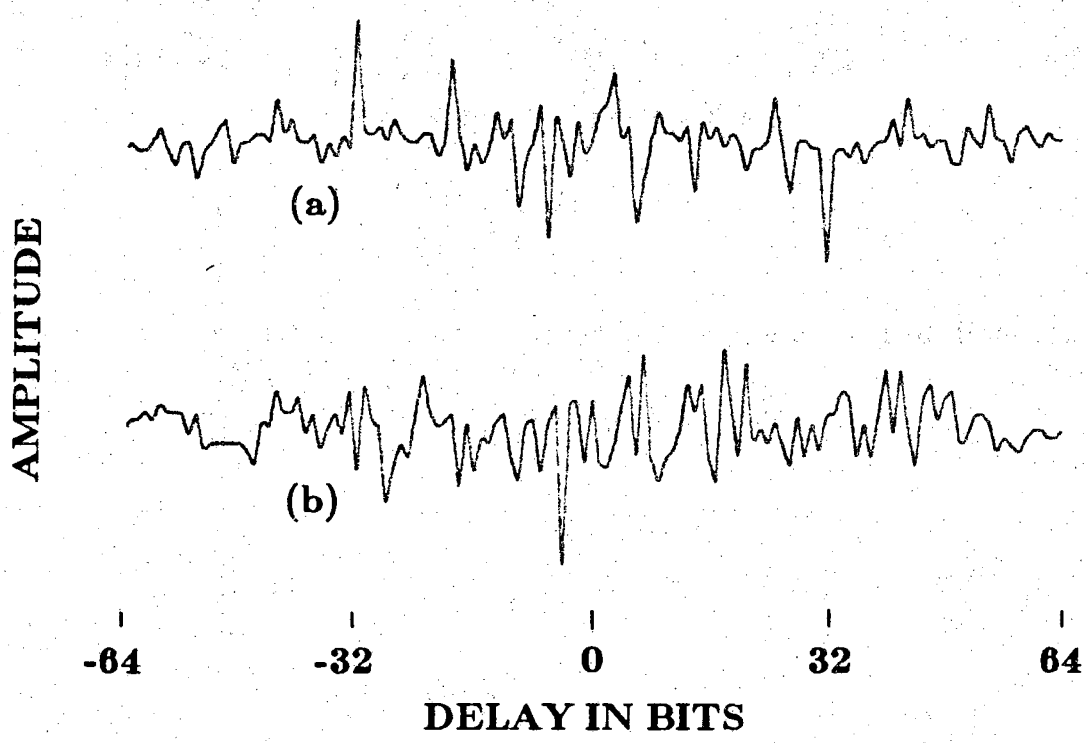

Figure 7–3 Comparison of cross-correlation functions for two Golay code pairs and two m-sequence pairs.

An exhaustive search has not yet been made and it may well be possible to synthesize a larger set of Golay codes with the same pairwise zero cross-correlation property. However, the eight pair set or any subset may be sufficient for many multi-mode applications.

In order to predict the cross-correlation levels which would exist under the filtering effect of a transducer and for much longer codes, the correlation system operation was simulated by computer and the peak cross-correlation amplitudes relative to the desired correlation output function were measured versus the code length. The maximum amplitude of the cross-correlation was then found to decrease roughly as the square root of the code length, as indicated by a least squares fit to a log-log plot of the data in Figure 7-4. This is the same variation that occurs in the cross-correlation of noise signals [17], and the range sidelobe height of pseudo-random codes [43].

As in the self-noise cancellation, the cancellation of the cross-correlation noise requires the addition of the correlation output for two consecutive transmit bursts. Because of the need for the proper alignment of the two waveforms, if movement of the target occurs, the cancellation can be degraded. The effects of moving targets on cross-correlation cancellation can be studied through a simulation of the cross-ambiguity function in the same manner as the ambiguity function simulation of Chapter VI.

A simulation of the cross-ambiguity function for a two pairs of 32 bit Golay codes which have the zero cross-correlation property is shown in Figure 7-5. As can be seen, the cross-correlation noise does not remain zero with increasing velocity. The average power of this cross-correlation signal was measured versus velocity and found to be essentially identical to the variation in the self-noise cancellation as measured in the section on *SNR* Effects of Moving Targets in Chapter VI. This is not suprising, because the self-noise and cross-correlation noise are very similar, and the cancellation properties are due to the same sign reversal property.

Multi-Mode SNR with Moving Targets and Clutter

An extension of the single-mode signal-to-noise ratio formula can be made for multi-mode systems by including the clutter noise from equation (7.9) and the cross-correlation noise term of equation (7.2), in a manner similar to that presented in reference [17] for a random signal system. If the noise signals from the interfering modes are considered to be uncorrelated with respect to each

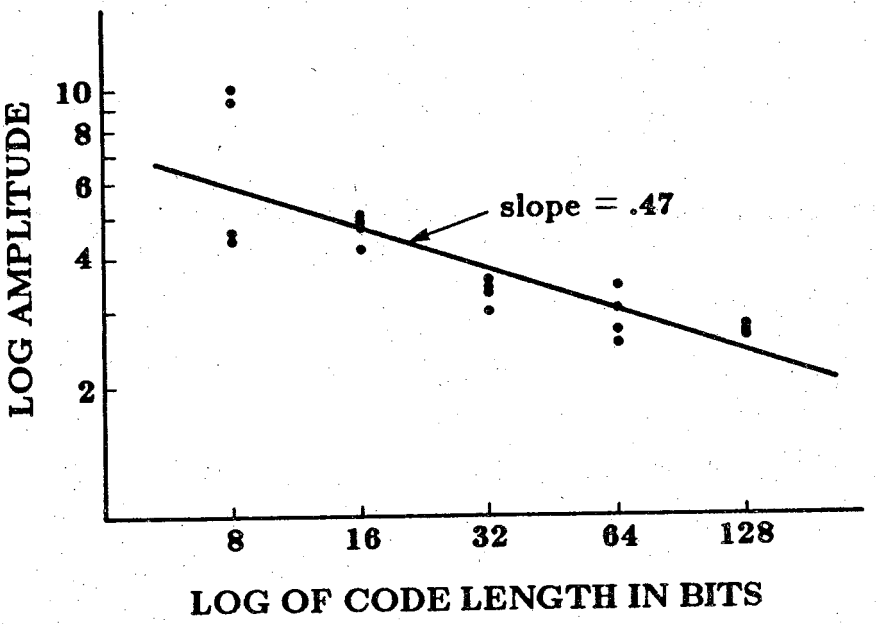

Figure 7–4 Maximum cross-correlation output amplitude versus code length.

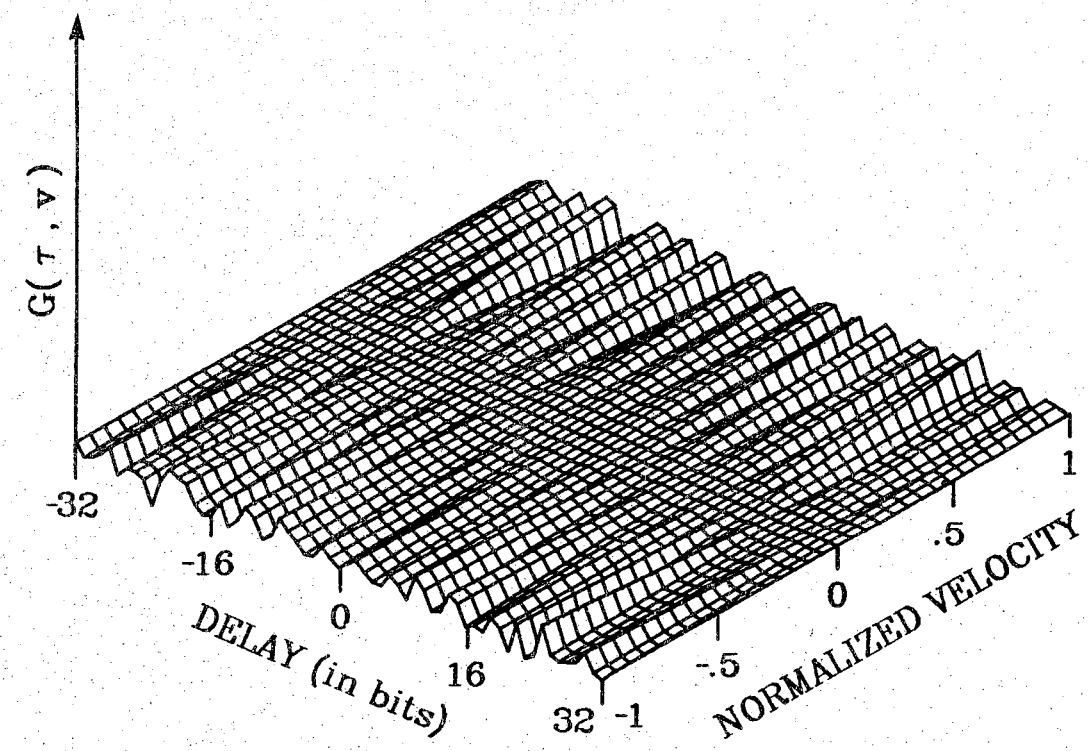

Figure 7–5 Simulated cross-ambiguity function for consecutive transmission of two 32-bit complementary Golay code pairs.

other and with respect to the other noise signals present in the single-mode *SNR* formula, the powers of the noise signals can be summed to determine the total interference poser. Assuming that the cross-correlation between the transmit signals varies in power with transmit burst length and receiver bandwidth in the same manner as the cross-correlation with background receiver noise (This has been verified experimentally for random signals [17]) then the signal-to noise ratio formula for a multi-mode system is

$$SNR = \frac{P_i\ S(v_t)}{C_i\ Q(v_c)+\eta(\frac{b}{nN})+\sum_{j=1}^{M}(\mu_j^i)^2(\frac{b}{nN})[R_j(v_t)\ P_j+R_j(v_c)C_j\ (\frac{2rn}{b})]} \quad (7.11)$$

This *SNR* formula can now be used to compare and evaluate the performance of different types of correlation systems under any conditions of interest.

Performance Comparison to Conventional Sequential Systems

Moving Targets

In order to reduce the complexity of equation (7.11), we assume that $C_j = C$ and $P_j = P$ for all j, $v_c = v_t = v$, $\mu_j^i = \mu$ for all $j \neq i$, and $u_i^i = 1$. In addition we also assume that $R_j = 1$, for all $j \neq i \neq c$, where the c-th term is isolated to designate the particular mode which produces zero cross-correlation in a Golay code system, and $R_i = R_c = R$. With these assumptions equation (7.11) then simplifies to

$$SNR = \frac{PS(v)}{C[Q(v)+\frac{2r}{N}R(v)]+\eta(\frac{b}{nN})+PR(v)(\frac{b}{nN})+\mu^2[R(v)+M-2][P(\frac{b}{nN})+\frac{C}{N}]} \quad (7.12)$$

If the *SNR* of the simultaneous multi-mode system is to be greater than or equal to a conventional sequential system then we must have

$$\frac{PS(v)}{C[Q(v)+\frac{2r}{N}R(v)]+\eta(\frac{b}{nN})+PR(v)(\frac{b}{nN})+\mu^2[R(v)+M-2][P(\frac{b}{nN})+\frac{C}{N}]} > \frac{P}{C+\eta} \tag{7.13}$$

Note that in a phased array each simultaneous mode would be connected to each array element so that the power for each mode might have to be reduced in order that the maximum average power is not exceeded for any array element. In this case the above comparison *SNR* would not be valid for the phased array system. We will assume, however, that the sequential phased array is not average power limited and that the average power limit is not exceeded in the simultaneous phased array. This *SNR* comparison formula will always be valid for a linear array since in a linear array each different code source would be connected to a different array element so that the same amount of power can be transmitted into each array element for both simultaneous and sequential excitation.

Since the value of n is typically fixed by the range to the target, the only variables which can be readily be controlled in equation (7.14) are N and μ^2. It would appear that one could then solve the inequality of equation (7.13) in terms of either N or μ^2 in order to determine a constraint on these variables. Unfortunately, the functions $S(v)$, $Q(v)$, and $R(v)$ are dependent on N since an increase in N increases the time over which the target can move. A solution for N would requires a determination of $R(v)$, $Q(v)$, and $S(v)$ for all N of interest using a simulation approach such as the one used in Chapter VI for $N = 2$. With these values the equation could then be solved using some type of iterative method. A study of this nature is beyond the scope of this work.

Equation (7.13) can, however, be readily rearranged as a constraint on μ^2 so that

$$\mu^2 < \frac{C[S(v)-Q(v)-\frac{2r}{N}R(v)]+\eta[S(v)-\frac{b}{nN}]-PR(v)(\frac{b}{nN})}{[P(\frac{b}{nN})+\frac{C}{N}][R(v)+M-2]}. \tag{7.14}$$

From this equation, for a given situation in which the target velocity and the clutter and noise levels are all known, as well as the speed of operation as given by N, and the transmit burst length n, it is then possible to determine the maximum beam overlap which will still provide the same signal-to-noise ratio as conventional sequential pulse-echo systems.

It is apparent from the various clutter and noise terms in equations (7.12) through (7.14) that the simultaneous transmission system will provide quite different performance levels depending upon the particular combination of clutter and noise level which is present. In order to analyze this complicated situation it is thus much simpler, and not necessarily any less informative, to evaluate the system performance in separate limiting cases where the system is limited by either clutter or noise, but not by combinations of these variables. With this in mind, in the following subsections we first analyze the performance of the simultaneous transmission system under clutter limited situations and then under receiver-noise limited conditions.

Clutter Limited System

The clutter limited case exists if n is large so that the terms involving $\eta b/(nN)$ and $Pb/(nN)$ can be ignored compared to the terms involving C. This will occur in a medium which has low level of attenuation and a high level of clutter.

In this clutter limited case equation (7.12) reduces to

$$SNR = \frac{PS(v)}{C\left[Q(v) + \frac{2r}{N}R(v) + \frac{\mu^2}{N}[R(v) + M-2]\right]}. \tag{7.15}$$

If the SNR of the simultaneous multi-mode system is to be greater than or equal to a conventional sequential system then we must have

$$\frac{PS(v)}{C\left[Q(v) + \frac{2r}{N}R(v) + \frac{\mu^2}{N}[R(v) + M-2]\right]} \geq \frac{P}{C + \eta}. \tag{7.16}$$

Rearranging equation (7.16) to produce a constraint on C/η, results in

$$\frac{C}{\eta} \leq \frac{NS(v)}{R(v) + \mu^2[R(v) + M - 2] - NS(v) + NQ(v)}, \tag{7.17}$$

for Golay codes with even values of N, and

$$\frac{C}{\eta} \leq \frac{1}{1 + \mu^2(M-1)}, \tag{7.18}$$

for Golay codes, m-sequences, or random signals with $N = 1$. For $N = 1$ the values of $R(v)$, $S(v)$, and $Q(v)$ were assumed to be unity since the effects of target movement are minimal in this case.

The right side of these equations then describes the maximum clutter-to-noise ratio which can be tolerated in order to produce a speed improvement of $M/2$ or M, while still providing the same signal-to-noise ratio as conventional sequential multi-mode systems. Remember of course that for this constraint to be valid the value of C/η is also bounded from below by our assumption that the system is clutter limited.

Using the values of $S(v)$, $Q(v)$, and $R(v)$ determined in Chapter VI, plots of the maximum C/η versus normalized target velocity v/v_a and M were made assuming $\mu^2 = .05$ for $N = 1$ and 2. The results are shown in Figure 7-6, for $N=2$, and Figure 7-7, for $N = 1$. As can be seen, the range of clutter-to-noise ratios which provides a speed increase without decreasing the *SNR* is much greater for the Golay code system operating with $N = 2$. This is due to the degrading presence of the self-noise for $N = 1$. Increases in the number of modes or the amount of cross-talk are shown to reduce the maximum clutter-to-noise ratio in both cases.

As a comparison the same maximum C/η ratio was determined for a pseudo-random m-sequence or random signal system operating with $N = 2$. In the case of pseudo-random m-sequences or random signals $R(v) \simeq 1$, and $S(v)$ and $Q(v)$ are the same as determined in Chapter VI, so that

$$\frac{C}{\eta} \leq \frac{2S(v)}{1 + \mu^2[M-1] - 2S(v) + 2Q(v)}, \tag{7.19}$$

for m-sequences and random signals with $N =2$. A plot of this constraint on

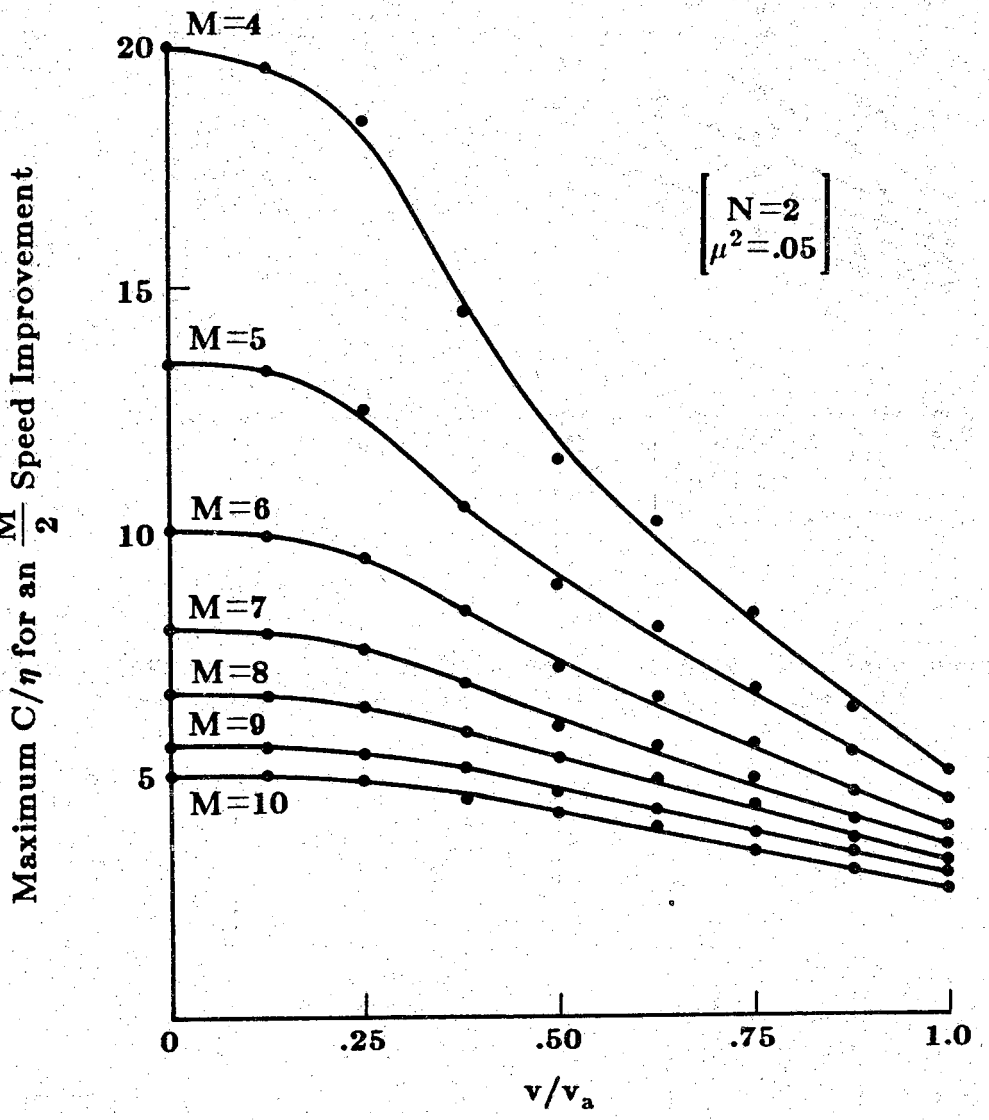

Figure 7–6 Maximum clutter-to-noise, C/η, for an M/2 speed improvement versus target velocity, v/v_a, and the number of modes, M.

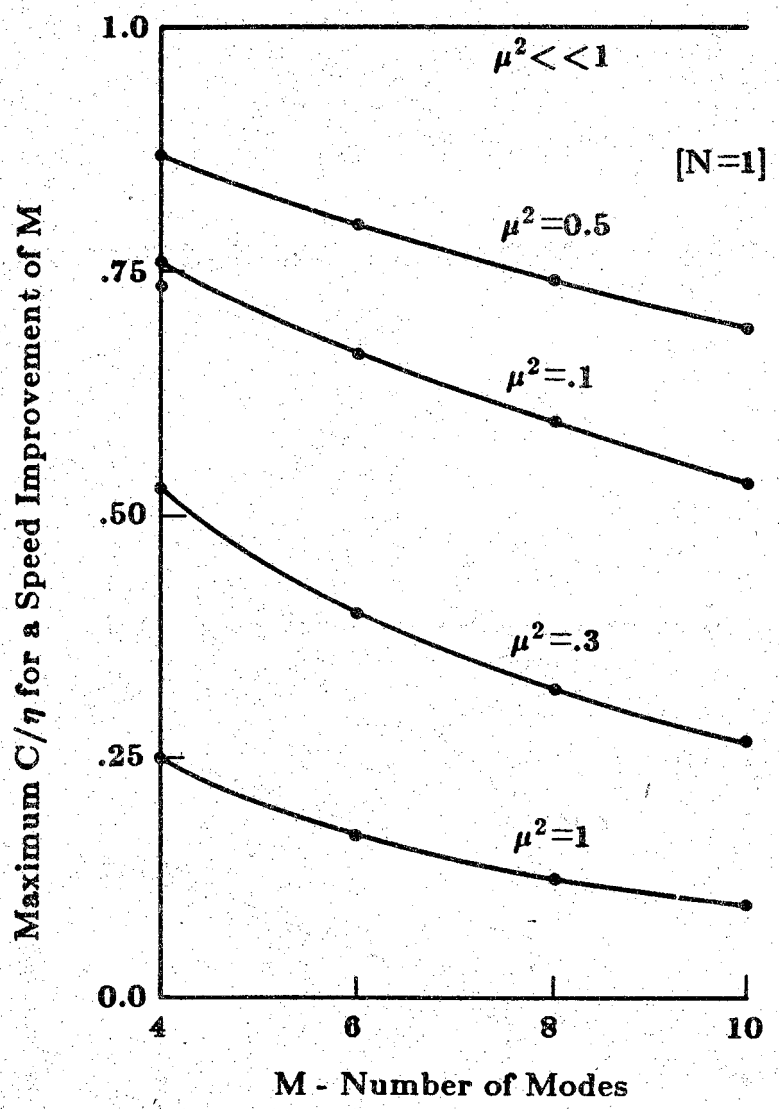

Figure 7–7 Maximum clutter-to-noise for a speed improvement of M versus the number of modes, M, and the cross-talk, μ^2.

C/η is shown in Figure 7-8. The curves are very similar to the curves of Figure 7-7 except that the values of C/η are doubled because of the extra signal-to-noise provided by $N = 2$ operation. It thus appears that if a speed improvement of $M/2$ is adequate, the Golay code system would be the best system choice, because of the much greater range of clutter-to-noise ratios in which it can provide a speed improvement without reducing the signal-to-noise ratio.

Receiver Noise Limited System

The noise limited condition will occur in highly attenuative media and at long ranges such that $C << \eta(\frac{b}{nN})$. In this situation the signal-to-noise ratio for a simultaneous transmission system reduces to

$$SNR = \frac{PS(v)}{\eta(\frac{b}{nN}) + PR(v)(\frac{b}{nN}) + \mu^2[R(v) + M - 2]\frac{Pb}{nN}} \tag{7.20}$$

Comparing this SNR equation to the SNR of a noise limited conventional system, $SNR = \frac{P}{\eta}$, results in a constraint on the maximum input signal-to-noise ratio which produces the maximum speed improvement of $M/2$, without degrading the SNR compared to conventional systems, such that

$$\frac{P}{\eta} \leq \frac{(nN/b)S(v) - 1}{R(v) + \mu^2[R(v) + M - 2]}. \tag{7.21}$$

Note that for this constraint to be valid the value of P/η may also be bounded from above by our assumption that the system is noise limited. If $N = 2$, and $n/b = 100$ is chosen as a typical value, and $\mu^2 = 1$ is chosen as a worst case, a plot of the constraint of equation (7.21) versus velocity produces the curves shown in Figure 7-9. As expected, an increase in velocity and/or the number of simultaneous modes results in a decrease in the maximum P/η which can be tolerated without reducing the SNR of the system.

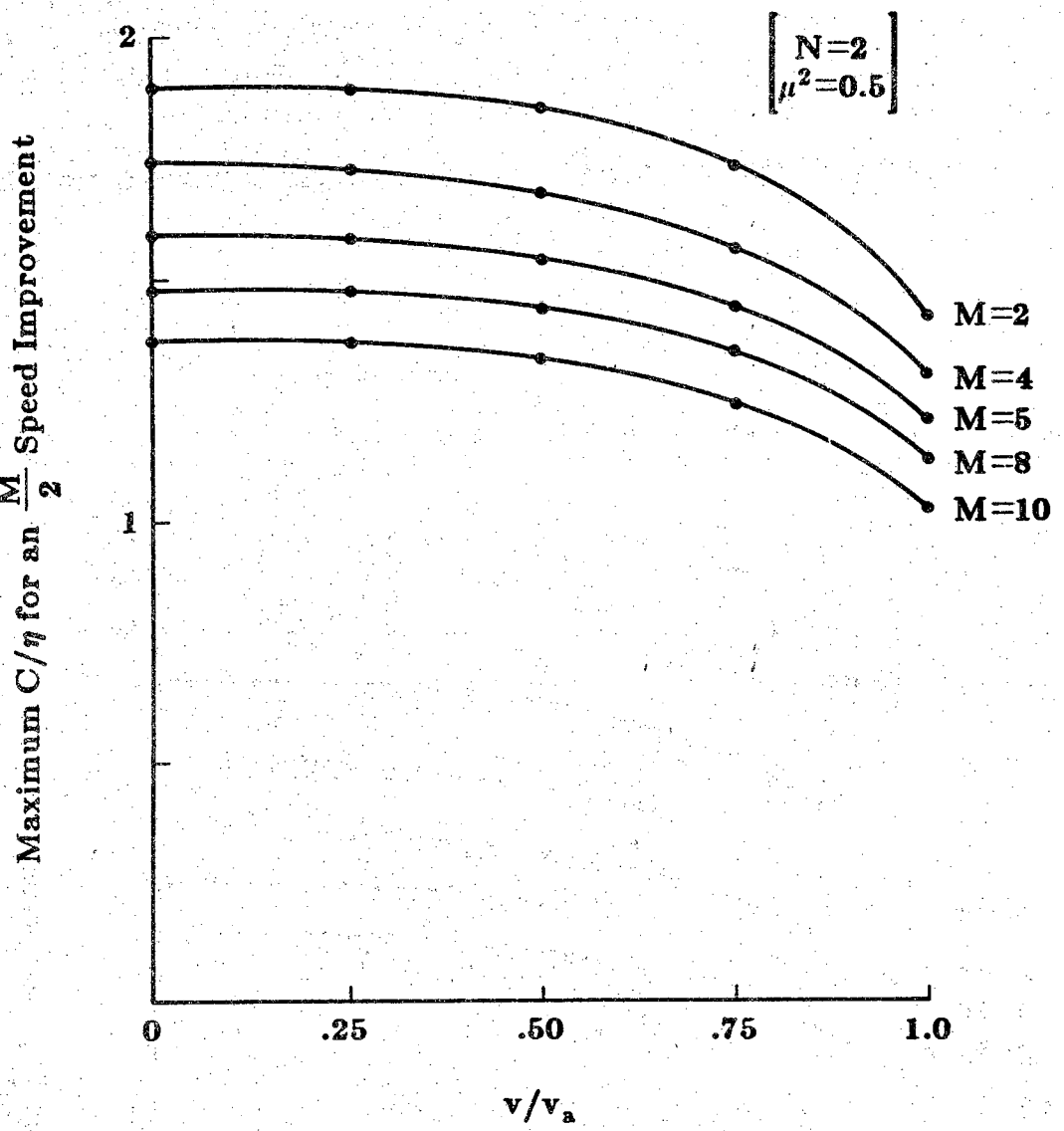

Figure 7–8 Maximum clutter-t-noise, C/η, for an M/2 speed improvement in an m-sequence system versus the number of modes, M, and the normalized target velocity, v/v_a.

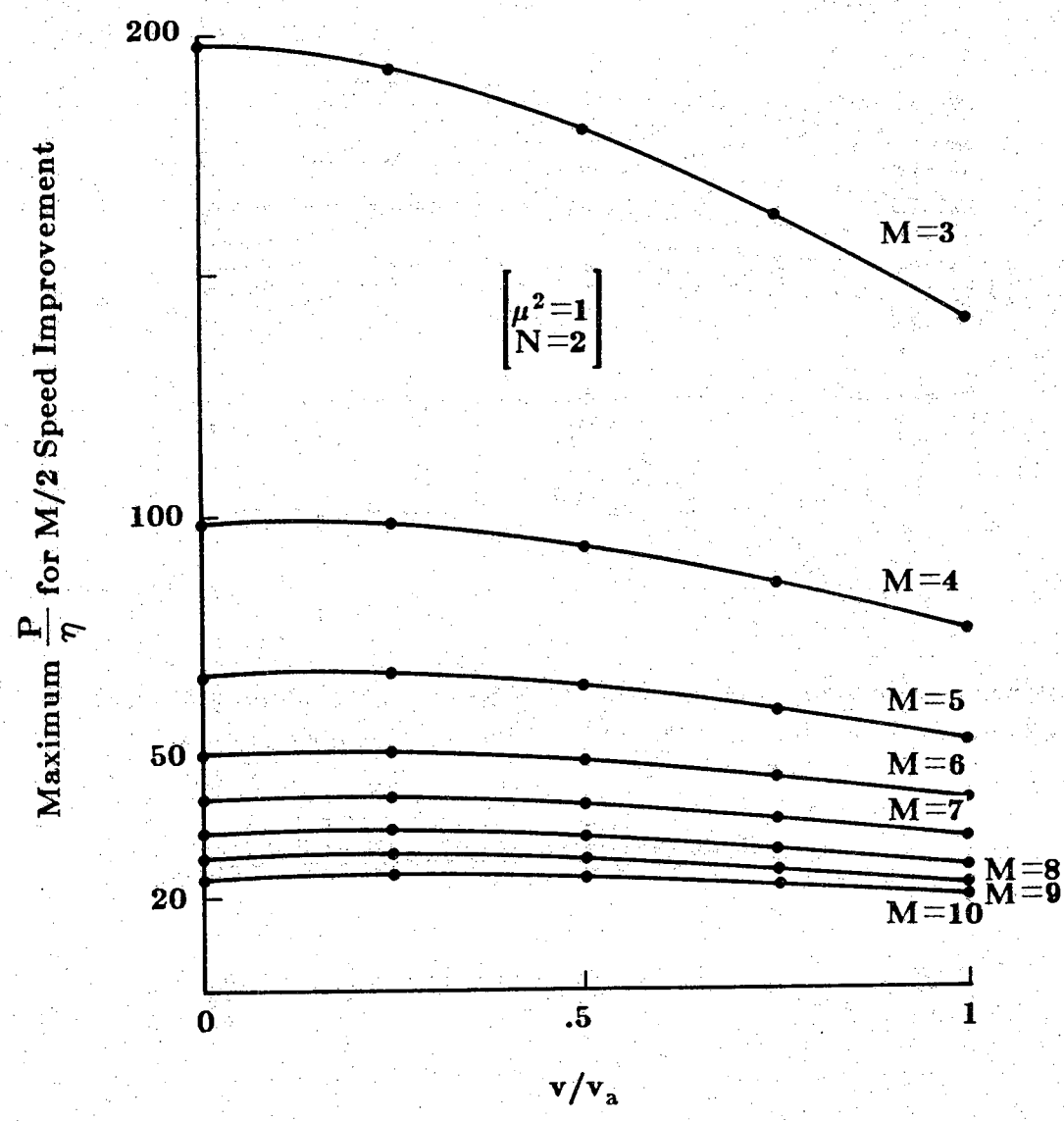

Figure 7–9 Maximum P/η, for an M/2 speed improvement in a Golay code system versus the number of modes, M, and the normalized target velocity, v/v_a.

For comparison the same constraint can be determined for pseudo-random m-sequences by setting $R(v)$ equal to unity in equation (7.2), so that

$$\frac{P}{\eta} \leq \frac{(nN/b)S(v) - 1}{1 + \mu^2[M - 1]}. \tag{7.22}$$

(This constraint also holds for the Golay code system when $N = 1$.) A plot of this constraint, Figure 7-10, shows that the pseudo-random code system again is constrained to a much lower range of P/η values than the Golay code system with $N = 2$. However, for large values of M, the performance of the m-sequence system is about the same as the Golay code system.

Low Velocity Analysis

In medical ultrasonic imaging applications, a wide range of target velocities will be encountered, depending upon the organ or body section under investigation. The highest velocities of about 120 cm/sec occur in the cardiovascular system in the aorta [69]. Maximum heart wall velocities on the order of 20 cm/sec are reached during the cardiac cycle [70]. In other imaging situations the velocities encountered are much lower, for example, the velocity of the foetal chest wall is only about 4 cm/sec [71]. In typical imaging applications the maximum scan distance is about 15 cm and the corresponding maximum repetition rate is 10 KHz, if the velocity of the tissue under study is approximately the velocity of water, 1500 m/sec. The maximum unambiguous velocity which can be imaged by a single-mode conventional pulse echo system is then about 75 cm/sec. A single-mode Golay code system can then image a target which moves at less than 25 cm/sec with more than 20 dB of self-noise cancellation and even for velocities up to 75 cm/sec the cancellation is still 10 dB. The Golay code system can thus image all but the fastest moving targets in the body with minimal degradation in signal-to-noise ratio.

As discussed in the moving target section, the value of N determines the speed of the simultaneous transmission system. The lowest value of $N = 1$ will thus produce the highest possible speed. We thus include the value of $N = 1$ as a special case in addition to evaluating the Golay code system for even N.

Assuming that the target and clutter velocities are less than 30% of the maximum unambiguous velocity, then $S(v_t)$ and $Q(v_c)$ are approximately unity, and $R_j(v_t)$ and $R_j(v_c)$ are approximately zero for $i = j$, and $i = c$ and letting $r = 1/2$ as a typical value, equation (7.12) then reduces to

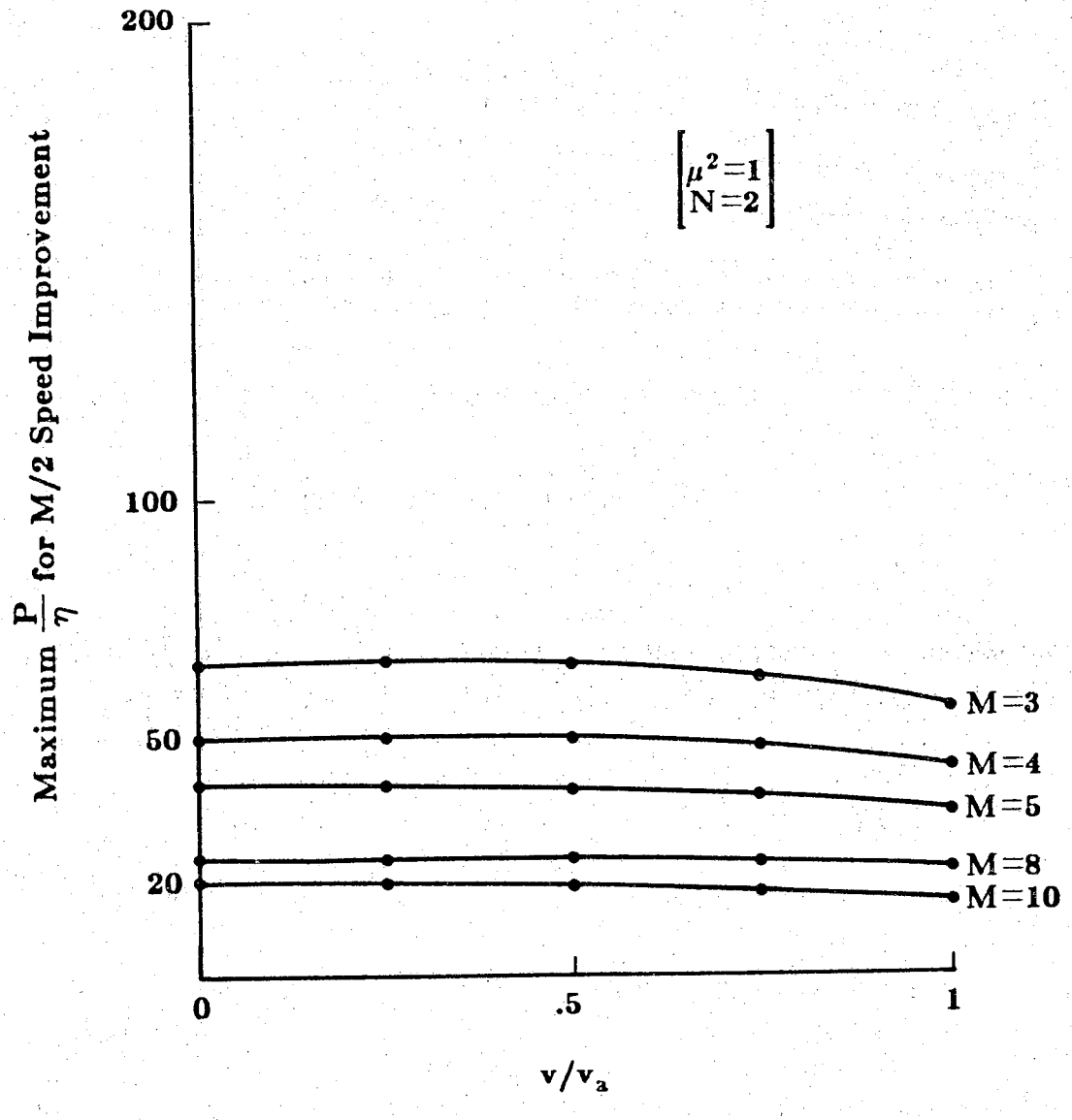

Figure 7–10 Maximum P/η, for an M/2 speed improvement in an m-sequence system versus the number of modes, M, and the normalized target velocity, v/v_a.

$$SNR = \frac{P}{C + \eta(\frac{b}{nN}) + \mu^2(M-2)[P(\frac{b}{nN}) + C(\frac{1}{N})]}, \tag{7.23}$$

for Golay codes with even values of N, and

$$SNR = \frac{P}{2C + \eta(\frac{b}{n}) + P(\frac{b}{n}) + \mu^2[M-1][P(\frac{b}{n}) + C]}, \tag{7.24}$$

for Golay codes, m-sequences, or random signals with $N = 1$.

If the SNR of the simultaneous array is to be greater than or equal to the sequential array system we must have

$$N \geq (\frac{b}{n}) + \mu^2(M-2)[\frac{P}{\eta}(\frac{b}{n}) + \frac{C}{\eta}], \tag{7.25}$$

for Golay codes with even values of N, and

$$N \geq \frac{b}{n} + [1 + \mu^2(M-1)][\frac{P}{\eta}(\frac{b}{n}) + \frac{C}{\eta}], \tag{7.26}$$

for Golay codes, m-sequences, or random signals with $N = 1$.

The maximum speed improvement, MSI, of the simultaneous system over the sequential system is the ratio of the number of modes M to the minimum number of transmit bursts N as given by the minimum N of equations (7.25) and (7.26) so that

$$MSI = \frac{M}{N} = \frac{M}{Int\left[(\frac{b}{n}) + \mu^2(M-2)[\frac{P}{\eta}(\frac{b}{n}) + \frac{C}{\eta}]\right]}, \tag{7.27}$$

for Golay codes with even N, where Int chooses the smallest integer greater than or equal to the argument, and

$$MSI = \frac{M}{Int\left[\frac{b}{n} + [1 + \mu^2(M-1)][\frac{P}{\eta}(\frac{b}{n}) + \frac{C}{\eta}]\right]}, \qquad (7.28)$$

for Golay codes with $n = 1$, and m-sequences and random signals for all N.

Plots of these speed improvement equations were made versus the number of simultaneous modes, M, and k, where $k = \frac{P}{\eta}(\frac{b}{n}) + \frac{C}{\eta}$. The values of $\mu^2 = .05$ and $\frac{b}{n} = .01$ were chosen as typical values, and the resulting plot is shown in Figure 7-11, for Golay codes, and Figure 7-12 for pseudo-random m-sequences. A comparison of the speed improvement shows that for low values of k corresponding to a low input SNR, the pseudo-random m-sequences produce the same speed improvement as the Golay codes. However, as the value of k is increased the Golay code system provides a much greater speed improvement.

It is apparent from these results that the simultaneous transmission system will provide greater operation speed than conventional pulse-echo systems, but a simultaneous transmission system will only provide equivalent or better signal-to-noise ratio for levels of C/η and P/η less than the values given by equation (7.17) and (7.21), respectively. The constraint on P/η being less restrictive than the constraint on C/η. These results are not suprising since the correlation system was shown to be optimal for noise limited situations.

The results also indicate that a Golay code simultaneous transmission system using zero cross-correlation pairs, provides as good as, or better performance than pseudo-random m-sequences or random signals under all conditions. For high-speed requirements, i.e. $N = 1$, the Golay codes provide the same performance as the m-sequences. For a lower speed requirement so that it is sufficient to have $N = 2$, the Golay code system provides a speed improvement of $M/2$ while retaining equivalent SNR to conventional systems for a much greater range of clutter and noise situations than the m-sequence system.

Note that the equations of speed improvement have no meaning for a two-mode simultaneous transmission system. If two modes are desired, as in the system of Figure 1-5 and if the proper zero interference codes are chosen, a Golay code simultaneous transmission system will operate at the same speed as a sequential two-mode pulse-echo system, with the increased signal-to-noise

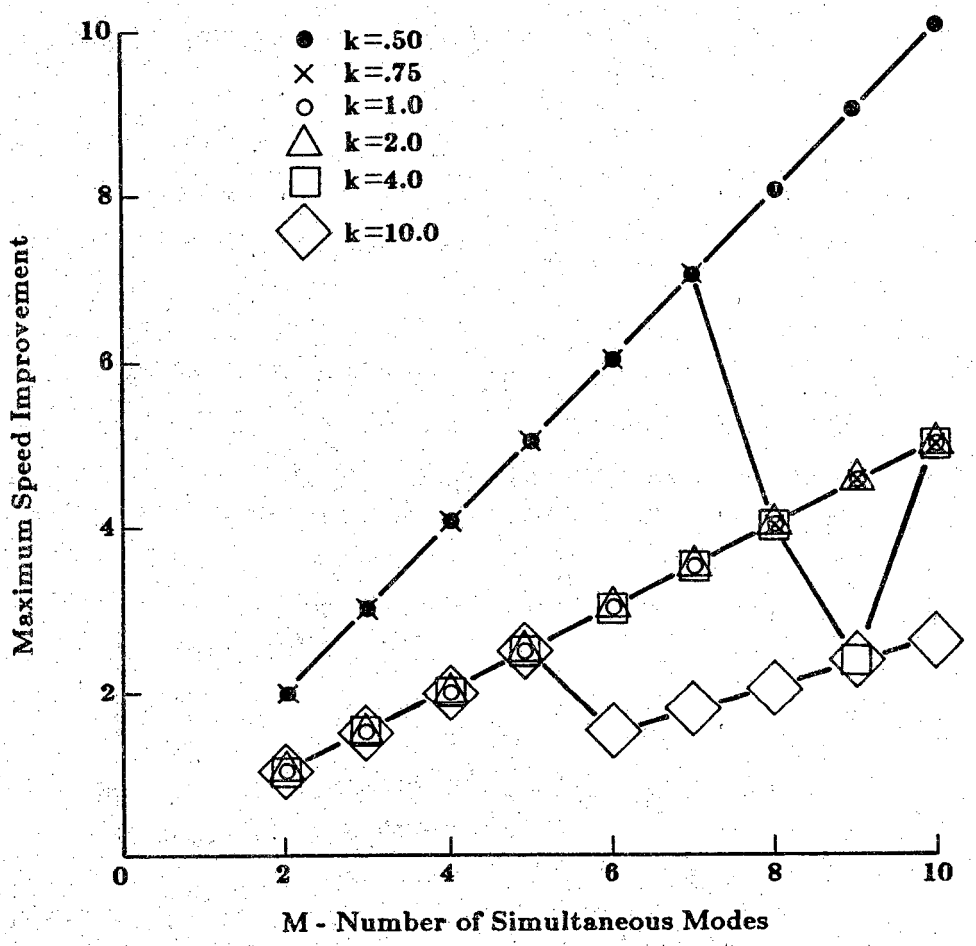

Figure 7–11 Maximum speed improvement versus the number of transmit modes, M, for a Golay code system with stationary targets.

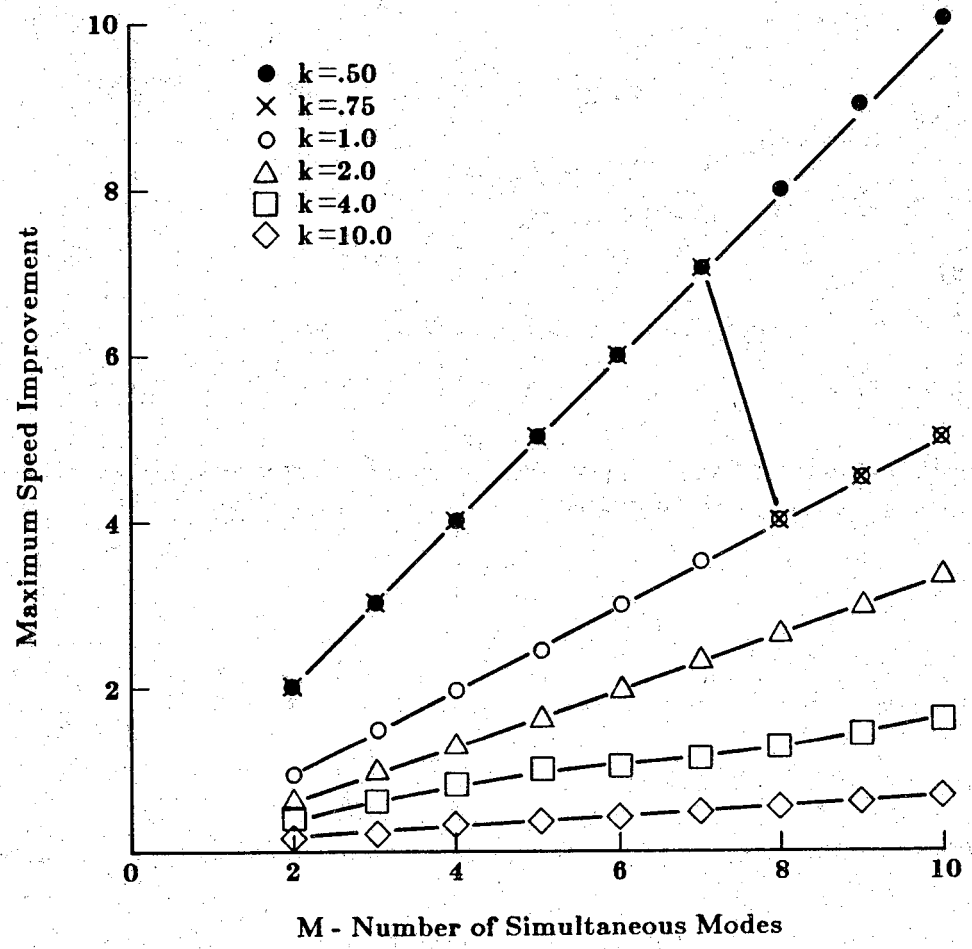

Figure 7–12 Maximum speed improvement versus the number of transmit modes, M, for an m-sequence system with stationary targets.

ratio provided by correlation, even in the worst case of completely overlapping beams. This two-mode system would have the same signal-to-noise ratio enhancement as the single-mode system, with the same good performance in the presence of clutter and interfering targets.

CHAPTER VIII - SUMMARY AND CONCLUSIONS

The detailed practical studies described in this thesis have demonstrated and analyzed the many promising advantages, as well as the limitations, of using correlation systems and pseudo-random transmit signals to improve the operation of conventional single-mode and multi-mode pulse-echo systems. In this chapter we summarize the important results and conclusions of each of these studies. Since the coverage is somewhat broad, the results are summarized and discussed in separate sections.

Single-Mode Systems

Subsequent to a background discussion in Chapter II which showed the important similarities and differences of correlation systems as applied to radar, sonar, and ultrasound, the fundamental principles of single-mode correlation systems were explored in detail. The presence of self-noise under finite correlation time was shown to be a fundamental limiting factor in correlation system operation under the presence of large targets and clutter. A signal-to-noise ratio formula which is useful for analyzing the performance of a correlation system was derived which includes the combined effects of self-noise, background receiver noise, and clutter. This formula was derived assuming a narrow beam of uniform cross-section illuminating and a uniform distribution of clutter targets. This formula was verified in Chapter V by actual measurements in a grainy medium.

In Chapter IV the many types of current methods for carrying out correlation processing were reviewed and compared in terms of their operating principles. The methods by which each of these systems approximates the correlation process were demonstrated in terms of their system equations. The second half of Chapter IV then reviewed and discussed the many different types of hardware which are currently used to carry out the important correlation functions of multiplication, delay generation, and integration.

Random and Pseudo-Random M-Sequence System

In Chapter V a new digital correlation system was described and demonstrated which uses a high-speed digital delay line, and can transmit either binary random or pseudo-random signals. A simulation of system operation was made which determined the clock frequency that produces the maximum output signal-to-noise ratio for the correlation system. At this optimum clock frequency, the correlation system was found to produce an output essentially equivalent in resolution to pulse-echo systems.

Actual measurements verified computer simulations of correlation system operation and showed that even under high-speed operation, using single burst correlation, the correlation system can retrieve signals buried in receiver noise, which a conventional pulse-echo system could not. However, in the correlation system, the presence of self-noise decreases system performance by limiting the dynamic range. When many more transmit bursts were correlated, as would be required in the case of very poor input signal-to-noise ratios, the self-noise was reduced and the dynamic range was significantly improved. The reduction in self-noise was found to be essentially the same for transmission of either sectioned m-sequences or clipped sampled random signals.

In order to produce the same signal-to-noise ratio enhancement in a pulse-echo system as in a correlation system, a coherent time-averaging technique would be required. A demonstration, in which a single bit of code was correlated over many transmit cycles, simulated time-averaging, and resulted in output signal-to-noise ratios slightly better than 256 bit single-burst operation, due to the lack of self-noise. However, a time-averaging system would be much slower than a correlation system, since the correlation system can produce signal-to-noise ratio enhancement in one burst through pulse-compression.

A more complete analysis of system operation was then made to include the effects of clutter, background receiver noise, and self-noise. To simplify derivations the clutter was assumed to be a random uniform distribution of equal cross-section targets with no multiple scattering or attenuation effects present. With these assumptions, a general signal-to-noise ratio formula was then developed and used to evaluate system performance under a variety of conditions.

Several different situations were considered which simplified the general signal-to-noise ratio formula. With an input signal-to-noise ratio much greater than unity, without clutter present, a pulse-echo system was found to produce a much higher dynamic range than a correlation system operating at high-

speed, but, in the presence of clutter the correlation system was found to have an output signal-to-noise ratio within 3 dB of the output signal-to-noise ratio of a pulse-echo system.

When the input signal-to-noise ratio is less than unity (a situation in which conventional pulse-echo systems cannot operate) the correlation system suffers some degradation in the presence of clutter due to self-noise overlap, but, with additional correlation time, the correlation system can retrieve a desired signal which is surrounded by clutter and buried in receiver noise.

Finally a formula was proferred which described the situation for which a correlation system would produce a higher signal-to-noise ratio than a conventional pulse-echo system. This formula indicated that for long transmit signals, n large, improvement occurs using the correlation system when the clutter-to-noise ratio is less than N. Using this result it is possible to select the appropriate system for a given application.

Golay Code System

Subsequent to the analysis of the random and pseudo-random code correlation system a new type of correlation flaw detection system was then described in Chapter VI. This new system transmits special paired pseudo-random codes called Golay codes and was shown to retain the theoretically unlimited signal-to-noise ratio enhancement capabilities of previous correlation systems. In addition the Golay code system has the benefit of being able to cancel unwanted self-noise in two consecutive transmit bursts. The absence of this self-noise allows the system to maintain optimal correlation operation under all signal-to-noise ratio conditions. Results of the analysis indicate that this new Golay code flaw detection system will provide substantially better performance in the presence of grains and large reflecting surfaces, while operating at much higher scan speeds, than previous single transducer correlation flaw detection systems.

A prototype Golay code system was demonstrated which transmits 64 bit Golay code pairs and successfully achieves cancellation of self-noise to -35 dB in two transmit bursts. This self-noise level was achieved 129 times faster than previous correlation flaw detection systems operating with the same length transmit burst.

Two useful methods of implementing self-noise cancellation were demonstrated. For very high-speed operation a high-speed integrator,

constructed from an operational amplifier, achieved good cancellation in two transmit bursts, and for lower speed operation a low-pass filter was able to achieve essentially the same cancellation as the high-speed integrator in 18 transmit bursts.

The disadvantages of self-noise in the presence of grains/clutter were also discussed and demonstrated using a large grained stainless steel sample. The results showed that the presence of self-noise in previous single transducer correlation systems increases the interference due to grains and that an increase in transmit burst length would not alleviate the problem. Results obtained using the prototype Golay code system indicated that the Golay code system can overcome the problem of self-noise inteference in the presence of grains.

In order to determine the factors which affect the amount of self-noise cancellation which occurs, further studies were made on the effects of DC offset and the pulse shape of the code pulses as determined by the turn-on and turn-off times of the pulses. Through computer simulations of these parameters, the self-noise cancellation was found to vary little with DC offset but was found to be very sensitive to misshaped pulses. It thus appears, in fact, that the present -35 dB self-noise cancellation present in the current prototype Golay code system could be improved by tuning or modifying the current transmitter design to improve the shape of the code pulses.

In order to investigate the applicability of Golay codes to situations where the targets are not stationary, such as in medical imaging applications, the limits of self-noise cancellation of a Golay code system were then determined under the presence of moving targets. This study was carried out through the a simulation of of the generalized ambiguity function developed by Kelly and Wishner [49]. The results showed that because self-noise cancellation requires a careful alignment of the correlation functions from consecutive transmit bursts, the self-noise cancellation is degraded by moving targets. Fortunately, the result indicate that the Golay code system will still produce self-noise cancellation of greater than 20 dB for velocities up to 30 % of the maximum velocity that a pulse-echo system can track.

Subsequent to the initial demonstration of the new Golay code system a full comparative system performance analysis was carried out under both stationary and moving targets. This analysis included the presence of background receiver noise and clutter.

In order to make the stationary target study more meaningful the analysis was carried out by considering a practical situation involving exponential attenuation with range. As expected, for stationary targets the Golay code

system was found to be optimal under all conditions and for all ranges. However the m-sequence and random signal systems were found to provide near equivalent performance in very low SNR conditions involving background receiver noise at long ranges. It is thus obvious that the Golay code system is the best system to choose for applications involving stationary targets. The Golay code system is ideal, therefore, for applications in the area of nondestructive testing.

In the analysis of a Golay code system under the presence of moving targets and clutter, a set of useful curves were determined, through the ambiguity function simulations described earlier, which can be used to determine under what situations a Golay code system will provide signal-to-noise ratio improvement over conventional systems. The curves indicate that the Golay code system is degraded by the presence of moving targets and is degraded even more when under the presence of moving clutter. The curves also indicate, however, that the the Golay code system will provide improvement over the other types of correlation systems and conventional systems over a significant range of target velocities and clutter levels.

It thus appears that the single-mode Golay code system should not be used under applications involving extremely high-velocity targets and clutter, which push the limits of conventional pulse-echo systems. The Golay code system could be used, however, to provide improved signal-to-noise ratio over conventional systems for a wide variety of more typical, slower moving target situations.

Simultaneous Multi-Mode Study

In Chapter VII of this thesis the single-mode study was extended to the study of a system which transmits in a number of different modes simultaneously and then uses correlation receivers to sort each mode out separately on reception.

The unique fundamental principles of this simultaneous transmission concept were first determined in terms of the fundamental equations which describe the correlation process. In this derivation the cross-talk between modes was shown to be a limiting factor in the performance of this system and was shown to relate to the amount of beam overlap and the cross-correlation level between transmit signals. The additional modes modes were then shown to reduce the dynamic range of target sizes which can be distinguished in

proportion to the inverse square root of the number of modes.

The clutter effects determined in the single-mode analysis were then extended to develop a signal-to-clutter ratio formula which includes the additional M−1 clutter signals due to the cross-talk inteferference between the simultaneous modes. Subsequent to this analysis of these fundamentals it was then possible to develop and analyze a general signal-to-noise ratio formula for a simultaneous transmission system.

Before this analysis was carried out, however, it was necessary to choose a good set of transmit signals. As in the single-mode analysis, the Golay codes have another useful unique property which occurs under the correlation of an even number of transmit bursts. Certain special pairs of complementary Golay code pairs have been discovered [68] which, besides providing zero self-noise cancellation in two transmit bursts, also have the the important unique property of zero cross-correlation in two transmit bursts. A promising set of eight basis complementary Golay code pairs was identified which includes 4 pairs of complementary Golay code pairs which have this zero cross-correlation property. In cross-correlation combinations between the complementary Golay code pairs which do not produce zero cross-correlation were found to have similar cross-correlation levels to special preferred m-sequence pairs which are noted for their low cross-correlation levels. Since longer Golay codes which are generated from these short basis codes using the generation processes of interleaving and appending retain the correlation properties of the shorter codes [68], this short set of eight code pairs can be used as a basis set for similar, much longer, eight pair sets. This is a useful feature since different length codes are required for different ranges in a pulse-echo imaging system.

An extension of the general single-mode signal-to-noise ratio formula was then made to develop a general simultaneous transmission signal-to-noise ratio formula which includes the effects of the interfering simultaneous modes under the presence of moving targets, clutter, and background receiver noise. This signal-to-noise ratio formula was then used to make a performance analysis and comparison of the use of Golay codes and, pseudo-random m-sequences or random signals, to conventional sequential multi-mode systems.

This equation was then simplified by assuming that all the interfering modes were identical in power and cross-talk overlap, and that certain noise terms could be made negligible by using long transmit bursts. A constraint was then derived from which for a given clutter, noise level, and target and clutter velocity, it is possible to determine the maximum permissable beam overlap in which a the simultaneous transmission system will still provide the

same signal-to-noise ratio as conventional sequential systems.

In order to simplify the performance evaluation under moving targets and clutter, the simultaneous transmission system was then analyzed under the two bounding cases of clutter limited and receiver noise limited operation. This simplification made it possible to isolate the separate effects of the clutter and receiver noise.

In the clutter limited case it was determined that there is a the maximum clutter-to-noise ratio above which the simultaneous transmission system will degrade the signal-to-noise ratio compared to conventional pulse-echo systems. This bound on the maximum clutter-to-noise ratio depends on the number of transmit bursts which are integrated, and was found to become more restrictive under the presence of higher velocity targets, increased beam overlap, and greater numbers of transmit modes. Below this bound the simultaneous transmission system will provide better signal-to-noise ratio and/or speed than the conventional system. The simultaneous transmission system which uses Golay codes was found to provide improved speed and signal-to-noise ratio over a much larger range of clutter-to-noise ratios than a simultaneous transmission system which uses m-sequences or random signals except in the case of one transmit burst integration.

In the receiver noise limited case it was determined that there is a maximum signal-to-receiver noise ratio above which the simultaneous transmission system will degrade the signal-to-noise ratio compared to conventional pulse-echo systems. Below this threshold the simultaneous transmission system provides better signal-to-noise ratio and/or speed compared to the conventional systems. This threshold again depends on the number of integrated transmit bursts and becomes more restrictive under the presence of moving targets, increased cross-talk and greater numbers of transmit modes. Unlike the clutter limited case, this signal-to-noise ratio constraint becomes less restrictive when the number of transmit bits can be increased. The Golay code system was again shown to provide improved performance over a greater range of signal-to-noise ratios than the m-sequence or random signal system except in the case of one transmit burst integration. In this one transmit burst case the performance of the two systems is again equivalent.

In many practical ultrasonic applications of a simultaneous multi-mode transmission system the velocity of the targets are low enough so that the self-noise and cross-correlation cancellation is nearly ideal. This low velocity assumption was then used to reduce the complexity of the general system

signal-to-noise ratio. Under the constraint of equal signal-to-noise ratio an equation was derived which describes the maximum speed improvement which a simultaneous transmission system will provide over conventional sequential pulse-echo systems. For typical values of cross-talk and burst length the maximum speed improvement was found to increase directly with an increasing number of transmit modes. But with decreasing signal-to-noise ratio, the incremental increase in speed with the number of modes became less. The maximum speed improvement was found to be greatest when the signal-to-noise ratio was low. This is not surprising since the performance of the correlation system has been found to be more optimal under low signal-to-noise ratio situations.

The Golay code simultaneous transmission system was shown to provide a greater speed improvement than the m-sequence system under input signal-to-noise ratios greater than unity. For signal-to-noise ratios less than unity, the performance of the Golay code system and the m-sequence or random signal system are the same.

To summarize these conclusions, it is apparent that the Golay codes will provide an improved system performance over either m-sequences or random signals over all conditions in either single or multi-mode operation. This is because of the advantage that Golay codes have with self-noise and cross-correlation cancellation when the integration time is greater than two transmit periods. It is also apparent that whether a single-mode or simultaneous multi-mode transmission system is better than the conventional pulse-echo systems depends on the situation. It is clear, however, that there are many situations to which a simultaneous transmission system using either Golay codes, m-sequences or random signals will provide an improved speed and/or signal-to-noise ratio compared to conventional sequential systems.

REFERENCES

[1] F. A. Firestone, "Reflectoscope," U. S. Patent 2,280,226, April 1942.

[2] Bilgutay, N. M., Furgason, E. S., and Newhouse, V. L., "Evaluation of a Random Signal Correlation System for Ultrasonic Flaw Detection," IEEE Trans. Sonics Ultrason. SU-23, 1976, pp. 329-333.

[3] Furgason, E. S., Newhouse, V. L., Bilgutay, N. M., and Cooper, G. R., "Application of Random Signal Correlation Techniques to Ultrasonic Flaw Detection," Ultrasonics, Vol. 13, No. 1, pp. 11-17, 1975.

[4] Cooper, G. R. and Gassner, R. L., "Analysis of a Wideband Random Signal Radar System," TR-EE 66-9, August, 1966.

[5] B. B. Lee and E. S. Furgason, "A New Digital Correlation Flaw Detection System," J. Nondestructive Evaluation, Vol. 2, No. 1, pp. 57-63, 1981.

[6] Elias, C. M., "An Ultrasonic Pseudorandom Signal-Correlation System," IEEE Trans. Sonics Ultrason. SU-27, pp. 1-7, January, 1980.

[7] Chapelon, J. Y., Cathignol, D., and Fourcade, C., "A New Pseudo-Random Binary Code Phase Modulated Ultrasonic High Resolution Echograph," presented at the Third International Symposium on Ultrasonic Imaging and Tissue Characterization, National Bureau of Standards, Gaithersburg, MD, June 5-7, 1978.

[8] Lam, F. K., and Hui, M. S., "An Ultrasonic Pulse Compression System for Non-Destructive Testing Using Maximal-Length Sequences," Ultrasonics, Vol. 20, No. 3, pp. 107-112, 1982.

[9] Pederson, N. E., "Method and Apparatus for Examining a Solid," U. S. Patent No. 4,167,879, Assigned to Panametric, Inc., Waltham, Mass., Sept. 18, 1979.

[10] Bilgutay, N. M., Newhouse, V. L., Saniie, J., and Furgason, E. S., "Flaw-to-Grain Echo Enhancement by Split-Spectrum Processing," Ultrasonics, Vol. 20, No. 2, pp. 59-68, 1982.

[11] Woodward, P. M., *Probability and Information Theory, With Applications to Radar,* New York: McGraw-Hill Book Co., Inc., London Pergamon Press Ltd., pp. 124-148, 1953.

[12] Winder, A. A., "II. Sonar System Technology," IEEE Trans. Sonics and Ultrason., Vol. SU-22, No. 5, pp. 291-332, 1975.

[13] Lee, B. B. and Furgason, E. S., "An Evaluation of Ultrasound NDE Correlation Flaw Detection Systems," IEEE Trans. Sonics and Ultrasonics, Vol. SU-29, No. 6, pp. 359-369, 1982.

[14] Von Ramm, O. T. and Smith, S. W., "Beam Steering with Linear Arrays," IEEE Trans. on Biomed. Eng., Vol. BME-30, No. 8, August 1983, pp 438-452.

[15] Miwa, H., Hayashi, H., Simura, T., and Murakami, K., "Simultaneous Multifrequency Ultrasonography the Principle and Technology," 1981 IEEE Ultrasonics Symposium Proceedings, Vol. 2, pp. 655-659, October 14-16, 1981.

[16] Tournois, P., "Acoustical Imaging Via Coherent Reception of Spatially Coloured Transmission," 1980 IEEE Ultrasonics Symposium, Boston, MA, pp. 747-750, November 5-7, 1980.

[17] Lee, B. B., and Furgason, E. S., "The Use of Noise Signals for Multi-Mode Operation of Phased Arrays," Journal of the Acoustical Society of America, Vol. 68, No. 1, pp. 320-328, July, 1980.

[18] Klauder, J. R., Price, A. C., Darlington S., and Albersheim, W. J., "The Theory and Design of Chirp Radars," Bell System Tech. J., Vol. 39, No. 4, July 1960, pp. 745-808.

[19] Cook, C. E., "Modification of Pulse Compression Waveforms," Proc. Natl. Electron. Conf. Vol. 14, 1958, pp. 1058-1067.

[20] Craig., S. E., Fishbein, W., and Rittenbach, O. E., " Continuous-Wave Radar with High Range Resolution and Unambiguous Velocity Determination," IRE Trans. on Military Electronics, April 1962, pp. 153-161.

[21] Lewis, B. L. and Kretschmer Jr., F. F., "A New Class of Polyphase Pulse Compression Codes and Techniques," IEEE Trans. on Aerospace and Electronic Systems, Vol. AES-17, No. 3, May 1981, pp. 364-371.

[22] Frank, R. L., "Polyphase Codes with Good Nonperiodic Correlation Properties," IEEE Trans. on Information Theory, Vol. IT-9, January 1963, pp. 43-45.

[23] Altes, R. A., "Radar/Sonar Signal Design For Bounded Doppler Shifts," IEEE Trans. on Aerospace and Electronic Systems, Vol. AES-18, No. 4, July 1982, pp. 369-379.

[24] Cloke, J. A., "Ambiguity Functions of Complementary Series," IEE International Conf. Radar 1982, The Royal Borough of Kensington and Chelsea Town Hall, Oct. 18-20, 1982, pp. 477-481.

[25] Wakasugi, K. and Fukao S., "Sidelobe Properties of a Complementary Code Used in MST Radar Observations," IEEE Trans. on Geoscience and Remote Sensing, Vol. GE-23, No.1, January 1985, pp. 57-59.

[26] Schmidt, G., Rüster, R., and Czechowsky, P., "Complementary Code and Digital Filtering for Detection of Weak VHF Radar Signals from The Mesosphere," IEEE Trans. on Geoscience Electronics, Vol. GE-17, No. 4, Oct. 1979, pp. 154-161.

[27] Skolnik, M. I., *Introduction to Radar Systems,* McGraw-Hill Book Company, New York, 1962.

[28] Deley, G. W., "Chapter 3 – Waveform Design," *Radar Handbook,* Merrill I. Skolnik, Editor, McGraw-Hill Book Company, 1970.

[29] Farnett, E. C., Howard, T. B., and Stevens, G. H., "Chapter 3 – Pulse-Compression Radar," *Radar Handbook,* Merrill I. Skolnik, Editor, McGraw-Hill Book Company, 1970.

[30] Winder, A. A., "II. Sonar System Technology," IEEE Trans. on Sonics and Ultrasonics, Vol. SU-22, No. 5, Sept. 1975, pp. 291-331.

[31] Stewart, J. L., Allen, W. B., Zarnowitz, R. M., and Brandon, M. K., " Pseudorandom Signal-Correlation Methods of Underwater Acoustic Research I: Principles," JASA, Vol. 37, June 1965, 1079-1090.

[32] Mitchell, G. T.,"Linear Correlators and High Resolution Random Signal Flaw Detection Systems," Purdue EE 696 Report, School of Electrical Engineering, Purdue University, April 1977.

[33] Skolnik, M. I., "Chapter I – An Introduction to Radar," *Radar Handbook,* Merrill I. Skolnik, Editor, McGraw-Hill Book Company, New York, N. Y., 1970, pp. 1-11 to 1-14.

[34] Carlin, B., *Ultrasonics,* McGraw-Hill Book Co., Inc., New York, N. Y., 1960, pp. 300-304.

[35] Tolstoy, I., Clay, C. S., *Ocean Acoustics Theory and Experiment in Underwater Sound,* McGraw-Hill Book Co., Inc., New York, N. Y., 1966, p. 3.

[36] Wild, J. J. and Reid, J. M., "Rotating Transducer for Tumor Location," Am. Inst. Ultrasonics Med., Vol. 4, 1955, p. 59.

[37] Lurch, C. S. Jr., "Chapter 32 – Satellite Surveillance Radar," *Radar Handbook,* Merrill I. Skolnik, Editor, McGraw-Hill Book Company, New York, N. Y., 1970, p. 32-11.

[38] Burckhardt, C. B., Grandchamp, P. A., and Hoffman, H., "Focusing Ultrasound over a Large Depth with an Annular Transducer - An Alternative Method," IEEE Trans. on Sonics and Ultrasonics, Vol. SU-22, No. 1, Jan. 1975, pp. 11-15.

[39] Furgason, E. S. and Newhouse, V. L., "The Use of Noise Signals for Multi-Mode Operation In Phased Arrays," Proc. of the Third International Symposium on Ultrasonic Imaging and Tissue Characterization, NBS, Gaithersburg, MD, June 1978, pp. 139-142.

[40] Furgason, E. S., Newhouse, V. L., and Lee, B. B., The Use of Noise Signals for Multi-Mode Beam Shaping," Abstracts of Scripps Inst. of Oceanography, La Jolla, California, July 1978, pp. 473-475.

[41] A. Papoulis, *Probability, Random Variables and Stochastic Processes,* McGraw-Hill, New York, pp. 326-331, 1965.

[42] P. W. Cooper, "Self-Noise of Random Binary Pulse Train of Fixed Pulse Width," IEEE Trans.

[43] Siebert, W. M., "A Radar Detection Philosophy," IRE Trans. on Infor. Theory, Vol. IT-2, No. 9, pp. 204-221, 1956.

[44] Vollman, W., "Resolution Enhancement of Ultrasonic B-Scan Images by Deconvolution," IEEE Trans. on Sonics and Ultrasonics, vol. SU-29, No. 2, March 1982, pp. 78-83.

[45] Bilgutay, N. M., "Split-Spectrum Processing for Flaw-to-Grain Echo Enhancement in Ultrasonic Detection," Purdue University Technical Report, TR-EE 81-20, pp. 210-219, 1981.

[46] Ishamaru, A., *Wave Propagation and Scattering in Random Medium,* Academic Press, 1978.

[47] Takeuchi, Y., "An Investigation of a Spread Energy Method for Medical Ultrasound Systems, Part One: Theory and Investigation Ultrasonics, Vol. 17, No. 4, pp. 219-224, 1979.

[48] Woodward, P. M., *Probability and Information Theory With Applications in Radar,* McGraw-Hill Book Co., Inc., New York, N. Y., 1953.

[49] Kelly, E. J. and Wishner, R. P., "Matched-Filter Theory for High-Velocity Accelerating Targets," IEEE Trans. on Military Electronics, Vol. MIL-9, No. 1, pp. 55-69, January, 1965.

[50] Chiang, A. M. and Burke, B. E., "A High-Speed Digitally Programmable CCD Transversal Filter," IEEE Journal of Solid-State Circuits, Vol. SC-18, No. 6, Dec. 1983, pp. 745-753.

[51] Burke, B. E., and Smythe, D. L. Jr., "A CCD Time-Integrating Correlator," IEEE Journal of Solid-State Circuits, vol. SC-18, No. 6, Dec. 1983, pp. 736-744.

[52] Blankenship, P. E., and Hofstetter, E. M., "Digital Pulse Compression via Fast Convolution," IEEE Trans. on Acoustics, Speech, and Signal Processing, April 1975, pp. 189-201.

[53] Butler, M. B. N., "S. A. W. Devices for Signal Processing," Case Studies in Advanced Signal Processing," IEE Conference Publication No. 180, Peebles Hotel Hydropropathic, Peebles, Scotland, Sept. 18-21, 1979, pp. 21-33.

[54] Hayt, W. H. Jr. and Kemmerly, J. E., *Engineering Circuit Analysis,* McGraw-Hill Book Co., Inc., New York, N. Y., 1971, pp. 542-543.

[55] Koral, W., "The Impact of Advanced LSI On Future Digital Signal Processing Architecture," *IEE Special Projects in Advanced Signal Processing,* 1980, pp. 244-247.

[56] Buckingham, M. J., "Noise in Electronic Devices and Systems," Ellis Horwood Limited, Market Cross House, Cooper Street, Chichester, West Sussex, England, 1983, pp. 22-23, p. 37,p. 39 and p. 73.

[57] Golomb, S. W., *Shift Register Sequences,* San Francisco, Holden-Day Inc., 1967.

[58] Cathignol, J., Fourcade, C., and Chapelon, J., "Transcutaneous Blood Flow Measurements Using Pseudorandom Noise Doppler System," IEEE Trans. Biom. Eng., Vol. BME-27, No. 1, pp. 30-36, 1980.

[59] Turyn, R. H., "On Barker Codes of Even Length," Proc. IEEE (Corr.), Vol. 51, No. 9, p. 1256, 1963.

[60] Golay, M. J. E., "Complementary Series," IRE Trans. on Info. Theory, Vol. IT-7, No. 4, pp. 82-47, April, 1961.

[61] Welti, G. R., "Quaternary Codes for Pulsed Radar," IRE Trans. on Info. Theory, Vol. IT-6, No. 6, pp. 400-408, 1960.

[62] Bernhardt, T., and Peacock, J. H., "Encoding Techniques for the Vibroseis System," Geophysical Prospecting, Vol. 26, pp. 184-193, 1978.

[63] Takeuchi, Y., "An Investigation of a Spread Energy Method for Medical Ultrasound Systems, Part One: Theory and Investigation," Ultrasonics, Vol. 17, No. 4, pp. 175-182, 1979.

[64] Takeuchi, Y., "An Investigation of a Spread Energy Method for Medical Ultrasound Systems, Part Two: Proposed System and Possible Problems," Ultrasonics, Vol. 17, No. 5, pp. 219-224, 1979.

[65] Turyn, R. H., "Ambiguity of Complementary Sequences," IEEE Trans. on Info. Theory, Vol. IT-9, No. 1, pp. 46-47, 1963.

[66] D. Nahamoo, and A. C. Kak, "Ultrasonic Echo Imaging With Pseudo-Random and Pulsed Sources: A Comparative Study," Ultrasonic Imaging, Vol. 3, pp. 1-36, 1981.

[67] Bar-Ness, Y., and Haimovich, A. M., "Synthesis of Random Antenna Array Patterns with Prescribed Nulls," IEEE Trans. on Antennas and Propagation, Vol. AP-32, No. 12, pp. 1298-1307, 1984.

[68] Sarwate, D. V., and Pursley, M. B., "Crosscorrelation Properties of Pseudorandom and Related Sequences," Proceedings of the IEEE, Vol. 68, No. 5, pp. 593-619, 1980.

[69] Renemen, R. S., and Spencer, M. P., "Local Doppler Audio Spectra in Normal and Stenosed Carotid Arteries," Ultrasound in Med. and Biol., Vol. 5, No. 1, pp. 1-11, 1979.

[70] Ambrose, J. A., King, B. D. , Teichholz, L. E. , LeBlanc, D. T., Schwinger, M., and Stein, J. H., "Early Diastolic Motion of the Posterior Aortic Root as an Index of Left Ventricular Filling," J. Clin. Ultrasound, Vol. 11, No. 7, pp. 357-364, 1983.

[71] Korba, L. W., Cobbold, R. S. C., Cousin, A. J., "An Ultrasonic Imaging and Differential Measurement System for the Study of Fetal Respiratory Movements," Ultrasound in Med. and Biol., Vol. 5, No. 2, pp. 139-148, 1979.